PRECISION CALCULATIONS FOR HIGGS PHYSICS IN THE STANDARD MODEL AND BEYOND

Von der Fakultät für Mathematik, Informatik und Naturwissenschaften der RWTH Aachen University zur Erlangung des akademischen Grades eines Doktors der Naturwissenschaften genehmigte Dissertation

vorgelegt von

JONAS KLAPPERT
M. Sc.

aus Meerbusch

Berichter: Prof. Dr. rer. nat. Robert Harlander
Prof. Dr. rer. nat. Michael Krämer

Tag der mündlichen Prüfung: 14.05.2020

ZUSAMMENFASSUNG

Spätestens seit der Entdeckung des Higgs-Bosons am Large Hadron Collider des CERNs ist der Higgs-Sektor des Standardmodells der Teilchenphysik eines der zentralen Forschungsgebiete der Hochenergiephysik. Durch mögliche Abweichungen von Messungen und theoretischen Vorhersagen innerhalb dieses Sektors erhofft man sich, ein vollständigeres Verständnis der Quantenfeldtheorien zu erhalten, die verwendet werden, um die Natur zu beschreiben. Neben immer genauer werdenden Messungen sind daher auch Hochpräzisions-Rechnungen notwendig, um bei Vergleichen von Messung und Vorhersage auf etwaige Abweichungen sensitiv zu sein.

Der Fokus dieser Arbeit liegt auf präzisen Vorhersagen von Observablen innerhalb des Higgs-Sektors.

Zum einen werden Studien der Higgsmassen-Berechnung innerhalb der minimalen supersymmetrischen Erweiterung des Standardmodells vorgestellt, die partielle Dreischleifenergebnisse beinhalten. Dafür werden verschiedene Berechnungsmethoden vorgestellt, welche in Kombination eine genaue Vorhersage der Masse des leichten CP-geraden Higgs für beliebige Parameterkonfigurationen erlauben. Durch die Verwendung der in dieser Arbeit entwickelten Ergebnisse kann die relative Unsicherheit in der Vorhersage der Masse des leichten CP-geraden Higgs auf unter 1% reduziert werden. Da zusätzlich alle zugehörigen Ergebnisse in ein öffentlich zugängliches Programm implementiert sind, können die Resultate dieser Arbeit in weiteren Studien genutzt werden.

Darüber hinaus wird die Higgs-Produktion in Kombination mit einem Vektor-Boson am Large Hadron Collider des CERNs untersucht. Durch die Ausnutzung einer Symmetrie der involvierten Vektor-Bosonen kann eine besondere Observable definiert werden, durch die sich ein Großteil der Unsicherheiten in sowohl Experiment als auch Vorhersage vermeiden lässt. Zur Veranschaulichung wird eine Analyse durchgeführt, die zum einen die erhöhte Sensitivität auf potentielle Abweichungen zwischen Theorie und Experiment zeigt, und zum anderen Evidenz für die Produktion eines Higgs-Bosons in Kombination mit einem Z-Boson durch Gluonfusion ermöglicht. Abschließend wird der aktuelle Fortschritt einer Zweischleifenrechnung für Higgs-Z-Produktion durch Gluonfusion vorgestellt, der eine volle Top-Quarkmassen-Abhängigkeit in den Schleifendiagrammen beinhaltet. Um die Quarkmassen-Effekte einzubeziehen, werden innovative Rechenmethoden entwickelt und in ein öffentlich zugängliches Programm implementiert, das breite Anwendung in der Berechnung von Mehrschleifendiagrammen finden kann.

ABSTRACT

At least since the discovery of the Higgs boson at the Large Hadron Collider at CERN, the Higgs sector of the Standard Model of particle physics has become one of the central research areas of high energy physics. Deviations between measurement and theoretical prediction within this sector have the potential to become a window on the quantum field theories describing nature. Besides the increasing precision of measurements, high-precision predictions are required to become sensitive on possible deviations.

The focus of this work is on precise predictions of observables within the Higgs sector.

On the one hand, studies of Higgs mass calculations within the context of the minimal supersymmetric extension of the Standard Model are presented, which include partial three-loop contributions. Different kinds of calculational methods are introduced, which, when combined, yield a reliable prediction of the light CP-even Higgs mass for in principle arbitrary parameter configurations. Utilizing the results of this work, the relative uncertainty of the predicted mass of the light CP-even Higgs can be reduced below the 1% level. Additionally, all corresponding results are implemented in an open-source program, which allows for further studies.

Moreover, Higgs production in association with a vector boson at the Large Hadron Collider at CERN is studied. By exploiting a symmetry connecting the final state gauge bosons, a particular observable can be defined, that leads to the cancellation of various sources of uncertainty in both measurement and prediction. For illustration, an experimental analysis for this observable is performed, which demonstrates an increased sensitivity to possible deviations between measurement and prediction, and, in addition, yields to evidence for the production of a Higgs boson associated with a Z boson through gluon fusion. Finally, the recent progress in the calculation of two-loop corrections to Higgs-Z production via gluon fusion including the full top-quark mass dependence are presented. To include these quark-mass effects, novel algebraic methods are developed and provided with an implementation into an open-source program, that can find wide application in the calculation of multi-loop Feynman diagrams.

LIST OF PUBLICATIONS

The research presented in this thesis was conducted at the Institute for Theoretical Particle Physics and Cosmology at RWTH Aachen University from January 2017 to January 2020. The contents of this thesis are partly based on work with other authors and have been published previously or are prepared for publication. Chap. 3, 4, and 5 are based on Refs. [JK1, JK4, JK6]. Chap. 7 is based on Ref. [JK3].

[JK1] R.V. Harlander, J. Klappert and A. Voigt, *Higgs mass prediction in the MSSM at three-loop level in a pure $\overline{DR}$ context*, *Eur. Phys. J.* **C 77** (2017) 814, arXiv:1708.05720 [hep-ph].

[JK2] R.V. Harlander, J. Klappert, S. Liebler and L. Simon, *vh@nnlo-v2: New physics in Higgs Strahlung*, *JHEP* **1805** (2018) 089, arXiv:1802.04817 [hep-ph].

[JK3] R.V. Harlander, J. Klappert, C. Pandini and A. Papaefstathiou, *Exploiting the WH/ZH symmetry in the search for New Physics*, *Eur. Phys. J.* **C 78** (2018) 760, arXiv:1804.02299 [hep-ph].

[JK4] R.V. Harlander, J. Klappert, A. D. Ochoa Franco and A. Voigt, *The light CP-even MSSM Higgs mass resummed to fourth logarithmic order*, *Eur. Phys. J.* **C 78** (2018) 874, arXiv:1807.03509 [hep-ph].

[JK5] J. Klappert and F. Lange, *Reconstructing Rational Functions with* `FireFly`, *Comp. Phys. Commun.* **247** (2020) 106951, arXiv:1904.00009 [cs.SC].

[JK6] R.V. Harlander, J. Klappert and A. Voigt, *The light CP-even MSSM Higgs mass including N^3LO+N^3LL QCD corrections*, arXiv:1910.03595 [hep-ph].

My contributions to these publications will be specified in detail in the course of this thesis.

CONTENTS

1 INTRODUCTION 1

I THE LIGHT CP-EVEN HIGGS MASS IN THE MSSM AT THE THREE-LOOP LEVEL

2 HIGGS MASS CALCULATIONS IN THE MSSM 5

3 FIXED-ORDER APPROACH 11

3.1 Higgs mass prediction at the three-loop level in the MSSM 12

3.1.1 Mass hierarchy selection 13

3.1.2 H3m renormalization scheme and its relation to $\overline{\text{DR}}'$ 14

3.1.3 Consistent determination of the MSSM $\overline{\text{DR}}'$ parameters 16

3.2 Numerical results including N^{3}LO QCD corrections 18

3.2.1 Size of three-loop contributions from different sources 18

3.2.2 Scale dependence of the Higgs pole mass 20

3.2.3 Comparison to other results 21

3.2.4 Tachyonic Higgs bosons 24

3.3 Conclusions 26

4 EFFECTIVE-FIELD-THEORY APPROACH 27

4.1 Renormalization-group improvement 28

4.2 Re-expanding the EFT calculation and ingredients for N^{3}LL accuracy 31

4.3 Extraction of the Higgs self-coupling at $\mathcal{O}(y_t^4 g_3^4)$ 32

4.3.1 Extraction procedure 32

4.3.2 Result in the degenerate-mass case 34

4.3.3 Extraction uncertainty 36

4.4 Numerical results including N^{3}LL QCD corrections 37

4.5 Conclusions 41

5 HYBRID APPROACH 43

5.1 Combination approaches 43

5.2 Numerical results including N^{3}LO+N^{3}LL QCD corrections 45

5.2.1 Size of the $\mathcal{O}(v^2/M_S^2)$ terms 45

5.2.2 Uncertainty estimate 47

5.2.3 Convergence for high SUSY scales 48

5.2.4 Convergence for low SUSY scales 51

5.3 Conclusions 52

II HIGGS STRAHLUNG IN THE STANDARD MODEL AND BEYOND

6 MEASUREMENT AND THEORY PREDICTION OF VH PRODUCTION 57

7 HIGGS-STRAHLUNG AS A PROBE FOR NEW PHYSICS 61

7.1 Motivation 61

7.2 Extraction of non-Drell-Yan contributions from data . . . 63
7.3 Theory prediction and sources of uncertainty of the Drell-Yan ratio . . . 65
7.4 Numerical results . . . 68
7.4.1 Outline of the simulation and analysis . . . 69
7.4.2 Impact of the hadron-level analysis on the Drell-Yan ratio . . . 71
7.4.3 Calculation of experimental uncertainties . . . 72
7.4.4 Semi-inclusive results . . . 73
7.4.5 Differential results . . . 74
7.5 Conclusions . . . 76
8 TOWARDS QUARK-MASS EFFECTS IN GLUON-INDUCED ZH PRODUCTION AT NLO QCD 77
8.1 Feynman diagrams and gauge choice . . . 78
8.2 Amplitude and tensor reduction . . . 80
8.3 Treatment of γ_5 . . . 85
8.4 Topologies . . . 86
8.5 Reduction to master integrals . . . 88
8.5.1 Integration-by-parts identities . . . 88
8.5.2 Sector relations . . . 90
8.5.3 Interpolation of multivariate rational functions over finite fields . . . 91
8.5.4 Rational reconstruction . . . 96
8.5.5 Integration-by-parts reductions over finite fields . . . 98
8.5.6 Reduction of two-loop integrals for gluon-induced ZH production . . . 100
8.6 Conclusions and Outlook . . . 102

III APPENDICES

A CONVENTIONS AND FEYNMAN RULES 105
B EXPLICIT FORMULÆ 109
B.1 Threshold corrections . . . 109
B.2 Projector coefficients . . . 110
BIBLIOGRAPHY 117
DANKSAGUNG 135
EIDESSTATTLICHE ERKLÄRUNG 137

1

INTRODUCTION

The success of the Standard Model of particle physics (SM)[1] at describing nature at the smallest known scales is undoubted. Its last missing piece, the Higgs boson H, was discovered by the ATLAS [2] and CMS [3] collaborations at the Large Hadron Collider (LHC) in 2012. In light of this discovery, the Higgs sector has become of foremost interest. Until today all measurements related to this sector are in agreement with SM predictions [4], thus raising the importance of precision calculations and measurements to enhance the sensitivity to potential beyond the SM (BSM) physics. This is especially relevant considering that, despite the success of the SM in describing nature, many puzzling observations remain which require BSM physics. For example, neutrino oscillations, the baryon asymmetry of the universe, dark matter and dark energy, and the smallness of the Higgs boson mass cannot be explained in the framework of the SM. As the Higgs sector is currently the least constrained part of the SM, potential inconsistencies in predictions that contribute to this sector could be a valuable hint towards a more complete picture of the underlying principles of BSM physics.

Several concepts and theories have been proposed to address these open questions, of which the extensively studied Supersymmetry (SUSY) is one.[2] Many realizations of SUSY provide a dark matter candidate, considering that dark matter is particle based, and come with an explanation for the size of the Higgs boson mass, for example. The primary idea of SUSY is to relate fermions and bosons by extending the Lorentz symmetry in the only possible non-trivial way. Among all possible SUSY realizations, the simplest one is the Minimal Supersymmetric Standard Model (MSSM) [9, 10]. It extends the SM in a minimal way to incorporate SUSY. As a consequence, each particle of the SM is accompanied by a so-called superpartner, whose spin is shifted by one half with respect to the SM partner. Additionally, a second complex Higgs doublet has to be introduced in order to ensure the holomorphicity of the superpotential. Therefore, the Higgs spectrum consists of five physical Higgs bosons. For real parameters the spectrum is given by two neutral CP-even h and H bosons,[3] the CP-odd A boson, and two charged $H^{\pm}$ bosons. One particular feature of SUSY is that, even at tree level, the mass of h, which could be identified as the SM Higgs, can be predicted. Thus, the measured mass of the discovered Higgs boson at the LHC can be used as an additional precision observable to constrain the mass spectrum of potential superpartners or to test SUSY theories in general. To complement precise measurements of the Higgs mass, precise predictions are needed in addition. Nonetheless, there has been no experimental

1 For a pedagogical introduction to the SM we refer the reader to Ref. [1], for example.
2 We refer the reader to Refs. [5–8] for an introduction to supersymmetric theories and the MSSM.
3 Note that the Higgs boson of the SM is denoted as H, whereas the SM-like Higgs of the MSSM is denoted as h.

evidence for supersymmetric particles so far, which are thus constrained to have masses above hundreds of GeV [11, 12].

Irrespective of specific extensions of the SM, precise theoretical predictions within the framework of the SM are currently indispensable to stay competitive to the shrinking measurement uncertainties and thus be sensitive to possible deviations from the SM. As state-of-the-art-calculation techniques are pushed to their limits with cutting-edge calculations of $2 \to 2$ and $2 \to 3$ scattering processes at the two-loop level, for example, the need of either conceptual advances within these calculations or novel algebraic approaches to at least ease computational bottlenecks are inevitable.

In addition, observables that are sensitive to potential BSM physics effects are well suited to complement both high-precision measurements and predictions. Furthermore, ratios, in which similar sources of uncertainties cancel, can help to alleviate the requirement of improved precision. Well-known examples of such observables are $R_{K^{(*)}}$ [13] and the ρ parameter [14].

Following the aforementioned observations, this thesis is dedicated to calculations, studies, and automatization of precision calculations in the SM and beyond. In Part I, we focus on Higgs mass predictions in the MSSM, apply and compare different approaches to Higgs mass calculations, and derive results, which are based on the calculation of Refs. [15, 16], up to the three-loop level. Afterwards, in Part II, we exploit a symmetry within the Higgs production associated with a vector boson at the LHC to define and study an observable that is highly sensitive to New-Physics phenomena. Guided by the latter idea and concerns regarding precision when trying to expose BSM physics using state-of-the-art analyses, we develop novel techniques that ease some bottlenecks in cutting-edge higher-order calculations. These methods are then applied to a proof-of-principle calculation within the context of the associated production of a Z and a Higgs boson.

Part I

THE LIGHT CP-EVEN HIGGS MASS IN THE MSSM AT THE THREE-LOOP LEVEL

In this part, we focus on the mass prediction of the light CP-even Higgs h in the MSSM, which in our studies is identified with the SM-like Higgs boson. Different computational approaches are compared and numerical studies up to three-loop accuracy are presented.

2

HIGGS MASS CALCULATIONS IN THE MSSM

With the discovery of the Higgs boson with a mass of [2, 3, 17, 18]

$$M_h = (125.10 \pm 0.14)\,\text{GeV}\,, \tag{2.1}$$

the SM is complete and appears to be a good description of nature around and below the electroweak scale. However, the SM does not describe gravity and cannot account for phenomena typically associated with dark matter, for example, or for CP-violation at the level required to explain the observed baryon anti-baryon asymmetry. SUSY has been an attractive proposal to address some of the deficits of the SM. As a realization of SUSY, the the MSSM exhibits a constrained Higgs sector which, for a given set of SUSY parameters, results in a theoretical prediction of the lightest CP-even Higgs boson mass M_h. Comparison to the measured mass of the observed Higgs boson as quoted above provides a stringent constraint of the MSSM. However, at tree level the mass of the lightest CP-even Higgs boson in the MSSM is bounded by the Z-boson mass, M_Z, in the decoupling limit, i.e. $M_A \gg M_Z$, where M_A is the mass of the CP-odd Higgs boson A:

$$M_h^2 \simeq v^2 \frac{\frac{3}{5}g_1^2 + g_2^2}{4} \cos^2 2\beta = M_Z^2 \cos^2 2\beta \leq M_Z^2\,, \tag{2.2}$$

where

$$v = \sqrt{v_u^2 + v_d^2} \approx 246\,\text{GeV}\,, \quad \tan\beta = \frac{v_u}{v_d}\,, \quad g_1 = \sqrt{\frac{5}{3}}g'\,, \quad g_2 = g. \tag{2.3}$$

g and g' are the gauge couplings of the $SU(2)_L$ and $U(1)_Y$, respectively. v_u and v_d are the vacuum expectation values (VEV) of the two Higgs doublets (cf. Eq. (2.7)). Without large radiative corrections to the Higgs mass, a realization of the MSSM in nature could have been ruled out already.

During the last decades, much effort has been invested in order to calculate radiative corrections, develop automated code to predict SUSY mass spectra, and to introduce new calculational approaches for different mass regions of the SUSY spectra. The latter can be divided into three categories, which will be discussed in more depth in the following chapters.

On the one hand, there are fixed-order (FO) calculations, where loop corrections to the Higgs mass are calculated in the full MSSM, and the perturbation series is truncated at a fixed order of the coupling constants. If the SUSY particles have masses not too far above the electroweak

scale, the FO calculation typically leads to a reliable value. However, if (some of) the SUSY particles are very heavy, the perturbative coefficients receive large logarithmic contributions, which spoil the convergence of the perturbative series. Currently, loop corrections up to the two-loop level are known in the on-shell scheme [19–34] and up to the three-loop level in the $\overline{\text{DR}}'$ scheme[1] [15, 16, 24–27, 35–49]. The corresponding FO Higgs pole mass results are available through implementations into publicly available spectrum generators [22, 50–59]. Spectrum generators are codes that calculate the mass spectrum, couplings, and observables for a given set of SM and model dependent input parameters. The contributions of this thesis to the FO approach are discussed in Chap. 3.

On the other hand, there are effective-field-theory (EFT) calculations, which are based on the assumption that the SUSY particles are very heavy compared to the electroweak scale. Integrating them out leaves the SM as an EFT. The latter retains the SUSY constraints through so-called threshold corrections between the MSSM and the SM parameters, which are applied at some large mass scale. The Higgs pole mass is then calculated from the SM $\overline{\text{MS}}$ parameters after evolving them down to the electroweak scale through SM renormalization-group equations (RGEs), thereby resumming contributions which are logarithmic in the ratio of the SUSY and the electroweak scale. Such kinds of logarithms are denoted as *large logarithms* in what follows. This procedure has been implemented through next-to-next-to-leading logarithmic order (NNLL[2] or third logarithmic order) in several publicly available pure-EFT spectrum generators [59–61]. Resummation through fourth logarithmic order (N^3LL) has recently been achieved through the calculation of the three-loop threshold correction for the quartic coupling λ [62], which complemented the available two-loop threshold corrections [60, 61, 63–67]. Our contributions to the EFT approach are discussed in Chap. 4.

The FO and the EFT approach have shown that the tree-level Higgs mass given in Eq. (2.2) indeed receives large radiative corrections. However, in order for the theoretical value of the light CP-even Higgs mass to be compatible with the observed Higgs mass of $M_h \approx 125\,\text{GeV}$, the SUSY spectrum requires TeV-scale stops (see Refs. [60, 64, 68–70], for example). Regarding uncertainties, it is not clear *a priori* whether a FO or an EFT approach provides the most reliable value for the Higgs mass at these mass scales. For this reason, so-called hybrid approaches have been devised [53, 59, 68, 69, 71–74]. They combine the virtues of a FO and an EFT calculation, and lead to a reliable value for the Higgs pole mass at arbitrary SUSY scales in principle. Comparison to the highest available FO result shows good agreement up to remarkably large SUSY scales of the order of 5–10 TeV [75], in accordance with earlier comparisons of FO and EFT results [47]. Our contributions to the hybrid approach are discussed in Chap. 5.

The aim of the first part of this thesis is to study the three-loop corrections obtained by a FO calculation in Refs. [15, 16]. Since the latter were not included in state-of-the-art spectrum generators before this thesis, we provide an implementation of these terms into

1 See Subsect. 3.1.2 and references therein for its definition.

2 Any N in shorthand notations like NLL corresponds to a *next-to*, e.g. NLL means next-to-leading logarithmic order. In combinations with LO, i.e. leading order, NLO represents next-to-leading order.

the C++ library Himalaya [47] and use it together with the spectrum generator FlexibleSUSY (FS) [58, 59]. With the help of Himalaya we are able to elevate the FO, the EFT, and the hybrid approach to the three-loop level, which is needed in order to reduce the theoretical uncertainty and be more competitive regarding the measured value of Eq. (2.1).

Before we turn to a more in-depth discussion of the approaches introduced above, we establish notational details in the following.

Masses denoted by capital letters, such as M_x, are meant to be pole masses, whereas masses denoted by lower case letters, such as m_x, are defined to be running masses in a specific renormalization scheme.

The set of SM $\overline{\text{MS}}$ parameters relevant to our calculation is denoted as

$$\bar{X} = \{\bar{\lambda}, \bar{g}_t, \bar{g}_3, \bar{v}\}\,, \tag{2.4}$$

where $\bar{\lambda}$ denotes the quartic Higgs coupling, $\bar{g}_t$ the SM top Yukawa coupling, $\bar{g}_3$ the strong gauge coupling, and $\bar{v}$ the vacuum expectation value of the Higgs field in the SM.

If SUSY would be an exact symmetry, the superpartners and their corresponding SM particles would have the same mass. As there are currently no hints for additional particles at the mass scale of the SM particles, SUSY has to be broken when realized in nature. Without assuming a specific SUSY breaking mechanism, cf. Refs. [76, 77], one is able to parametrize this breaking by adding terms to the Lagrangian that explicitly break SUSY. For our studies, the relevant parts of the MSSM Lagrangian read[3]

$$\begin{aligned}
-\mathcal{L}^{\text{MSSM}}_{\text{soft-breaking}} \supset\ & \frac{1}{2}\left(M_1 \tilde{B}\tilde{B} + M_2 \tilde{W}\tilde{W} + m_{\tilde{g}}\tilde{g}\tilde{g} + \text{h.c.}\right) \\
& + (y_u A_u)_{ij}\left(\tilde{Q}_i H_2\right)\tilde{U}_j^* + (y_d A_d)_{ij}\left(H_1 \tilde{Q}_i\right)\tilde{D}_j^* \\
& + \left(m_Q^2\right)_{ij}\tilde{Q}_i^*\tilde{Q}_j + \left(m_U^2\right)_{ij}\tilde{U}_i^*\tilde{U}_j + \left(m_D^2\right)_{ij}\tilde{D}_i^*\tilde{D}_j \\
& + B\mu\left(H_1 H_2 + \text{h.c.}\right)\,.
\end{aligned} \tag{2.5}$$

Here, $\tilde{B}$, referred to as bino, is the superpartner of the SM B_μ boson, $\tilde{W}_\mu$, referred to as winos, are the superpartners of the SM W_μ bosons, and $\tilde{g}$, referred to as gluino, is the superpartner of the SM gluon g. M_1, M_2, and $m_{\tilde{g}}$ are the masses of the bino, wino, and gluino, respectively. $(y_u)_{ij}$ and $(y_d)_{ij}$ are the Yukawa coupling matrices of up-type or down-type quarks in the MSSM. The trilinear coupling matrices $(A_{u/d})_{ij}$ are soft-breaking parameters in the MSSM. Note that we are assuming flavor diagonal matrices, i.e. $(y_{u/d}A_{u/d})_{ij} = \delta_{ij} y_{u/d} A_{u/d}$, with δ_{ij} being the Kronecker symbol and $u/d \in \{u, s, t\}/\{d, c, b\}$. $\tilde{Q}$, $\tilde{U}$, and $\tilde{D}$ are the superpartner fields of the quarks, referred to as squarks, containing the $SU(2)_L$ doublet squarks, the up-type singlet squarks, and down-type singlet squarks, respectively. Their mass matrices $(m_Q^2)_{ij}$ contain the squared soft breaking masses $m_{Q,i}$, $m_{U,i}$, and $m_{D,i}$ for $i \in \{1, 2, 3\}$ as

3 For a comprehensive introduction to the MSSM, we refer the reader to Refs. [6–8].

diagonal elements. Note that all gauge indices are suppressed in Eq. (2.5). $B\mu$ is the soft bilinear term of the μ-parameter of the Higgs potential,

$$V_{\text{Higgs}} \supset |\mu|^2|H_1|^2 + |\mu|^2|H_2|^2\,, \tag{2.6}$$

where the two Higgs doublets can be decomposed as

$$H_1 = \begin{pmatrix} \frac{1}{\sqrt{2}}\left[v_d + (\phi_1 - \mathrm{i}\chi_1)\right] \\ -\phi_1^- \end{pmatrix}, \qquad H_2 = \begin{pmatrix} \phi_2^+ \\ \frac{1}{\sqrt{2}}\left[v_u + (\phi_2 - \mathrm{i}\chi_2)\right] \end{pmatrix}. \tag{2.7}$$

ϕ_i, χ_i are real and $\phi_i^\pm$ are complex scalar fields. v_u and v_d are the VEVs of the two Higgs doublets. Since we are interested in studies of M_h, only the fields ϕ_i are considered, which can be converted into their mass eigenstates h and H at tree level by diagonalizing the matrix:

$$\mathsf{M}^{\text{tree}} = \frac{\sin 2\beta}{2}\begin{pmatrix} M_Z^2\cot\beta + M_A^2\tan\beta & -M_Z^2 - M_A^2 \\ -M_Z^2 - M_A^2 & M_Z^2\tan\beta + M_A^2\cot\beta \end{pmatrix}. \tag{2.8}$$

At tree level, the running sfermion masses $m_{\tilde{f}_1} \leq m_{\tilde{f}_2}$ are the eigenvalues of the ith generation squark mass matrix $\mathsf{M}_{q,i}$,

$$\mathsf{M}_{q,i} = \begin{pmatrix} m_q^2 + m_{Q,i}^2 + \Delta_1 & m_q X_q \\ m_q X_q & m_q^2 + m_{U,i}^2 + \Delta_2 \end{pmatrix}, \tag{2.9}$$

with the SUSY breaking parameters $m_{Q,i}$, $m_{U,i}$, and $m_q = v_{u/d}\,y_q/\sqrt{2}$ being the running $\overline{\text{DR}}'$ quark mass. The Δ_i in Eq. (2.9) are electroweak contributions and read

$$\Delta_1 = M_Z^2\left(I_q - e_q\sin^2\theta_w\right)\cos 2\beta\,, \tag{2.10}$$

$$\Delta_2 = e_q M_Z^2\sin^2\theta_w\cos 2\beta\,, \tag{2.11}$$

where I_q is the third component of the corresponding quark's isospin, e_q is its electric charge, and θ_w is the weak mixing angle.

For our studies, the relevant set of MSSM parameters, renormalized in the $\overline{\text{DR}}'$ scheme, read

$$Y = \{y_t, g_3, v, m_{\tilde{t}_1}, m_{\tilde{t}_2}, X_t, m_{\tilde{g}}, m_{\tilde{q}}\}\,, \tag{2.12}$$

with

$$v_u = v\sin\beta\,, \quad v_d = v\cos\beta\,, \quad m_{\tilde{q}} = \left(\prod_{f\in\{u,d,c,s,b\}}\prod_{n=1}^{2} m_{\tilde{f}_n}\right)^{1/10}, \tag{2.13}$$

whereas y_t denotes the MSSM top Yukawa coupling, g_3 the strong gauge coupling, $X_t = A_t - \mu/\tan\beta$ the stop mixing parameter, $m_{\tilde{g}}$ the gluino mass, and $m_{\tilde{q}}$ the average mass of

all squarks but the stops. Combining the latter squark masses through a geometric mean is justified since we are only interested in studies where these masses are of comparable size. A_t is the up-type trilinear coupling of the third generation. Note that, due to the SUSY constraints, Y does not contain a separate parameter for the quartic Higgs coupling.

When mentioning the electroweak scale, we estimate its magnitude by the value of v. It is used as a representative for SM mass scales such as the top mass $\bar{m}_t = \bar{v}\bar{g}_t/\sqrt{2}$. The SUSY scale is identified with M_S, which is treated as an input parameter for our calculations. M_S is also used as a representative for MSSM mass scales such as one of the stop masses $m_{\tilde{t}_i}$, and we refer to the decoupling limit if $M_S \gg v$.

Additionally, we introduce the short hand notations:

$$\kappa = \frac{1}{16\pi^2}\,, \quad x_t = \frac{X_t}{M_S}\,, \quad s_x = \sin x\,, \quad c_x = \cos x\,. \tag{2.14}$$

If not stated differently, we follow the SUSY Les Houches Accord (SLHA) standard [78] and use the subsequent set of SM parameters as input for numerical studies:

$$\begin{aligned}
&\bar{\alpha}_{\text{em}}^{\text{SM}(5)}(M_Z) = \frac{1}{127.944}\,, \quad \bar{\alpha}_s^{\text{SM}(5)}(M_Z) = 0.1184\,, \quad M_Z = 91.1876\,\text{GeV}\,,\\
&G_F = 1.1663787\cdot 10^{-5}\,\text{GeV}^{-2}\,, \quad M_e = 510.998902\,\text{keV}\,, \quad M_\mu = 105.6583715\,\text{MeV}\,,\\
&M_\tau = 1.777\,\text{GeV}\,, \quad \bar{m}_u(2\,\text{GeV}) = 2.4\,\text{MeV}\,, \quad \bar{m}_d(2\,\text{GeV}) = 4.75\,\text{MeV}\,,\\
&\bar{m}_s(2\,\text{GeV}) = 104\,\text{MeV}\,, \quad \bar{m}_c^{\text{SM}(4),\overline{\text{MS}}}(\bar{m}_c) = 1.27\,\text{GeV}\,, \quad \bar{m}_b^{\text{SM}(5),\overline{\text{MS}}}(\bar{m}_b) = 4.18\,\text{GeV}\,,\\
&M_t = 173.34\,\text{GeV}\,,
\end{aligned} \tag{2.15}$$

where $\bar{\alpha}_{\text{em}}^{\text{SM}(5)}(M_Z)$ and $\bar{\alpha}_s^{\text{SM}(5)}(M_Z)$ denote the fine-structure and strong coupling in the $\overline{\text{MS}}$ scheme in the SM with five active quark flavours, and G_F is the Fermi constant. M_e, M_μ, M_τ, and M_t denote the pole masses of the electron, muon, and tau lepton as well as top quark, respectively. The input masses of the up, down, and strange quark are defined in the $\overline{\text{MS}}$ scheme at the scale 2 GeV. The charm and bottom quark masses are defined in the $\overline{\text{MS}}$ scheme at their mass scale in the SM with four and five active quark flavours, respectively. The conversion of the SM input parameters to MSSM $\overline{\text{DR}}'$ parameters will be discussed in detail in Subsect. 3.1.3.

The SUSY input parameters are chosen such that the degenerate soft-breaking mass parameters are all set to M_S. Furthermore, we set $\mu(M_S) = m_A(M_S) = M_S$, $\tan\beta(M_S) = 20$, $A_t = X_t + \mu/\tan\beta$, while all other trilinear couplings are set to zero unless otherwise stated. M_S and X_t are left as free parameters. As a notational definition, we refer to the limit $m_{U,3} = m_{Q,3} = m_{\tilde{g}} = m_{\tilde{q}} = M_S$ as the *degenerate-mass case*.

3

FIXED-ORDER APPROACH

In the FO approach, also commonly known as the Feynman-diagrammatic approach, the prediction of the mass of the CP-even neutral Higgs bosons is based on the calculation of self-energy and tadpole Feynman diagrams involving contributions from SM particles as well as their superpartners. Corrections emerging from different sectors, e.g. quantum chromodynamics (QCD) or electroweak (EW), can be incorporated order by order in couplings and, equivalently, additional loops. The Higgs mass matrix M of the CP-even states can thus be written as

$$\mathsf{M} = \mathsf{M}^{\text{tree}} - \underbrace{\begin{pmatrix} \hat{\Sigma}_{11}(p^2) & \hat{\Sigma}_{12}(p^2) \\ \hat{\Sigma}_{12}(p^2) & \hat{\Sigma}_{22}(p^2) \end{pmatrix}}_{\hat{\Sigma}(p^2)} . \tag{3.1}$$

Here, $\hat{\Sigma}_{ij}$ are understood as the renormalized self-energy contributions to the Higgs mass matrix (cf. Ref. [79], for example) and p^2 is the external momentum. As $p^2 \neq 0$ in general, we are interested in solving the pole mass equation

$$0 = \det\left\{ p^2 \delta_{ij} - \mathsf{M}^{\text{tree}}_{ij} + \operatorname{Re} \hat{\Sigma}(p^2)_{ij} \right\} \tag{3.2}$$

for p^2. Since $\hat{\Sigma}$ itself depends on p^2, Eq. (3.2) has to be solved iteratively. In the decoupling limit and considering only the real part of $\hat{\Sigma}_{ij}$, Eq. (3.2) simplifies to

$$p^2 - m_h^{2,\text{tree}} + \hat{\Sigma}_{11}(p^2) = 0 \,, \tag{3.3}$$

where $m_h^{2,\text{tree}}$ is given by Eq. (2.2) and is used as an initial value for p^2. Solving Eq. (3.3) iteratively yields an expression for the light CP-even Higgs pole mass

$$M_h^2 = m_h^{2,\text{tree}} - \hat{\Sigma}_{11}(m_h^{2,\text{tree}}) + \hat{\Sigma}'_{11}(m_h^{2,\text{tree}})\hat{\Sigma}_{11}(m_h^{2,\text{tree}}) + \dots \,, \tag{3.4}$$

where the prime indicates the derivative of the self-energy with respect to the momentum squared. The ellipsis indicates higher-order derivatives and products of self-energies. Usually, Eq. (3.2) is solved numerically until a fixed point is found with sufficient precision.

Despite the seemingly straightforwardness, the FO approach suffers from unreliable predictions if the splitting between the electroweak and the SUSY scale becomes sizable, leading to logarithms of the form $\ln(v^2/M_S^2)$ that spoil the convergence of the perturbative expansion. However, this approach is perfectly suited for SUSY scales which are of the same order as

the electroweak scale and, in addition, FO calculations are an important ingredient in the calculation of threshold corrections when using an EFT framework (cf. Chap. 4).

In this chapter, which is largely based on Refs. [47,74], we present an implementation of the three-loop corrections calculated in Refs. [15,16] into the C++ library Himalaya [47]. After a discussion how some technicalities regarding the results of Refs. [15,16] are handled in Subsect. 3.1.1, renormalization-scheme changing shifts are derived in Subsect. 3.1.2 that allow for a conversion to the commonly used $\overline{\text{DR}}'$ scheme. To provide a consistent analysis of the three-loop results within the $\overline{\text{DR}}'$ scheme, which was first done as part of this thesis, we define the required input parameters in Subsect. 3.1.3. Afterwards, in Sect. 3.2, the numerical effects including the three-loop corrections are studied by comparing to earlier results and different codes. Further, deficits of the FO approach are emphasized. One of the central aspects in Refs. [47,74] is the program Himalaya, which has been developed during this thesis. This includes the supplementary calculations to the results of Refs. [15,16] presented in this chapter. The interface to FlexibleSUSY was created in collaboration with A. Voigt.

3.1 HIGGS MASS PREDICTION AT THE THREE-LOOP LEVEL IN THE MSSM

The results for the three-loop $\mathcal{O}(y_t^4 g_3^4)$ corrections, i.e. N^{3}LO, to the Higgs mass in the MSSM have been obtained in Refs. [15,16] in a Feynman-diagrammatic calculation of the relevant one- and two-point functions with external Higgs fields in the limit of vanishing external momenta, i.e. $p^2 = 0$. The dependence of these terms on the squark and gluino masses was approximated through asymptotic expansions, assuming various hierarchies among the masses of the SUSY particles. The considered approximations are motivated by the Snowmass Points and Slopes scenarios of Refs. [80,81] and thus split into six cases:

$$\begin{aligned}
&\text{(h3)} && m_{\tilde{q}} \approx m_{\tilde{t}_1} \approx m_{\tilde{t}_2} \approx m_{\tilde{g}}\,, \\
&\text{(h4)} && m_{\tilde{q}} \gg m_{\tilde{t}_1} \approx m_{\tilde{t}_2} \approx m_{\tilde{g}}\,, \\
&\text{(h5)} && m_{\tilde{q}} \gg m_{\tilde{t}_2} \gg m_{\tilde{t}_1} \approx m_{\tilde{g}}\,, \\
&\text{(h6)} && m_{\tilde{q}} \gg m_{\tilde{t}_2} \gg m_{\tilde{g}} \gg m_{\tilde{t}_1}\,, \\
&\text{(h6b)} && m_{\tilde{q}} \approx m_{\tilde{t}_2} \approx m_{\tilde{g}} \approx m_{\tilde{t}_1}\,, \\
&\text{(h9)} && m_{\tilde{q}} \approx m_{\tilde{t}_1} \approx m_{\tilde{t}_2} \gg m_{\tilde{g}}\,.
\end{aligned} \tag{3.5}$$

Note that different expansion depths are obtained for each hierarchy, partly omitting terms of $\mathcal{O}(X_t^4)$. Recently, Ref. [48] provided a calculation of the same three-loop contributions without an expansion in different mass hierarchies. However, since these formulæ are not publicly available, our work focuses on the results of Refs. [15,16].

The results of Refs. [15,16], which we refer to as the *H3m result* in the following, are implemented in the program H3m. Using H3m requires the user to complement it by FeynHiggs [22,50–53,68,69,82] to include full one-loop and partial two-loop corrections in the

calculation of the light CP-even Higgs mass. Since `FeynHiggs` performs its calculations in the on-shell scheme and `H3m` uses a modified version of the $\overline{\text{DR}}$ scheme, higher-order effects of mixed renormalization schemes are implicitly generated during the diagonalization of the Higgs mass matrix. These terms could potentially lead to large corrections, spoiling the convergence of the perturbative series. Additionally, due to the restrictive implementation of the `H3m` result, it was not considered in state-of-the-art spectrum generators so far. In order to provide consistency of renormalization schemes, we reimplemented the `H3m` result into the library `Himalaya` and made it accessible with an interface that can be used seamlessly by spectrum generators. In the following, we describe details regarding the implementation and the involved renormalization schemes. Afterwards, we study the impact of the three-loop results using a consistent renormalization scheme and compare to results obtained by different programs.

In principle one could use the corrections of $\mathcal{O}(y_t^4 g_3^4)$ to obtain terms of $\mathcal{O}(y_b^4 g_3^4)$. However, to provide a consistent result the currently unknown corrections of $\mathcal{O}(y_t^2 y_b^2 g_3^4)$ would be needed in addition. Moreover, Ref. [47] showed that the $\mathcal{O}(y_b^4 g_3^4)$ terms are negligible compared to the $\mathcal{O}(y_t^4 g_3^4)$ corrections. Hence, we do not include terms of $\mathcal{O}(y_b^4 g_3^4)$ in our studies.

3.1.1 *Mass hierarchy selection*

A particular set of mass parameters typically matches several of the hierarchies mentioned in Eq. (3.5). Therefore, a criterion to define one of those hierarchies as the most suitable hierarchy is needed. Ref. [16] suggested a pragmatic definition, namely the comparison of the various asymptotic expansions to the exact expression at the two-loop level. The expansion which fits the exact two-loop result best is then selected. Due to instabilities of this selection, Ref. [47] extended this criterion to also include convergence properties of each hierarchy in a given parameter point (see also Ref. [83]). Combining both criteria, a smooth hierarchy selection for a large parameter space can be assured. This selection algorithm is implemented in the `Himalaya` library and summarized below.

Following Ref. [16], in a first step the Higgs pole mass M_h is calculated at the two-loop level including $\mathcal{O}(y_t^4 + y_t^4 g_3^2)$ corrections by using the result of Ref. [24] in the form of the associated `FORTRAN` code provided by the authors. We refer to this quantity as M_h^{DSZ} in what follows. Subsequently, for all hierarchies i that fit the given mass spectrum, M_h is calculated again using the expanded expressions of Ref. [16] up to the two-loop level, i.e. $\mathcal{O}(y_t^4 + y_t^4 g_3^2)$, resulting in $M_{h,i}$. The most suited hierarchy is then defined as the value of i for which the difference

$$\delta_i^{\text{2L}} = \left| M_h^{\text{DSZ}} - M_{h,i} \right| \tag{3.6}$$

is minimal. However, we found that this criterion alone causes instabilities in the hierarchy selection in regions where several hierarchies lead to similar values of δ_i^{2L}. To refine the

selection criterion we also take into account the quality of the convergence in the respective hierarchies, quantified by

$$\delta_i^{\text{conv}} = \sqrt{\sum_{j=1}^{n} \left(M_{h,i} - M_{h,i}^{(j)} \right)^2}. \tag{3.7}$$

While $M_{h,i}$ includes all available terms of the expansion in mass ratios (and mass differences), in $M_h^{(j)}$ the highest terms of the expansion for the mass ratio (and mass difference) j are dropped. We then define the *best* hierarchy to be the one which minimizes the quadratic mean of Eqs. (3.6) and (3.7),

$$\delta_i = \sqrt{\left(\delta_i^{\text{2L}}\right)^2 + \left(\delta_i^{\text{conv}}\right)^2}. \tag{3.8}$$

3.1.2 *H3m renormalization scheme and its relation to $\overline{DR}'$*

When calculating higher-order corrections, it is tempting to utilize the $\overline{\text{MS}}$ scheme since its behaviour is well understood to all orders in perturbation theory. However, shifting the dimensionality of vector bosons in supersymmetric theories and not adjusting the degrees of freedom of their corresponding superpartners will break supersymmetry explicitly. Therefore, Ref. [84] proposed to use a different regularization scheme called *dimensional reduction*. Its mathematically consistent formulation was derived in Ref. [85]. In this scheme, vector bosons are treated four-dimensionally whereas the extra degrees of freedom, emerging from the analytic continuation of the space-time dimension, are introduced as so-called *ϵ-scalars*. Complemented with modified minimal subtraction, this renormalization scheme is called $\overline{\text{DR}}$ scheme [86]. Since the ϵ-scalar is unphysical, it is appealing to set its mass, m_ϵ, to zero. Refs. [87–90] pointed out that if the mass of the ϵ-scalar is set to zero, inconsistencies arise once renormalization-group running is considered, because m_ϵ will become non-zero and contributes to the running of other parameters. Additionally, they proposed a modification of the $\overline{\text{DR}}$ scheme that introduces finite shifts in the masses of scalar sparticles. These shifts lead to a decoupling of m_ϵ from all β-functions. This modified $\overline{\text{DR}}$ scheme, denoted as $\overline{\text{DR}}'$, is most convenient for higher-order calculations in supersymmetric theories. Note, however, that it is still unproven whether the $\overline{\text{DR}}$ or the $\overline{\text{DR}}'$ scheme does preserve supersymmetry to all orders in perturbation theory. Recently, checks up to three-loop order were presented in Ref. [91] verifying that there are no ambiguities within the calculations presented in this thesis.

Following the former definitions, the renormalization scheme used in the `H3m` calculation slightly differs from the original $\overline{\text{DR}}$ scheme concerning the treatment of the ϵ-scalars. In practice, an on-schell renormalization condition for the ϵ-scalars is imposed by setting $m_\epsilon = 0$. Hence, we denote the latter renormalization scheme as the *H3m scheme*.

In order to seamlessly combine the three-loop result in the H3m scheme with existing lower-order calculations, it is necessary to convert it to the more commonly used $\overline{\text{DR}}'$ scheme, where m_ϵ completely decouples from the particle spectrum. To do that, we need to reconstruct the m_ϵ-terms in the H3m result. This can be done by noting that, up to two-loop $\mathcal{O}(y_t^4 g_3^2)$, the analytic form of the corrections to the Higgs mass are identical in the $\overline{\text{DR}}$, the $\overline{\text{DR}}'$, and the H3m scheme for $m_\epsilon = 0$.

Since the $\overline{\text{DR}}'$ result is independent of m_ϵ to all orders in perturbation theory, we can convert the known two-loop $\mathcal{O}(y_t^4 g_3^2)$ $\overline{\text{DR}}'$ expression to the $\overline{\text{DR}}$ scheme by shifting the stop masses according to Refs. [35, 90, 92]. Expanding the resulting expression to $\mathcal{O}(y_t^4 g_3^4)$ generates all m_ϵ-dependent terms up to this order in the $\overline{\text{DR}}$ scheme. From there, we can convert the stop masses and m_ϵ to the H3m scheme, using the formulæ of Ref. [16]. This generates a non-vanishing term at $\mathcal{O}(y_t^4 g_3^4)$, which is non-zero even when the on-shell condition $m_\epsilon = 0$ is applied. We computed the conversion terms for both the squared light CP-even Higgs mass and the Higgs mass matrix. For $m_\epsilon = 0$ and the squared Higgs mass, this shift reads

$$\begin{aligned}(\Delta M_h^2)_{\text{H3m}\to\overline{\text{DR}}'} = \frac{8\kappa^3 v^2 y_t^4 g_3^4 s_\beta^4}{m_{\tilde{t}_1}^2 m_{\tilde{t}_2}^2 \Delta_{12}^3}\left[-6\left(1+l_{S\tilde{g}}\right)m_{\tilde{g}}^2 + 10\left(1+l_{S\tilde{q}}\right)m_{\tilde{q}}^2 + \sum_{i=1}^{2}(1+l_{S\tilde{t}_i})m_{\tilde{t}_i}^2\right] \\ \times\left[(\Delta_{12}^3 + \Delta_{12}X_t^4)\sum_{i=1}^{2} m_{\tilde{t}_i}^2 - 2\Delta_{12}^3 X_t^2 + 4m_{\tilde{t}_1}^2 m_{\tilde{t}_2}^2 X_t^4 \ln\left(\frac{m_{\tilde{t}_2}}{m_{\tilde{t}_1}}\right)\right],\end{aligned} \tag{3.9}$$

with $l_{Sx} = \ln\left(Q^2/m_x^2\right)$. Q is the renormalization scale and $\Delta_{12} = m_{\tilde{t}_1}^2 - m_{\tilde{t}_2}^2$. For the mass matrix the shift yields

$$(\Delta \mathsf{M}_{11})_{\text{H3m}\to\overline{\text{DR}}'} = C\mu^2 X_t^2\left\{m_{\tilde{t}_1}^4 - 2m_{\tilde{t}_1}^2 m_{\tilde{t}_2}^2 \ln\left(\frac{m_{\tilde{t}_1}^2}{m_{\tilde{t}_2}^2}\right) - m_{\tilde{t}_2}^4\right\}, \tag{3.10}$$

$$\begin{aligned}(\Delta \mathsf{M}_{12})_{\text{H3m}\to\overline{\text{DR}}'} = C\mu X_t\Bigg\{ &- m_{\tilde{t}_1}^4\left(A_t X_t + 3m_{\tilde{t}_2}^2\right) + 2A_t m_{\tilde{t}_1}^2 m_{\tilde{t}_2}^2 X_t \ln\left(\frac{m_{\tilde{t}_1}^2}{m_{\tilde{t}_2}^2}\right) \\ &+ A_t m_{\tilde{t}_2}^4 X_t + m_{\tilde{t}_1}^6 + 3m_{\tilde{t}_1}^2 m_{\tilde{t}_2}^4 - m_{\tilde{t}_2}^6\Bigg\},\end{aligned} \tag{3.11}$$

$$(\Delta \mathsf{M}_{21})_{\text{H3m}\to\overline{\text{DR}}'} = (\Delta \mathsf{M}_{12})_{\text{H3m}\to\overline{\text{DR}}'}, \tag{3.12}$$

$$\begin{aligned}(\Delta \mathsf{M}_{22})_{\text{H3m}\to\overline{\text{DR}}'} = C\Bigg\{\Delta_{12}\Big[m_{\tilde{t}_1}^2\left(A_t^2 X_t^2 + 4A_t m_{\tilde{t}_2}^2 X_t - m_{\tilde{t}_2}^4\right) - m_{\tilde{t}_1}^4\left(2A_t X_t + m_{\tilde{t}_2}^2\right) \\ + \left(m_{\tilde{t}_2}^3 - A_t m_{\tilde{t}_2} X_t\right)^2 + m_{\tilde{t}_1}^6\Big] - 2A_t^2 m_{\tilde{t}_1}^2 m_{\tilde{t}_2}^2 X_t^2 \ln\left(\frac{m_{\tilde{t}_1}^2}{m_{\tilde{t}_2}^2}\right)\Bigg\},\end{aligned} \tag{3.13}$$

with

$$C = \frac{8\kappa^3 y_t^4 g_3^4 v^2 s_\beta^2}{m_{\tilde{t}_1}^2 m_{\tilde{t}_2}^2 \Delta_{12}^3}\left\{-6(l_{S\tilde{g}}+1)m_{\tilde{g}}^2 + 10(l_{S\tilde{q}}+1)m_{\tilde{q}}^2 + \sum_{i=1}^{2}(1+l_{S\tilde{t}_i})m_{\tilde{t}_i}^2\right\}. \tag{3.14}$$

The indices ij of M_{ij} imply the corresponding matrix entry (cf. Eq. (3.1)). Adding these terms to the `H3m` result provides the three-loop Higgs mass corrections in the $\overline{\text{DR}}'$ scheme. For the squared Higgs mass and Higgs mass matrix this transformation reads

$$M_h^2\Big|_{\overline{\text{DR}}'} = M_h^2\Big|_{\texttt{H3m}} + (\Delta M_h^2)_{\texttt{H3m}\to\overline{\text{DR}}'} \tag{3.15}$$

and

$$\mathsf{M}_{ij}\Big|_{\overline{\text{DR}}'} = \mathsf{M}_{ij}\Big|_{\texttt{H3m}} + (\Delta \mathsf{M}_{ij})_{\texttt{H3m}\to\overline{\text{DR}}'}\,, \tag{3.16}$$

respectively.

We checked that the resulting $\overline{\text{DR}}'$ expression is renormalization-scale independent by using the corresponding stop-mass β-functions in the $\overline{\text{DR}}'$ scheme [92].

3.1.3 *Consistent determination of the MSSM $\overline{DR}'$ parameters*

In our approach, we link the `Himalaya` library to `FlexibleSUSY`, which provides us with the required input parameters. To produce a consistent result, the values of the input parameters have to be provided at the correct perturbative order to be compatible with the genuine loop corrections. As an additional free parameter, the scale at which the parameters of the SM are converted to the MSSM has to be fixed. In order to do this, `FlexibleSUSY` determines the running $\overline{\text{DR}}'$ gauge and Yukawa couplings as well as the running vacuum expectation value of the MSSM along the lines of Ref. [79] by setting the conversion scale to the Z-boson pole mass M_Z.

The MSSM $\overline{\text{DR}}'$ gauge couplings g_1, g_2, and g_3 are given in terms of the $\overline{\text{DR}}'$ parameters $\alpha_{\text{em}}^{\text{MSSM}}(M_Z)$ and $\alpha_s^{\text{MSSM}}(M_Z)$ in the MSSM as:

$$g_1(M_Z) = \sqrt{\frac{5}{3}}\frac{\sqrt{4\pi\alpha_{\text{em}}^{\text{MSSM}}(M_Z)}}{\cos\theta_w(M_Z)}\,, \tag{3.17}$$

$$g_2(M_Z) = \frac{\sqrt{4\pi\alpha_{\text{em}}^{\text{MSSM}}(M_Z)}}{\sin\theta_w(M_Z)}\,, \tag{3.18}$$

$$g_3(M_Z) = \sqrt{4\pi\alpha_s^{\text{MSSM}}(M_Z)}\,. \tag{3.19}$$

The couplings $\alpha_{\text{em}}^{\text{MSSM}}(M_Z)$ and $\alpha_s^{\text{MSSM}}(M_Z)$ are calculated from the corresponding input parameters as

$$\alpha_{\text{em}}^{\text{MSSM}}(M_Z) = \frac{\bar{\alpha}_{\text{em}}^{\text{SM}(5)}(M_Z)}{1-\Delta\alpha_{\text{em}}(M_Z)}\,, \tag{3.20}$$

$$\alpha_s^{\text{MSSM}}(M_Z) = \frac{\bar{\alpha}_s^{\text{SM}(5)}(M_Z)}{1-\Delta\alpha_s(M_Z)}\,, \tag{3.21}$$

where the threshold corrections $\Delta\alpha_i(M_Z)$ have the form given in Eq. (B.1) and (B.2). The $\overline{\text{DR}}'$ weak mixing angle in the MSSM, θ_w, is determined at the scale M_Z from the Fermi constant G_F and the Z pole mass via the relation

$$\sin^2\theta_w \cos^2\theta_w = \frac{\pi\,\alpha_{\text{em}}^{\text{MSSM}}}{\sqrt{2}M_Z^2 G_F(1-\delta_r)}\,, \tag{3.22}$$

where

$$\delta_r = \hat{\rho}\frac{\text{Re}\,\Sigma_{W,T}(0)}{M_W^2} - \frac{\text{Re}\,\Sigma_{Z,T}(M_Z^2)}{M_Z^2} + \delta_{VB} + \delta_r^{(2)}\,, \tag{3.23}$$

$$\hat{\rho} = \frac{1}{1-\Delta\hat{\rho}}\,, \qquad \Delta\hat{\rho} = \text{Re}\left[\frac{\Sigma_{Z,T}(M_Z^2)}{\hat{\rho}\,M_Z^2} - \frac{\Sigma_{W,T}(M_W^2)}{M_W^2}\right] + \Delta\hat{\rho}^{(2)}\,. \tag{3.24}$$

Here, $\Sigma_{V,T}(p^2)$ denotes the transverse part of the $\overline{\text{DR}}'$-renormalized one-loop self-energy of the vector boson V in the MSSM. The vertex and box contributions δ_{VB}, the two-loop contributions $\delta_r^{(2)}$ as well as the corrections up to two-loop ($\Delta\hat{\rho}^{(2)}$) to the ρ parameter are taken from Ref. [79].

The $\overline{\text{DR}}'$ vacuum expectation values of the up- and down-type Higgs doublets are calculated as

$$v_u(M_Z) = \frac{2m_Z(M_Z)\sin\beta(M_Z)}{\sqrt{3/5g_1^2(M_Z)+g_2^2(M_Z)}}\,, \tag{3.25}$$

$$v_d(M_Z) = \frac{2m_Z(M_Z)\cos\beta(M_Z)}{\sqrt{3/5g_1^2(M_Z)+g_2^2(M_Z)}}\,, \tag{3.26}$$

where $\tan\beta(M_Z)$ is an input parameter and $m_Z(M_Z)$ is the Z boson $\overline{\text{DR}}'$ mass in the MSSM, which is calculated from the Z pole mass at the one-loop level as

$$m_Z^2(M_Z) = M_Z^2 + \text{Re}\,\Sigma_{Z,T}(M_Z^2)\,. \tag{3.27}$$

In order to calculate the Higgs pole mass in the $\overline{\text{DR}}'$ scheme at the three-loop level $\mathcal{O}(y_t^4 g_3^4)$, the $\overline{\text{DR}}'$ top Yukawa coupling must be extracted from the input parameter M_t at the two-loop level at $\mathcal{O}(g_3^4)$. To achieve that, we make use of the known two-loop QCD corrections to the top Yukawa coupling of Refs. [93–96], as described in the following: We calculate the $\overline{\text{DR}}'$ Yukawa coupling y_t at the scale M_Z from the $\overline{\text{DR}}'$ top mass m_t and the $\overline{\text{DR}}'$ up-type VEV v_u as

$$y_t(M_Z) = \sqrt{2}\frac{m_t(M_Z)}{v_u(M_Z)}\,, \tag{3.28}$$

where we relate the $\overline{\text{DR}}'$ top mass to the top pole mass M_t at the scale M_Z as

$$\begin{aligned} m_t(M_Z) = M_t + \operatorname{Re}\Sigma_t^S(M_t^2, M_Z) + M_t\Big[\operatorname{Re}\Sigma_t^L(M_t^2, M_Z) + \operatorname{Re}\Sigma_t^R(M_t^2, M_Z) \\ + \Delta m_t^{(1),\text{QCD}}(M_Z) + \Delta m_t^{(2),\text{QCD}}(M_Z)\Big], \end{aligned} \tag{3.29}$$

where $\Sigma_t^{S,L,R}(p^2, Q)$ denote the scalar (superscript S), and the left- and right-handed parts (L, R) of the $\overline{\text{DR}}'$ renormalized one-loop top self-energy without QCD contributions. $\Delta m_t^{(1),\text{QCD}}$ and $\Delta m_t^{(2),\text{QCD}}$ are the full one- and two-loop QCD corrections taken from Refs. [93, 94] (cf. Eq. (B.3) and (B.4)).

3.2 NUMERICAL RESULTS INCLUDING N^{3}LO QCD CORRECTIONS

`FlexibleSUSY` calculates the two CP-even Higgs pole masses M_h and M_H by solving the pole mass equation, introduced in Eq. (3.2), numerically at the momenta $p^2 = M_h^2$ and $p^2 = M_H^2$, respectively. At the one-loop level, `FlexibleSUSY` contains the full one-loop MSSM Higgs self energy and tadpole contributions, including electroweak corrections and the momentum dependence. At the two-loop level the known corrections of $\mathcal{O}(g_3^2(y_t^4 + y_b^4) + (y_t^2 + y_b^2)^3 + y_\tau^6)$ [24–27, 38] are implemented for $p^2 = 0$. For the three-loop level the terms of $\mathcal{O}(y_t^4 g_3^4)$ from the `Himalaya` package, as described in Sect. 3.1, are incorporated. They are also only known for $p^2 = 0$. All contributions are defined in the $\overline{\text{DR}}'$ scheme by default. The renormalization scale is chosen to be $Q = M_S = \sqrt{m_{\tilde{t}_1} m_{\tilde{t}_2}}$ and the $\overline{\text{DR}}'$parameters that enter Eq. (3.2) are evolved from M_Z to that scale by using the three-loop renormalization-group equations of the MSSM [97, 98]. To account for the momentum dependence while diagonalizing M, the eigenvalues for M_h and M_H are inserted iteratively into Eq. (3.2) until a fixed point for the Higgs masses is reached with sufficient precision. Note that we are only interested in M_h.

3.2.1 *Size of three-loop contributions from different sources*

The three sources affecting the Higgs pole mass at $\mathcal{O}(y_t^4 g_3^4)$ in the $\overline{\text{DR}}'$ calculation within `FlexibleSUSY+Himalaya` (`FS+H`) are

- the one-loop threshold correction of $\mathcal{O}(g_3^2)$ to the strong coupling constant,
- the two-loop threshold correction of $\mathcal{O}(g_3^4)$ to the top Yukawa coupling,
- the genuine three-loop contribution to the Higgs mass matrix.

In Fig. 1, the impact of these three sources on the Higgs pole mass is shown relative to the two-loop calculation without these three corrections. The left panel shows the impact as a function of the SUSY scale M_S, and the right panel as a function of the relative stop mixing parameter x_t for the scenario defined in Chap. 2. We use the two-loop ingredients

as reference point, i.e. g_3 at tree level (g_3^{0L}), y_t at one loop (y_t^{1L}), and the genuine two loop corrections to M_h (M_h^{2L}) as described above, and replace each of them separately by the ingredients required at three-loop accuracy.

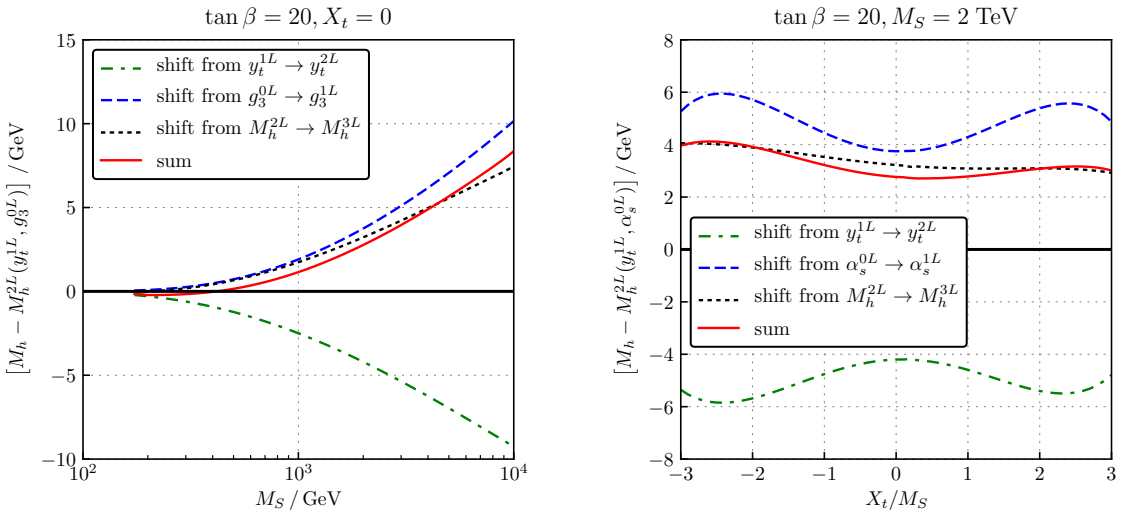

Figure 1: *Impact of different three-loop contributions on the Higgs pole mass M_h. In the left panel we show the shift in the Higgs pole mass with respect to $M_h^{2L}(y_t^{1L}, g_3^{0L})$ as a function of the SUSY scale. In the right panel we vary the relative stop mixing parameter x_t.*

First, we observe that the inclusion of the one-loop threshold correction to g_3, Eq. (B.2), (blue dashed line) leads to a significant positive shift of the Higgs pole mass of around $+2.5\,\text{GeV}$ for $M_S \approx 1\,\text{TeV}$. For larger SUSY scales the shift increases logarithmically as is to be expected from the logarithmic terms on the r.h.s. of Eq. (B.2). The inclusion of the full two-loop QCD corrections to y_t (green dash-dotted line) leads to a shift of similar magnitude, but in the opposite direction. Thus, there is a significant cancellation between the three-loop contributions from the one-loop threshold correction to g_3 and the two-loop QCD corrections to y_t. The genuine three-loop contribution to the Higgs pole mass (black dotted line) is again positive and around $+2\,\text{GeV}$ for $M_S \approx 1\,\text{TeV}$. This is consistent with the findings of Ref. [16]. As a result, the sum of these three three-loop effects (red solid line) leads to a net positive shift of the Higgs mass relative to the two-loop result without all these corrections.

The size of the individual three-loop contributions depends on the relative stop mixing parameter x_t, as can be seen from the right panel of Fig. 1. Between minimal ($x_t = 0$) and maximal stop mixing ($x_t \approx \pm\sqrt{6}$) the size of the individual three-loop contributions changes by 1–2 GeV. For maximal (minimal) mixing, their impact is maximal (minimal). The direction of the shift is independent of x_t.

Note that the nominal two-loop result of the original `FlexibleSUSY` calculation includes by default the one-loop threshold correction to g_3 and the SM QCD two-loop contributions to the top Yukawa coupling [58, 71]. This means that the two-loop Higgs mass as evaluated by the original `FlexibleSUSY` already incorporates partial three-loop contributions. Hence, the

two-loop result of the original FlexibleSUSY does not correspond to the zero-line in Fig. 1, but is rather close to the blue dashed line. This implies that, compared to the two-loop result of the original FlexibleSUSY, the effect of the remaining $\mathcal{O}(y_t^4 g_3^4)$ contributions in the Higgs mass prediction is *negative*.

3.2.2 *Scale dependence of the Higgs pole mass*

To estimate the size of the missing higher-order contributions, Fig. 2 shows the renormalization scale dependence of the one-, two-, and three-loop Higgs pole masses for the scenario defined in Chap. 2 at $x_t = 0$ as a function of M_S. The one- and two-loop calculations

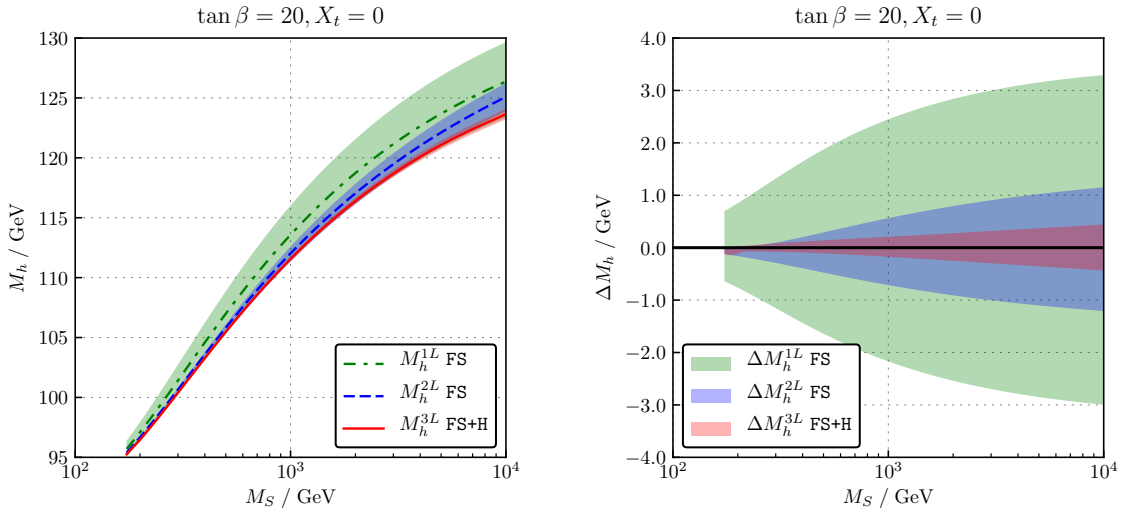

Figure 2: *Variation of the Higgs pole mass when the renormalization scale is varied by a factor two around the scale at which M_h is calculated.*

correspond to the original FlexibleSUSY calculation. In the one-loop calculation the threshold corrections to g_3 and y_t are set to zero, and in the two-loop calculation the one-loop threshold corrections to g_3 and the two-loop QCD corrections to y_t are taken into account. The three-loop result of FlexibleSUSY+Himalaya includes all three-loop contributions at $\mathcal{O}(y_t^4 g_3^4)$ as discussed in the previous subsection, i.e. the one-loop threshold correction to g_3, the full two-loop QCD corrections to y_t, and the genuine three-loop correction to the Higgs pole mass from Himalaya. The bands show the corresponding variation of the Higgs pole mass when the renormalization scale is varied using the three-loop renormalization-group equations [97–103] for all parameters except for the vacuum expectation values, where the β-functions are known only up to the two-loop level [104, 105]. In FlexibleSUSY and FlexibleSUSY+Himalaya, the renormalizaion scale is varied in the full MSSM within the interval $[M_S/2, 2M_S]$. The plot shows that the successive inclusion of higher-order corrections reduces the scale dependence, as expected. In particular, the three-loop corrections to the Higgs mass reduce the scale dependence by around a factor two, compared to the two-loop

calculation. Note that the variation of the renormalization scale only serves as an indicator of the theoretical uncertainty due to missing higher-order effects.

3.2.3 *Comparison to other results*

In this section, we compare the results obtained with `FlexibleSUSY+Himalaya` to different MSSM spectrum generators employing the fixed-order approach. We choose the same scenario as in Subsect. 3.2.1, where the lightest CP-even Higgs pole mass is calculated at the scale $Q = M_S = \sqrt{m_{\tilde{t}_1} m_{\tilde{t}_2}}$. The results are shown in Figs. 3–4 and compared against `FlexibleSUSY` and `FeynHiggs`. The blue dashed line corresponds to `FlexibleSUSY 2.3.0` at the two-loop level, which coincides with `SOFTSUSY 3.5.1` [54,106] by construction. The green dash-dotted line shows the Higgs mass prediction using `FeynHiggs 2.14.3 (FH)`, which employs the on-shell scheme, when disabling the option of large logarithms resummation [22, 50–53, 68].[1] `FeynHiggs 2.14.3` includes the two-loop contributions of $\mathcal{O}(g_3^2(y_t^4 + y_b^4) + (y_t^2 + y_b^2)^3)$.

We consider Fig. 3 first. The left panel shows the Higgs mass prediction as a function of M_S according to the two codes discussed above, together with the `FlexibleSUSY+Himalaya` result (solid red). The stop mixing parameter X_t is set to zero. The right panel shows the difference of these curves to the latter.

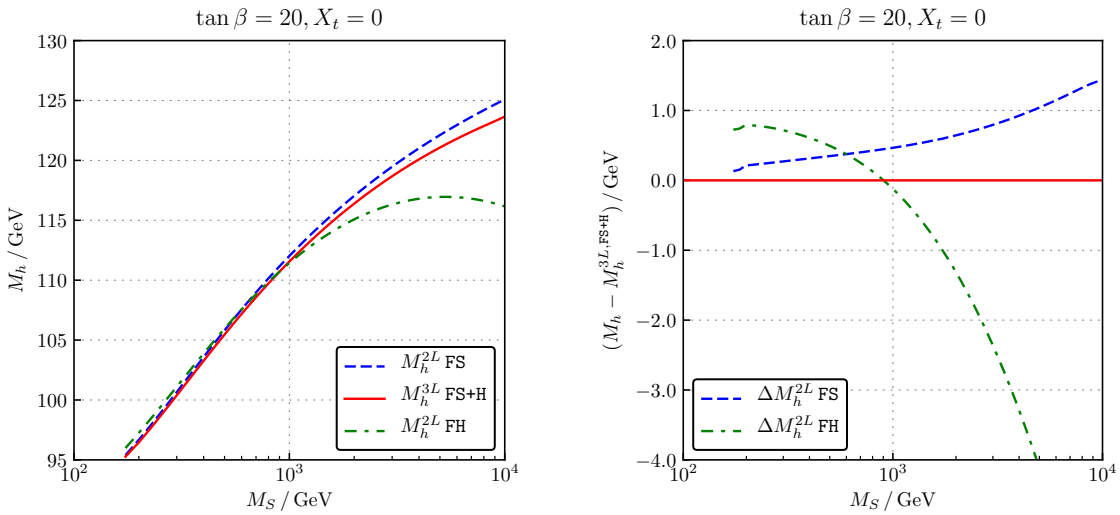

Figure 3: *Comparison of Higgs mass predictions between two- and three-loop fixed-order programs as a function of the SUSY scale for the absolute Higgs pole mass (left) and the difference w.r.t. the three-loop calculation (right).*

The effect of the three-loop $\mathcal{O}(y_t^4 g_3^4)$ terms on the fixed-order result is negative compared to the original `FlexibleSUSY` calculation, as discussed in Subsect. 3.2.1, and amounts to a few

1 We use the SLHA input interface of `FeynHiggs`, which performs a conversion of the $\overline{\text{DR}}'$ input parameters to the on-shell scheme. Resummation is disabled, as it would lead to an inconsistent result in combination with the $\overline{\text{DR}}'$ to on-shell conversion of `FeynHiggs` [69]. We call `FeynHiggs` with the flags 42420110.

hundred MeV up to regions of $M_S = 1\,\text{TeV}$. In addition, the M_S dependence and predicted Higgs mass are comparable among all three codes up to $M_S = 1\,\text{TeV}$. At scales above 1 TeV, the result obtained with `FeynHiggs` starts to deviate from the $\overline{\text{DR}}'$ calculations. At those SUSY scales, the fixed-order approach suffers from large logarithmic contributions due to sizable mass splittings, which spoil the perturbative convergence unless higher logarithmic orders are included. Note that the behavior of the $\overline{\text{DR}}'$ results in the few-TeV region is accidental and based on implicit higher-order logarithms, as shown in Ref. [71], and one would expect a similar trend as for the `FeynHiggs` result in principle.

Fig. 4 shows the three-loop effects as a function of X_t with $M_S = 2\,\text{TeV}$. The figure shows that, for $|X_t| \lesssim 3M_S$, the qualitative features of the discussion above are mostly independent of the mixing parameter, whereupon the quantitative differences between the fixed-order results are typically larger for non-zero stop mixing. Additionally, there is an interesting feature of the $\overline{\text{DR}}'$ codes, which suffer from tachyonic states introduced by positive values of X_t and large scale splittings between v and M_S. However, this can be circumvented by inserting the absolute values of the tachyonic running masses into the loop corrections within `FlexibleSUSY`. The reason for this behaviour is discussed in Subsect. 3.2.4 in more detail.

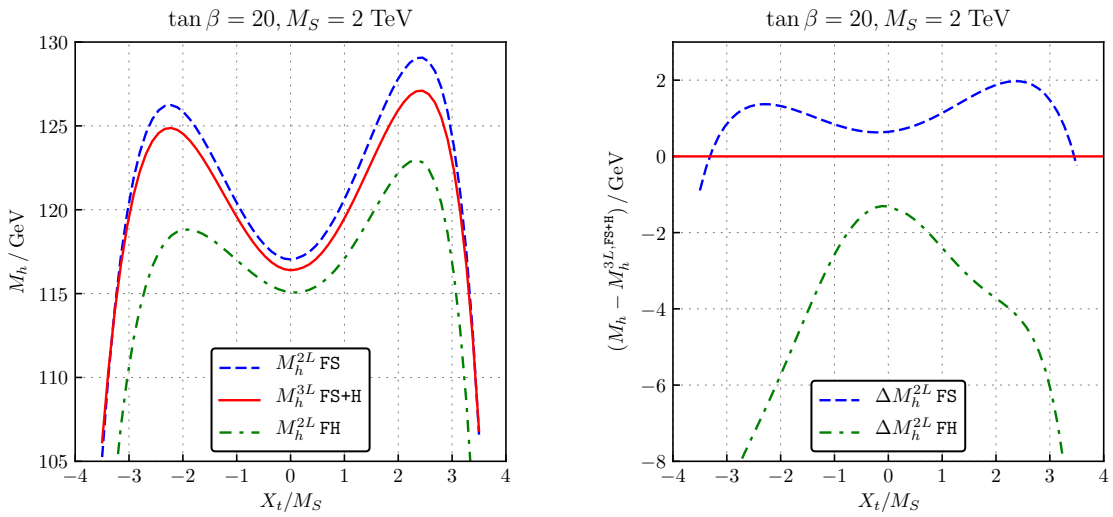

Figure 4: *Comparison of Higgs mass predictions between two- and three-loop fixed-order programs as a function of the relative stop mixing parameter x_t for the absolute Higgs pole mass (left) and the difference w.r.t. the three-loop calculation (right).*

As the three-loop corrections were originally implemented in the `H3m` code, we now turn to a comparison of our `FlexibleSUSY+Himalaya` implementation to `H3m`. We checked that our implementation of the $\mathcal{O}(y_t^4)$ and $\mathcal{O}(y_t^4 g_3^2)$ terms in `Himalaya` leads to the same numerical results as in `H3m` if the same set of $\overline{\text{DR}}'$ parameters is used as input. Since the $\mathcal{O}(y_t^4 g_3^4)$ terms of `Himalaya` are derived from their implementation in `H3m`, they also result in the same numerical value if the same set of input parameters is given *and* the same mass hierarchy is selected. But since `Himalaya` has a slightly more sophisticated way of choosing this hierarchy

(see Subsect. 3.1.1), its numerical $\mathcal{O}(y_t^4 g_3^4)$ contribution does occasionally differ slightly from the one of H3m. Note that recently a different calculation of the three-loop $\mathcal{O}(y_t^4 g_3^4)$ corrections was presented in Ref. [48]. Since their result is not publicly available, we cannot compare to those. However, Ref. [48] claims that combining their new calculation with FeynHiggs at the two-loop level leads to similar numerical values of the light CP-even Higgs mass as obtained by H3m.

In Fig. 5 we compare our results to the three-loop calculation presented in Ref. [107], assuming the input parameters for the *heavy sfermions* scenario defined in detail in the example directory of Ref. [108]. In the left panel the blue circles show the H3m result, including

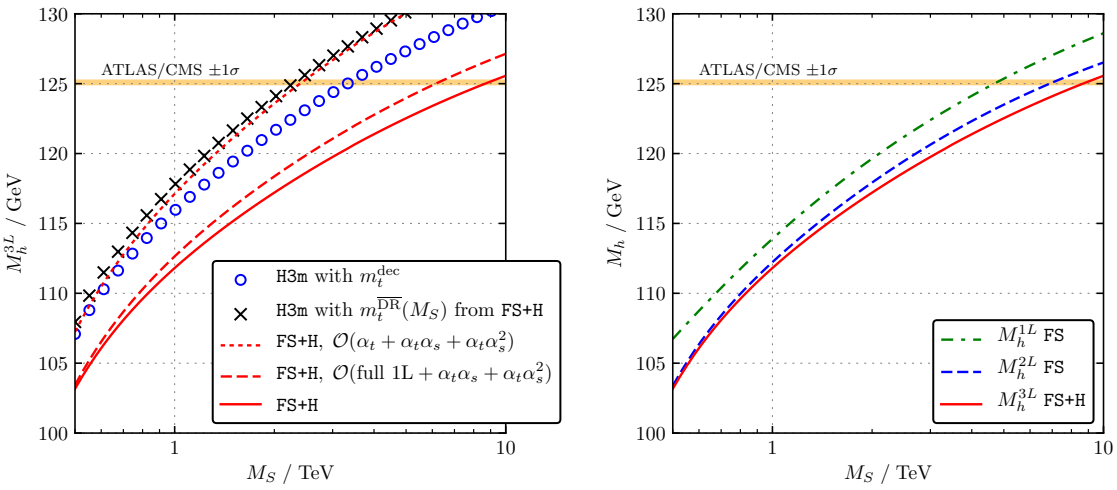

Figure 5: *Comparison of the lightest Higgs pole mass calculated at the one-, two-, and three-loop level with* FlexibleSUSY *and* FlexibleSUSY+Himalaya *as a function of the SUSY scale for the heavy sfermions scenario of Ref. [107]. These plots are taken from Ref. [47].*

only the terms of $\mathcal{O}(y_t^4(1 + g_3^2 + g_3^4))$, where the MSSM $\overline{\rm DR}'$ top mass is calculated using the *running and decoupling* procedure described in Ref. [107]. The black crosses show the same result, except that the $\overline{\rm DR}'$ top mass at the SUSY scale is taken from the spectrum generator FlexibleSUSY+Himalaya. We can reproduce the latter result with FlexibleSUSY+Himalaya if we take the same terms into account, i.e. $\mathcal{O}(y_t^4(1 + g_3^2 + g_3^4))$, see the dotted red line in Fig. 5. The small differences between the two results are due to the fact that H3m works with on-shell electroweak parameters, while FlexibleSUSY+Himalaya uses $\overline{\rm DR}'$ parameters. The inclusion of all one-loop contributions to M_h and the momentum iteration reduces the Higgs mass by 4–6 GeV, as shown by the red dashed line. Including all two- and three-loop corrections which are available in FlexibleSUSY+Himalaya, i.e. $\mathcal{O}(g_3^2(y_t^4 + y_b^4) + (y_t^2 + y_b^2)^3 + y_\tau^6 + y_t^4 g_3^4)$, further reduces the Higgs mass by up to 2 GeV, as shown by the red solid line. The right panel of Fig. 5 shows again our one-, two-, and three-loop predictions obtained with FlexibleSUSY and FlexibleSUSY+Himalaya. Similar to Fig. 3, we observe that the higher-order terms lead to a lower predicted Higgs mass.

As a final study, we compare the results obtained with `FlexibleSUSY+Himalaya` to the ones presented in Figure 1 of Ref. [109]. Our results are shown in Fig. 6. As not all parameters

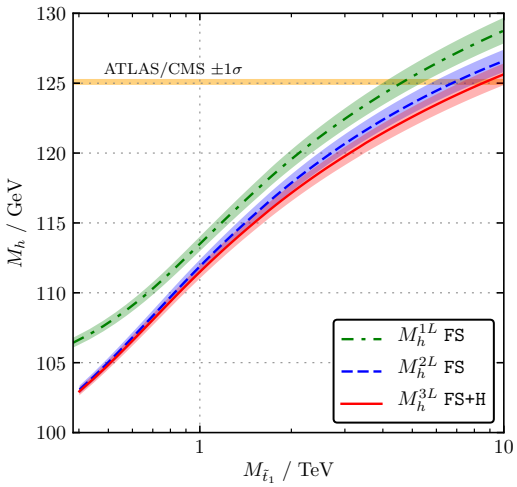

Figure 6: *Comparison of the lightest Higgs pole mass calculated at the one-, two-, and three-loop level with `FlexibleSUSY` and `FlexibleSUSY+Himalaya` as a function of the lightest stop pole mass for the benchmark point of Figure 1 of Ref. [109]. This plot is taken from Ref. [47].*

in Ref. [109] are fully defined, we need to specify a value for m_A and the sfermion mixing parameters other than X_t. Hence, we set $m_A(M_S) = M_S$, with $Q = M_S = \sqrt{m_{\tilde{t}_1} m_{\tilde{t}_2}}$, $x_t(M_S) = 0$, $\mu(M_S) = 200\,\text{GeV}$, and all remaining trilinear couplings are selected to be zero. The soft-breaking mass parameters of the left- and right-handed stops are set equal at the SUSY scale, i.e. $m_{Q,3}(M_S) = m_{U,3}(M_S)$, whereas all other soft-breaking sfermion mass parameters are set to $m_{\tilde{f}}(M_S) = m_{Q/U,3}(M_S) + 1\,\text{TeV}$. The gaugino mass parameters are set to $M_1(M_S) = M_2(M_S) = m_{\tilde{g}}(M_S) = 1.5\,\text{TeV}$. Note that the bands around the calculated Higgs mass values in Fig. 6 show the parametric uncertainty from $M_t = (173.34 \pm 0.98)\,\text{GeV}$ [110] and $\tilde{\alpha}_s^{\text{SM}(5)}(M_Z) = 0.1184 \pm 0.0007$ [111]. Again, we observe a reduction of M_h towards higher loop order, thus leading to the opposite conclusion of a heavy SUSY spectrum in this scenario, given the measured value for the Higgs mass as in Eq. (2.1) (cf. Figure 1 of Ref. [109]).

3.2.4 *Tachyonic Higgs bosons*

As observed in the previous subsection, in the fixed-order calculation the $\overline{\text{DR}}'$ masses of the heavy CP-even, the CP-odd, and the charged Higgs bosons can become tachyonic at the scale $Q = M_Z$ for $x_t \gtrsim 0$. The origin of this behavior is the $B\mu$ parameter, which becomes negative when performing renormalization-group running to $Q = M_Z$, as shown in the left panel of Fig. 7. In our scenario, the value of $B\mu$ is fixed at the SUSY scale by the $\overline{\text{DR}}'$ CP-odd

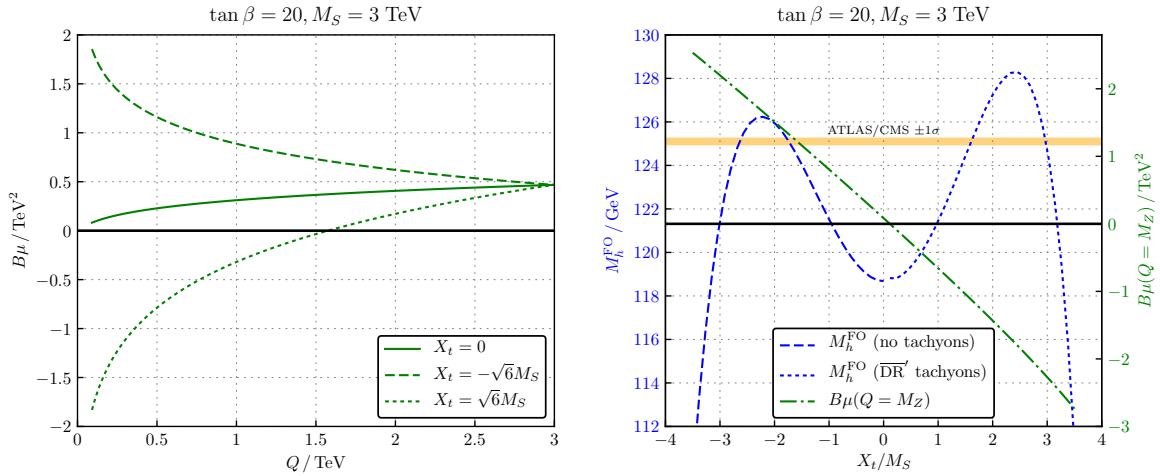

Figure 7: *Left panel: Renormalization-group running of $B\mu(Q)$ for different values of X_t. Right panel: Three-loop fixed-order Higgs pole mass (blue lines) and $B\mu(Q = M_Z)$ as a function of x_t (green dash-dotted line). These plots are taken from Ref. [74].*

Higgs mass $m_A(M_S)$ to

$$B\mu(M_S) = \frac{1}{2}\sin[2\beta(M_S)]\, m_A^2(M_S) \approx 0.05 M_S^2\,, \tag{3.30}$$

where we have set $\tan\beta(M_S) = 20$ and $m_A^2(M_S) = M_S^2$ in the last step. For such a large value of $\tan\beta$, the one-loop β-function of the $B\mu$ parameter is approximately given by

$$\beta_{B\mu} \approx 3\kappa y_t^2\,(B\mu + 2\mu A_t) \approx 3\kappa y_t^2\,(0.05 + 2x_t)\, M_S^2\,. \tag{3.31}$$

From Eq. (3.31) it follows that $\beta_{B\mu}$ is negative for $x_t < -0.025$. Hence, $B\mu$ increases during the renormalization-group running from M_S down to M_Z, which is illustrated by the green dashed line in the left panel of Fig. 7. However, if $x_t > -0.025$ $\beta_{B\mu}$ is positive so that $B\mu$ decreases when running to M_Z and changes sign at some low scale Q_{tach}, see green dotted line. The value of the scale Q_{tach} can be larger than M_Z if x_t and/or M_S are large enough, for example for $x_t > 0$ and $M_S \gtrsim 3\,\text{TeV}$. When this happens, the $\overline{\text{DR}}'$ masses of the heavy CP-even, the CP-odd, and the charged Higgs bosons are tachyonic at $Q = M_Z$, because

$$m_H^2(M_Z) \approx m_{H^\pm}^2(M_Z) \approx m_A^2(M_Z) = \frac{2B\mu(M_Z)}{\sin[2\beta(M_Z)]} < 0\,. \tag{3.32}$$

In the right panel of Fig. 7 the value of $B\mu(M_Z)$ is shown as a function of x_t as green dash-dotted line for the scenario with $\tan\beta = 20$ and $M_S = 3\,\text{TeV}$. The value for M_S is increased compared to our other studies for better illustration. In accordance with the estimate above, $B\mu(M_Z)$ is in fact negative for positive values of x_t, and the fixed-order Higgs mass calculation (see blue dashed/dotted lines) involves tachyonic $\overline{\text{DR}}'$ masses at the electroweak scale.

In some spectrum generators, the occurrence of heavy Higgs tachyons is bypassed by using the pole masses of the heavy Higgs boson masses in the loop calculations at the low scale instead of the $\overline{\text{DR}}'$ masses. In `FlexibleSUSY`, on the other hand, an error is flagged by default if $\overline{\text{DR}}'$ tachyons appear at any scale. Optionally, `FlexibleSUSY` uses the absolute values of the tachyonic masses in the loop integrals, which is done for all fixed-order calculations in this thesis when $x_t > 0$.

In general, the occurrence of these tachyonic states due to higher-order effects appears to make the approach proposed in Ref. [79] of matching SM and MSSM parameters at the scale M_Z questionable. For SUSY scales above the TeV scale it might thus be advisable to perform the matching at a larger scale to avoid tachyonic states. To our knowledge, this program has not been pursued in all generality up to now (see Ref. [107], however). For very large SUSY scales, the fixed-order approach is bound to fail anyway due to large logarithmic contributions as encountered in Subsect. 3.2.3.

3.3 CONCLUSIONS

In this chapter we have presented a consistent inclusion of the $\mathcal{O}(y_t^4 g_3^4)$ corrections to the light CP-even Higgs mass in the MSSM using the $\overline{\text{DR}}'$ scheme. We reimplemented these contributions including renormalization-scheme changing shifts in the `Himalaya` library to make them accessible to state-of-the-art spectrum generators. Including all relevant three-loop contributions of $\mathcal{O}(y_t^4 g_3^4)$, the mass of the light CP-even Higgs gets negatively shifted by approximately 1 GeV compared to a two-loop $\overline{\text{DR}}'$ calculation. The genuine three-loop corrections lead to an overall positive shift, whereas the two-loop threshold correction in the top Yukawa coupling leads to a reduction of the Higgs mass prediction by about 2 GeV, depending on the value of the stop masses and stop mixing. To indicate the remaining theory uncertainty due to higher-order effects, we have varied the renormalization scale by a factor of two. The results show that the inclusion of the three-loop contributions reduces the scale uncertainty of the Higgs mass by around a factor of two. Thus, the inclusion of the three-loop terms implemented in the `Himalaya` library leads to an overall improvement compared to a two-loop prediction.

For SUSY masses above the TeV scale the fixed-order approach suffers from large logarithmic contributions. Furthermore, such sizable scale splittings lead to running tachyonic masses in the Higgs sector of the MSSM for positive values of X_t, when following the prescription of [79]. To obtain a prediction of the light CP-even Higgs mass, which is comparable to the measurement of 125 GeV [2, 3, 17, 18], SUSY spectra in the TeV range are required, however. This observation is in accordance with the literature [60, 62, 64, 68–70]. Therefore, we will focus on different approaches in the next chapters, which directly address the issues of the fixed-order approach for large scale splittings between v and M_S. Additionally, we will apply proper uncertainty estimates to quantitatively compare the validity in different parameter regions of these methods.

4

EFFECTIVE-FIELD-THEORY APPROACH

Besides the FO approach, one can also employ EFT methods to calculate the SM-like Higgs boson mass in the MSSM. One of their benefits is that these techniques allow the resummation of large logarithmic contributions. These logarithms are only taken into account up to a specific order when evaluating the Higgs mass in the FO approach. However, without including higher-dimensional operators in the effective Lagrangian, contributions that are suppressed by the heavy scale, i.e. terms of $\mathcal{O}(v^2/M_S^2)$, are not captured. The basic idea is thus to introduce the SM as the low-energy EFT of the MSSM. Therefore, the SUSY particles are integrated out from the full theory at specific mass scales. In the simplest case, which we are interested in, all SUSY particles are chosen to have the mass $M_S = \sqrt{m_{\tilde{t}_1} m_{\tilde{t}_2}}$. The SM Higgs self-coupling $\bar{\lambda}$ is determined at M_S by applying relations that translate the SM to the MSSM. That is

$$\bar{\lambda} = \frac{(g^2 + g'^2)}{4} c_{2\beta}^2 + \Delta\lambda \,, \tag{4.1}$$

where $\Delta\lambda$ summarizes generic higher-order corrections to $\bar{\lambda}$ which are usually denoted as threshold corrections. The logarithms occurring in $\bar{\lambda}$ are resummed by evolving the Higgs self-coupling between the low- and high-energy scale, using renormalization-group equations. As several SM parameters are involved in this running, the corresponding system of coupled differential equations is usually solved numerically with boundary values at the scales M_t and M_S. Afterwards, the mass of the SM Higgs can be calculated as

$$M_h^2 = \bar{\lambda} \bar{v}^2 \,. \tag{4.2}$$

The aforementioned approach has already been studied up to the two-loop level in Refs. [60, 61, 63–66]. The first three-loop study has been provided in Ref. [62], which also includes the calculation of the three-loop threshold correction to the Higgs self-coupling including $\mathcal{O}(y_t^4 g_3^4)$, as part of this thesis.

We start this chapter, which is largely based on Ref. [62], by introducing the deficits of the FO approach concerning large mass splittings and the benefits of the EFT approach in such scenarios more formally in Sect. 4.1. Afterwards, in Sect. 4.2, we derive a third approach, which can be interpreted as the perturbative version of the EFT approach, and summarize the ingredients required for N^{3}LL resummation. In Sect. 4.3, we derive the threshold corrections to the Higgs self-coupling at the three-loop level employing the results of Refs. [15, 16]. Finally, numerical studies of the EFT approach including N^{3}LL resummation are presented and compared to FO calculations in Sect. 4.4. D. Ochoa provided the building blocks of the

calculation presented in this chapter, which were revised in the course of this thesis. As a central result of Ref. [62], the latter ingredients were combined with the `H3m` result and implemented into `Himalaya` in order to perform the studies presented in Ref. [62] as part of this thesis. The numerical studies were performed together with R. V. Harlander and A. Voigt.

4.1 RENORMALIZATION-GROUP IMPROVEMENT

Before we turn to an improved treatment of large logarithms in Higgs mass calculations in the MSSM, we describe the explicit problem of the fixed-order approach concerning large scale splittings, which was already illustrated in Subsect. 3.2.3, more formally. The calculational formalism and notational details are introduced, in addition. Note that we only focus on contributions with powers of y_t and g_3.

In the Standard Model, the pole mass of the Higgs boson can be expressed as a series expansion in terms of the SM couplings and logarithms. The dominant terms in the expansion are those that involve the strong and the top Yukawa coupling. In the following, we consider only corrections to the tree-level Higgs mass of the form $\mathcal{O}(\bar{g}_t^4 \bar{g}_3^{2n})$ with $n \geq 0$, in which case the pole mass of the Higgs boson can be expressed in terms of $\overline{\text{MS}}$ parameters as

$$M_h^2 = \bar{v}^2(Q_t) \left[\bar{\lambda}(Q_t) + \kappa \bar{g}_t^4(Q_t) \sum_{n=0}^{\infty} \sum_{p=0}^{n+1} \kappa^n \bar{g}_3^{2n}(Q_t) c_{\text{SM}}^{(n,p)} \bar{l}_{\mu t}^p \right], \tag{4.3}$$

where

$$\bar{l}_{\mu t} = \ln \frac{Q_t^2}{\bar{m}_t^2}, \quad \bar{m}_t^2 = \frac{\bar{g}_t^2 \bar{v}^2}{2}, \tag{4.4}$$

with Q_t being the renormalization scale. The $c_{\text{SM}}^{(n,p)}$ are pure numbers. Up to three-loop order ($n = 2$), the non-logarithmic coefficients read [43, 112, 113]

$$\begin{aligned} c_{\text{SM}}^{(0,0)} &= c_{\text{SM}}^{(1,0)} = 0, \\ c_{\text{SM}}^{(2,0)} &= -\frac{1888}{9} + 160\zeta_3 + \frac{7424}{45}\zeta_2^2 - \frac{1024}{3}\text{Li}_4\left(\frac{1}{2}\right) - \frac{512}{9}\text{Li}_2^2\left(\frac{1}{2}\right) - \frac{1024}{9}\text{Li}_2\left(\frac{1}{2}\right)\zeta_2, \end{aligned} \tag{4.5}$$

where

$$\begin{aligned} \zeta_2 &= \frac{\pi^2}{6} = 1.64493\ldots, \qquad \zeta_3 = 1.20206\ldots, \\ \text{Li}_2\left(\frac{1}{2}\right) &= 0.582241\ldots, \qquad \text{Li}_4\left(\frac{1}{2}\right) = 0.517479\ldots. \end{aligned} \tag{4.6}$$

The logarithmic coefficients ($p \neq 0$) can be obtained from the renormalization-group invariance of M_h^2 and the RGEs of the parameters,

$$Q\frac{\mathrm{d}}{\mathrm{d}Q}\bar{x}_i(Q) = \beta_{\bar{x}_i}(\bar{X}(Q))\,, \tag{4.7}$$

with $\bar{x}_i \in \bar{X}$ and Q being an arbitrary scale. The terms in the SM β-functions, which are relevant for our discussion, read [43]

$$\begin{aligned}
\beta_{\bar{g}_3} &= -7\kappa\bar{g}_3^3 - 26\kappa^2\bar{g}_3^5 + \mathcal{O}(\kappa^3)\,,\\
\beta_{\bar{g}_t} &= -\bar{g}_t\left[8\kappa\bar{g}_3^2 + 108\kappa^2\bar{g}_3^4 - \left(640\zeta_3 - \frac{4166}{3}\right)\kappa^3\bar{g}_3^6 + \mathcal{O}(\kappa^4)\right]\,,\\
\beta_{\bar{\lambda}} &= -\kappa\bar{g}_t^4\left[12 + 64\kappa\bar{g}_3^2 + 8\left(\frac{133}{3} - 16\zeta_3\right)\kappa^2\bar{g}_3^4 - 16616.3\kappa^3\bar{g}_3^6 + \mathcal{O}(\kappa^4)\right]\,.
\end{aligned} \tag{4.8}$$

In the MSSM one can write an analogous expression for the light CP-even Higgs boson mass in terms of the MSSM parameters Y. Neglecting sub-leading terms of $\mathcal{O}(v^2/M_S^2)$, one obtains an expansion in the decoupling limit, which reads

$$M_h^2 = M_Z^2\cos^2 2\beta + \kappa v^2(Q_t)y_t^4(Q_t)s_\beta^4\sum_{n=0}^{\infty}\sum_{p=0}^{n+1}\kappa^n g_3^{2n}(Q_t)c_{\mathrm{MSSM}}^{(n,p)}(Y(Q_t))\,l_{\mu t}^p\,, \tag{4.9}$$

with

$$l_{\mu t} = \ln\frac{Q_t^2}{m_t^2}\,,\quad m_t^2 = \frac{y_t^2 v_u^2}{2}\,. \tag{4.10}$$

The coefficients $c_{\mathrm{MSSM}}^{(n,p)}$ have been calculated analytically through $n = 1$ and can be extracted from Refs. [24, 35–37]. The result for $n = 2$ is contained in the `H3m` result by Ref. [15, 16], which was calculated neglecting contributions of $\mathcal{O}(v^2/M_S^2)$, in terms of mass hierarchies. The coefficients $c_{\mathrm{MSSM}}^{(n,p)}$ contain logarithmic contributions of the form $l_{tS} \equiv \ln(m_t/M_S)$, which spoil the convergence properties of Eq. (4.9) if $M_S \gg m_t$ regardless of the choice of Q_t. These type of logarithms are called *large logarithms* when a sizable scale splitting between the SM and its superpartners is apparent. The impact of these logarithms on M_h is shown in the previous chapter explicitly, for example. Note that one usually evolves the running MSSM parameters perturbatively in addition, see, e.g., Ref. [79]. However, the further usage of RGEs does not change the discussion about the problems of a fixed-order calculation for large scale splittings introduced above.

In a fixed-order calculation, the perturbative expansion is truncated at finite order in κ. Keeping terms through order κ^N, we denote this result as

$$M_{h,\mathrm{FO},N}^2(Q_t)\,. \tag{4.11}$$

Eq. (4.11) with $N = 3$ is essential for the extraction of the three-loop correction of $\bar{\lambda}$ as shown in Sect. 4.3.

In addition to the fixed-order approach there exists a different technique called EFT approach [63]. The idea of the EFT calculation consists of two steps. First, heavy (i.e. SUSY) particles are integrated out and are thus decoupled from the SM. As a result, one obtains relations between the parameters of the effective theory (the SM) and the full theory (the MSSM) of the form

$$\bar{x}_i(Q) = f_i(Y(Q), Q)\,. \tag{4.12}$$

In particular, one obtains a relation between $\bar{\lambda}$ and the MSSM parameters, which means that the Higgs mass in the SM, given by Eq. (4.3), is fixed in terms of the parameters Y. The f_i in Eq. (4.12) are known as perturbative expansions, neglecting terms of $\mathcal{O}(v^2/M_S^2)$. They depend explicitly on the renormalization scale Q_S in the form of $\ln(Q_S/M_S)$. Therefore, if Eq. (4.12) is employed at the scale $Q_S \sim M_S$, no large logarithms appear in the matching. For our purpose, the relevant threshold corrections of Eq. (4.12) take the form

$$\begin{aligned}
\bar{\lambda} &= \frac{M_Z^2}{v^2}\cos^2 2\beta + \kappa y_t^4 s_\beta^4 (\Delta\lambda)_{y_t^4} + \kappa^2 y_t^4 g_3^2 s_\beta^4 (\Delta\lambda)_{y_t^4 g_3^2} + \kappa^3 y_t^4 g_3^4 s_\beta^4 (\Delta\lambda)_{y_t^4 g_3^4} + \mathcal{O}(\kappa^4)\,,\\
\bar{g}_3 &= g_3\left(1 + \kappa g_3^2 (\Delta g_3)_{g_3^2} + \kappa^2 g_3^4 (\Delta g_3)_{g_3^4} + \mathcal{O}(\kappa^4)\right)\,,\\
\bar{g}_t &= y_t s_\beta\left(1 + \kappa g_3^2 (\Delta y_t)_{g_3^2} + \kappa^2 g_3^4 (\Delta y_t)_{g_3^4} + \mathcal{O}(\kappa^4)\right)\,,\\
\bar{v} &= v + \mathcal{O}(\kappa)\,,
\end{aligned} \tag{4.13}$$

where the perturbative coefficients (Δy_i) can be found in Refs. [62, 64, 93, 94]. Explicit expressions for these threshold corrections are given in Subsect. 4.3.2 for the degenerate-mass case. Their dependence on the renormalization scale Q, indicated in Eq. (4.12), is suppressed here.

Secondly, we apply RGEs to resum logarithmic contributions. Therefore, it is convenient to introduce two scales as boundary conditions, Q_S and Q_t, which are chosen such that large logarithms do not occur. Starting with numerical values of $Y(Q_S \sim M_S)$ obtained by a spectrum generator, Eq. (4.12) is used to provide numerical values for the $\overline{\text{MS}}$ SM parameters $\bar{x}_i(Q_S)$. Afterwards, one solves the SM $\overline{\text{MS}}$ RGEs of Eq. (4.7) numerically to evolve the $\bar{x}_i(Q_S)$ down to $Q_t \sim M_t$. In solving the RGEs numerically, one effectively resums large logarithms of the form l_{tS}. This is in contrast to the fixed-order calculation, where these large logarithms appear explicitly in M_h^2 up to a fixed order. The $\bar{x}_i(Q_t)$ are then inserted into Eq. (4.3) in order to calculate M_h^2 up to terms of $\mathcal{O}(v^2/M_S^2)$. We denote this result as

$$M_{h,\text{EFT}}^2(Q_t, Q_S)\,. \tag{4.14}$$

The only fixed-order logarithms involved in this result are of the form $\ln(Q_S/M_S)$ from Eq. (4.12), and $\ln(Q_t/\bar{m}_t)$ from Eq. (4.3). They can be made small by choosing $Q_S \sim M_S$

and $Q_t \sim M_t$, respectively. Due to the improvement regarding the used RGEs, we denote this procedure as *renormalization-group improvement*. The renormalization-group improved Higgs mass calculation produces reliable results for sizable scale splittings, where terms of $\mathcal{O}(v^2/M_S^2)$ can be neglected. However, for scenarios in which M_S is of the same order as v, the fixed-order approach, which usually includes these contributions of $\mathcal{O}(v^2/M_S^2)$, is preferable.

4.2 RE-EXPANDING THE EFT CALCULATION AND INGREDIENTS FOR N^{3}LL ACCURACY

The perturbative version of the EFT approach described in Sect. 4.1 would be to start with Eq. (4.3) and first set the scale at which the matching to the MSSM is performed to $Q_S \sim M_S$. It would be more convenient, however, to perform RGE running within the SM to Q_S but for our calculations this is not required. By setting the renormalization scale to Q_S, large logarithms of the form $\ln(Q_S^2/\bar{m}_t{}^2)$ are generated:

$$M_h^2 = \bar{v}^2(Q_S)\left[\bar{\lambda}(Q_S) + \kappa \bar{y}_t^4(Q_S) \sum_{n=0}^{\infty}\sum_{p=0}^{n+1} \kappa^n \bar{g}_3^{2n}(Q_S) c_{\mathrm{SM}}^{(n,p)} \ln\left(\frac{Q_S^2}{\bar{m}_t^2}\right)^p\right]. \tag{4.15}$$

Subsequently, one expresses the $\bar{x}_i(Q_S)$ by the $Y(Q_S)$ through Eq. (4.12). This last step only introduces small logarithms of the form $\ln(Q_S/M_S)$. Re-expanding in κ and keeping terms through order κ^N, this result is denoted as

$$M_{h,\mathrm{EFT},N}^2(Q_S)\,. \tag{4.16}$$

Obviously, the following formal relation applies:

$$M_{h,\mathrm{EFT}}^2(Q_S, Q_S) = M_{h,\mathrm{EFT},N}^2(Q_S) + \mathcal{O}(\kappa^{N+1}) \tag{4.17}$$

if the same order of the threshold corrections, the same values for $Y(Q_S)$, and the same SM expression for M_h^2 are used in deriving the results on both sides of this equation. Note, however, that $M_{h,\mathrm{EFT},N}^2$ does not profit from renormalization-group improvement. We also have

$$M_{h,\mathrm{FO},N}^2(Q_S) = M_{h,\mathrm{EFT},N}^2(Q_S)\,, \tag{4.18}$$

with the fixed-order result of Eq. (4.11), when expanding in κ to $\mathcal{O}(\kappa^N)$ and setting $Q_t = Q_S$. This relation is used in the next section to extract the three-loop threshold correction for the quartic Higgs coupling $\bar{\lambda}(Q_S)$.

In this chapter we aim for a calculation of the light CP-even Higgs pole mass of the MSSM in the decoupling limit including the fixed-order through $\mathcal{O}(y_t^4 g_3^4)$ (N^{3}LO), as well as resummation in $\bar{g}_t^4 \bar{g}_3^{2n}$ through fourth logarithmic order (N^{3}LL), while neglecting all terms of $\mathcal{O}(v^2/M_S^2)$. This calculation requires to include

- the four-loop β-function for $\bar{\lambda}$ to order $\kappa^4 \bar{g}_t^4 \bar{g}_3^6$,
- the three-loop β-function for $\bar{g}_t$ to order $\kappa^3 \bar{g}_t \bar{g}_3^6$,
- the two-loop β-function for $\bar{g}_3$ to order $\kappa^2 \bar{g}_3^5$,
- the three-loop threshold correction for $\bar{\lambda}$ to order $\kappa^3 \bar{g}_t^4 \bar{g}_3^4$,
- the two-loop threshold correction for $\bar{g}_t$ to order $\kappa^2 \bar{g}_t \bar{g}_3^4$,
- the one-loop threshold correction for $\bar{g}_3$ to order $\kappa \bar{g}_3^3$,
- the three-loop SM contributions to the Higgs mass, Eq. (4.3), to order $\kappa^3 \bar{g}_t^4 \bar{g}_3^4$.

Note that our identification of the logarithmic order refers to the required order of the β-function of the SM-Higgs self-coupling $\bar{\lambda}$. Specifically, our N^{n}LL terms involve the β-function to $\mathcal{O}(\bar{g}_t^4 \bar{g}_3^{2n})$.

Until recently, all of the necessary expressions were known, except for the three-loop threshold correction for $\bar{\lambda}$ to $\mathcal{O}(\bar{g}_t^4 \bar{g}_3^4)$. The latter was calculated in Ref. [62] as a part of this thesis. In the next section, we show details of this derivation utilizing the `H3m` result.

4.3 EXTRACTION OF THE HIGGS SELF-COUPLING AT $\mathcal{O}(y_t^4 g_3^4)$

This section describes how we use the formalism introduced in Sect. 4.1 and 4.2 to calculate the three-loop contributions to $\bar{\lambda}$ at $\mathcal{O}(y_t^4 g_3^4)$.

4.3.1 *Extraction procedure*

Using Eqs. (4.3), (4.5), (4.8), (4.13), and setting $Q_t = Q_S$, the three-loop result for $M^2_{h,\mathrm{EFT},3}(Q_S)$ including terms up to $\mathcal{O}(y_t^4 g_3^4)$ can be written in the following form:

$$\begin{aligned} M^2_{h,\mathrm{EFT},3}(Q_S) = M^2_{h,\mathrm{EFT},2}(Q_S) \\ + \kappa^3 v^2 y_t^4 g_3^4 s_\beta^4 \Bigg\{ & 368\, l_{St}^3 + \Big[80 + 96(\Delta g_3)_{g_3^2} + 192(\Delta y_t)_{g_3^2}\Big] l_{St}^2 \\ & - \Big[64\zeta_3 + \frac{1028}{3} + 32(\Delta g_3)_{g_3^2} + 256(\Delta y_t)_{g_3^2} \\ & \quad - 36(\Delta y_t)^2_{g_3^2} - 24(\Delta y_t)_{g_3^4}\Big] l_{St} \\ & + 32(\Delta y_t)_{g_3^2} - 42(\Delta y_t)^2_{g_3^2} - 12(\Delta y_t)_{g_3^4} + (\Delta\lambda)_{y_t^4 g_3^4} + c_{\mathrm{SM}}^{(2,0)} \Bigg\}, \end{aligned} \tag{4.19}$$

where $l_{St} = \ln(Q_S^2/m_t^2)$ and, as before, the Q_S dependence of y_t, g_3, Δy_t, Δg_3, and $\Delta\lambda$ is suppressed. Until recently, the only unknown term on the r.h.s. of Eq. (4.19) was the three-loop threshold correction for the quartic Higgs coupling $(\Delta\lambda)_{y_t^4 g_3^4}$, which we calculate

in the following. Assuming that the three-loop fixed-order result $M^2_{h,\mathrm{FO},3}(Q_S)$ is known, we can insert (4.19) into Eq. (4.18) and solve for the unknown threshold correction:

$$M^2_{h,\mathrm{FO},3}(Q_S) - M^2_{h,\mathrm{EFT},3}(Q_S)\Big|_{(\Delta\lambda)_{y_t^4 g_3^4}=0} = \kappa^3 v^2 y_t^4 g_3^4 s_\beta^4 (\Delta\lambda)_{y_t^4 g_3^4} \,. \tag{4.20}$$

Note that all large logarithms l_{St} cancel on the l.h.s. of Eq. (4.20). Thus, we may write Eq. (4.20) as

$$\kappa^3 v^2 y_t^4 g_3^4 s_\beta^4 (\Delta\lambda)_{y_t^4 g_3^4} = M^2_{h,\mathrm{FO},3}(Q_S) - M^2_{h,\mathrm{EFT},2}(Q_S) - \Delta M^2_{h,3}(Q_S) \,, \tag{4.21}$$

where

$$\Delta M^2_{h,3}(Q_S) = \kappa^3 v^2 y_t^4 g_3^4 s_\beta^4 \left[32(\Delta y_t)_{g_3^2} - 42(\Delta y_t)^2_{g_3^2} - 12(\Delta y_t)_{g_3^4} + c^{(2,0)}_{\mathrm{SM}} \right] . \tag{4.22}$$

The threshold correction $(\Delta\lambda)_{y_t^4 g_3^4}$ obtained in this way is defined in the $\overline{\mathrm{MS}}$ scheme and expressed in terms of the MSSM $\overline{\mathrm{DR}}'$ parameters y_t and g_3, in accordance with Eq. (4.13). Inverting the threshold corrections for y_t and g_3,

$$\begin{aligned} g_3 &= \bar{g}_3 \left\{ 1 - \kappa \bar{g}_3^2 (\Delta g_3)_{g_3^2} - \kappa^2 \bar{g}_3^4 \left[(\Delta g_3)_{g_3^4} - 3(\Delta g_3)^2_{g_3^2} \right] + \mathcal{O}(\kappa^3) \right\} , \\ y_t s_\beta &= \bar{g}_t \left\{ 1 - \kappa \bar{g}_3^2 (\Delta y_t)_{g_3^2} - \kappa^2 \bar{g}_3^4 \left[(\Delta y_t)_{g_3^4} - 2(\Delta g_3)_{g_3^2} (\Delta y_t)_{g_3^2} - (\Delta y_t)^2_{g_3^2} \right] + \mathcal{O}(\kappa^3) \right\} , \end{aligned} \tag{4.23}$$

it can also be expressed in terms of SM $\overline{\mathrm{MS}}$ parameters according to

$$\bar{\lambda} = \frac{M_Z^2}{\bar{v}^2} \cos^2 2\beta + \kappa \bar{g}_t^4 (\Delta\lambda)_{\bar{g}_t^4} + \kappa^2 \bar{g}_t^4 \bar{g}_3^2 (\Delta\lambda)_{\bar{g}_t^4 \bar{g}_3^2} + \kappa^3 \bar{g}_t^4 \bar{g}_3^4 (\Delta\lambda)_{\bar{g}_t^4 \bar{g}_3^4} + \mathcal{O}(\kappa^4) \,, \tag{4.24}$$

where

$$\begin{aligned} (\Delta\lambda)_{\bar{g}_t^4} &= (\Delta\lambda)_{y_t^4} \,, \\ (\Delta\lambda)_{\bar{g}_t^4 \bar{g}_3^2} &= (\Delta\lambda)_{y_t^4 g_3^2} - 4(\Delta\lambda)_{y_t^4} (\Delta y_t)_{g_3^2} \,, \\ (\Delta\lambda)_{\bar{g}_t^4 \bar{g}_3^4} &= (\Delta\lambda)_{y_t^4 g_3^4} + (\delta\lambda)_{y_t^4 g_3^4} \,, \end{aligned} \tag{4.25}$$

and

$$\begin{aligned} (\delta\lambda)_{y_t^4 g_3^4} = &-(\Delta\lambda)_{y_t^4 g_3^2} \left[2(\Delta g_3)_{g_3^2} + 4(\Delta y_t)_{g_3^2} \right] \\ &+ (\Delta\lambda)_{y_t^4} \left[10(\Delta y_t)^2_{g_3^2} - 4(\Delta y_t)_{g_3^4} + 8(\Delta y_t)_{g_3^2} (\Delta g_3)_{g_3^2} \right] . \end{aligned} \tag{4.26}$$

Eq. (4.20) shows how the three-loop threshold correction for the quartic Higgs coupling can be extracted from the three-loop fixed-order result for the MSSM Higgs mass. The latter has been calculated in Refs. [15, 16] in the form of a set of expansions around various limiting cases for the SUSY masses (cf. Eq. (3.5)). In all of the different expansions, terms of $\mathcal{O}(v^2/M_S^2)$ have been neglected. Since the `H3m` result was obtained in a scheme that differs from the

commonly used $\overline{\text{DR}}'$ scheme, the shift presented in Eq. (3.9) has to be applied to Eq. (4.20) in order to receive a consistent result.

With Eq. (4.20) we are able to extract the three-loop threshold correction for the quartic Higgs coupling expressed in terms of the H3m hierarchies defined in Eq. (3.5) taken from Ref. [16]. We denote this result as $(\Delta\lambda_{\texttt{H3m}})_{y_t^4 g_3^4}$ in what follows. Using renormalization-group invariance, we can improve on the logarithmic part of $(\Delta\lambda_{\texttt{H3m}})_{y_t^4 g_3^4}$ by replacing their hierarchy dependence with general MSSM particle masses. This can be done by deriving logarithmic terms of the form $\ln(Q^2/M_S^2)$ by requiring that

$$Q\frac{\mathrm{d}}{\mathrm{d}Q}\left[M_{h,\text{FO},2}^2(Q) + \Delta M_{h,3}^2(Q) + \kappa^3 v^2 y_t^4(Q) g_3^4(Q) s_\beta^4 (\Delta\lambda(Q))_{y_t^4 g_3^4}\right] = 0 + \mathcal{O}(\kappa^4)\,, \quad (4.27)$$

with $\Delta M_{h,3}^2$ from Eq. (4.22), and using the three-loop MSSM β-functions [97, 98]. We refer to the corresponding threshold correction, which includes the exact mass dependence of the logarithmic terms, reconstructed in this way as $(\Delta\lambda_{\texttt{EFT}})_{y_t^4 g_3^4}$. Note that only the non-logarithmic term of the fixed-order three-loop result of Ref. [16] enters this result. Of course, expanding $(\Delta\lambda_{\texttt{EFT}})_{y_t^4 g_3^4}$ in terms of the H3m hierarchies up to the appropriate orders, we recover $(\Delta\lambda_{\texttt{H3m}})_{y_t^4 g_3^4}$ as defined above.

4.3.2 *Result in the degenerate-mass case*

Since we have made the x_t dependence explicit in our result and we neglect all but the leading terms in $y_t^2 \propto m_t^2$, we can set $m_{\tilde{t}_1} = m_{\tilde{t}_2} = M_S$ in our expressions.

Using the degenerate-mass limit, the expression for $(\Delta\lambda)_{y_t^4 g_3^4}$ is simple enough to be quoted here. In this case, the threshold corrections for the top Yukawa coupling, defined by Eq. (4.13), are given by

$$(\Delta y_t)_{g_3^2} = -\frac{4}{3}\left(-1 + l_{SS} + x_t\right)\,, \quad (4.28)$$

$$(\Delta y_t)_{g_3^4} = \frac{2099 - 1748 l_{SS} + 372 l_{SS}^2}{54} + \frac{-416 + 32 l_{SS}}{27} x_t\,, \quad (4.29)$$

where $l_{SS} = \ln(Q_S^2/M_S^2)$ and the one-loop threshold correction of the strong coupling,

$$(\Delta g_3)_{g_3^2} = -\frac{1}{2} - 2 l_{SS}\,, \quad (4.30)$$

is used. Following Eq. (4.22), this leads to a subtraction term

$$\begin{aligned}\Delta M_{h,3}^2(Q_S) = \kappa^3 v^2 y_t^4 g_3^4 s_\beta^4 \Bigg[&- \frac{2\left(2243 - 2228 l_{SS} + 708 l_{SS}^2\right)}{9} \\ &- \frac{2\left(-1312 + 736 l_{SS}\right) x_t}{9} - \frac{224 x_t^2}{3} + c_{\text{SM}}^{(2,0)}\Bigg]\,,\end{aligned} \quad (4.31)$$

with $c_{\rm SM}^{(2,0)}$ from Eq. (4.5). Using the `h3` hierarchy of `H3m`, where all SUSY masses are assumed to be of comparable size and the expansion is performed in the mass differences, the `H3m` result for the degenerate-mass case reads

$$\begin{aligned} M_{h,\rm FO,3}^2\Big|_{l_{St}=0} = \frac{8}{27}\kappa^3 v^2 y_t^4 g_3^4 s_\beta^4 \Big[&-1246 - 2132 l_{SS} + 1326 l_{SS}^2 - 504 l_{SS}^3 - 1926\zeta_3 \\ &+ 216 l_{SS}\zeta_3 \\ &+ x_t\left(-2776 + 400 l_{SS} - 1464 l_{SS}^2 + 1908\zeta_3\right) \\ &+ x_t^2\left(3678 - 6 l_{SS} + 126 l_{SS}^2 - 1485\zeta_3\right) \\ &+ x_t^3\left(2722 + 20 l_{SS} + 108 l_{SS}^2 - 2259\zeta_3\right)\Big] + \mathcal{O}(x_t^4)\,. \end{aligned} \tag{4.32}$$

Note that in the expansion of the `h3` hierarchy, higher orders of x_t are not included in the `H3m` result. The shift to convert from the `H3m` to the $\overline{\rm DR}'$ scheme as defined by Eq. (3.9) is

$$(\Delta M_h^2)_{\texttt{H3m}\to\overline{\rm DR}'} = 16\kappa^3 v^2 y_t^4 g_3^4 s_\beta^4\,(1 + l_{SS})\left(6 - 6x_t^2 + x_t^4\right)\,. \tag{4.33}$$

Combining Eqs. (4.31)–(4.33) according to Eq. (4.20), we obtain

$$\begin{aligned} (\Delta\lambda(Q_S))_{y_t^4 g_3^4} = \frac{1}{27}\Big\{ &6082 - 27832 l_{SS} + 14856 l_{SS}^2 - 4032 l_{SS}^3 \\ &- 15408\zeta_3 + 1728 l_{SS}\zeta_3 - 27 c_{\rm SM}^{(2,0)} \\ &+ x_t\left[7616 l_{SS} - 11712 l_{SS}^2 + 32(-940 + 477\zeta_3)\right] \\ &+ x_t^2\left[28848 - 2640 l_{SS} + 1008 l_{SS}^2 - 11880\zeta_3\right] \\ &+ x_t^3\left[160 l_{SS} + 864 l_{SS}^2 + 8(2722 - 2259\zeta_3)\right]\Big\} + \mathcal{O}(x_t^4) \end{aligned} \tag{4.34}$$

for the threshold correction in terms of $\overline{\rm DR}'$ parameters.

If one re-expresses the one- and two-loop corrections in terms of SM $\overline{\rm MS}$ parameters, the following shift must be added to Eq. (4.34) in the degenerate-mass case,

$$\begin{aligned} (\delta\lambda(Q_S))_{y_t^4 g_3^4} = \frac{1}{27}\Big[&26916 l_{SS} - 18816 l_{SS}^2 - 5904 l_{SS}^3 \\ &- x_t\left(-3744 + 14016 l_{SS} + 18816 l_{SS}^2\right) \\ &- x_t^2\left(29652 - 5424 l_{SS} - 9936 l_{SS}^2\right) \\ &- x_t^3\left(-6768 - 13152 l_{SS} - 2688 l_{SS}^2\right)\Big] + \mathcal{O}(x_t^4)\,. \end{aligned} \tag{4.35}$$

To obtain Eq. (4.35) we used the threshold corrections

$$(\Delta\lambda)_{y_t^4} = -6 l_{SS} + 6x_t^2 - \frac{x_t^4}{2} \tag{4.36}$$

and

$$(\Delta\lambda)_{y_t^4 g_3^2} = -\frac{4}{3}\Big\{4\left[6l_{SS} + 3l_{SS}^2 + 6\left(1 + l_{SS}\right)x_t - \left(3 + 6l_{SS}\right)x_t^2 - \left(1 + 2l_{SS}\right)x_t^3\right] + x_t^4\Big\} \quad (4.37)$$

in accordance with Eq. (4.23), (4.25), and (4.26).

4.3.3 *Extraction uncertainty*

In order to combine the three-loop threshold correction of $(\Delta\lambda)_{y_t^4 g_3^4}$ with existing EFT codes such as `HSSUSY` [59] or `SusyHD` [60], where the one- and two-loop corrections are expressed in terms of SM $\overline{\text{MS}}$ parameters, we extended the functionality of `Himalaya` to provide $(\Delta\lambda_{\texttt{EFT}})_{y_t^4 g_3^4}$ by implementing Eq. (4.20), including the conversion from the `H3m` to the $\overline{\text{DR}}'$ scheme. In addition, we included the shift of Eq. (4.26) that converts the parameters in the threshold correction from the $\overline{\text{DR}}'$ to the $\overline{\text{MS}}$ scheme.

When using the `H3m` result for the extraction of $(\Delta\lambda)_{y_t^4 g_3^4}$, it is important to provide an uncertainty estimate due to missing higher-order terms regarding the expansions of Eq. (3.5). We employ two largely complementary ways to estimate this uncertainty, referring to the expansion and the x_t uncertainty, respectively.

Concerning the expansion uncertainty, we proceed as follows. As described in Subsect. 4.3.1, within the $\overline{\text{DR}}'$ scheme, there are two possible extractions of the threshold correction for the quartic Higgs coupling. Both of them use the hierarchy expansions of `H3m` for the non-logarithmic terms. However, while $(\Delta\lambda_{\texttt{H3m}})_{y_t^4 g_3^4}$ uses these expansions also for the logarithmic terms, $(\Delta\lambda_{\texttt{EFT}})_{y_t^4 g_3^4}$ contains their exact mass dependence, derived from renormalization-group invariance. We thus use the difference of $(\Delta\lambda_{\texttt{EFT}})_{y_t^4 g_3^4}$ to $(\Delta\lambda_{\texttt{H3m}})_{y_t^4 g_3^4}$ at the scale Q_S as an uncertainty estimate regarding the hierarchy expansion of the non-logarithmic contribution:

$$\delta_{\text{exp}} = \kappa^3 y_t^4 g_3^4 s_\beta^4 \left|(\Delta\lambda_{\texttt{H3m}})_{y_t^4 g_3^4} - (\Delta\lambda_{\texttt{EFT}})_{y_t^4 g_3^4}\right|. \quad (4.38)$$

For the x_t uncertainty, on the other hand, we consider the conversion term $(\delta\lambda)_{y_t^4 g_3^4}$ defined in Eq. (4.26), whose mass dependence is known exactly. Since the main source of uncertainty occurs for large mixing, we determine the highest power n_{max} of x_t taken into account in the specific `H3m` hierarchy, and use the size of the terms of order x_t^n with $n_{\text{max}} < n \leq 4$ in the non-logarithmic part of $(\delta\lambda)_{y_t^4 g_3^4}$ as uncertainty estimate, labeled δ_{x_t}. Note that powers higher than x_t^4 cannot appear in $(\Delta\lambda)_{y_t^4 g_3^4}$ when the result is expressed in terms of the MSSM top Yukawa coupling. The reason is that the one-loop correction $(\Delta\lambda)_{y_t^4}$ contains no terms with $x_t^{n>4}$, and up to the three-loop level the involved (s)quarks, gluons, and gluinos do not introduce any additional x_t-dependence. To be specific, let us again consider the limit of degenerate MSSM mass parameters. In this case, `H3m` uses the `h3` hierarchy defined in

Eq. (3.5), which includes only terms through x_t^3 though. The uncertainty is thus estimated with the help of the non-logarithmic terms of order x_t^4 in $(\delta\lambda)_{y_t^4 g_3^4}$, given by

$$\delta_{x_t} = \frac{5735}{27}\kappa^3 y_t^4 g_3^4 s_\beta^4 \, x_t^4 \,. \tag{4.39}$$

We combine these two uncertainties linearly and define the total uncertainty due to the hierarchy expansions as

$$\delta\left(\kappa^3 y_t^4 g_3^4 s_\beta^4 (\Delta\lambda_{\texttt{EFT}})_{y_t^4 g_3^4}\right) = \delta_{x_t} + \delta_{\text{exp}}. \tag{4.40}$$

Note that for cases in which $\delta_{x_t} = 0$, δ_{exp} still serves as an estimate for the uncertainty regarding the expansions of the `H3m` result.

After the derivation of $(\Delta\lambda_{\texttt{EFT}})_{y_t^4 g_3^4}$ and the definition of its uncertainty, all ingredients for a consistent calculation of the light CP-even Higgs mass including N^{3}LL corrections are known. Therefore, we close this chapter by discussing the impact of $(\Delta\lambda_{\texttt{EFT}})_{y_t^4 g_3^4}$ by including it into the EFT code `HSSUSY`, which then fulfills all requirements introduced in Sect. 4.2. In the following we will only use $(\Delta\lambda_{\texttt{EFT}})_{y_t^4 g_3^4}$ for the determination of $(\Delta\lambda)_{\bar{g}_t^4 \bar{g}_3^4}$.

4.4 NUMERICAL RESULTS INCLUDING N^{3}LL QCD CORRECTIONS

To study the numerical impact of the three-loop threshold correction $(\Delta\lambda)_{\bar{g}_t^4 \bar{g}_3^4}$ on the value of the light CP-even MSSM Higgs mass, we link `Himalaya` to `HSSUSY`, a spectrum generator from the `FlexibleSUSY` package that follows the EFT approach outlined in Sect. 4.1. It assumes a high-scale MSSM scenario, where the quartic Higgs coupling of the SM is evaluated at the SUSY scale $Q_S = M_S$ by the matching to the MSSM. The scenario assumes that all SUSY particles have masses around M_S and the SM is the appropriate EFT below that scale. In the original version of `HSSUSY`, the quartic Higgs coupling is determined using the two-loop expressions of $\mathcal{O}(\bar{g}_3^2(\bar{g}_t^2 + \bar{g}_b^2)^2 + (\bar{g}_t^2 + \bar{g}_b^2)^3 + \bar{g}_\tau^2(\bar{g}_b^2 + \bar{g}_\tau^2)^2)$ from Refs. [64,65][1], thereby ignoring terms of $\mathcal{O}(v^2/M_S^2)$. The known three- and four-loop SM $\overline{\text{MS}}$ β-functions of Refs. [101,103,113–117] are used to evolve the SM parameters to the electroweak scale, where the gauge and Yukawa couplings as well as the Higgs VEV are extracted from the known low-energy observables at full one-loop level plus the known two- and three-loop QCD corrections of Refs. [118–121]. The Higgs pole mass is calculated by default at the scale $Q_t = M_t$ at the full one-loop level with additional two-, three-, and four-loop SM corrections of $\mathcal{O}(\bar{g}_3^2(\bar{g}_t^4 + \bar{g}_b^4) + (\bar{g}_t^2 + \bar{g}_b^2)^3 + \bar{g}_\tau^6)$, $\mathcal{O}(\bar{g}_t^8 + \bar{g}_t^6\bar{g}_3^2 + \bar{g}_t^4\bar{g}_3^4)$, and $\mathcal{O}(\bar{g}_t^4\bar{g}_3^6)$ from Refs. [112,113,122]. Thus, by including $(\Delta\lambda)_{\bar{g}_t^4 \bar{g}_3^4}$ in the calculation, `HSSUSY` provides a resummed Higgs mass prediction in the decoupling limit of the MSSM through N^{3}LO+N^{3}LL at $\mathcal{O}(\bar{g}_t^4\bar{g}_3^4)$, including the full NLO+NLL and the NNLO+NNLL result at $\mathcal{O}(\bar{g}_3^2(\bar{g}_t^4 + \bar{g}_b^4) + (\bar{g}_t^2 + \bar{g}_b^2)^3 + \bar{g}_\tau^6)$.

1 We thank Thomas Kwasnitza for making the two-loop y_b corrections in `HSSUSY` publicly available.

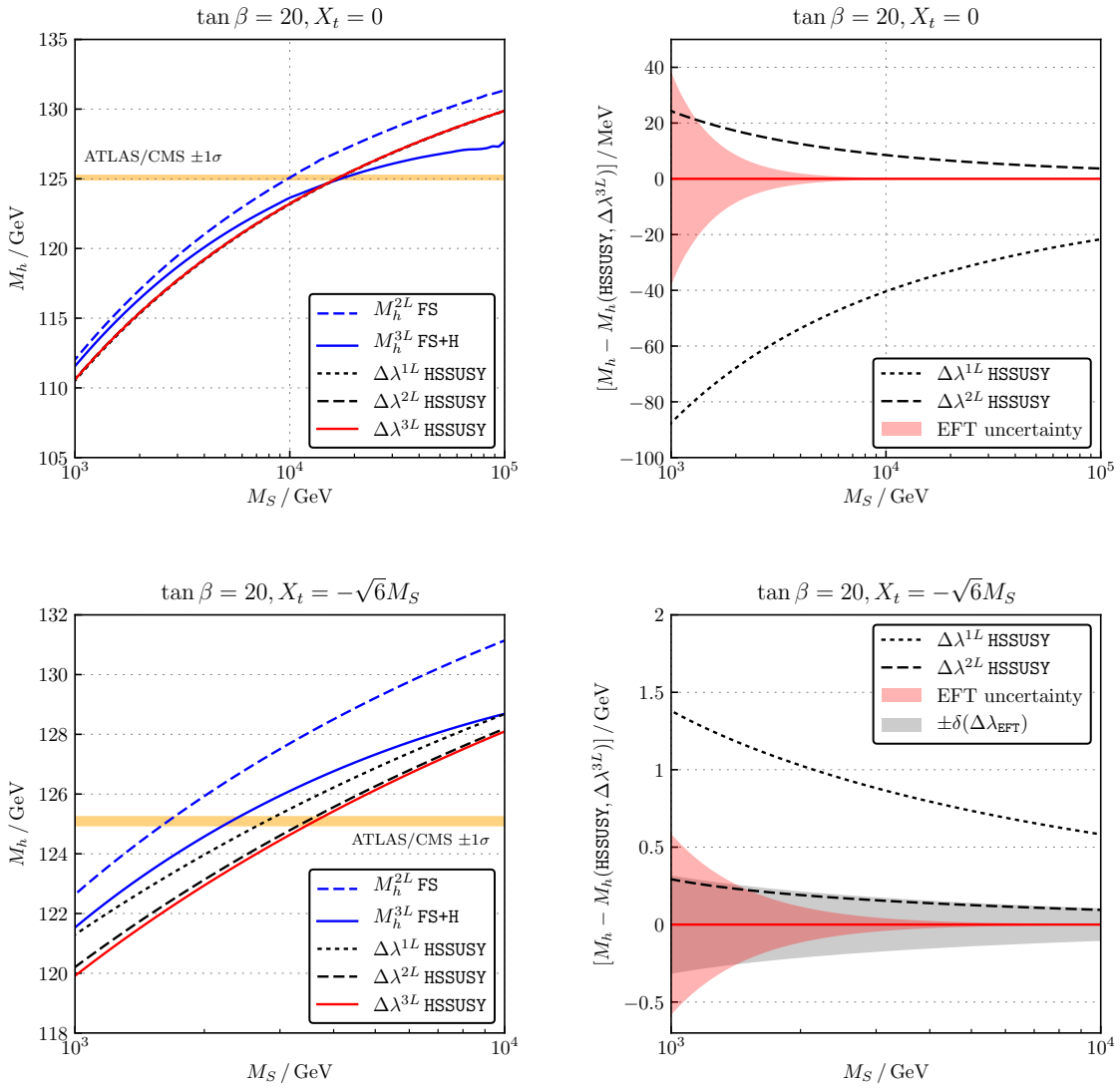

Figure 8: *Comparison of the three-loop* `HSSUSY` *(EFT) calculation with lower order EFT and fixed-order MSSM calculations from the* `FlexibleSUSY` *package as a function of the SUSY scale.*

In Fig. 8 the effect of $(\Delta\lambda)_{\tilde{g}_t^4 \tilde{g}_3^4}$ on the pure EFT calculation of `HSSUSY` is shown as a function of the SUSY scale M_S for the scenario defined in Chap. 2. The upper row shows a scenario with vanishing stop mixing, $x_t(Q_S) = 0$, the lower row shows one with maximal stop mixing, $x_t(Q_S) = -\sqrt{6}$. The left column of Fig. 8 displays the value of the calculated SM-like Higgs boson mass for these two scenarios. The blue dashed line and the blue solid line show the two- and three-loop fixed-order calculations of `FlexibleSUSY 2.3.0` and `FlexibleSUSY 2.3.0+Himalaya 2.0.1`, respectively. The black dotted, dashed, and red solid line depict the EFT calculations of `HSSUSY` with $\bar{\lambda}(Q_S)$ calculated at the one-, two-, and three-loop level, respectively. Here, $\Delta\lambda^{1L}$ and $\Delta\lambda^{2L}$ denote all available one- and two-loop corrections, respectively, and $\Delta\lambda^{3L} = (\Delta\lambda)_{\tilde{g}_t^4 \tilde{g}_3^4}$. For comparison, the orange horizontal band shows the current experimental value for the Higgs mass, see Eq. (2.1). As was already observed for example in Refs. [59, 70, 71], we find that in the range $M_S \geq 1\,\text{TeV}$ the fixed-order and the

EFT calculations deviate by several GeV. This is to be expected, because the EFT calculation resums the large logarithmic corrections in contrast to the fixed-order calculation and the terms of $\mathcal{O}(v^2/M_S^2)$ become negligible for M_S being above a few TeV [59, 69, 72, 74].[2]

As the black dashed and solid red line are hardly distinguishable in these plots, we show the shift relative to the one- and two-loop calculations of HSSUSY in the right column of Fig. 8. The gray band in the lower right panel of Fig. 8 corresponds to the theoretical uncertainty on the result due to the hierarchy expansions of the H3m result, evaluated according to Eq. (4.40). It amounts to more than 100% of the central shift for maximal mixing. For $x_t = 0$, this uncertainty is zero, see Eq. (4.39), because we also set $Q_S = M_S$. This is consistent with the fact that in this case, the degenerate-mass limit of the H3m result is exact. The red band shows the *EFT uncertainty* as defined in Refs. [60, 64, 70], estimating effects from missing terms of $\mathcal{O}(v^2/M_S^2)$. We see that the impact of $(\Delta\lambda)_{\bar{g}_t^4\bar{g}_3^4}$ is largely negative with respect to the two-loop threshold correction, $\Delta\lambda^{2L}$, and may reduce the Higgs mass by up to 0.6 GeV for maximal mixing when considering all values in the grey uncertainty band. For zero stop mixing, the shift is significantly smaller ($\lesssim 20$ MeV).

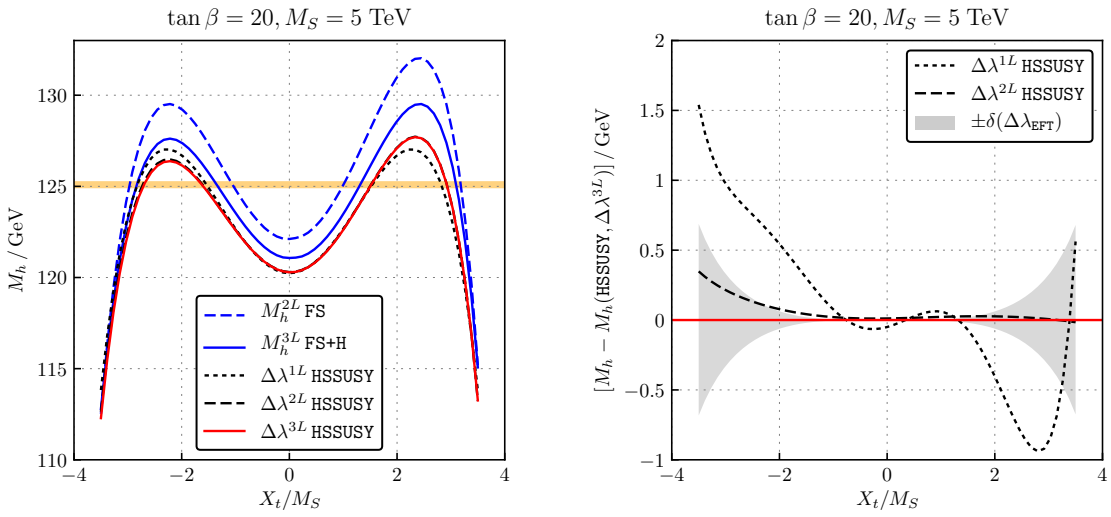

Figure 9: *Comparison of the three-loop* HSSUSY *(EFT) calculation with lower order EFT and fixed-order MSSM calculations from the* FlexibleSUSY *package as a function of the relative stop mixing.*

In Fig. 9, the Higgs mass prediction is shown as a function of the relative stop-mixing parameter x_t for the scenario defined in Chap. 2 with $M_S = 5$ TeV, where both the fixed-order and the EFT approach can accommodate for the experimentally observed value of M_h, Eq. (2.1), as long as $|x_t|$ is sufficiently large. The right panel shows again the difference of the three-loop calculation of HSSUSY with respect to the one- and two-loop calculations. In accordance with Fig. 8, we find that the shift induced by including $(\Delta\lambda)_{\bar{g}_t^4\bar{g}_3^4}$ is negative by trend, and below about 200 MeV for $x_t > -2$. Below that value, the effects could be of order

2 The magnitude of the terms of $\mathcal{O}(v^2/M_S^2)$ is discussed quantitatively in Subsect. 5.2.1.

1 GeV, but the uncertainty of our approximation grows to about 100% in this case, because the x_t^4 term is not included in the hierarchy expansion of the H3m result for this scenario.

To estimate the maximal effect that $(\Delta\lambda)_{\bar{g}_t^4\bar{g}_3^4}$ can have on the Higgs mass prediction, the blue band of Fig. 10 shows the variation of M_h when the SUSY mass parameters $m_{Q,3}$, $m_{U,3}$, $m_{D,3}$, and $m_{\tilde{g}}$ are varied simultaneously and independently within the interval $[M_S/\sqrt{2}, \sqrt{2}M_S]$ as a function of M_S, including the uncertainty $\delta((\Delta\lambda_{\text{EFT}})_{\bar{g}_t^4\bar{g}_3^4})$.[3] The hatched region marks the range of SUSY scales where the lightest running stop mass is below 1 TeV for at least one of the scanned points. In this case, the EFT may not be applicable. For zero stop mixing (left panel), we find that $(\Delta\lambda)_{\bar{g}_t^4\bar{g}_3^4}$ can have an effect up to ≈ -150 MeV for $M_S \geq 1$ TeV. In the region where $m_{\tilde{t}_1} > 1$ TeV, the correction reduces to -130 MeV at most. The three-loop correction decreases for larger SUSY scales, mainly due to the fact that the SM couplings become smaller. For maximal stop mixing, $x_t = -\sqrt{6}$, the effect of the three-loop correction is significantly larger, and can reach -1.25 GeV for $m_{\tilde{t}_1} \gtrsim 1$ TeV. The correction becomes particularly large when the soft-breaking stop-mass parameters $m_{Q,3}$ and $m_{U,3}$ become small.

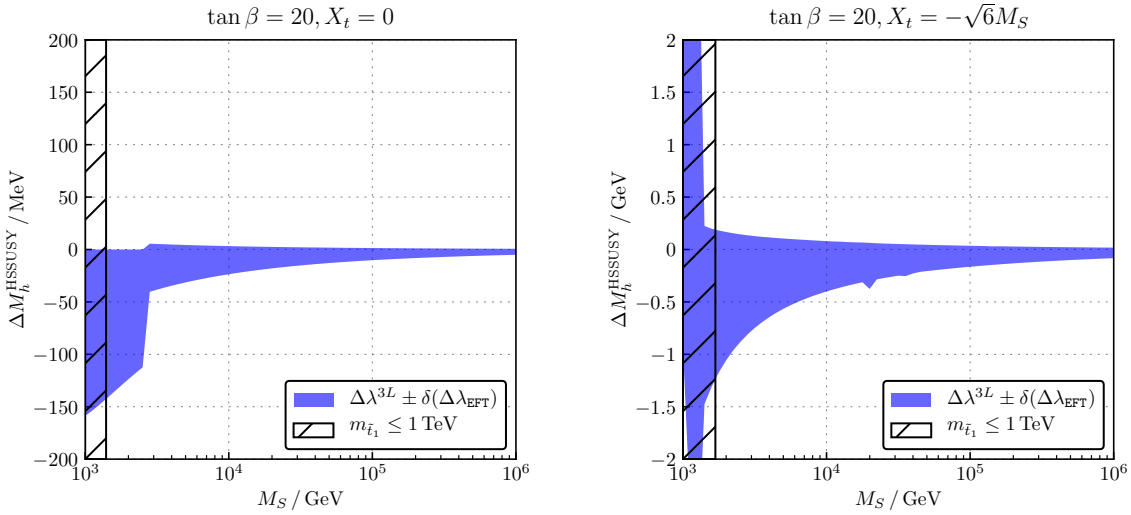

Figure 10: *Variation of M_h when the SUSY mass parameters are varied within the interval $[M_S/\sqrt{2}, \sqrt{2}M_S]$ in HSSUSY. The left panel shows $X_t = 0$ and the right panel $X_t = -\sqrt{6}M_S$. The blue band shows the maximal variation of M_h when the three-loop correction $(\Delta\lambda)_{\bar{g}_t^4\bar{g}_3^4} \pm \delta((\Delta\lambda_{\text{EFT}})_{y_t^4\bar{g}_3^4})$ is included, with respect to the two-loop calculation. In the hatched region there is $m_{\tilde{t}_1}(M_S) \leq 1$ TeV for at least one of the scanned parameter points.*

3 The choice of the interval $[M_S/\sqrt{2}, \sqrt{2}M_S]$ ensures that for all scanned points there exists a suitable mass hierarchy which fits the parameter point with a moderate uncertainty $(\Delta\lambda_{\text{EFT}})_{\bar{g}_t^4\bar{g}_3^4}$. In the scanned parameter region, the most frequently chosen hierarchy is h3.

4.5 CONCLUSIONS

In this chapter, we have introduced an alternative method to the FO approach to calculate the light CP-even Higgs mass in the MSSM, namely the EFT approach. The improvement employing renormalization-group equations leads to a resummation of large logarithms, which is desirable when sizable scale splittings between v and M_S arise. However, for regions in which contributions of $\mathcal{O}(v^2/M_S^2)$ become significant, the EFT approach turns out to be unreliable.

To provide a study in this framework including N^{3}LL resummation, we derived a result for the quartic Higgs coupling from the known three-loop corrections to the light CP-even Higgs mass of Refs. [15,16]. The latter is provided both in terms of $\overline{\text{DR}}'$ and $\overline{\text{MS}}$ parameters through its implementation into the public `Himalaya` library. This should facilitate its inclusion into spectrum generators which implement the EFT approach. In addition, an uncertainty estimate is provided to account for missing higher order terms in the mass-hierarchy expansions.

Combining `Himalaya` and `HSSUSY`, our numerical analysis shows that the three-loop correction tends to be negative and may decrease the predicted Higgs pole mass by up to 0.6 GeV for maximal stop mixing. In scenarios with zero stop mixing, the shift is significantly smaller, dropping to about -25 MeV for SUSY mass parameters of around 1 TeV. For non-degenerate spectra with $m_{\tilde{t}_1} \gtrsim 1$ TeV, the three-loop correction can be of the same size and reach up to -1.25 GeV for low stop masses in scenarios where a suitable mass hierarchy exists. In scenarios where no such hierarchy exists, the correction may be significantly larger, accompanied by a large expansion uncertainty. Due to the minor impact of the three-loop contribution of $\mathcal{O}(y_t^4 g_3^4)$ on the Higgs mass and its uncertainty, importance is raised towards the inclusion of the missing electroweak contributions at the two-loop level, which have not yet been calculated.

Although the EFT approach yields reliable results for multi-TeV scales, missing terms of $\mathcal{O}(v^2/M_S^2)$ could be important at intermediate scales between a few hundred GeV and the low TeV range. However, at these scales the FO approach tends to become inaccurate as well. In order to account for a reliable prediction of the light CP-even Higgs mass at arbitrary scales, the so-called hybrid approach has been developed in Refs. [53,68]. It combines the virtues of both the FO and the EFT approach. To overcome the deficits of the EFT and the FO approach, we provide a prescription to elevate the hybrid approach to the three-loop level in the next chapter.

5

HYBRID APPROACH

As seen in the previous chapters, the FO approach, on the one hand, yields reliable results if the masses of the SM and MSSM particles are of comparable size, and the EFT approach, on the other hand, yields reliable results if the mass splitting between the SM particles and their SUSY partners becomes sizable. However, it is unclear which of both approaches is the most suited one for intermediate SUSY scales ranging from a few hundred GeV up to a few TeV. Therefore, Refs. [53, 68] proposed a combined approach, which includes both contributions of $\mathcal{O}(v^2/M_S^2)$ and renormalization-group improvement. In practice, such a combination is tedious as one has to provide full perturbative control over all required intermediate pieces. However, if applied properly, one achieves a prediction for the light CP-even Higgs mass, which is in principle reliable for arbitrary mass splittings within the theory. In this chapter, we only focus on the simplest mass hierarchy, where the mass spectrum of the SUSY particles is given at a common scale M_S.

In Sect. 5.1, we summarize different combination approaches known in the literature and outline our procedure to obtain a result including N^{3}LO and N^{3}LL contributions, where we incorporate full one-loop, $\mathcal{O}(y_t^4 g_3^2 + y_t^6)$ two-loop, and $\mathcal{O}(y_t^4 g_3^4)$ three-loop corrections. Afterwards, in Sect. 5.2, we study the numerical impact of our hybrid approach, quantize the magnitude of the $\mathcal{O}(v^2/M_S^2)$ terms, and provide an uncertainty estimate. The required parts for a proper combination are implemented into the `Himalaya` library. This chapter is largely based on Ref. [74], where the way to combine the available results has been developed in the course of this thesis. This includes the implementation of the required parts into `Himalaya`, which are essential for all presented studies in this chapter. In collaboration with R. V. Harlander and A. Voigt, we studied the numerical impact of our combined result.

5.1 COMBINATION APPROACHES

So far, two approaches to combine FO and EFT results in the context of the light CP-even Higgs mass have been pursued in the literature:

- **Subtraction approach**: In this approach, the squared Higgs pole mass is written as

$$(M_h^{\text{subtr}})^2 = (M_h^{\text{FO}})^2 - (M_h^{\text{logs}})^2 + (M_h^{\text{res}})^2, \tag{5.1}$$

  where $(M_h^{\text{FO}})^2$ denotes the fixed-order result, $(M_h^{\text{logs}})^2$ are the large logarithmic fixed-order corrections, and $(M_h^{\text{res}})^2$ are the resummed logarithmic corrections.

An advantage of this approach is that existing fixed-order results can be used and different effective theories can be considered in a straightforward way. The generalization of this approach to models beyond the MSSM is non-trivial, because it requires model-specific FO and EFT loop calculations.

This approach is implemented into `FeynHiggs` at the two-loop level, see for example [53, 68, 69].

- **FlexibleEFTHiggs approach** [59,71,72]: The matching condition in this approach reads

$$(M_h^{\text{SM}})^2 = (M_h^{\text{MSSM}})^2 \,, \tag{5.2}$$

where M_h^{SM} denotes the Higgs pole mass as a function of SM $\overline{\text{MS}}$ parameters, and M_h^{MSSM} is the Higgs pole mass calculated in the MSSM in the $\overline{\text{DR}}'$ scheme. The $\overline{\text{MS}}$ and $\overline{\text{DR}}'$ parameters appearing in Eq. (5.2) depend on the renormalization scale Q_S, which is set close to the SUSY scale. In this way, the SM quartic Higgs coupling is determined in the $\overline{\text{MS}}$ scheme at the scale Q_S, which is then evolved down to the electroweak scale using SM RGEs in order to evaluate the Higgs pole mass from it.

Due to the simplicity of the matching condition (5.2), this approach can be generalized to other models in a rather straightforward way. However, the extension of this approach to the two-loop level is non-trivial with regards to the proper cancellation of potentially large logarithmic corrections in the matching.

The *FlexibleEFTHiggs* approach is implemented at one-loop level into `FlexibleSUSY` [59, 71], and at two-loop level into `SARAH/SPheno` [72].[1]

In this thesis, we adopt a hybrid scheme that is similar to the subtraction approach of Eq. (5.1). However, we work in the $\overline{\text{DR}}'$ scheme and include three-loop QCD corrections, when combining the FO and EFT results. In our framework, the light CP-even Higgs pole mass is calculated as

$$(M_h^{\text{hyb}})^2 = (M_h^{\text{EFT}})^2 + \Delta_v \,, \tag{5.3}$$

where M_h^{EFT} denotes the three-loop EFT result of `FlexibleSUSY/HSSUSY+Himalaya` [62] presented in Chap. 4. It resums large logarithms of $\mathcal{O}(y_t^4 g_3^4)$ to N^{3}LL, while others are resummed to NNLL. Its fixed-order expansion would reproduce the full fixed-order result in the limit $v^2/M_S^2 \to 0$, including the known two-loop corrections in the gaugeless limit and the three-loop terms of $\mathcal{O}(y_t^4 g_3^4)$ from `Himalaya` [15, 16, 47]. Δ_v supplies the terms that are suppressed by powers of v^2/M_S^2 as $M_S \gg v$ at fixed order up to the two-loop level, i.e. at $\mathcal{O}(y_t^6 + y_t^4 g_3^2)$ for the two-loop part. We separate Δ_v into a tree-level plus one-loop and a two-loop part,

$$\Delta_v = \Delta_v^{\text{0L+1L}} + \Delta_v^{\text{2L}} \,. \tag{5.4}$$

1 Note that in the implementation of the *FlexibleEFTHiggs* approach in `SARAH/SPheno`, large higher-order logarithmic corrections are induced at the matching scale. As a result, `SARAH/SPheno` resums large logarithms only up to (including) the leading-logarithmic level.

The first term on the r.h.s. of Eq. (5.4) is extracted from the *FlexibleEFTHiggs* result implemented in `FlexibleSUSY` and the second term from the two-loop contributions implemented into the `Himalaya` library, as described in what follows. The tree-level and one-loop contribution $\Delta_v^{\text{0L+1L}}$ is obtained by taking the difference between the one-loop *FlexibleEFTHiggs* result M_h^{FEFT} and the one-loop pure EFT result obtained from `HSSUSY` as

$$\Delta_v^{\text{0L+1L}} = \left[(M_h^{\text{FEFT}})^2 - (M_h^{\text{EFT}})^2\right]_{\text{0L+1L}} . \tag{5.5}$$

Due to the structure of the *FlexibleEFTHiggs* calculation, this difference contains all tree-level and one-loop SUSY contributions of higher order in v^2/M_S^2, and formally two-loop non-logarithmic electroweak SUSY terms (see below). In particular, large logarithmic corrections as well as two-loop non-electroweak SUSY contributions are absent. The two-loop contribution Δ_v^{2L} is obtained by

$$\Delta_v^{\text{2L}} = \Delta^{\text{2L}}_{\mathcal{O}(y_t^4 g_3^2 + y_t^6)} - \Delta^{\text{2L}}_{\mathcal{O}(y_t^4 g_3^2 + y_t^6)}\Big|_{v^2 \ll M_S^2} . \tag{5.6}$$

The terms on the r.h.s. of Eq. (5.6) represent the difference between the two-loop fixed-order contribution $\mathcal{O}(y_t^4 g_3^2 + y_t^6)$ calculated with `Himalaya`, and the same two-loop FO contribution where all $\mathcal{O}(v^2/M_S^2)$ terms are neglected. This difference thus contains all two-loop $\mathcal{O}(v^2/M_S^2)$ terms at $\mathcal{O}(y_t^4 g_3^2 + y_t^6)$. Large logarithmic as well as non-electroweak three-loop corrections of order $(v^2/M_S^2)^0$ are absent. To ensure this cancellation, the momentum iteration for the first term on the r.h.s. of Eq. (5.6) is only performed once as shown in Eq. (3.4), whereas the second term on the r.h.s. of Eq. (5.6) is derived as in Sect. 4.2.

5.2 NUMERICAL RESULTS INCLUDING N^{3}LO+N^{3}LL QCD CORRECTIONS

Following the prescription of the previous section, we present numerical studies for our hybrid approach in this section. First, we investigate the size of terms of $\mathcal{O}(v^2/M_S^2)$ in Subsect. 5.2.1 as a function of the SUSY scale M_S, which is followed by the definition of our uncertainty estimate in Subsect. 5.2.2. Afterwards, in Subsect. 5.2.3–5.2.2, we discuss our hybrid approach in comparison to a pure FO and EFT calculation.

5.2.1 *Size of the $\mathcal{O}(v^2/M_S^2)$ terms*

The main advantage of the hybrid approach is the inclusion of $\mathcal{O}(v^2/M_S^2)$ terms into the EFT result. To estimate at which scales these terms Δ_v can be neglected, we study their effect on the Higgs pole mass as a function of the SUSY scale in this section. For convenience we define the (non-squared) contribution of these terms as

$$\bar{\Delta}_v = \bar{\Delta}_v^{\text{0L+1L}} + \bar{\Delta}_v^{\text{2L}} , \tag{5.7}$$

$$\bar{\Delta}_v^{\text{0L+1L}} = \left[(M_h^{\text{EFT}})^2 + \Delta_v^{\text{0L+1L}}\right]^{1/2} - M_h^{\text{EFT}}\,, \tag{5.8}$$

$$\bar{\Delta}_v^{\text{2L}} = \left[(M_h^{\text{EFT}})^2 + \Delta_v^{\text{0L+1L}} + \Delta_v^{\text{2L}}\right]^{1/2} - \left[(M_h^{\text{EFT}})^2 + \Delta_v^{\text{0L+1L}}\right]^{1/2}\,. \tag{5.9}$$

Setting the input to the scenario defined in Chap. 2, we find that the $\mathcal{O}(v^2/M_S^2)$ terms can

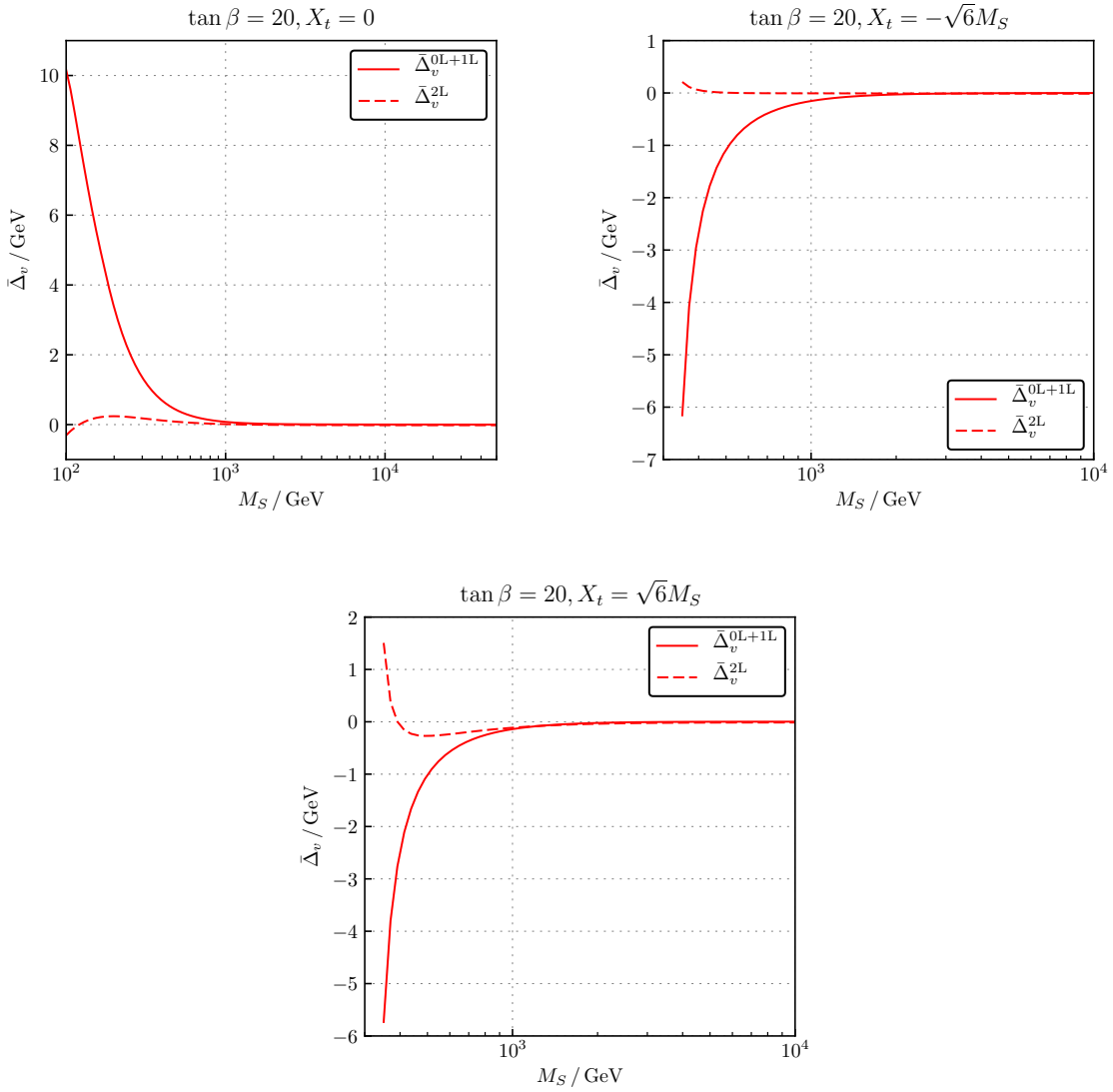

Figure 11: *Size of the $\mathcal{O}(v^2/M_S^2)$ terms as a function of M_S for different stop-mixing parameters X_t. The data of these plots is taken from Ref. [74].*

be sizable below $M_S \lesssim 0.5\,\text{TeV}$, while they are small as long as $M_S \gtrsim 1\,\text{TeV}$, see Fig. 11. Specifically, we find for $M_S \gtrsim 1\,\text{TeV}$

$$x_t = 0 \quad : \quad |\bar{\Delta}_v| \lesssim 0.10\,\text{GeV}\,, \tag{5.10}$$

$$x_t = -\sqrt{6} : \quad |\bar{\Delta}_v| \lesssim 0.15\,\text{GeV}\,, \tag{5.11}$$

$$x_t = \sqrt{6} \quad : \quad |\bar{\Delta}_v| \lesssim 0.25\,\text{GeV}\,. \tag{5.12}$$

Other values of $\tan\beta$ lead to similar observations.

The sign and the order of magnitude of these results are in agreement with the contribution of higher-dimensional operators as presented in Ref. [65]. Since the remaining uncertainty on the light CP-even Higgs pole mass is dominated by the uncertainty induced by the extraction of the running top Yukawa coupling, which has been estimated to be between 0.2–0.6 GeV [60, 65, 70, 115], we conclude that for $M_S \gtrsim 1\,\text{TeV}$ the $\mathcal{O}(v^2/M_S^2)$ terms are negligible and the EFT approach leads to a more precise value of the Higgs pole mass than the fixed-order result. This confirms the transition region of $M_S^{\text{equal}} = 1.0$–$1.3\,\text{TeV}$ estimated in Ref. [70].

5.2.2 *Uncertainty estimate*

We estimate the uncertainty of the hybrid result conservatively by taking the minimum uncertainty of the FO and EFT results for each parameter point:

$$\Delta M_h^{\text{hyb}} = \min\left\{\Delta M_h^{\text{FO}}, \Delta M_h^{\text{EFT}}\right\} . \tag{5.13}$$

The uncertainty of the three-loop fixed-order calculation, ΔM_h^{FO}, is estimated by:

- variation of the renormalization scale Q_S at which the Higgs pole mass is calculated ($\Delta^{(Q_S)} M_h^{\text{FO}}$),
- in-/exclusion of the two-loop threshold correction for the strong gauge coupling g_3 in the MSSM [96, 123, 124] ($\Delta^{(g_3)} M_h^{\text{FO}}$),

Thus, ΔM_h^{FO} yields

$$\Delta M_h^{\text{FO}} = \Delta^{(Q_S)} M_h^{\text{FO}} + \Delta^{(g_3)} M_h^{\text{FO}} , \tag{5.14}$$

with

$$\Delta^{(Q_S)} M_h^{\text{FO}} = \max_{Q_S \in [M_S/2, 2M_S]} \left| M_h^{\text{FO}}(Q_S) - M_h^{\text{FO}}(M_S) \right| , \tag{5.15}$$

$$\Delta^{(g_3)} M_h^{\text{FO}} = \left| M_h^{\text{FO}}(g_3^{\text{1L}}) - M_h^{\text{FO}}(g_3^{\text{2L}}) \right| . \tag{5.16}$$

The uncertainty of the three-loop EFT calculation, ΔM_h^{EFT}, is estimated by:

- variation of the renormalization scale Q_t at which the Higgs pole mass is calculated ($\Delta^{(Q_t)} M_h^{\text{EFT}}$),
- variation of the renormalization scale Q_S at which the MSSM is matched to the SM ($\Delta^{(Q_S)} M_h^{\text{EFT}}$),
- in-/exclusion of the four-loop QCD threshold correction for the SM top Yukawa coupling [125] ($\Delta^{(y_t^{\text{SM}})} M_h^{\text{EFT}}$),

- estimation of the effect of $\mathcal{O}(v^2/M_S^2)$ terms from the quartic Higgs coupling along the lines of Refs. [60, 64, 70] ($\Delta^{(v^2/M_S^2)} M_h^{\text{EFT}}$).[2]

Hence, by combining these sources of uncertainty linearly ΔM_h^{EFT} yields

$$\Delta M_h^{\text{EFT}} = \Delta^{(Q_t)} M_h^{\text{EFT}} + \Delta^{(Q_S)} M_h^{\text{EFT}} + \Delta^{(y_t^{\text{SM}})} M_h^{\text{EFT}} + \Delta^{(v^2/M_S^2)} M_h^{\text{EFT}}\,, \tag{5.17}$$

with

$$\Delta^{(Q_t)} M_h^{\text{EFT}} = \max_{Q \in [M_t/2, 2M_t]} \left| M_h^{\text{EFT}}(Q) - M_h^{\text{EFT}}(M_t) \right|\,, \tag{5.18}$$

$$\Delta^{(Q_S)} M_h^{\text{EFT}} = 0.5\,\text{GeV}\,, \tag{5.19}$$

$$\Delta^{(y_t^{\text{SM}})} M_h^{\text{EFT}} = \left| M_h^{\text{EFT}}(y_t^{\text{SM,3L}}) - M_h^{\text{EFT}}(y_t^{\text{SM,4L}}) \right|\,, \tag{5.20}$$

$$\Delta^{(v^2/M_S^2)} M_h^{\text{EFT}} = \left| M_h^{\text{EFT}} - M_h^{\text{EFT}}(v^2/M_S^2) \right|\,. \tag{5.21}$$

The matching-scale uncertainty $\Delta^{(Q_S)} M_h^{\text{EFT}}$ has been estimated in Ref. [60, 64, 70]. It was found that for scenarios as those considered here, the uncertainty does not exceed 0.5 GeV for $M_S \gtrsim 1$ TeV. Rather than extending the procedure of Ref. [60, 64, 70] to N^{3}LL which would involve the logarithmic terms at N^{4}LO, we conservatively associate this maximal value of 0.5 GeV to the matching-scale uncertainty, independently of M_S.

5.2.3 *Convergence for high SUSY scales*

Convergence properties of our hybrid result to the pure FO or EFT calculation, depending on the scale M_S, can be used as a check for our calculation. Therefore, in Fig. 12, we compare the hybrid result defined in Eq. (5.3) (red solid line) with the three-loop $\overline{\text{DR}}'$ fixed-order calculation M_h^{FO} of `FlexibleSUSY+Himalaya` [47] (blue dashed line) and the three-loop EFT result M_h^{EFT} of `HSSUSY+Himalaya` [62] (black dash-dotted line), which resums large logarithms through N^{3}LO. The red band indicates our uncertainty estimate as defined in Sect. 5.2.2. Note that we only include $\mathcal{O}(y_t^6 + y_t^4 g_3^2)$ contributions at the two-loop level.

Since $\Delta_v \to 0$ for $M_S \to \infty$, the hybrid curve converges towards the EFT curve in this limit. Note that in the scenario with $x_t = -\sqrt{6}$ for values of M_S below ~ 600 GeV, no suitable mass hierarchy is available in `Himalaya`. The three-loop fixed-order contribution is set to zero in this case, which means that the EFT curve and the hybrid calculation is formally consistent only at the two-loop level for lower scales. On the other hand, for $M_S \to M_Z$ one may expect the hybrid curve to converge towards the three-loop fixed-order curve. However, we find a finite offset at low energies of up to ~ 0.5 GeV for $x_t = 0$ and ~ 1.5 GeV for $x_t = -\sqrt{6}$. This offset results from higher order $\mathcal{O}(v^2/M_S^2)$ terms, which are not suppressed in the low M_S region. The origin of these will be investigated in the following subsection.

2 $M_h^{\text{EFT}}(v^2/M_S^2)$ of Eq. (5.21) is obtained by scaling the individual terms in the one-loop threshold correction $\Delta\lambda^{1\text{L}}$ for the quartic coupling by factors of the order $(1 + v^2/M_S^2)$.

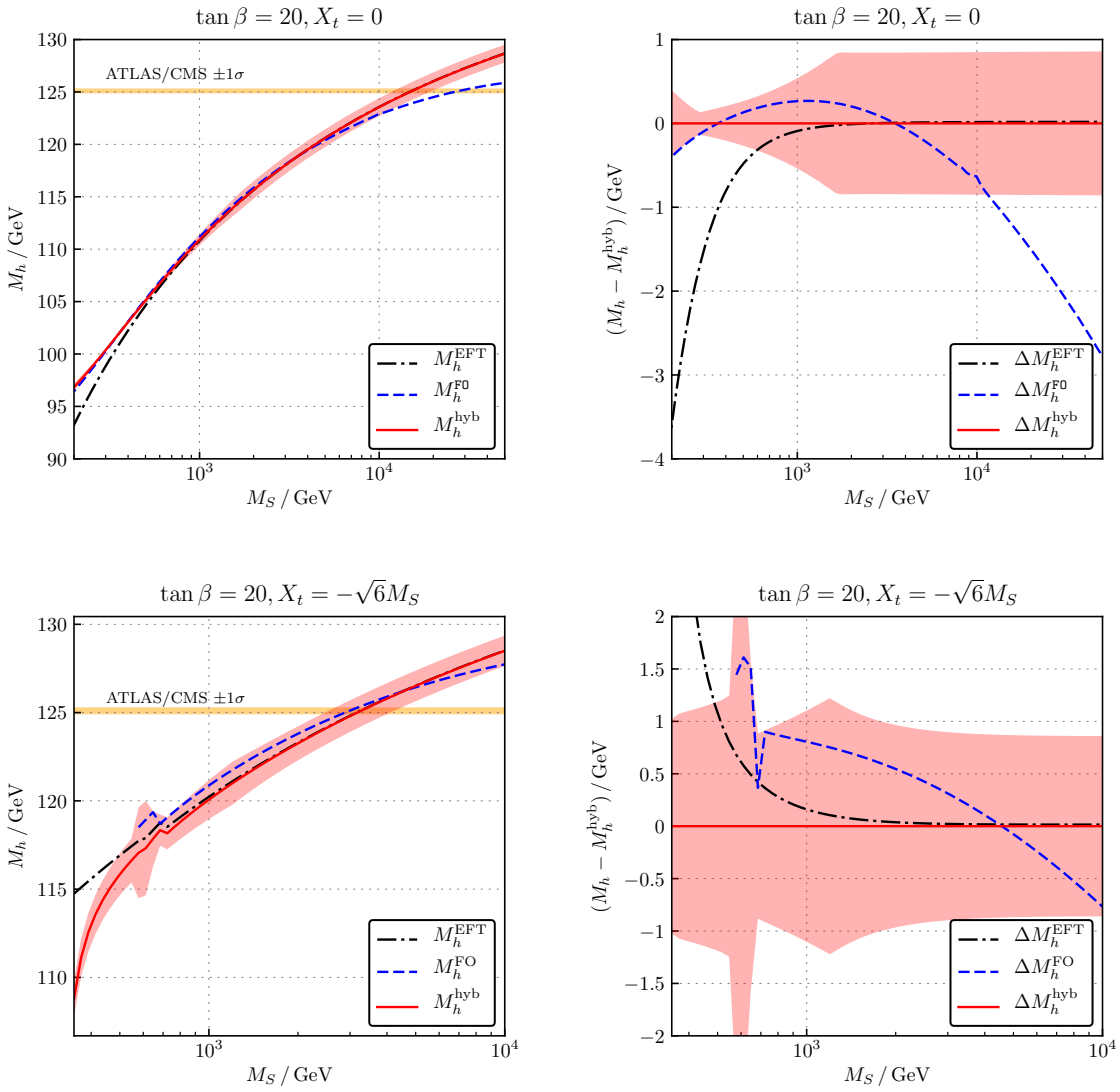

Figure 12: *Comparison of the three-loop FO, EFT, and hybrid results as functions of M_S. The red band shows our uncertainty estimate. The data of these plots is taken from Ref. [74].*

In Fig. 13 a comparison of the hybrid results with the three-loop FO and EFT results is shown as a function of x_t for the degenerate-mass scenario with $\tan\beta = 20$ and $M_S = 3\,\text{TeV}$, where the MSSM value of the Higgs pole mass can be in agreement with the experimentally measured value. As our derivation of the Δ_v terms from above suggests, we find agreement of the hybrid result with the EFT within 0.5 GeV for such a large SUSY scale. The largest deviations of 0.5 GeV occur in the region $|x_t| > 3$, while in the region $|x_t| < 3$ the deviation is smaller than 0.1 GeV. However, the latter region suffers from a problematic feature of the fixed-order calculation, which is the occurrence of tachyonic $\overline{\text{DR}}'$ masses of the heavy CP-even, the CP-odd, and the charged Higgs bosons at the electroweak scale for $x_t > 0$ as already discussed in Chap. 3. The kink at $\sim x_t = 0$ of the FO curve is due to the replacement of the tachyonic running masses by their absolut values, which leads to a discontinuous transition.

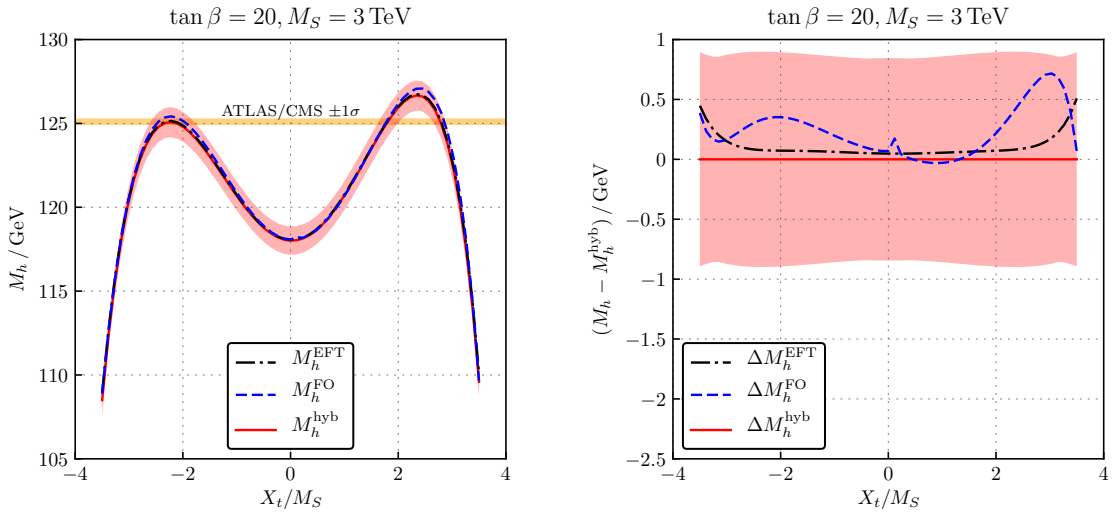

Figure 13: *Comparison of the three-loop FO, EFT, and hybrid results as functions of X_t/M_S. The red band shows our uncertainty estimate. The data of these plots is taken from Ref. [74].*

Our combined uncertainty as defined by Eq. (5.13) is shown as the red band in Figures 12–13. In the studied scenario, the uncertainty is nearly constant and around $\Delta M_h^{\text{hyb}} \approx 1\,\text{GeV}$. Very rarely it happens that the central value of the approach (EFT or FO) that determines the hybrid uncertainty through Eq. (5.13) is not itself contained in the resulting uncertainty band. In this case, we widen the band correspondingly.

As shown in Fig. 12, for SUSY scales below 1–2 TeV, the fixed-order uncertainty defined by Eq. (5.14) is the smaller of the two on the r.h.s. of Eq. (5.13). Due to the occurrence of large logarithmic loop corrections, ΔM_h^{FO} becomes larger when M_S is increased and reaches about $\Delta M_h^{\text{FO}} \approx 1\,\text{GeV}$ for $M_S \approx 1\,\text{TeV}$. A larger uncertainty of up to $\Delta M_h^{\text{FO}} \approx 1.5\,\text{GeV}$ occurs only for $x_t = -\sqrt{6}$ around $M_S \approx 0.6\,\text{TeV}$, where a hierarchy switch occurs in the three-loop fixed-order result of `Himalaya`.

The EFT uncertainty as defined by Eq. (5.17) is composed as follows. $\Delta^{(Q_t)} M_h^{\text{EFT}}$ is approximately independent of the SUSY scale and amounts to about 0.2 GeV whereas the uncertainty $\Delta^{(y_t^{\text{SM}})} M_h^{\text{EFT}}$ from the extraction of the SM top Yukawa coupling amounts to approximately 0.1 GeV and increases slightly with the SUSY scale. For SUSY scales above 1–2 TeV, the total uncertainty of the EFT calculation ΔM_h^{EFT} is dominated by these two contributions and $\Delta^{(Q_S)} M_h^{\text{EFT}}$, while amounting to slightly less than 1 GeV. In contrast, $\Delta^{(v^2/M_S^2)} M_h^{\text{EFT}}$ is negligible at these scales. This is in agreement with the results from Subsect. 5.2.1, where it was found that the $\mathcal{O}(v^2/M_S^2)$ terms are below 0.25 GeV for $M_S \gtrsim 1\,\text{TeV}$. Finally, we find that the extraction uncertainty $|\delta_{x_t} + \delta_{\text{exp}}|$ of the three-loop threshold correction $\bar{\lambda}$ introduced in the previous chapter is below 2 MeV for the degenerate-mass scenarios considered here with $M_S \gtrsim 1\,\text{TeV}$, and is thus negligible.

Quite generally, the SUSY scale M_S^{equal}, where both the FO and the EFT calculation have the same uncertainty, is between $M_S \gtrsim$ 1–2 TeV, which is in agreement with the findings in Refs. [70, 126].

5.2.4 *Convergence for low SUSY scales*

As described in Refs. [59, 71], the *FlexibleEFTHiggs* calculation implemented in `FlexibleSUSY` since version `2.0.0` includes all one-loop contributions and resums all large logarithmic corrections at the next-to-leading logarithmic level. When compared to the one-loop fixed-order $\overline{\text{DR}}'$ result of `FlexibleSUSY`, one finds splendid agreement in the limit $M_S \to M_Z$ if $\tan\beta \to 1$ and $x_t = 0$, corresponding to scenarios where incomplete higher-order effects gathered by both calculations, e.g. through momentum iteration, are small. The first row in Tab. 1 shows a scenario with $\tan\beta = 3$, $M_S = M_Z$, and $x_t = 0$, where both results agree within 5 MeV (0.01%). When increasing $\tan\beta$, the two-loop differences between the two

Table 1: *Comparison of the one-loop FlexibleEFTHiggs and n-loop fixed-order $\overline{DR}'$ Higgs pole mass with `FlexibleSUSY`.*

n	$\tan\beta$	M_S	x_t	M_h^{FEFT}	M_h^{FS}	$(M_h^{\text{FEFT}} - M_h^{\text{FS}})$
1	3	M_Z	0	57.584 GeV	57.590 GeV	−0.005 GeV
1	20	M_Z	0	88.725 GeV	88.636 GeV	+0.089 GeV
1	20	M_t	0	95.612 GeV	95.999 GeV	−0.387 GeV
1	20	200 GeV	0	96.733 GeV	97.378 GeV	−0.645 GeV
1	20	500 GeV	0	105.489 GeV	107.059 GeV	−1.570 GeV
2	20	500 GeV	0	105.489 GeV	105.411 GeV	−0.078 GeV

Higgs mass values become more sizable, increasing to 0.089 GeV (0.1%) for $\tan\beta = 20$, see the second row of Tab. 1. There are several sources of such $\tan\beta$-dependent higher-order terms in both calculations: In the fixed-order calculation, for example, an iteration over the squared momentum p^2 is used to find the solution of Eq. (3.2). This iteration leads to higher-order SUSY contributions of $\mathcal{O}(y_t^n y_b^m v^2/M_S^2)$ $(n+m \geq 6)$ which increase with $\tan\beta$, for example, due to the increasing bottom Yukawa coupling y_b. In the *FlexibleEFTHiggs* approach such terms are absent because p^2-terms are taken into account only at the one-loop level, and thus no momentum iteration needs to be performed. However, in the *FlexibleEFTHiggs* calculation other $\tan\beta$-dependent higher-order terms are generated. These arise, for example, by inserting the one-loop threshold corrections for the MSSM $\overline{\text{DR}}'$ electroweak gauge couplings g_1 and g_2 into the tree-level term $m_h^{2,\text{tree}}$ on the r.h.s. of Eq. (5.2) in order to express the quartic Higgs coupling of the SM in terms of SM $\overline{\text{MS}}$ gauge couplings:

$$(M_h^{\text{MSSM}})^2 = m_h^{2,\text{tree}} + \Delta^{1\text{L}}(m_h^{\text{MSSM}})^2\,, \tag{5.22}$$

$$m_h^{2,\text{tree}} = v^2 \frac{\left(\frac{3}{5}g_1^2 + g_2^2\right)}{4} c_{2\beta}^2 \left[1 + \left(\frac{3}{5}g_1^2 + g_2^2\right)(c_{2\beta}^2 - 1)\frac{v^2}{4m_A^2}\right] + \mathcal{O}\left(\frac{v^4}{m_A^4}\right). \tag{5.23}$$

Since the tree-level MSSM $\overline{\text{DR}}'$ Higgs mass m_h^{tree} initially depends on g_1^2, g_2^2, and $c_{2\beta}$, the insertion of the threshold corrections generates two-loop terms, which are of electroweak order $\mathcal{O}(g_1^n g_2^m c_{2\beta}^{2k} v^2/m_A^2)$ and depend on $\tan\beta$. Note that these are just two of several possible sources for incomplete higher-order $\tan\beta$-dependent terms by which the two formally one-loop approximations differ.

When the SUSY scale is increased to $M_S = M_t$ (third row in Tab. 1), renormalization-group effects arise, because the scale at which the running couplings are extracted ($Q = M_Z$) is no longer identical to the scale where the Higgs pole mass is calculated ($Q = M_S = M_t$). While in *FlexibleEFTHiggs* the SM RGEs are used to evolve the running couplings from $M_Z \to M_t$, the fixed-order calculation uses MSSM RGEs. This increases the difference between the two results to $-0.387\,\text{GeV}$ (-0.4%) in our example. For larger SUSY scales, this difference increases further, as shown in the fourth and fifth rows of Tab. 1 for $M_S = 200\,\text{GeV}$ and $M_S = 500\,\text{GeV}$, respectively. For these scales, logarithmic corrections of the form $\ln(M_S/M_t)$ occur, which get resummed in the *FlexibleEFTHiggs* calculation, but not in the fixed-order one. In the latter, the inclusion of two-loop corrections must account for this difference. In fact, when two-loop corrections are included in the fixed-order calculation, see the bottom row of Tab. 1, the difference is reduced again to $-0.078\,\text{GeV}$ (-0.07%).

This analysis shows that one cannot expect perfect agreement between the *FlexibleEFTHiggs* and the fixed-order results at low SUSY scales $M_S \lesssim 200\,\text{GeV}$, even though both calculations are formally consistent at their respective accuracy level. Since the *FlexibleEFTHiggs* result is part of our hybrid scheme defined in Eq. (5.3)–(5.6), the described deviation translates into a non-convergence of M_h^{hyb} towards the three-loop fixed-order result at low SUSY scales in Fig. 12.

5.3 CONCLUSIONS

In this chapter, we presented a hybrid calculation of the light CP-even Higgs pole mass in the MSSM by combining FO and EFT results in the $\overline{\text{DR}}'$ scheme up to three-loop accuracy. To be exact, beyond the relevant two-loop FO corrections and the corresponding resummation of large logarithms through NNLL, our result includes the three-loop FO corrections and the resummation through N^{3}LL w.r.t. the strong coupling. This hybrid result is in principle reliable at arbitrary SUSY scales.

The size of terms of $\mathcal{O}(v^2/M_S^2)$ was estimated by comparing our hybrid calculation with the EFT calculation. We find that these terms are smaller than $0.25\,\text{GeV}$ as long as $M_S \gtrsim 1\,\text{TeV}$, which is the region where the degenerate-mass scenarios can be compatible with the experimental value for the Higgs mass [64]. Combining this with the fact that for $M_S \gtrsim 1.0$–$1.3\,\text{TeV}$ the EFT calculation has a smaller uncertainty than the FO calculation (see also Ref. [70, 126]), we conclude that an EFT calculation provides an excellent approximation in the MSSM for degenerate-mass scenarios, when neglecting terms of $\mathcal{O}(v^2/M_S^2)$.

The estimated uncertainty of our hybrid result is below 1 GeV in most of the relevant parameter space. Since we use the three-loop results of Ref. [15, 16] for the FO Higgs mass, which are based on approximations in various SUSY mass hierarchies, the uncertainty becomes a bit larger in specific regions of the SUSY parameter space, where none of the available approximations matches. The same holds for split SUSY spectra, where the EFT results used in our calculation become inaccurate.

Overall, we have studied the FO, the EFT, and the hybrid approach and discussed their benefits and drawbacks concerning different parameter regions in the previous three chapters. Using the implementation of all required parts into the `Himalaya` library, which has been accomplished as part of this thesis, we were able to elevate all three approaches to the three-loop level in the $\overline{\text{DR}}'$ scheme. In addition, `Himalaya` facilitates the inclusion of these three-loop contributions into spectrum generators.

Part II

HIGGS STRAHLUNG IN THE STANDARD MODEL AND BEYOND

This part is focused on the Higgs-Strahlung process at the LHC. It is one of the four most relevant production channels of the Higgs at the LHC and, in addition, provides unique features that could help detecting potential New-Physics phenomena. Specifically, we exploit a relation between the final state gauge bosons to study a particular observable based on ratios of inclusive and differential production cross sections. Further, we discuss recent progress in the inclusion of quark-mass effects to a process that can be found exclusively in Higgs production associated with a Z boson using novel algebraic techniques.

6

MEASUREMENT AND THEORY PREDICTION OF VH PRODUCTION

The relevance of Higgs production associated with a vector boson V, where $V \in \{Z, W^{\pm}\}$, was first described in Ref. [127]. This process is also commonly denoted as *Higgs Strahlung*. Although it has a lower cross section at hadron colliders compared to other Higgs production channels like gluon fusion ($gg \to H$, cf. [128]), its additional final state particles originating from the decay of the associated vector boson are able to yield clean signatures in a detector. The discovery of the Higgs-Strahlung process has been achieved in combination with the discovery of the Higgs boson decaying into a pair of bottom quarks [129, 130]. The latter yields a perfect agreement with SM predictions within the given uncertainties. Although the Higgs boson decays prevalently into bottom quarks [131], its signature is contaminated by the dominating background of $gg \to b\bar{b}$ events and only the unstable vector bosons allowed for a discovery. The V boson decays that are of foremost interest can be categorized into three channels:

- 0-lepton channel: $Z \to \nu\nu$,
- 1-lepton channel: $W \to \ell\nu$,
- 2-lepton channel: $Z \to \ell\ell$,

where ℓ denotes a charged lepton and ν a neutrino. The leptonic decay modes lead to clean signatures that can be efficiently triggered on, while rejecting most of the mutli-jet backgrounds. Already at the Tevatron the CDF and D0 collaborations reported an excess of events in VH associated production in the mass range of 120–135 GeV, with a global significance of 3.1σ [132], just four days before the Higgs boson was discovered at the LHC [2, 3]. Further evidence for VH production was announced by ATLAS and CMS in Refs. [133, 134] before its discovery was announced in Refs. [129, 130].

From the theoretical perspective, representative types of Feynman diagrams for VH production in the SM are depicted in Fig. 14. One distinguishes between the Drell-Yan (DY) type

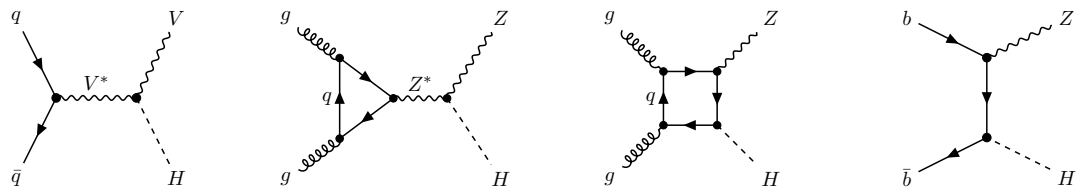

Figure 14: *Representative Feynman diagrams for VH production at hadron colliders. The first diagram from the left depicts the DY process, the second and third the gluon-initiated non-DY ZH production, and the fourth the non-DY initial $b\bar{b}$ ZH production.*

processes (left diagram of Fig. 14) and non-DY type processes (second, third, and fourth diagram from the left of Fig. 14), where the latter type only exist for ZH production. Note that the gluon-initiated process is already loop induced. The inclusive cross section of VH production is thus decomposed as:

$$\sigma^{VH} = \sigma^{VH}_{\text{DY}} + \sigma^{VH}_{\text{non-DY}}\,, \tag{6.1}$$

where, by definition, the DY component can be factorized as

$$\sigma^{VH}_{\text{DY}} = \int \mathrm{d}q^2\, \sigma_V(q^2)\, \frac{\mathrm{d}\Gamma_{V^*\to VH}}{\mathrm{d}q^2} + \Delta\sigma^{VH}_{\text{EW}}\,, \tag{6.2}$$

with σ_V being the production cross section of a V boson via the DY process and Γ is the decay rate of V to the VH final state. In Eqs. (6.1) and (6.2), the electroweak corrections $\Delta\sigma^{VH}_{\text{EW}}$ are understood to be fully attributed to σ^{VH}_{DY}, i.e. $\sigma^{VH}_{\text{non-DY}}$ does not receive any electroweak corrections by definition.

At LO in perturbation theory, one can relate the DY-like terms for WH and ZH production by changing external parameters like the gauge boson mass, the gauge coupling, or the parton distribution function (PDF), all of which can be determined independently through other processes. The effect of higher orders on this similarity between the DY components is studied in Chap. 7. In addition, it is plausible that any New Physics respects the gauge symmetry between the W and the Z boson, and thus preserves the relation between the DY-components for WH and ZH production. For example, in a general 2-Higgs-Doublet-Model (2HDM), whose Higgs sector is comparable to the MSSM, the ratio of the DY components for WH and ZH production is the same as in the SM.

In the non-DY term of Eq. (6.1) ($\sigma^{VH}_{\text{non-DY}}$) the dominant contribution in the SM is due to the gluon-initiated process $gg \to ZH$, denoted by σ_{gg}. The latter is well-defined considering QCD only since it is separately finite and gauge invariant to all orders of perturbation theory. Despite the fact that in the SM the $b\bar{b}$-initiated contributions, denoted by $\sigma_{b\bar{b}}$, are tiny compared to σ^{ZH}_{DY} or σ_{gg}, they may become important in BSM theories. Note that in $\sigma_{b\bar{b}}$ the $b\bar{b}$-DY component is not included. None of the non-DY processes have a correspondence in WH production in the SM. Therefore, we assume $\sigma^{WH}_{\text{non-DY}} = 0$ throughout this thesis.

The current theoretical precision is quite different for the two components of Eq. (6.1). While σ^{VH}_{DY} is known through NNLO QCD [135–140], i.e. $\mathcal{O}(\alpha_s^2)$, and results at threshold are even known up to N^{3}LO QCD [141, 142], the current theory prediction for the total inclusive cross section of σ_{gg} is based on the full LO calculation, which is also of $\mathcal{O}(\alpha_s^2)$ [143, 144]. At this order, σ_{gg} amounts to about 6% of the total ZH cross section for $M_H = 125\,\text{GeV}$ in proton-proton (pp) collisions at a center of mass energy $\sqrt{s} = 13\,\text{TeV}$. A full calculation of the relevant NLO corrections, i.e. $\mathcal{O}(\alpha_s^3)$, is not yet available, but in Chap. 8 we present recent

progress on the inclusion of quark-mass effects. However, assuming that it depends only weakly on the top-quark mass, the NLO K-factor,

$$K = \frac{\sigma_{gg}^{\text{NLO}}(M_t \to \infty, M_b = 0)}{\sigma_{gg}^{\text{LO}}(M_t \to \infty, M_b = 0)}\,, \tag{6.3}$$

has been found to be of the order of two, which increases the gluon-induced contribution to the total cross section accordingly [145, 146]. Higher-order terms in $1/M_t$ were evaluated in Ref. [147], but their validity is restricted to an invariant mass M_{ZH} of the ZH system of $M_{ZH} < 2M_t$. Concerning differential distributions, the amplitudes for 2- and 3-parton final states including the full quark-mass dependence have been merged in order to obtain a reliable prediction at large transverse momenta of the Higgs boson [148, 149].

For associated ZH production, additional contributions to the DY process at $\mathcal{O}(\alpha_s^2)$ exist, where a Z boson couples to a closed top- or bottom-quark loop. Their impact on the inclusive cross section is below 1% [150]. The extra non-DY component $\sigma_{b\bar{b}}$, which is known up to $\mathcal{O}(\alpha_s^2)$ in massless QCD [151], is about three orders of magnitude smaller compared to σ_{DY}^{ZH}.

For σ_{DY}^{VH}, also electroweak corrections are known [152–154], while they are unavailable for any non-DY contribution in the SM at the time of this writing. As a consequence, the estimated theoretical accuracy due to scale variation for the DY-like component is at the sub-percent level, while it reaches up to about 25% for σ_{gg} at NLO. Including NLL resummation, this reduces to about 7% [146]. The PDF uncertainties are at the 2% and 4% level for the DY and the σ_{gg} component, respectively, employing the `PDF4LHC15_100` [155] PDF sets. Implementations including NNLO with parton shower matching have been presented in Refs. [156, 157].

For illustration, Fig. 15 depicts the DY and non-DY contributions in the SM for ZH production

$$\sqrt{s} = 13\,\text{TeV}\,, \quad M_H = 125\,\text{GeV}\,, \quad M_t = 173\,\text{GeV}\,, \quad \texttt{PDF4LHC15\_nnlo\_100}$$

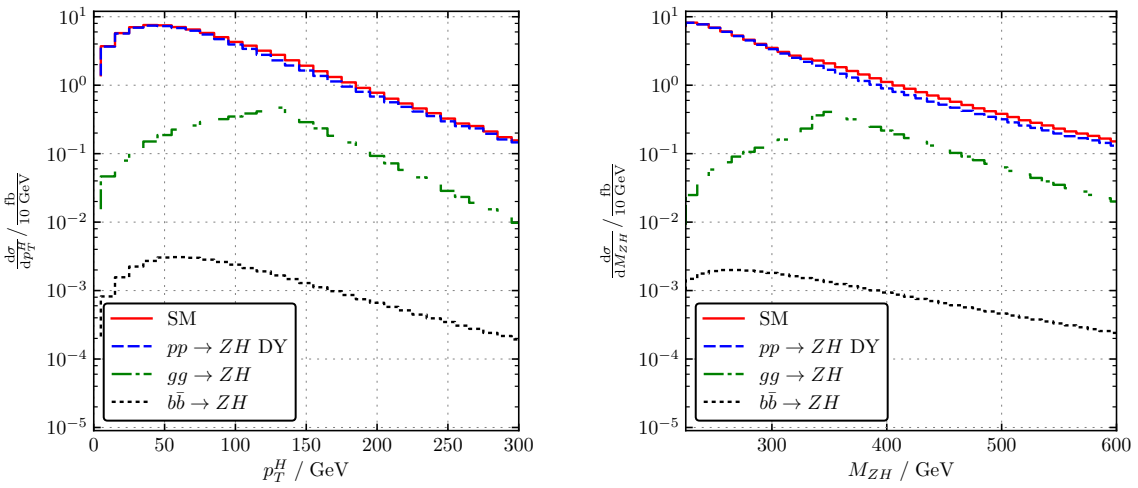

Figure 15: *Transverse-momentum (left) and invariant-mass distribution (right) of ZH production at the LHC in the SM divided into their contributions.*

including up to $\mathcal{O}(\alpha_s^2)$ corrections as distributions of transverse momentum of the Higgs, p_T^H, and invariant mass of the ZH system M_{ZH}. The latter two are defined as:

$$p_T^H = p^H \sin\theta\,, \qquad M_{ZH}^2 = \left(p^Z + p^H\right)^2\,, \tag{6.4}$$

where p^x is the four-momentum of particle x and the polar angle θ is defined as in Ref. [133]. Fig. 15 is obtained by utilizing `MCFM` [140, 158, 159] for the DY and `vh@nnlo` [160, 161] for the non-DY component. Note that only LO QCD contributions for $\sigma_{b\bar{b}}$ are included.

To set the contribution of WH and ZH production into perspective, Fig. 16 shows the same kinematical distributions as Fig. 15, but compares the complete differential cross section, i.e. the combination of DY and non-DY components, of the different final state vector bosons. The results are obtained with `MCFM` at $\mathcal{O}(\alpha_s^2)$. Adding the W^+H and W^-H results into approximately twice the contribution of ZH production. Additionally, the similarity of the DY components is evident, whereas the non-DY components in ZH production are subleading, but visible around the top-quark threshold.

$$\sqrt{s} = 13\,\text{TeV}\,, \quad M_H = 125\,\text{GeV}\,, \quad M_t = 173\,\text{GeV}\,, \quad \texttt{PDF4LHC15\_nnlo\_100}$$

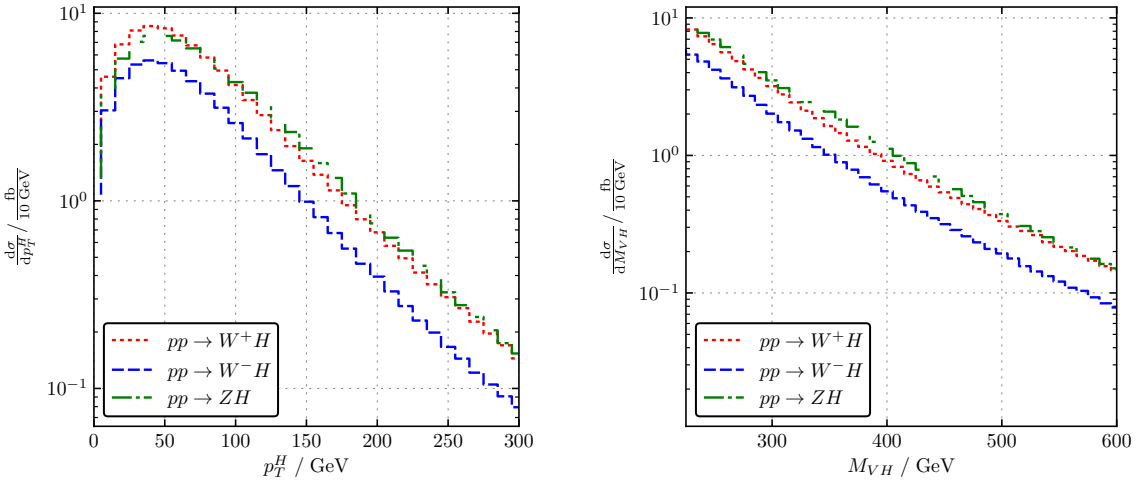

Figure 16: *Comparison of complete VH contributions to transverse momentum (left) and invariant mass distributions (right) at the LHC including $\mathcal{O}(\alpha_s^2)$ corrections.*

7

HIGGS-STRAHLUNG AS A PROBE FOR NEW PHYSICS

As already pointed out in the previous chapter, the DY processes in VH production provide many similarities, whereas the non-DY-type contributions are exclusively present for the ZH final state. This raises the question if there is a way of exploiting the symmetry of DY induced production to be sensitive to any non-DY processes, which might hint to New-Physics phenomena.[1]

Within this chapter, we try to answer this question by simulating a state-of-the-art analysis used in the discovery of the $H \to b\bar{b}$ decay. In Sect. 7.1 we start by motivating a particular ratio and present the effect of different extensions of the SM on the latter. Afterwards, in Sect. 7.2, a modified ratio is defined, that allows for an extraction of any non-DY type contributions by relating measured quantities to theoretical predictions. In Sect. 7.3 more focus is given to possible sources of theoretical uncertainties, which leads to a rough uncertainty estimate. This insight is followed in Sect. 7.4 by mimicking the analysis performed in the $H \to b\bar{b}$ discovery to estimate the significance of any non-DY contributions. These findings are then projected to the High-Luminosity-LHC (HL-LHC). The studies of this chapter are based on Ref. [163], to which A. Papaefstathiou provided the Monte-Carlo simulation. Here, we present an updated analysis using the results recently published in Ref. [129].

7.1 MOTIVATION

The gluon-initiated component reveals some interesting features which makes it particularly suited as a probe for New Physics. First of all, it is loop induced, which introduces a peculiar sensitivity to currently unknown particles that might couple the initial-state gluons to the ZH final state. Secondly, the dominant contribution in the SM is due to top-quark loops, which lead to a characteristic threshold structure in various kinematical distributions of the cross section. The application of appropriate cuts thus allows for enriching the ZH production with gluon-initiated events, as pointed out in Ref. [164]. Through the box diagrams of Fig. 14 the cross section also receives a dependence on the top Yukawa coupling, which is amplified by the fact that the box diagrams interfere destructively with the triangle diagrams of Fig. 14. Another interesting feature which appears in many BSM models are s-channel contributions due to additional Higgs bosons [165]. They either add to the triangle-component of σ_{gg}, or

1 We note that, at the level of the actual DY process of virtual V production, $pp \to V^*$, the symmetry between $V = W$ and $V = Z$ has been used before as an alternative way to measure the W-boson mass at hadron colliders [162].

they occur in the non-DY-type process $\sigma_{b\bar{b}}$. Many of such New-Physics effects on σ_{gg} as well as $\sigma_{b\bar{b}}$ can be investigated with the help of the program `vh@nnlo` [160, 161].

Deviations from the SM, like modified Yukawa couplings, new colored particles, or an extended Higgs sector, are thus likely to manifest themselves in the ZH final state through the gluon- or $b\bar{b}$-initiated component of the cross section. Apart from direct measurements, these effects could be enhanced if one considers a suitable observable. An appropriate choice might be given by the ratio

$$R^{ZH}_{\text{DY}} \equiv \frac{\sigma^{ZH}}{\sigma^{ZH}_{\text{DY}}} \equiv R^{ZH}_{\text{DY}}(x) = \frac{\mathrm{d}\sigma^{ZH}/\mathrm{d}x}{\mathrm{d}\sigma^{ZH}_{\text{DY}}/\mathrm{d}x} \tag{7.1}$$

for a distribution in a specific kinematic variable x. For illustration, Fig. 17 shows the impact of New Physics (a non-SM-Yukawa coupling in this case) on Eq. (7.1) for $x = p_T^H$. Indeed, this observable exhibits a significant dependence on New-Physics effects. Note that the local minimum at $p_T^H \sim 230\,\text{GeV}$ for $y_t = 2\,y_{t,\text{SM}}$ is an effect from the box-triangle interference. As

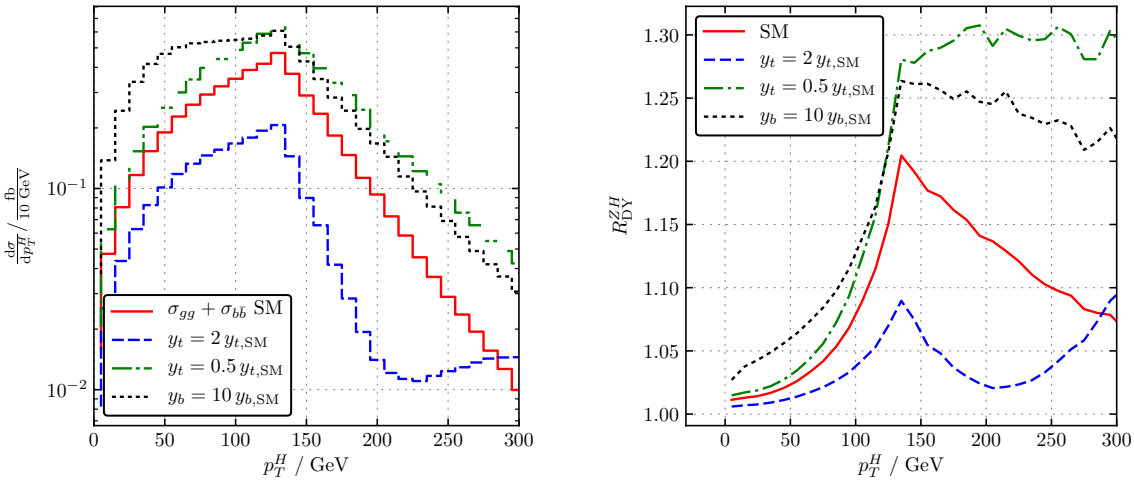

Figure 17: *The p_T^H spectrum (left) of the Higgs boson produced through the gg- and $b\bar{b}$-processes for different values of the top and bottom Yukawa couplings and their impact on R^{ZH}_{DY} (right).*

input for all numerical studies, we set

$$\sqrt{s} = 13\,\text{TeV}\,, \qquad M_H = 125\,\text{GeV}\,, \qquad M_t = 173\,\text{GeV}\,, \tag{7.2}$$

and use the `PDF4LHC15_mc` PDF sets [155] with $\alpha_s(M_Z) = 0.118$ unless otherwise stated.

In addition to p_T^H, we find that the invariant mass M_{ZH} of the ZH system is particularly well suited, since it reveals distinct features that allow to identify various New-Physics models, especially when normalized to the DY-like ZH contribution. Examples for modified Yukawa couplings are shown in Fig. 18, which include the effect of both σ_{gg} and $\sigma_{b\bar{b}}$, the latter of which becomes relevant in scenarios with enhanced bottom Yukawa coupling.

Experimentally, the invariant mass for the M_{ZH} system may be difficult to access, and other observables such as the p_T^H spectrum may be more advantageous. However, the general idea of Eq. (7.1) is independent of the choice of x and the optimal observable is best determined within an experimental analysis where all the systematic uncertainties are available.

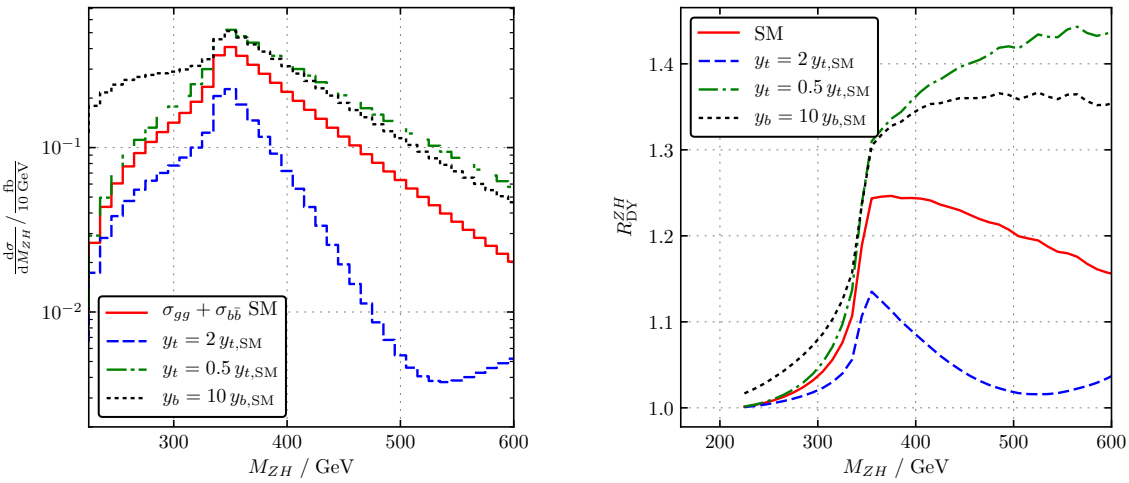

Figure 18: *The invariant mass spectrum (left) of the Higgs boson produced through the gg- and $b\bar{b}$-processes for different values of the top and bottom Yukawa couplings and their impact on R_{DY}^{ZH} (right).*

As already pointed out in Ref. [164], the contribution of σ_{gg} to the total cross section is typically rather small in the kinematical region below the top-quark threshold. The distribution above $2M_t$, on the other hand, distinctly reflects the impact of New Physics. Specifically, this region crucially depends on the top Yukawa coupling, as shown in Fig. 18. In addition, new heavy particles which contribute to the effective $ggZH$ coupling might also reveal extra threshold structures in Eq. (7.1) as a function of the invariant mass, as shown using the example of a vector-like top-quark partner T in the left panel of Fig. 19. Additional Higgs bosons which contribute through s-channel exchange lead to further features in this spectrum, see the right panel of Fig. 18, which shows R_{DY}^{ZH} for a 2HDM.[2] The peak structure is dominated by the $b\bar{b} \to ZH$ process in this case (see also Refs. [161, 163]).

7.2 EXTRACTION OF NON-DRELL-YAN CONTRIBUTIONS FROM DATA

The high accuracy to which the DY component is known theoretically suggests a simple comparison of the experimentally determined ZH rate to the theoretical prediction of its DY component in order to extract the non-DY part:

$$\frac{\sigma_{\text{non-DY}}^{ZH}}{\sigma_{\text{DY}}^{ZH}} = R_{\text{DY}}^{ZH} - 1 = \frac{\sigma^{ZH}}{\sigma_{\text{DY}}^{ZH}} - 1\,, \tag{7.3}$$

2 Details of the implementation of these models can be found in Ref. [161] and the references therein.

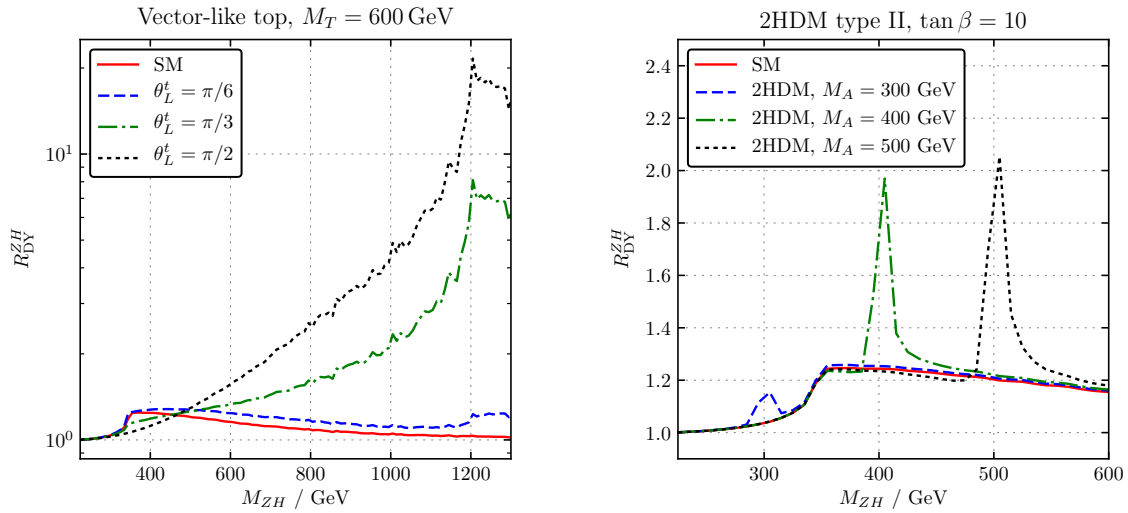

Figure 19: *Impact on R_{DY}^{ZH} of a vector-like top partner T for different mixing angles (left) and a pseudoscalar Higgs boson of the 2HDM (right).*

with the DY-like cross section, σ_{DY}^{ZH}, taken from theory, and the full ZH cross section σ^{ZH} from experiment. Such an experiment/theory comparison suffers from potential systematic uncertainties though, due to detector simulation, unfolding, and the like.

Here, we propose to analyze the data from Higgs Strahlung by making use of a very specific feature for this process which has been alluded to in Chap. 6, namely, the similarity between the ZH and the WH process. For this purpose, we define the double ratio

$$R_R^{ZW} = \frac{\sigma^{ZH}/\sigma^{WH}}{\sigma_{\text{DY}}^{ZH}/\sigma^{WH}} \equiv \frac{R^{ZW}}{R_{\text{DY}}^{ZW}}\,. \tag{7.4}$$

Obviously, if all quantities are evaluated theoretically, it is $R_R^{ZW} = R_{\text{DY}}^{ZH}$, cf. Eq. (7.1). Here, however, we suggest to take the numerator $R^{ZW} = \sigma^{ZH}/\sigma^{WH}$ of the double ratio in Eq. (7.4) from measured data. Despite the different final states for ZH and WH production, we expect that a number of systematic experimental uncertainties cancel, in particular if the parameters of the analyses for ZH and WH are aligned as much as possible. We focus more on these uncertainties in Sect. 7.4.

The denominator of Eq. (7.4), on the other hand, referred to as the DY ratio in what follows, can be calculated within the SM with rather high precision, as will be discussed in Sect. 7.3. In addition, it can hardly be affected by any New-Physics effects, because of the strong theoretical and experimental constraints on the electroweak gauge couplings (cf. Refs. [4, 131, 166–168]).

We note that the comparison of WH to ZH as a probe for New Physics has been first suggested in Ref. [165], where the 2HDM was considered as an example at the level of total cross sections, partly with boosted topology. Here, we provide a much more elaborate investigation of that proposal, on the basis of differential quantities and including an

estimate of the expected experimental uncertainty through the analysis of a simulated event sample.

7.3 THEORY PREDICTION AND SOURCES OF UNCERTAINTY OF THE DRELL-YAN RATIO

Before turning to the details of a full analysis, we study different contributions to the theory prediction of R_{DY}^{ZW} and their corresponding uncertainties in this section. Hence, we compare different orders in perturbation theory for QCD, electroweak, and initial photon contributions and their impact on R_{DY}^{ZW} for the fully inclusive as well as the fiducial cross section. In addition, scale variations are used to estimate missing higher-order corrections. The studied processes can be summarized as follows:

- $pp \to ZH \to \ell^+\ell^- + b\bar{b}$,
- $pp \to W^-H \to \ell^-\bar{\nu}_\ell + b\bar{b}$,
- $pp \to W^+H \to \ell^+\nu_\ell + b\bar{b}$,

where only the DY part for $pp \to ZH$ is included. We define the fiducial cross section according to the cuts proposed in Ref. [131], namely

$$p_T^\ell > 15\,\text{GeV}\,, \qquad \eta_\ell < 2.5\,, \qquad p_T^\nu > 15\,\text{GeV}\,, \qquad 75\,\text{GeV} < m_{\ell\ell} < 105\,\text{GeV}\,, \tag{7.5}$$

where p_T^ℓ and η_ℓ are the transverse momentum and rapidity of a charged lepton, respectively. p_T^ν is the transverse momentum of the neutrino associated with $W^\pm H$ production and $m_{\ell\ell}$ is the invariant mass of a charged lepton pair. The cut on $m_{\ell\ell}$ only applies to ZH production, of course. As we also consider the decay of the Higgs boson into a pair of b quarks, all jets are clustered according to the anti-k_T jet algorithm [169] with distance parameter $R = 0.4$. The two jets emerging from the b quark pair have to satisfy the cuts

$$p_T^{b\text{-jet}} > 25\,\text{GeV}\,, \qquad |\eta_{b\text{-jet}}| < 2.5\,. \tag{7.6}$$

Note that the clustering of jets is only considered in studies with `MCFM` since jet-clustering algorithms are not implemented in `HAWK` [153, 170, 171].

The renormalization (Q_R) and factorization scale (Q_F) are equally chosen to the invariant mass of the VH system for `MCFM` and to the sum of the pole masses of M_V and M_H for `HAWK`:

$$\texttt{MCFM}: \quad Q = Q_R = Q_F = M_{VH}\,, \qquad \texttt{HAWK}: \quad Q = Q_R = Q_F = M_V + M_H\,. \tag{7.7}$$

QCD CONTRIBUTIONS. To quantify the higher-order QCD effects to R_{DY}^{ZW} for both the total and the differential cross section we utilize `MCFM`. As PDFs we choose the `NNPDF30` [172] sets with $\alpha_s(M_Z) = 0.118$ and consider all contributions up to NNLO, i.e. $\mathcal{O}(\alpha_s^2)$. The final state leptons are selected as electrons and their corresponding neutrino.

At the level of the total cross section, R_{DY}^{ZW} receives corrections of only 0.2% at NLO, while the NNLO corrections on top of that are at the per-mill level. This is quite remarkable as the NLO corrections on the numerator and denominator in that ratio amount to 16%. The NNLO corrections amount to less than 1% on top of that.

As a function of M_{VH}, the NLO corrections on the DY-ratio are at or below the 1% level without jet clustering, as shown in Fig. 20. Including NNLO contributions, the impact on the DY-ratio is below the 1% level in relation to the NLO result. This holds for both the fully inclusive as well as the fiducial cross section. Therefore, we neglect the NNLO corrections to the DY process in the following and estimate the uncertainty due to uncalculated QCD corrections to be less than 1% for the NLO prediction.

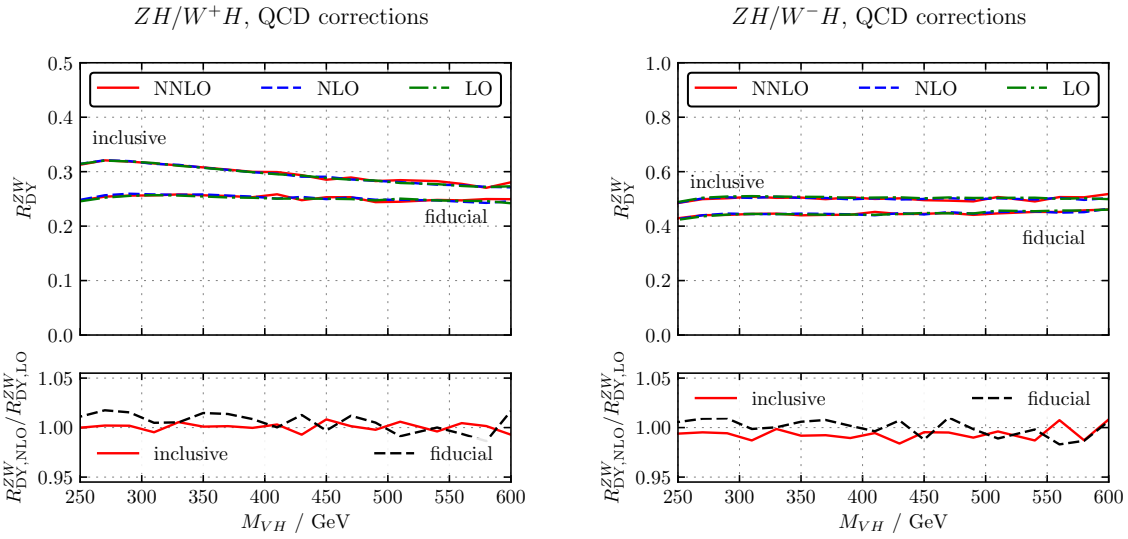

Figure 20: *QCD corrections to the ratio R_{DY}^{ZW} for (left) $W = W^+$ and (right) $W = W^-$ as a function of the VH invariant mass. The lines in the upper parts of the plots show the LO, NLO, and NNLO QCD result. The lower parts show the ratio of the NLO to the LO result.*

Applying jet clustering with the anti-k_T algorithm, the discussion from above does not change qualitatively. Comparing NNLO and NLO QCD corrections results to a comparable impact on R_{DY}^{ZW} as without jet clustering, see Fig. 21. Note that the total cross section remains unaffected by employing the anti-k_T algorithm. As we give just a rough estimate on the theoretical uncertainty incorporating QCD corrections, we do not include the effect of jet clustering in our uncertainty estimate and postpone it to a more comprehensive analysis.

PDF uncertainties for the QCD contributions and scale variations have been estimated in Ref. [163], resulting in uncertainties that are almost constant over the studied invariant mass spectrum and below 1% at NLO, when the scales $Q_R = Q_F$ were varied by a factor of two. This low uncertainty is due to cancellations within R_{DY}^{ZW} when assuming that the individual uncertainties are fully correlated between the *ZH* and the *WH* process. This assumption is justified from the identical form of the DY-like QCD corrections.

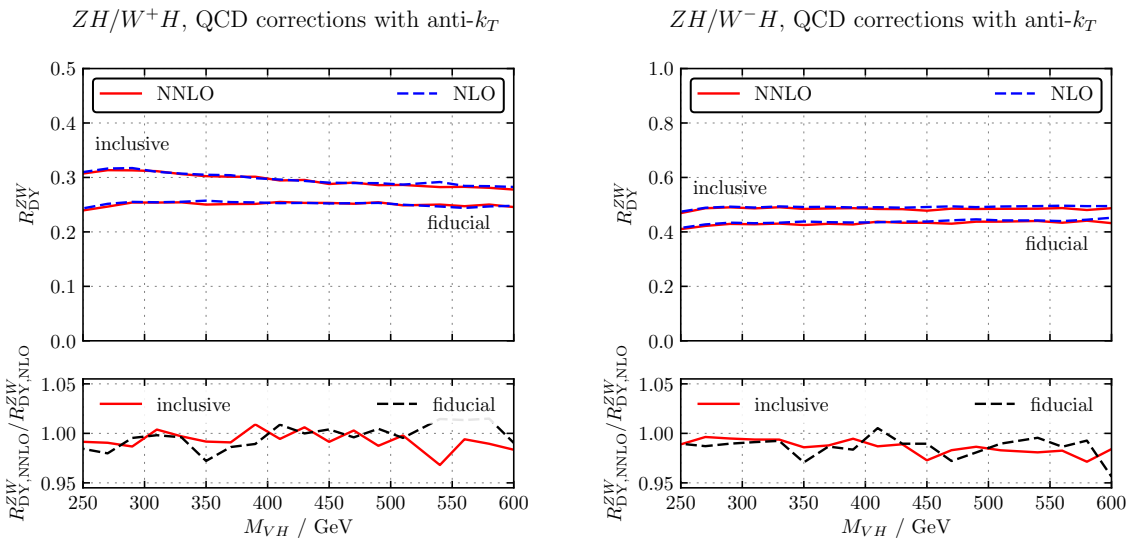

Figure 21: *Effects of jet clustering for QCD corrections to the ratio R^{ZW}_{DY} for (left) $W = W^+$ and (right) $W = W^-$ as a function of the VH invariant mass. The lines in the upper parts of the plots show the NLO and NNLO QCD result. The lower parts show the ratio of the NNLO to the NLO result.*

ELECTROWEAK CONTRIBUTIONS. Due to the different electric charge of W and Z bosons and their different decay patterns, one may expect a larger sensitivity of the ratio R^{ZW}_{DY} to electroweak corrections in comparison to the QCD effects. Indeed, employing HAWK to

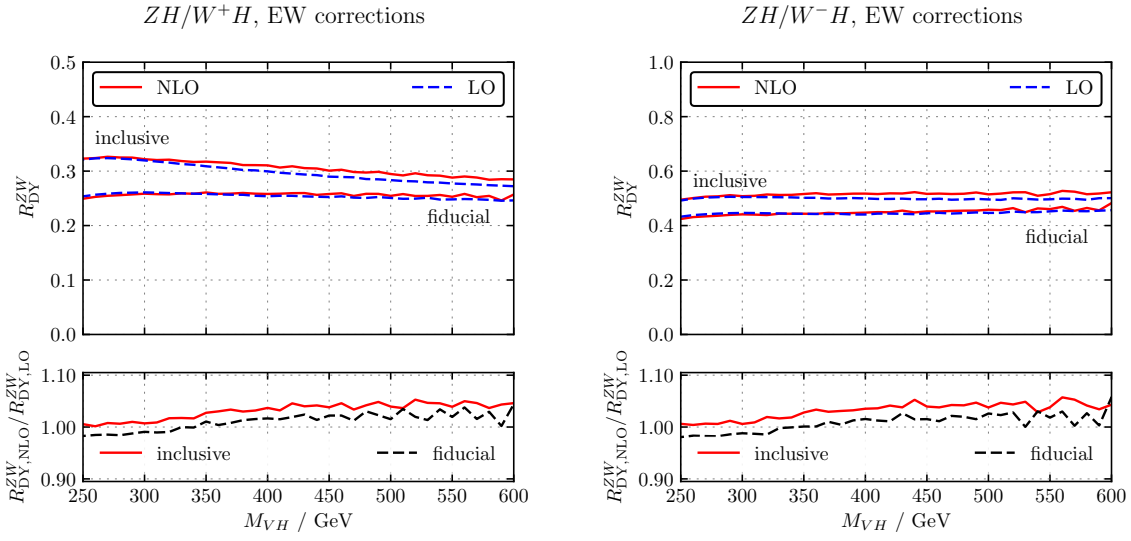

Figure 22: *Electroweak corrections to the ratio R^{ZW}_{DY} for (left) $W = W^+$ and (right) $W = W^-$ as a function of the VH invariant mass. The lines in the upper parts of the plots show the LO, NLO electroweak result. The lower parts show the ratio of NLO to LO.*

study these effects, we find that they amount up to about 5% on R^{ZW}_{DY} without considering recombination of final-state leptons, see Fig. 22. Compared to the QCD corrections, the electroweak effects on R^{ZW}_{DY} show a stronger dependence on M_{VH}, albeit in a continuous and monotonous way.

INCOMING PHOTON CORRECTIONS. An additional electroweak contribution is due to photon-induced processes, $\gamma q \to qVH$, referred to as σ_γ in what follows. Although σ_γ amounts to at most about 7% to the inclusive VH production cross section, its effect on the M_{VH} distribution of the ZH/WH ratio reaches the 20% level at $M_{VH} = 600\,\text{GeV}$, as illustrated in Fig. 23 using the `LUXqed17_plus_PDF4LHC15` PDF set [173]. Recent theoretical progress in the determination of the photon PDFs [173] allows us to neglect this source of uncertainty in our analysis, because the uncertainty on σ_γ has been reduced significantly [174]. The inclusion of both NLO EW and photon-induced corrections is usually performed by adding correction factors δ_x, $x \in \{\text{EW}, \gamma\}$ to the tree-level DY cross section σ_0 as $\sigma_0(1 + \delta_{\text{EW}} + \delta_\gamma)$ [153]. δ_γ is understood to be the correction factor for photon-induced contributions. A variation of the electroweak factorization scale by a factor of two around the central value of $M_V + M_H$ changes $\delta_{\text{EW}} + \delta_\gamma$ by less than 4% and would thus be invisible in Fig. 22 and 23.

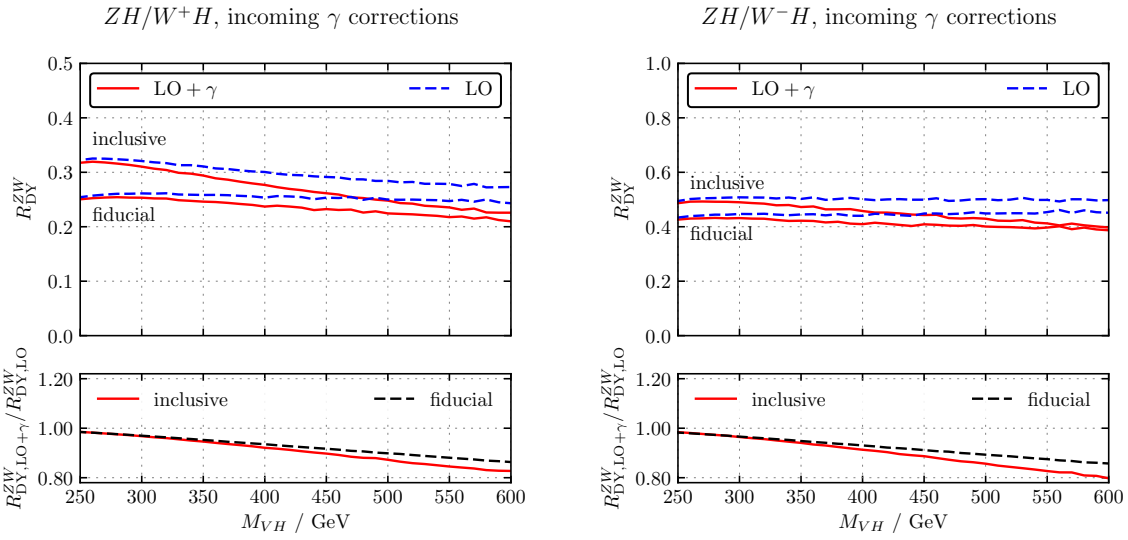

Figure 23: Incoming photon corrections to the ratio R^{ZW}_{DY} for (left) $W = W^+$ and (right) $W = W^-$ as a function of the VH invariant mass. The lines in the upper parts of the plots show the LO and LO with incoming γ corrections. The lower parts show the ratio of photon-induced corrections to the LO contribution.

7.4 NUMERICAL RESULTS

In this section, we study the double ratio defined in Eq. (7.4) and provide a rough estimate of the uncertainty on R^{ZW}_R by combining the theoretical uncertainty on R^{ZW}_{DY} with the experimental one on R^{ZW} through

$$\left(\frac{\delta R^{ZW}_R}{R^{ZW}_R}\right)^2 = \left(\frac{\delta R^{ZW}_{\text{DY}}}{R^{ZW}_{\text{DY}}}\right)^2_{\text{th}} + \left(\frac{\delta R^{ZW}}{R^{ZW}}\right)^2_{\text{exp}}, \tag{7.8}$$

where the subscripts indicate that the first term is obtained through a theoretical calculation and the second through an experimental measurement. The quadratic sum of theoretical and experimental uncertainties is justified by the low level of correlation between the two. We assume total integrated luminosities for pp collisions at $\sqrt{s} = 13\,\text{TeV}$ of (a) $\mathcal{L} = 36.1\,\text{fb}^{-1}$, (b) $\mathcal{L} = 300\,\text{fb}^{-1}$, and (c) $\mathcal{L} = 3000\,\text{fb}^{-1}$, corresponding to (a) the ATLAS luminosity underlying the analysis of Ref. [133], (b) the end of LHC run 3, and (c) the future HL-LHC run.

We begin by outlining the details of our event simulation and their respective analysis in Subsect. 7.4.1. In Subsect. 7.4.2 and 7.4.3 we study the impact of our analysis on R_R^{ZW} and estimate the experimental uncertainty of Eq. (7.8). Afterwards, in Subsect. 7.4.4 and 7.4.5, we turn to a quantitative study of R_R^{ZW} including rough uncertainty estimates for Eq. (7.8) and provide a significance to detect the gluon-initiated ZH production process.

7.4.1 *Outline of the simulation and analysis*

We construct a hadron-level simulation, including decays of the vector bosons and the Higgs boson. As in Subsect. 7.3, we consider leptonic decays of the vector bosons,

$$W^+ \to \ell^+ \nu_\ell\,, \qquad W^- \to \ell^- \bar{\nu}_\ell\,, \qquad Z \to \ell^+ \ell^-\,, \tag{7.9}$$

where $\ell \in \{e, \mu\}$, and Higgs boson decays to $b\bar{b}$ pairs. The parton-level events for signal and backgrounds are generated at NLO QCD using `MadGraph5_aMC@NLO` [175, 176] for all samples, except for gluon-induced ZH production which is generated at leading order. To take into account the NLO QCD corrections on $gg \to ZH$, we apply a global K-factor of $K = 2$ [145, 147]. For all samples, we employ the `PDF4LHC15_nlo_mc` PDF set [155]. Parton showering as well as hadronization and modeling of the underlying event is performed within the general-purpose Monte-Carlo event generator `HERWIG 7` [177, 178]. Since electroweak corrections largely cancel in the double ratio R_R^{ZW}, they can be neglected in our event simulation.

As background processes we consider $pp \to t\bar{t}$, $pp \to W^\pm b\bar{b}$, $pp \to Zb\bar{b}$ and single top production. In this simplified phenomenological analysis, we do not consider any backgrounds of jets emerging from u, d, and s quarks, or gluons, which are mis-identified as b-jets, nor those coming from mis-identified leptons. These events are expected to be sub-dominant with respect to the irreducible backgrounds, as is indeed the case in Ref. [133], for example. To approximately take into account the NNLO corrections on the $pp \to t\bar{t}$ background, we apply a global K-factor of $K = 1.2$ [179].

Jets are reconstructed employing the anti-k_T algorithm, implemented in the `FastJet` package [180, 181] with distance parameter $R = 0.4$. The jet transverse momentum is required to be larger than 20 GeV for *central jets*, i.e. $|\eta| < 2.5$, and larger than 30 GeV for *forward jets*, i.e. $2.5 < |\eta| < 5$. Selected central jets are labeled as *b-tagged* if a b-hadron is found within the jet. A b-tagging efficiency of 70% is considered, flat over the transverse momentum of the

jets, to reproduce the efficiency of the experimental b-tagging algorithm of Ref. [133]. The leading b-jet is required to have a transverse momentum larger than 45 GeV. The missing transverse energy, E_T^{miss}, is taken as the negative sum of transverse momenta of all visible particles. Electrons and muons are subject to isolation criteria by requiring the scalar sum of the transverse momenta of tracks in $R = 0.2$ around them to be less than one tenth of their transverse momentum:

$$\sum_{R<0.2} p_T^{\text{tracks}} < 0.1\, p_T^{\ell}\,. \tag{7.10}$$

The 13 TeV ATLAS analysis of Ref. [133] considered three event selections, corresponding to the $Z \to \nu\bar{\nu}$, the $W \to \ell\nu$, and the $Z \to \ell\ell$ channels. In our analysis, we only consider the 1- and 2-lepton channel. All selections require exactly two b-tagged central jets, used to define the invariant mass $M_{b\bar{b}}$. For the $W \to \ell\nu$ selections, events with more than three central and forward jets are discarded.

In order to suppress top-quark-related background in the $W \to \ell\nu$ analysis, we set a cut (see below) on the reconstructed top-quark mass m_{top}. The latter is calculated as follows. First, the neutrino four-momentum is reconstructed by assuming that its transverse component is equal to the missing transverse momentum, $p_T^{\nu} = E_T^{\text{miss}}$, and then the quadratic equation

$$(p^{\nu} + p^{\ell})^2 = M_{\text{W}}^2 \tag{7.11}$$

is solved for the z-component p_z^{ν}. Afterwards, the two resulting solutions are used to construct two possible W four-momenta.[3] These two W four-momenta are then combined with the four-momentum of one of the b-jet candidates, and out of those combinations the one with an invariant mass m_{top} closest to the top mass of $M_t = 173$ GeV is selected. A cut on m_{top} combined with an additional cut on the invariant mass of the $b\bar{b}$ system reduces the background originating from $V + b\bar{b}$ signatures that emerge from $t\bar{t}$ and single top productions significantly [133].

Further requirements on the 1- and 2-lepton channels are as follows:

$Z \to \ell\ell$:

Exactly two same-flavor leptons with $p_T > 7$ GeV and $|\eta| < 2.5$, of which at least one has $p_T > 25$ GeV are required. Due to charge misidentification of electrons, only for muons an opposite charge is mandatory. The invariant mass of the two leptons is restricted to 81 GeV $< m_{\ell\ell} <$ 101 GeV and the transverse momentum of the Z needs to be larger than 150 GeV.

$W \to \ell\nu$:

Exactly one lepton with $p_T > 25$ GeV and $|\eta| < 2.5$ is required. The transverse momentum of the W boson has to be greater than 150 GeV and the transverse missing

3 In the case of a negative discriminant in the quadratic equation, the E_T^{miss} vector is rescaled such that the discriminant becomes zero. The rescaling factor on the two E_T^{miss} vector components is chosen to be the same.

energy is enforced to be $E_T^{\text{miss}} > 30\,\text{GeV}$ in the electron sub-channel. Finally, cuts on the invariant mass of the $b\bar{b}$ system and the reconstructed top mass are set to $m_{b\bar{b}} > 75\,\text{GeV}$ or $m_{\text{top}} \leq 225\,\text{GeV}$.

The events passing the selection cuts are subject to a *dijet-mass analysis*, following closely that of Ref. [133], where the boosted-decision-tree discriminant (labeled BDT_{VH} in Ref. [133]) of the multivariate analysis is replaced by the invariant mass of the b-tagged jets. This results in ten signal regions, shown in the second and third rows of Tab. 12 in Ref. [133]. In our analysis, only signal regions with $p_T^V > 150\,\text{GeV}$ are included. We have further applied the requirement $110\,\text{GeV} \leq m_{b\bar{b}} \leq 140\,\text{GeV}$, which efficiently selects events containing $H \to b\bar{b}$. The expected number of events predicted by the Monte-Carlo level analysis at the selection level are similar to those of Ref. [133].

7.4.2 *Impact of the hadron-level analysis on the Drell-Yan ratio*

To estimate the impact of the hadron-level analysis on the DY ratio defined in Eq. (7.1), Fig. 24 compares the hadron-level prediction of the ratio R_{DY}^{ZW} after analysis cuts to the parton-level prediction. The parton-level prediction is obtained from the truth-level W and Higgs boson momenta, whereas the hadron-level curve is constructed through the combination of the reconstructed four-momenta of the W boson and the Higgs boson. For the W boson, a random choice is made between the two solutions for the z-component of the neutrino momentum. Fig. 24 shows that this ratio is only moderately affected by the analysis and can be thus calculated fairly reliably within perturbation theory for the inclusive cross section. It is conceivable that the analysis could be modified appropriately to preserve more closely the parton-level form of R_{DY}^{ZW}.

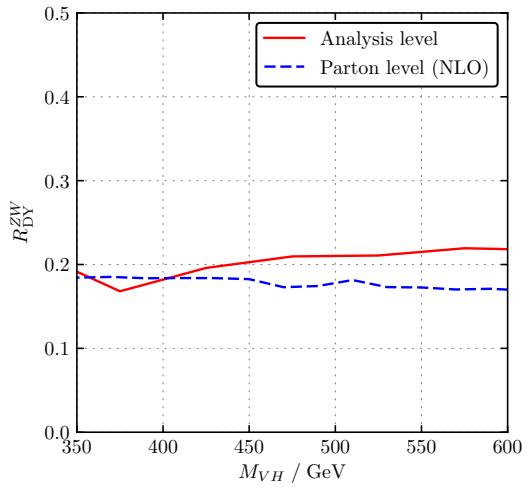

Figure 24: *Comparison of the hadron-level to the parton-level analysis on R_{DY}^{ZW}. The data is taken from [163].*

7.4.3 *Calculation of experimental uncertainties*

The experimental ratio R^{ZW} is evaluated from

$$R^{ZW} = \frac{\mathrm{d}N^{ZH}}{\mathrm{d}N^{WH}} = \frac{\mathrm{d}N^{\ell\ell} - \mathrm{d}N^{\ell\ell}_{\mathrm{bkg}}}{\mathrm{d}N^{\ell} - \mathrm{d}N^{\ell}_{\mathrm{bkg}}}, \tag{7.12}$$

where $\mathrm{d}N^X$ and $\mathrm{d}N^X_{\mathrm{bkg}}$, with $X \in \{\ell, \ell\ell\}$, represent the total number of events and the number of background events per bin, with an $Xb\bar{b}$ final state, respectively. The uncertainty due to background subtraction will be included in the estimate of the overall systematic uncertainty. The statistical uncertainty on R^{ZW} originating from the expected total number of collected event samples is given by

$$\left(\frac{\delta R^{ZW}}{R^{ZW}}\right)^2_{\mathrm{stat.}} = \left(\frac{\partial R^{ZW}}{\partial(\mathrm{d}N^{\ell\ell})}\right)^2 \delta(\mathrm{d}N^{\ell\ell})^2 + \left(\frac{\partial R^{ZW}}{\partial(\mathrm{d}N^{\ell})}\right)^2 \delta(\mathrm{d}N^{\ell})^2 . \tag{7.13}$$

If we assume the expected number of events in each bin to be large enough, then $\mathrm{d}N^X$ is Gaussian-distributed with uncertainty $\delta(\mathrm{d}N^X) = \sqrt{\mathrm{d}N^X}$, yielding:

$$\left(\frac{\delta R^{ZW}}{R^{ZW}}\right)^2_{\mathrm{stat.}} = \frac{\mathrm{d}N^{\ell\ell}}{(\mathrm{d}N^{\ell\ell} - \mathrm{d}N^{\ell\ell}_{\mathrm{bkg}})^2} + \frac{\mathrm{d}N^{\ell}}{(\mathrm{d}N^{\ell} - \mathrm{d}N^{\ell}_{\mathrm{bkg}})^2} . \tag{7.14}$$

We define the systematic uncertainty on R^{ZW} to include all uncertainties that contribute to its experimental measurement. A precise determination of these systematics would require a comprehensive experimental analysis that takes into account all the correlations between the different contributing components. In this work, however, we content ourselves with an estimate of the uncertainty derived from the separate *ZH* and *WH* signal strengths of Eq. (7.15), presented in the ATLAS analysis of Ref. [129] which uses the same cuts as Ref. [133]:

$$\begin{aligned} \mu_{ZH} &= 1.20^{+0.23}_{-0.23}(\mathrm{stat.})^{+0.23}_{-0.20}(\mathrm{syst.}) , \\ \mu_{WH} &= 1.08^{+0.27}_{-0.27}(\mathrm{stat.})^{+0.38}_{-0.34}(\mathrm{syst.}) . \end{aligned} \tag{7.15}$$

The systematic uncertainty of these results includes all sources of experimental nature, related to the background- and signal-Monte-Carlo simulation and data-driven estimates, and to the finite size of the simulated samples.

We assume that the (symmetrized) systematic uncertainties $(\delta\mu_{VH})_{\mathrm{syst.}}$ can be propagated directly to the experimental ratio defined by Eq. (7.12), and thus to the double ratio by

$$\begin{aligned} \left(\frac{\delta R^{ZW}_R}{R^{ZW}_R}\right)^2_{\mathrm{syst.}} &= (\delta\mu_{ZH})^2_{\mathrm{syst.}} + (\delta\mu_{WH})^2_{\mathrm{syst.}} - 2\, p_{ZW}\, (\delta\mu_{ZH})_{\mathrm{syst.}} (\delta\mu_{WH})_{\mathrm{syst.}} \\ &= 0.046 + 0.130 - 0.155\, p_{ZW} , \end{aligned} \tag{7.16}$$

where p_{ZW} parameterizes the correlation of the systematic uncertainties between ZH and WH production. In the next section, we present results for R_R^{ZW} assuming different values of p_{ZW} and luminosities for integrated quantities.

7.4.4 *Semi-inclusive results*

Tab. 2 shows the results for no correlation ($p_{ZW} = 0$), 50% correlation ($p_{ZW} = 0.5$), and full correlation ($p_{ZW} = 1$) for different luminosities and kinematic regions.[4] The statistical

Table 2: *Numerical results for the double ratio R_R^{ZW} and the associated statistical and systematic uncertainties, obtained by mimicking the analysis of Ref. [133]. We assume that restricting M_{VH} does not effect the systematic uncertainty.*

		stat. ($\mathcal{L}/\text{fb}^{-1}$)			syst. (p_{ZW})		
	R_R^{ZW}	36.1	300	3000	0	0.5	1
all M_{VH}	1.49	$\pm$0.90	$\pm$0.31	$\pm$0.10	$\pm$0.63	$\pm$0.47	$\pm$0.22
restricted M_{VH}	1.55	$\pm$1.08	$\pm$0.38	$\pm$0.12	$\pm$0.63	$\pm$0.47	$\pm$0.22

uncertainty is evaluated for three values of the integrated luminosity ($\mathcal{L} = 36.1$, 300, and $3000\,\text{fb}^{-1}$). From the hadron-level selection described in Subsect. 7.4.1, it has been found that the analysis of Ref. [133] favors events with $M_{VH} \gtrsim 350\,\text{GeV}$. Furthermore, we find that, in the present analysis, the gluon-induced ZH production process contributes substantially up to $M_{VH} \sim 650\,\text{GeV}$. Therefore, we also present results where the events are restricted to $350\,\text{GeV} < M_{VH} < 650\,\text{GeV}$ in the second line of Tab. 2. Note that only the signal regions with $p_T^V > 150\,\text{GeV}$ are included. Beyond enhancing the $gg \to ZH$ process contribution, this also ensures that the 1-lepton and 2-lepton analyses select similar phase space regions so as to facilitate the cancellation of systematic uncertainties in the ratio. Due to the present rudimentary treatment of systematic uncertainties, these are only considered inclusively, and thus assumed unchanged by this restriction on the M_{VH} range. Future experimental analyses, which exhibit information on the correlations between systematics, should be able to provide a more differential estimation.

As expected, at luminosities that are projected for the HL-LHC ($3000\,\text{fb}^{-1}$) the statistical uncertainty decreases significantly. Further studies on the correlation of systematics and a more tailored analysis would help to decrease the systematic uncertainty as well. The restriction on the invariant mass of the VH system only affects the statistical uncertainty mildly.

4 An earlier version of these results, based on lower statistics of our simulation, has been presented in Ref. [182] and with full statistics in [163].

From the numbers of Tab. 2, one may evaluate the significance s to which the non-DY component can be observed through

$$s/\sigma = \frac{\sigma^{ZH}_{\text{non-DY}}}{\delta\sigma^{ZH}_{\text{non-DY}}} = \frac{R^{ZW}_R - 1}{\delta R^{ZW}_R} = \frac{R^{ZW}_R - 1}{\sqrt{(\delta R^{ZW}_R)^2_{\text{stat.}} + (\delta R^{ZW}_R)^2_{\text{syst.}}}} \,. \tag{7.17}$$

For $\mathcal{L} = 3000\,\text{fb}^{-1}$, we thus find that the gluon-initiated component for ZH production as predicted by the SM gives only a 2.2σ effect for the restricted M_{VH} sample assuming full correlation of the systematic uncertainties between ZH and WH production. In case the systematic uncertainties can be decreased down to half the current value, the significance increases to 3.4σ. Note that these projected significances are slightly improved in comparison to Ref. [163] due to the reduced systematic uncertainty of Ref. [129]. Considering the fact that New-Physics models typically enhance the gluon-initiated component, a dedicated experimental analysis which is tailored to isolate this component and optimized for the ZH/WH ratio measurement therefore seems appealing.

Let us close this section by comparing these results to the direct extraction of the non-DY component from R^{ZH}_{DY} as sketched at the beginning of Sect. 7.2. In this case and for $\mathcal{L} = 3000\,\text{fb}^{-1}$, the statistical and systematic uncertainty is given by

$$\left(\delta R^{ZH}_{\text{DY}}\right)_{\text{stat.}} = 0.14\,\left(R^{ZH}_{\text{DY}} - 1\right) \qquad \text{and} \qquad \left(\delta R^{ZH}_{\text{DY}}\right)_{\text{syst.}} = R^{ZH}_{\text{DY}}\,(\delta\mu_{ZH})_{\text{syst.}}\,, \tag{7.18}$$

respectively, if we follow the analogous reasoning as above. Using our central value for the double ratio in the restricted-M_{VH} region for R^{ZH}_{DY}, this leads to a signal significance of 1.6σ. Assuming that the systematic uncertainty can be reduced by a factor of two, the significance for $R^{ZH}_{\text{DY}} \neq 1$ increases to 3σ. Comparing this to R^{ZW}_R, we find that the direct measurement of R^{ZH}_{DY} is competitive as long as the correlation between the systematic ZH and WH uncertainties is smaller than about 85%, i.e. roughly the value of p_{ZW} where the correlation term in Eq. (7.16) cancels $(\delta\mu_{WH})_{\text{syst.}}$. At this point it is important to keep in mind that, as argued at the beginning of Sect. 7.2, we also expect significant contributions to the uncertainty from the theoretical input to R^{ZH}_{DY}, while they should be negligible for R^{ZH}_R. This means that already a significantly lower ZH/WH correlation should lead to an improved extraction of the non-DY contribution by using the double ratio R^{ZW}_R.

7.4.5 *Differential results*

In this section, we turn to differential results of R^{ZW}_R using the M_{VH} distribution. Fig. 25a demonstrates how an experimental measurement would look like, assuming that a gluon-

initiated ZH production exists in the measurement at the level of the SM prediction. The double ratio R_R^{ZW} is then given by:

$$R_R^{ZW} = 1 + \frac{\mathrm{d}N_{gg}^{ZH}}{\mathrm{d}N_{\mathrm{DY}}^{ZH}} \tag{7.19}$$

Fig. 25a also shows the theoretical parton-level distribution as blue dashes, where no cuts are applied. The theoretical prediction and experimental expectation are in good agreement in this range of invariant masses of the VH system. Note that the ATLAS analysis of Ref. [133] was not constructed to detect the $gg \to ZH$ component. It is thus conceivable that an analysis can be devised to increase its contribution to the total ZH production with respect to the parton-level prediction. Fig. 25b shows the resulting fractional uncertainties originating from

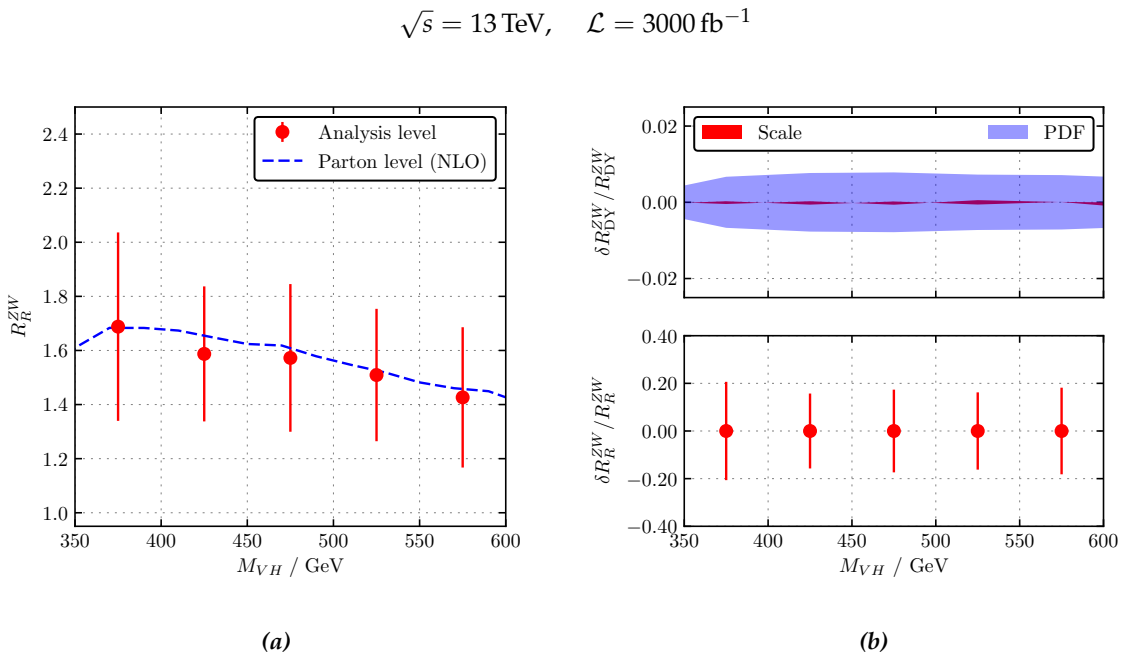

(a) ***(b)***

Figure 25: *(a): Hadron-level result of the differential double ratio R_R^{ZW} in comparison to the parton-level result. The size of the uncertainty bars indicates the total theoretical and statistical uncertainty as given by Eq. (7.8). (b): Theoretical uncertainty (upper panel) and experimental uncertainty (lower panel) as defined by Eq. (7.8). The data is taken from [163].*

theory or data statistics as a function of the VH-system's invariant mass. The upper panel shows the theoretical uncertainty, i.e. the first term in Eq. (7.8), obtained by considering the scale and PDF variations after applying the hadron-level analysis. In the lower panel, the error bars show the total uncertainty as dictated by Eq. (7.8), i.e. the combination of the theoretical and statistical uncertainties for an integrated luminosity of $\mathcal{L} = 3000\,\mathrm{fb}^{-1}$, but excluding experimental systematic uncertainties. We refrain from assessing the latter as their differential behavior would be challenging to predict at this stage. It is evident that the statistical uncertainty originating from the equivalent data sample size for an integrated luminosity of $\mathcal{L} = 3000\,\mathrm{fb}^{-1}$, $\mathrm{d}N^X$, dominates over the theoretical uncertainty.

7.5 CONCLUSIONS

In this chapter, we investigated New-Physics effects in the gluon-initiated Higgs-Strahlung process and demonstrated that the ZH invariant mass distribution provides a particularly sensitive probe for physics beyond the SM. While the invariant-mass distribution below the $t\bar{t}$ threshold, $M_{ZH} < 2M_t$, remains rather unperturbed and thus may serve as a gauge for the experimental data, all New-Physics effects studied here can be clearly identified, and to a large extent even distinguished, by the kinematic region above that threshold. Recall that the low-M_{ZH} region is also under fairly good theoretical control due to existing higher-order perturbative calculations in the large-M_t limit [147].

Mimicking the phenomenological analysis of Ref. [133] at the hadronic level, we find that the SM σ_{gg} component can be established at the $\sim 3.4\sigma$-level at the HL-LHC by comparing the experimental data to the theory prediction for the ratio of DY-like ZH production to WH production in the one- and two-lepton channels. We found that the estimate of systematic uncertainties becomes the limiting factor for the measurement, highlighting the importance of a detailed investigation of systematic effects, and potentially an optimization of the experimental analysis towards the extraction of this ratio from data. However, including the zero-lepton channel and optimizing the current analyses for the $gg \to ZH$ process would most likely allow to reveal an $\mathcal{O}(5\sigma)$-level signal.

Nonetheless, in order to uniquely establish New-Physics effects from this method, the theoretical control of the $gg \to ZH$ component needs to be increased further, for example by including SM top-mass effects at NLO QCD. Therefore, the next chapter is dedicated to achieve progress on incorporating quark-mass effects at NLO QCD for gluon-induced ZH production. Additionally, novel algebraic techniques and their implementation are presented, which ease the computational complexity of comparable calculations.

8

TOWARDS QUARK-MASS EFFECTS IN GLUON-INDUCED ZH PRODUCTION AT NLO QCD

The two-loop QCD corrections to the gluon-induced ZH production have been calculated in Refs. [145, 147] in the limit of an infinitly heavy top-quark mass while setting the bottom-quark mass to zero. Using these approximations, it was shown that the two-loop results enhance the gluon-initiated process by roughly 100% and lead to a K-factor of $K \approx 2$ [145, 147]. However, following the analysis of the previous chapter, these approximations are not sufficient if one tries to search for New-Physics effects using the double ratio defined in Eq. (7.4) due to theoretical uncertainties. Therefore, we summarize the progress achieved within this thesis in the calculation of the NLO QCD, i.e. $\mathcal{O}(\alpha_s^3)$, corrections incorporating quark-mass effects in this chapter.

For a full NLO QCD calculation, which is part of the hadronic N^{3}LO calculation, real and virtual corrections that contribute to $\mathcal{O}(\alpha_s^3)$ are needed. Thus, the required ingredients are:

1. Leading-order (one-loop) amplitude $\mathcal{A}_{1\mathrm{L}}(\alpha_s)$ with a gg initial state, where $\mathcal{A}_{n\mathrm{L}}$ depicts the amplitude at n-loop level,
2. Interference of the one-loop amplitude with its virtual corrections at the two-loop level,

$$\mathcal{A}_{1\mathrm{L}}^{*}(\alpha_s) \cdot \mathcal{A}_{2\mathrm{L}}(\alpha_s^2)\,, \tag{8.1}$$

3. Real corrections at the one-loop level with $q\bar{q}$, qg, $\bar{q}g$, and gg initial states.

Within the scope of this thesis, we only focus on virtual contributions and exclude any one-particle-reducible two-loop subgraphs. At the current stage, we do not aim for a complete result including renormalization and the calculation of master integrals, but rather concentrate on the reduction of integrals occurring in the amplitude to a set of master integrals (cf. Sect. 8.5) by keeping intermediate steps as general as possible.

The remainder of this chapter is structured as follows. We start by summarizing the setup of the calculation followed by a brief interlude of finite-field-interpolation techniques, which have been developed during this thesis and are essential for this calculation. This chapter is closed with an overview of recent progress, which includes an almost complete reduction to a set of master integrals. We stress again that the results obtained in this chapter are still incomplete at the time of this writing and that we only aim to provide a proof-of-principle study concerning the reduction of Feynman integrals of comparable complexity using functional-interpolation techniques over finite fields.

8.1 FEYNMAN DIAGRAMS AND GAUGE CHOICE

The LO contribution to gluon-induced ZH production is already loop induced and, in a general R_ξ gauge, three classes of Feynman diagrams, shown in Fig. 26, contribute. On the

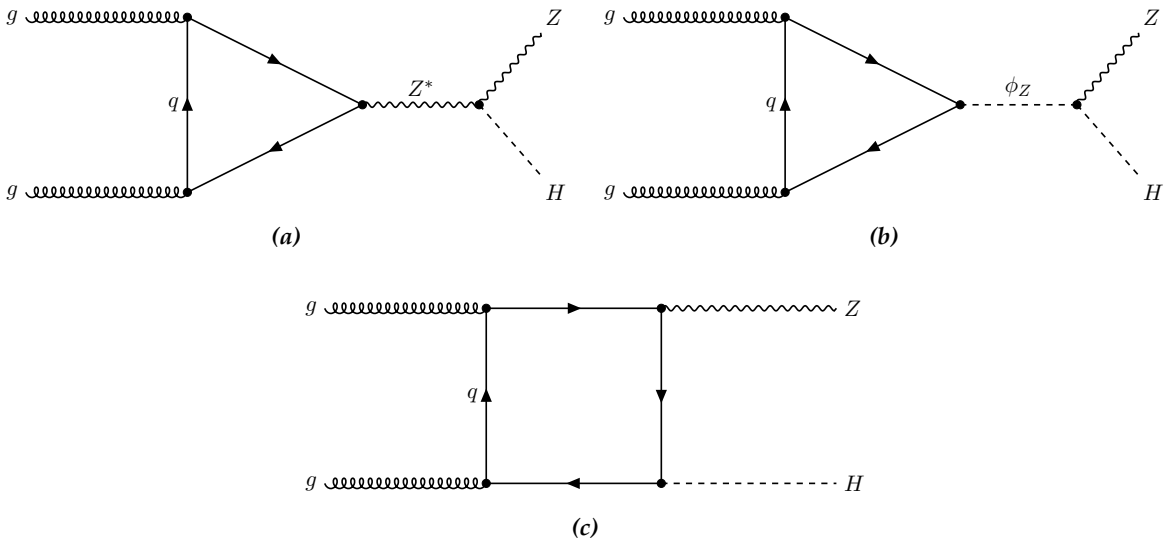

Figure 26: *The three classes of Feynman diagrams that contribute to the LO amplitude of gluon-induced ZH production. Fig. 26a and Fig. 26b differ by the intermediate particle, which can be a virtual Z boson, Z^*, or a Goldstone boson ϕ_Z. The loop mediator is a quark labeled q.*

one hand, there are one-particle reducible diagrams (Fig. 26a and 26b), in which a triangle quark loop mediates between the incoming gluons and either a virtual Z boson, Z^*, or a neutral Goldstone boson ϕ_Z. On the other hand, different types of box-quark loops (Fig. 26c) contribute in addition. Since diagrams like Fig. 26b and 26c involve the quark Yukawa coupling, only heavy quarks have to be considered for these contributions. For diagrams like Fig. 26a one also needs to only contemplate third-generation quarks due to Furry's theorem [183], which leads to a cancellation of the vector coupling in the sum of diagrams. Additionally, the axial-vector coupling vanishes when summing over mass-degenerate isospin doublets.

To further simplify the calculation, as done e.g. in Ref. [145], one can utilize the consequence of the Landau-Yang theorem [184, 185], which forbids the decay of a massive spin-1 vector particle into two massless spin-1 vector particles. More precisely, the vertex function $\mathcal{V}$ describing Fig. 26a,

$\mathcal{V}^{\mu_1\mu_2\mu_3} =$ 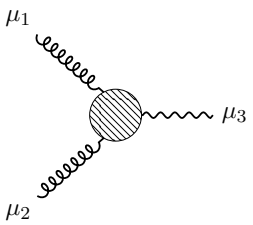 , (8.2)

vanishes to all orders in perturbation theory, when contracted with its corresponding polarization vectors. Thus, by noting that the sum over the polarization modes of the Z boson is the same as its propagator in Landau gauge, $\xi_Z = 0$, all contributions of diagrams like Fig. 26a vanish. For internal gluons, emerging at the two-loop level, we use the Feynman gauge, $\xi_g = 1$.

The virtual NLO QCD contributions of interest for this work are two-loop diagrams based on Fig. 26. A few representative diagrams of the latter are depicted in Fig. 27. To generate all

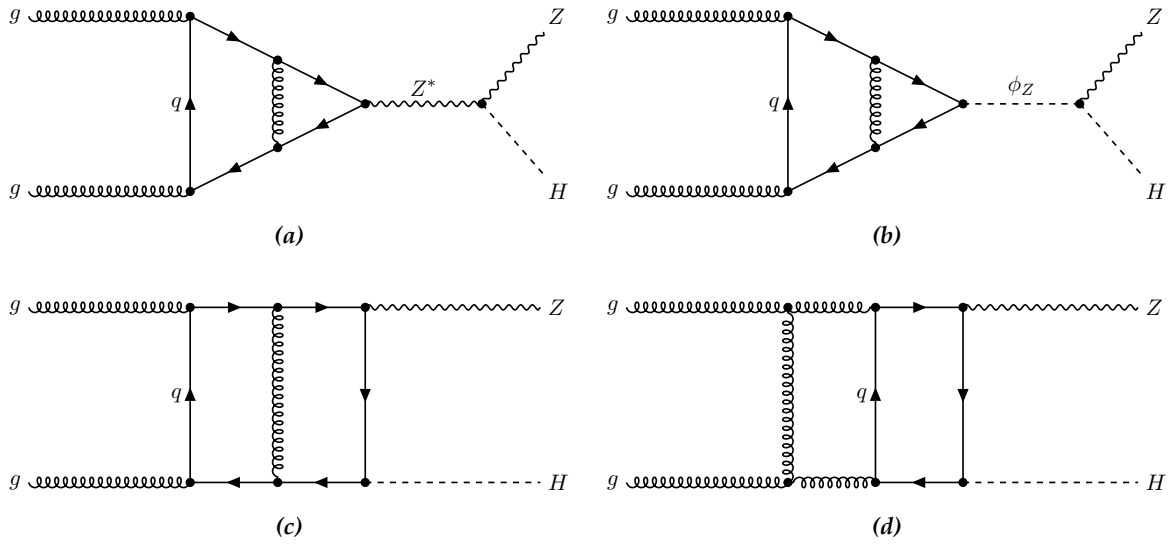

Figure 27: *Representative Feynman diagrams that contribute to the two-loop virtual corrections of gluon-induced ZH production.*

possible diagrams, we utilize the `qgraf` package [186]. The latter does not only generate all Feynman diagrams, but also calculates the required symmetry factors and signs associated with closed fermion loops. Removing diagrams that involve Z propagators, the number of diagrams generated by `qgraf` at the one-loop level is eleven and increases to 188 at the two-loop level only considering contributions of $\mathcal{O}(\alpha_s)$ and $\mathcal{O}(\alpha_s^2)$, respectively.

After all Feynman diagrams have been obtained, the Feynman rules have to be inserted. We employ the tool `q2e` [187, 188] for this task. `q2e` splits the diagrams into a QCD-color factor, which will be later processed by the `FORM` [189] package `color` [190], and a part dependent on the momenta. Since the color factorization is impossible for diagrams that contain four-gluon vertices, we use the well known technique of introducing an auxiliary scalar particle σ.[1] The Feynman rule of the four-gluon vertex can be constructed by the sum

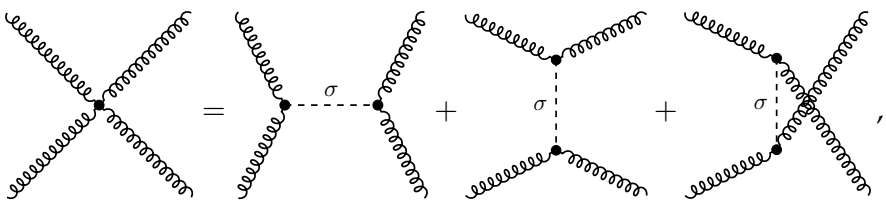

(8.3)

1 For the Feynman rules of σ we refer to App. A.

which obviously increases the number of Feynman diagrams, but the color factor can be factorized. Note that in the 188 diagrams at the two-loop level additional contributions due to the σ particle are already included.

8.2 AMPLITUDE AND TENSOR REDUCTION

To write down the generic form of the amplitude for the gluon-induced ZH production, we choose the gluon momenta, $q_1^{\mu_1}$ and $q_2^{\mu_2}$, as well as the momentum of the Z boson, $q_3^{\mu_3}$, as incoming. Their polarization vectors are labeled as $\epsilon^a_{\mu_1}(q_1)$, $\epsilon^b_{\mu_2}(q_2)$, and $\epsilon_{\mu_3}(q_3)$ for the two gluons and the Z boson, respectively. The amplitude of interest can be written as

$$\mathrm{i}\mathcal{A} = \epsilon^a_{\mu_1}(q_1)\epsilon^b_{\mu_2}(q_2)\epsilon_{\mu_3}(q_3)\delta^{ab}\sum_q I_q \mathcal{T}^{\mu_1\mu_2\mu_3}\,, \tag{8.4}$$

where we sum over the color indices $a, b = 1, \ldots, 8$, and quark flavors q. $I_q = \pm\frac{1}{2}$ is the third component of the weak isospin of the quark q and $\mathcal{T}^{\mu_1\mu_2\mu_3}$ is a polarization tensor, which will be derived below. The kinematic invariants of this process are defined as

$$s = (q_1+q_2)^2\,, \quad t = (q_1+q_3)^2\,, \quad u = (q_2+q_3)^2\,, \quad z = q_3^2\,, \quad h = (q_1+q_2+q_3)^2\,, \tag{8.5}$$

where $z = M_Z^2$ and $h = M_H^2$. In addition, momentum conservation leads to the identity

$$s + t + u = z + h\,. \tag{8.6}$$

As already mentioned in Sect. 8.1, as a consequence of charge-conjugation invariance, the Z boson couples only axially to the internal quark loops. As a result, any contribution from a mass-degenerate weak isodoublet of quarks vanishes. Thus, we consider only third generation quarks, namely the top and bottom quark. Their mass is labeled as M_q with $q \in \{t, b\}$.

The polarization tensor is uniquely defined by the external vector bosons and can be decomposed into a basis of Lorentz structures and scalar form factors. Note, however, that there exist further methods in the literature like Ref. [191], for example, which use projections onto physical helicity states.

For three external vector bosons, of which one contributes only with an axial coupling, and one scalar, we can specify four different kinds of Lorentz structures as building blocks for the polarization tensor $\mathcal{T}^{\mu_1\mu_2\mu_3}$,

$$\epsilon^{\mu_1\mu_2\mu_3 q_i}\,, \quad g^{\mu_i\mu_j}\epsilon^{\mu_k q_1 q_2 q_3}\,, \quad q_i^{\mu_j}\epsilon^{\mu_k\mu_l q_n q_m}\,, \quad q_i^{\mu_j} q_k^{\mu_l}\epsilon^{\mu_m q_n q_o q_p}\,, \tag{8.7}$$

where the indices $i, j, k, l, m, n, o, p \in \{1, 2, 3\}$ are mapped such that the Levi-Civita symbol does not vanish. Note that we use the shorthand notation

$$\epsilon^{\nu q_1 q_2 q_3} = \epsilon^{\nu\mu\rho\sigma} q_{1,\mu} q_{2,\rho} q_{3,\sigma} \tag{8.8}$$

with $\epsilon^{0123} = +1$. All possible non-zero index combinations lead to three terms for the first, three terms for the second, 27 terms for the third, and 27 terms for the fourth Lorentz structure of Eq. (8.7). These 60 structures are accompanied with scalar form factors $\tilde{a}_1, \ldots, \tilde{a}_{60}$. However, one can exploit symmetry relations between these $\tilde{a}_i \equiv \tilde{a}_i(t, u, z, h, M_q^2)$ to further reduce the size of the form-factor basis. To remove redundancies, we first utilize the Schouten identity in four dimensions,

$$g^{\alpha[\beta}\epsilon^{\gamma\delta\rho\sigma]} = 0\,, \tag{8.9}$$

and re-combine the coefficients of the remaining Lorentz structures, which are linear combinations of $\tilde{a}_i$ and kinematic invariants, to new form factors labeled a_i afterwards. Applying Eq. (8.9) iteratively leads to the following decomposition of the polarization tensor $\mathcal{T}^{\mu_1\mu_2\mu_3}$:

$$\begin{aligned}
\mathcal{T}^{\mu_1\mu_2\mu_3} = {} & a_1(t,u)\epsilon^{\mu_1\mu_2\mu_3 q_1} + a_2(t,u)\epsilon^{\mu_1\mu_2\mu_3 q_2} + a_3(t,u)\epsilon^{\mu_1\mu_2\mu_3 q_3} + a_4(t,u) g^{\mu_1\mu_2}\epsilon^{\mu_3 q_1 q_2 q_3} \\
& + \epsilon^{\mu_2\mu_3 q_1 q_2}\left[a_5(t,u)q_1^{\mu_1} + a_6(t,u)q_2^{\mu_1} + a_7(t,u)q_3^{\mu_1}\right] \\
& + \epsilon^{\mu_2\mu_3 q_1 q_3}\left[a_8(t,u)q_1^{\mu_1} + a_9(t,u)q_2^{\mu_1}\right] \\
& + \epsilon^{\mu_2\mu_3 q_2 q_3}\left[a_{10}(t,u)q_1^{\mu_1} + a_{11}(t,u)q_2^{\mu_1} + a_{12}(t,u)q_3^{\mu_1}\right] \\
& + \epsilon^{\mu_1\mu_3 q_1 q_2}\left[a_{13}(t,u)q_1^{\mu_2} + a_{14}(t,u)q_2^{\mu_2} + a_{15}(t,u)q_3^{\mu_2}\right] \\
& + \epsilon^{\mu_1\mu_3 q_1 q_3}\left[a_{16}(t,u)q_1^{\mu_2} + a_{17}(t,u)q_2^{\mu_2} + a_{18}(t,u)q_3^{\mu_2}\right] \\
& + \epsilon^{\mu_1\mu_3 q_2 q_3}\left[a_{19}(t,u)q_1^{\mu_2} + a_{20}(t,u)q_2^{\mu_2}\right] \\
& + q_3^{\mu_3}\left[a_{21}(t,u)\epsilon^{\mu_1\mu_2 q_2 q_3} + a_{22}(t,u)\epsilon^{\mu_1\mu_2 q_1 q_3}\right] \\
& + a_{23}(t,u)q_1^{\mu_1}q_2^{\mu_2}\epsilon^{\mu_3 q_1 q_2 q_3} \\
& + q_1^{\mu_1}\epsilon^{\mu_3 q_1 q_2 q_3}\left[a_{24}(t,u)q_1^{\mu_2} + a_{25}(t,u)q_3^{\mu_2}\right] \\
& + q_2^{\mu_2}\epsilon^{\mu_3 q_1 q_2 q_3}\left[a_{26}(t,u)q_2^{\mu_1} + a_{27}(t,u)q_3^{\mu_1}\right] \\
& + a_{28}(t,u)q_3^{\mu_1}q_3^{\mu_3}\epsilon^{\mu_2 q_1 q_2 q_3} + a_{29}(t,u)q_3^{\mu_2}q_3^{\mu_3}\epsilon^{\mu_1 q_1 q_2 q_3}\,.
\end{aligned} \tag{8.10}$$

Note that we have suppressed the dependence of the a_i on the squared masses of the Z boson, the Higgs boson, and the quark.

In addition, we impose Bose symmetry for the incoming gluons,

$$\mathcal{T}^{\mu_1\mu_2\mu_3} = \mathcal{T}^{\mu_2\mu_1\mu_3}\Big|_{q_1 \leftrightarrow q_2}\,, \tag{8.11}$$

which reveals the following set of identities for the remaining form factors:

$$\begin{aligned}
a_2(t,u) &= -a_1(u,t)\,, & a_3(t,u) &= -a_3(u,t)\,,\\
a_4(t,u) &= -a_4(u,t)\,, & a_{13}(t,u) &= -a_6(u,t)\,,\\
a_{14}(t,u) &= -a_5(u,t)\,, & a_{15}(t,u) &= -a_7(u,t)\,,\\
a_{16}(t,u) &= a_{11}(u,t)\,, & a_{17}(t,u) &= a_{10}(u,t)\,,\\
a_{18}(t,u) &= a_{12}(u,t)\,, & a_{19}(t,u) &= a_9(u,t)\,,\\
a_{20}(t,u) &= a_8(u,t)\,, & a_{22}(t,u) &= -a_{21}(u,t)\,,\\
a_{23}(t,u) &= -a_{23}(u,t)\,, & a_{26}(t,u) &= -a_{24}(u,t)\,,\\
a_{27}(t,u) &= -a_{25}(u,t)\,, & a_{29}(t,u) &= -a_{28}(u,t)\,.
\end{aligned} \tag{8.12}$$

Hence, the total number of form factors reduces to 16, including permutations of t and u. Finally, by employing gauge invariance with respect to the gluons,

$$q_{1,\mu_1}\epsilon^b_{\mu_2}(q_2)\epsilon_{\mu_3}(q_3)\mathcal{T}^{\mu_1\mu_2\mu_3} = \epsilon^a_{\mu_1}(q_1)q_{2,\mu_2}\epsilon_{\mu_3}(q_3)\mathcal{T}^{\mu_1\mu_2\mu_3} = 0\,, \tag{8.13}$$

we can establish a minimal basis of form factors for our calculation. The additional constraints given by Eq. (8.13) can be summarized as:

$$\begin{aligned}
a_4(t,u) &= 2\frac{a_3(t,u)}{s}\,, & a_6(t,u) &= -2\frac{a_2(t,u)}{s} + a_7(t,u)\frac{z-t}{s}\,,\\
a_9(t,u) &= -2\frac{a_3(t,u)}{s}\,, & a_{11}(t,u) &= a_{12}(t,u)\frac{z-t}{s}\,,\\
a_{13}(t,u) &= 2\frac{a_2(u,t)}{s} - a_7(u,t)\frac{z-u}{s}\,, & a_{16}(t,u) &= a_{12}(u,t)\frac{z-u}{s}\,,\\
a_{19}(t,u) &= 2\frac{a_3(t,u)}{s}\,.
\end{aligned} \tag{8.14}$$

For convenience, we relabel the physical form factors occurring in Eq. (8.14) as follows,

$$2\frac{a_2(t,u)}{s} = f_1(t,u)\,, \quad a_7 = -f_2\,, \quad a_{12} = f_3\,, \quad 2\frac{a_3}{s} = f_4\,, \tag{8.15}$$

where we have dropped the t and u dependence of $f_{2,3,4}$ for simplicity. The remaining a_i that do not contribute to Eq. (8.13) due to transversality conditions for the vector bosons,

$$q_1\cdot\epsilon^a(q_1) = q_2\cdot\epsilon^b(q_2) = q_3\cdot\epsilon(q_3) = 0\,, \tag{8.16}$$

are relabeled as $a_i = f_i$. Hence, the polarization tensor has the decomposition

$$\begin{aligned}
\mathcal{T}^{\mu_1\mu_2\mu_3} = &\left[\frac{s}{2}\epsilon^{\mu_1\mu_2\mu_3 q_2} - q_2^{\mu_1}\epsilon^{\mu_2\mu_3 q_1 q_2}\right] f_1(t,u) - \left[\frac{s}{2}\epsilon^{\mu_1\mu_2\mu_3 q_1} - q_1^{\mu_2}\epsilon^{\mu_1\mu_3 q_1 q_2}\right] f_1(u,t) \\
&+ \left[q_3^{\mu_1} + \frac{z-t}{s}q_2^{\mu_1}\right]\epsilon^{\mu_2\mu_3 q_2 \nu}\left[q_{1,\nu} f_2(t,u) + q_{3,\nu} f_3(t,u)\right] \\
&+ \left[q_3^{\mu_2} + \frac{z-u}{s}q_1^{\mu_2}\right]\epsilon^{\mu_1\mu_3 q_1 \nu}\left[q_{2,\nu} f_2(u,t) + q_{3,\nu} f_3(u,t)\right] \\
&+ \left[\frac{s}{2}\epsilon^{\mu_1\mu_2\mu_3 q_3} - q_2^{\mu_1}\epsilon^{\mu_2\mu_3 q_1 q_3} + q_1^{\mu_2}\epsilon^{\mu_1\mu_3 q_2 q_3} + g^{\mu_1\mu_2}\epsilon^{\mu_3 q_1 q_2 q_3}\right] f_4(u,t) \\
&+ q_1^{\mu_1}\epsilon^{\mu_2\mu_3 q_1 q_2} f_5(t,u) - q_2^{\mu_2}\epsilon^{\mu_1\mu_3 q_1 q_2} f_5(u,t) \\
&+ q_1^{\mu_1}\epsilon^{\mu_2\mu_3 q_1 q_3} f_8(t,u) + q_2^{\mu_2}\epsilon^{\mu_1\mu_3 q_2 q_3} f_8(u,t) \\
&+ q_1^{\mu_1}\epsilon^{\mu_2\mu_3 q_2 q_3} f_{10}(t,u) + q_2^{\mu_2}\epsilon^{\mu_1\mu_3 q_1 q_3} f_{10}(u,t) \\
&+ q_3^{\mu_3}\left[\epsilon^{\mu_1\mu_2 q_2 q_3} f_{21}(t,u) - \epsilon^{\mu_1\mu_2 q_1 q_3} f_{21}(u,t)\right] \\
&+ q_1^{\mu_1} q_2^{\mu_2}\epsilon^{\mu_3 q_1 q_2 q_3} f_{23}(t,u) \\
&+ q_1^{\mu_1} q_1^{\mu_2}\epsilon^{\mu_3 q_1 q_2 q_3} f_{24}(t,u) - q_2^{\mu_1} q_2^{\mu_2}\epsilon^{\mu_3 q_1 q_2 q_3} f_{24}(u,t) \\
&+ q_1^{\mu_1} q_3^{\mu_2}\epsilon^{\mu_3 q_1 q_2 q_3} f_{25}(t,u) - q_2^{\mu_2} q_3^{\mu_1}\epsilon^{\mu_3 q_1 q_2 q_3} f_{25}(u,t) \\
&+ q_3^{\mu_1} q_3^{\mu_3}\epsilon^{\mu_2 q_1 q_2 q_3} f_{28}(t,u) - q_3^{\mu_2} q_3^{\mu_3}\epsilon^{\mu_1 q_1 q_2 q_3} f_{28}(u,t)\,,
\end{aligned} \tag{8.17}$$

where gauge invariance and Bose symmetry with respect to the gluons is manifest. Eq. (8.17) is in accordance with the findings of Ref. [143], but includes additional terms which were dropped in the latter due to the transversality conditions for the vector bosons.

In order to compute the form factors that contribute to the cross section, $f_{1,\dots,4}$, we need to construct projectors to isolate each f_i. In full generality, a form factor f_j can be obtained by applying a projector $p_{j,\mu_1\dots\mu_n}$ with n Lorentz indices as

$$f_j = p_{j,\mu_1\dots\mu_n}\mathcal{T}^{\mu_1\cdots\mu_n}\,, \tag{8.18}$$

where $\mathcal{T}^{\mu_1\cdots\mu_n}$ is given by

$$\mathcal{T}^{\mu_1\cdots\mu_n} = \sum_j t_j^{\mu_1\cdots\mu_n} f_j \tag{8.19}$$

and $t_j^{\mu_1\cdots\mu_n}$ is a generic Lorentz structure accompanied by the corresponding form factor f_j. The projectors $p_{j,\mu_1\dots\mu_n}$ can be obtained with

$$p_{j,\mu_1\dots\mu_n} = \sum_k t_{k,\mu_1,\dots,\mu_n} t^{-1}_{jk}\,, \tag{8.20}$$

where the matrix t_{jk} is defined as

$$t_{jk} = t_j^{\mu_1,\dots,\mu_n} t_{k,\mu_1,\dots,\mu_n}\,. \tag{8.21}$$

For our calculation, we have to obtain projectors for the four physical form factors $f_{1,\dots,4}$. Therefore, we start by calculating the matrix t_{jk} for all 22 structures given in Eq. (8.17). The entries of t_{jk} are rational functions in the kinematic invariants defined in Eq. (8.5). Using the t_i basis of Eq. (8.17) as defined by Eq. (8.19), we find that f_{10} and f_{23} result to zero after contracting with any t_i thus being removed from t_{jk}. Additionally, the structures of f_8, f_{24}, and f_{25} can only be used to project to a combination of these three Lorentz structures. Since we are not interested in any of the latter, we remove them from t_{jk} as well. Finally, for the inversion of t_{jk}, we only need to consider the remaining 13 t_i, namely $t_{1,\dots,9,14,15,21,22}$. Note that we have suppressed the Lorentz indicies of the t_i in this paragraph. We get a total amount of 169 nonzero entries of t_{jk}^{-1}, which are calculated by utilizing finite-field-interpolation techniques combined with the rational-reconstruction method (cf. Subsect. 8.5.3 and Subsect. 8.5.4). Instead of using explicit projectors for $f_{1,\dots,4}$, we pursue a more general approach, in which just one projector ($p_{\mu_1\mu_2\mu_3}$) with generic coefficients (c_i) is used:

$$p_{\mu_1\mu_2\mu_3} = \sum_{k=1}^{9} c_k t_{k,\mu_1\mu_2\mu_3} + c_{14} t_{14,\mu_1\mu_2\mu_3} + c_{15} t_{15,\mu_1\mu_2\mu_3} + c_{21} t_{21,\mu_1\mu_2\mu_3} + c_{22} t_{22,\mu_1\mu_2\mu_3} \,. \tag{8.22}$$

Therefore, we only get one expression for the whole amplitude containing the full set of relevant Feynman integrals. The explicit results can be found in App. B.2.

Considering only QCD corrections, the form factors themselves can be written as a perturbative series in the strong coupling constant α_s as

$$f_i(t,u) = \alpha_s \Delta f_i^{1\mathrm{L}}(t,u) + \alpha_s^2 \Delta f_i^{2\mathrm{L}}(t,u) + \mathcal{O}(\alpha_s^3) \,, \tag{8.23}$$

where $\Delta f_i^{n\mathrm{L}}(t,u)$ is the n-loop correction to the form factor f_i.

In addition to the isolation of the form factors, we also have to consider the color structure of the amplitude. As already shown in Eq. (8.4), the only color tensor with two indices in the adjoint representation is the Kronecker symbol δ^{ab}. This factor can be projected out by

$$p^{ab} = \frac{\delta^{ab}}{N_A} \,, \tag{8.24}$$

where $N_A = N_C^2 - 1 = 8$ is the dimension of the adjoint representation.

Both projectors, $p_{\mu_1\mu_2\mu_3}$ and p^{ab}, have been implemented in a `FORM`-code.

Utilizing the procedures described in the next sections, inserting explicit expressions for c_i, and choosing unitary gauge, we find agreement with the result of Ref. [143] for $\mathcal{T}^{\mu_1\mu_2\mu_3}$ at the one-loop level. Note that due to the usage of Eq. (8.9) in four dimensions terms proportional to ϵ, which arise in $d = 4 - 2\epsilon$ dimensions, might not be captured by the tensor decomposition of Ref. [143]. However, the set of integrals over loop momenta, which we are aiming for, should remain unaffected. We have checked this by using all 60 possible Lorentz structures of Eq. (8.7) as a basis in d dimensions, constructed projectors, and extracted the integrals from the amplitude.

8.3 TREATMENT OF γ_5

As we utilize dimensional regularization [192, 193] in our calculation to perform the analytic continuation of the SM to a non-integer number $d = 4 - 2\epsilon$ of space-time dimensions, we have to take care of genuinely four-dimensional objects, like the Levi-Civita symbol,

$$\epsilon_{\mu_1\mu_2\mu_3\mu_4}\,, \qquad \epsilon^{0123} = +1\,, \tag{8.25}$$

and the fifth Dirac matrix γ_5,

$$\gamma_5 = \mathrm{i}\gamma_0\gamma_1\gamma_2\gamma_3 = \frac{\mathrm{i}}{4!}\epsilon_{\mu_1\mu_2\mu_3\mu_4}\gamma^{\mu_1}\gamma^{\mu_2}\gamma^{\mu_3}\gamma^{\mu_4}\,. \tag{8.26}$$

To deal with these objects in d dimensions, we need to define a prescription. In the literature quite a few approaches have been suggested [194], to which we refer the reader. Our focus is based on the prescription developed in Refs. [195–198], where we will treat the Levi-Civita symbol merely as a symbol with d-dimensional indices. In this scheme, also referred to as the Larin scheme, the axial-vector matrix is continued enforcing a specific order of the two Dirac matrices by

$$\gamma_\mu\gamma_5 = \frac{\mathrm{i}}{3!}\epsilon_{\mu\mu_1\mu_2\mu_3}\gamma^{\mu_1}\gamma^{\mu_2}\gamma^{\mu_3}\,. \tag{8.27}$$

As an alternative one can also use

$$\gamma_5 = \frac{\mathrm{i}}{4!}\epsilon_{\mu_1\mu_2\mu_3\mu_4}\gamma^{\mu_1}\gamma^{\mu_2}\gamma^{\mu_3}\gamma^{\mu_4}\,, \tag{8.28}$$

when the axial-vector matrix is replaced by its symmetric Hermitian counterpart [199]

$$\gamma_\mu\gamma_5 \to \frac{1}{2}\left(\gamma_\mu\gamma_5 - \gamma_5\gamma_\mu\right)\,. \tag{8.29}$$

Both replacements lead in our calculation to products of two Levi-Civita symbols, which are evaluated in terms of the d-dimensional metric tensor g^μ_ν as

$$\epsilon^{\mu_1\mu_2\mu_3\mu_4}\epsilon_{\mu_5\mu_6\mu_7\mu_8} = \begin{vmatrix} g^{\mu_1}_{\mu_5} & g^{\mu_1}_{\mu_6} & g^{\mu_1}_{\mu_7} & g^{\mu_1}_{\mu_8} \\ g^{\mu_2}_{\mu_5} & g^{\mu_2}_{\mu_6} & g^{\mu_2}_{\mu_7} & g^{\mu_2}_{\mu_8} \\ g^{\mu_3}_{\mu_5} & g^{\mu_3}_{\mu_6} & g^{\mu_3}_{\mu_7} & g^{\mu_3}_{\mu_8} \\ g^{\mu_4}_{\mu_5} & g^{\mu_4}_{\mu_6} & g^{\mu_4}_{\mu_7} & g^{\mu_4}_{\mu_8} \end{vmatrix}\,. \tag{8.30}$$

We have implemented both prescriptions, Eq. (8.27) and Eq. (8.28) with Eq. (8.29), into a FORM-code following the steps summarized in Ref. [194]. In practice, traces in which a γ_5 occurs will be rewritten as

$$\mathrm{Tr}\left(\gamma_{\mu_1}\gamma_{\mu_2}\ldots\gamma_\mu\gamma_5\right)\,, \tag{8.31}$$

using the cyclicity of the trace, and either Eq. (8.27) or Eq. (8.28) with Eq. (8.29) are used to replace γ_5. Afterwards, d-dimensional trace identities for the Dirac matrices are used followed by an evaluation of products of Levi-Civita symbols as given by Eq. (8.30). We have checked that our implementation yields the same result for both replacements.

Note that the prescription discussed above comes with a caveat, namely the violation of the axial Ward identity. However, the latter can be addressed by including additional renormalization factors that restore this identity as studied in Ref. [197], for example. Since we only present preliminary results in this chapter, we do not cover a proper renormalization in the our calculation and focus on the reduction to master integrals in Sect. 8.5 instead.

8.4 TOPOLOGIES

As a next step, all occurring Feynman diagrams are mapped onto a smaller number of generic user-defined topologies with the tool `exp` [187, 188]. The required topologies by `exp` are depicted in Fig. 28, where we do not distinguish different mass distributions at this point. `exp` outputs `FORM` files, which are further processed with a modified version of the `FORM` code originating from `MINCER` [200] and `MATAD` [201] to evaluate traces of Dirac matrices, where, in addition, γ_5 is treated as described in Sect. 8.3.

After all traces have been evaluated, four-momentum conservation has to be inserted, the tensor reduction has to be performed, and the scalar Feynman integrals have to be rewritten in a form that is suitable for further processing. This procedure has to be performed for each topology. Note that our setup is partly based on code developed in Ref. [202] and modified to be applicable to $2 \to 2$ scattering processes. To express occurring integrals over loop momenta to a commonly used notation, we want to rewrite them as scalar functions of the form

$$F(\mathrm{id}; d, \{q_j\}, \{M_i\}, \{a_i\}) = \int_{l_1,\ldots,l_L} \frac{1}{P_1^{a_1} \cdots P_N^{a_N}}\,, \tag{8.32}$$

where L is the number of loops, id is an identifier that specifies the topology, and the inverse propagators $P_1, \ldots, P_N$ are given by $P_i = k_i^2 - M_i^2 + \mathrm{i}0$ in Minkowski space. We denote the set of integrals with the same id as an integral family. M_i denotes the mass of the i^{th} propagating particle with momentum k_i, of which the latter is a linear combination of loop momenta l_j and external momenta q_j. Each integral measure is defined as

$$\int_l \equiv \int \frac{\mathrm{d}^d l}{(2\pi)^d}\,. \tag{8.33}$$

The scalar function F depends on the space-time dimension d, the set of masses $\{M_i\}$, the set of external momenta $\{q_j\}$, and the propagator powers $\{a_i\}$ that take integer values.

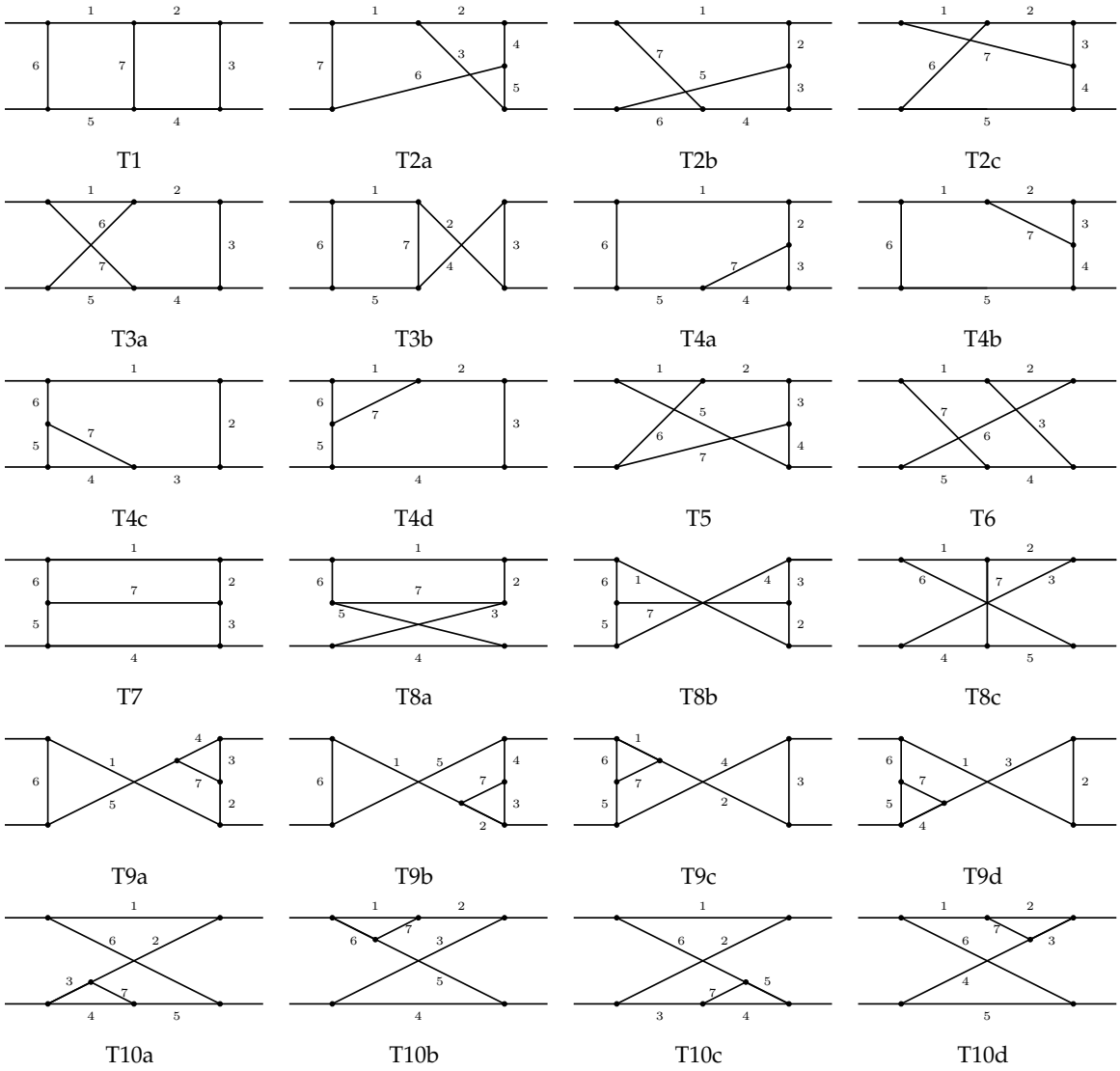

Figure 28: *The* 24 *required topologies for $gg \to ZH$ by* exp *at the two-loop level. The upper left incoming line carries momentum q_1, the lower left incoming line q_2, and the upper right incoming line q_3.*

For a given value of L and number of external momenta E, N can be calculated by

$$N = EL + \frac{L\,(L+1)}{2}\,, \tag{8.34}$$

which is the number of possible scalar products involving at least one loop momentum. These scalar products are used internally to express any occurring numerator structure in terms of functions F. For our two-loop calculation, we have $L = 2$ and $E = 3$, which leads to $N = 9$. Seven of the nine propagators are determined by the momentum flowing through the lines of each topology and the mass distribution. The remaining two are fixed as scalar products of external and loop momenta that are linearly independent with respect to the propagators dictated by the respective topology. We have automatized this procedure by first assigning a momentum flow through each line of a topology that respects momentum conservation at each vertex. Afterwards, the two extra propagators have to be specified. Any

possible scalar product is thus considered and tested whether it fulfills the criterion to be linearly independent with respect to the already fixed ones.

After all propagators have been fixed, `FORM` code is generated that includes specific replacement rules obtained by considering all kinds of scalar products completed to squares. These rules can then map any occurring numerator structure to functions F by raising and lowering the propagator powers a_i. Finally, all functions F are gathered as a list which can be further processed by different approaches. Here, we only focus on integration-by-parts (IBP) reductions introduced in the next section.

8.5 REDUCTION TO MASTER INTEGRALS

After expressing amplitudes as a sum of scalar integrals, usually a huge number of integrals has to be computed. For the two-loop contributions of gluon-induced ZH productions, roughly 15000 scalar integrals occur in the amplitude. Luckily, not all of these integrals are linearly independent and they can thus be reduced to a smaller number of so-called master integrals.

In Subsect. 8.5.1 integration-by-parts identities are introduced, which are used for the reduction of single integral families to a set of master integrals. Subsect. 8.5.2 discusses so-called sector relations, which, in addition, can be used to identify integral relations among different integral families. However, when performed fully algebraically, the IBP approach tends to become unfeasible for cutting edge calculations. Therefore, in Subsect. 8.5.3 and Subsect. 8.5.4, novel techniques developed within this thesis and partly published in Ref. [203] are presented, which perform the reduction fully numerically over so-called finite fields multiple times and process these evaluations by functional-interpolation algorithms. Their benefits over conventional approaches, several optimizations, and hybrid algorithms are discussed in Subsect. 8.5.5. These techniques are applied in Subsect. 8.5.6 to reduce the two-loop integrals occurring in the amplitude of $gg \to ZH$.

8.5.1 *Integration-by-parts identities*

In 1981, Chetyrkin and Tkachov [204, 205] observed that by inserting the scalar product of a derivative with respect to a loop momentum and another momentum into Eq. (8.32) the corresponding integral vanishes in dimensional regularization:

$$\int_{l_1,\dots,l_L} \frac{\partial}{\partial l_i^\mu} \left(\tilde{q}_j^\mu \frac{1}{P_1^{a_1} \cdots P_N^{a_N}} \right) = 0 \,, \tag{8.35}$$

where $\tilde{q}_j^\mu$ can either be another loop momentum or an external momentum. These identities can be used to derive relations among integrals of different sets of $\{a_i\}$ within the same integral family by explicitly evaluating the derivative,

$$0 = \sum_n c_n F(\mathrm{id}; d, \{q_j\}, \{M_i\}, \{a_i^{(n)}\}) \,. \tag{8.36}$$

The coefficients in these relations, c_n, are in general rational functions in d, $\{M_i\}$, and $\{q_j\}$. For a given integral family, this leads in total to $L(L+E)$ of such identities that are denoted as IBP identities or relations.

After all relations for a given integral family are found, one is able to express the scalar integrals occurring in an amplitude by a smaller subset of linearly independent integrals. This procedure is called *reduction* and the elements of the set of linearly independent integrals are known as *master integrals*. Since there is no unique definition of the term master integral, a reduction algorithm has to specify some kind of order among the different integrals. Usually, one chooses an order in which the master integrals are the easiest ones to evaluate. Note, in addition, that the number of master integrals is finite [206]. Therefore, the master integrals build a basis for a finite dimensional vector space of scalar integrals.

Currently, two different procedures employing IBP identities for a reduction to master integrals exist in the literature. One of these two methods tries to find recursion relations, which express an integral by easier integrals. This strategy has been successfully applied to contributions for massless propagator-type diagrams [200,205,207], massive tadpoles [201,208], and on-shell propagators [120, 209, 210] at the three-loop level. Usually, such recursion relations have to be found manually, which makes them less attractive for sufficiently complicated calculations. However, once these recursions are found, the reduction is straightforward. A general algorithm to find these relations has been published in Refs. [211, 212], which, unfortunately, tends to become slow for complicated cases. Additionally, even if recursion relations can be found, their application can often become slow due to their complexity.

A different approach was presented by Laporta in 2001 [213]. By inserting different integer values of a_i in the Eq. (8.36), one obtains a homogenous system of equations of integrals. One can solve this system by Gaussian elimination and since it is homogenous, all integrals are expressed by master integrals. As straightforward this algorithm might seem, one major drawback is that one has to build huge systems of equations for state-of-the-art calculations, which become expensive to solve both in terms of memory and runtime. Within this thesis, we address this drawback by interpolation techniques (cf. Subsect. 8.5.5). There exist several public implementations of the Laporta algorithm, `AIR` [214], `FIRE` [215–218], `Reduze` [219,220], and `Kira` [221,222]. As the IBP relations are linear, the solution strategies thus only involve addition, subtraction, multiplication, and division. Additionally, the coefficients of the master integrals are rational functions in d, $\{M_i\}$, and $\{q_j\}$. This feature is of particular interest as will be discussed in Subsect. 8.5.5 in more detail.

For more details on IBP reductions, we refer the reader to Refs. [223, 224] for a general overview.

8.5.2 *Sector relations*

In addition to relations among integrals belonging to the same integral family, there also exist relations among integrals of different integral families, which are called *sector relations*.

The sector S of a scalar integral given in the form of Eq. (8.32) is represented as the index set of positive a_i, i.e. $\{i|a_i > 0\}$. A subset of the latter represents a different sector, that is called a *subsector* of S. One can interpret the concept of a sector and subsector also graphically, in which one draws a generic diagram for the sector S, where its subsector is obtained by shrinking its missing propagator to a point. Additionally, integral families that are related just by crossing of external legs can be identified.

For illustration, let us consider the full sectors of two integral families shown on the left-hand side of Fig. 29. The subsector $S_1 = \{1, 2, 3, 4, 5\}$ of family F_1 and the subsector

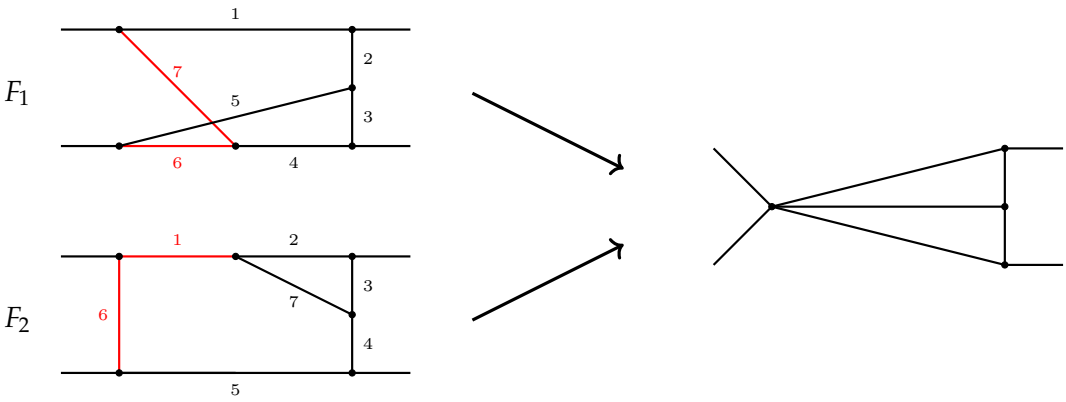

Figure 29: *Sector relations between the two integral families F_1 and F_2. The red lines denote propagators not present in the considered subsectors.*

$S_2 = \{2, 3, 4, 5, 7\}$ of family F_2 have isomorphic graphs, see right hand side of Fig. 29. Therefore, any integral belonging to S_1 of family F_1 can always be expressed as a linear combination of integrals belonging to sector S_2 and family F_2 and subsectors of S_2 or vice versa. These types of mappings are called sector relations.

Sector relations can help to relate master integrals belonging to different integral families, thus reducing the total number of master integrals. Further, the total number of integrals that have to be reduced in the first place can also be decreased. A particular application are Feynman integrals that belong to mirrored topologies, which can be mapped to each other.

We utilize the tool `Reduze 2` [220] for the detection of sector relations and apply them as `FORM` identities in our calculation.

8.5.3 *Interpolation of multivariate rational functions over finite fields*

As the complexity of state-of-the-art multi-loop calculations pushes conventional computer algebra systems (CAS) like `Fermat` [225] to their limits, a different approach that is actively studied in Computer Science since decades, attracted the attention of physicist in the last years [203, 226–229]. It is known under the name of *functional interpolation*, where the main goal is to interpolate the function of interest, i.e. getting a functional prescription from a set of numerical data, also called *probes*, rather than performing all steps algebraically with a CAS. Usually, no knowledge is provided from the function of interest, which is thus called *black box*. The evaluation of the black box can be easily parallelized since, in practice, each probe can be computed independently. In the context of IBP reductions this method was proposed in Ref. [226] and further applied to scattering amplitudes in Ref. [227], where the occurring functions are multivariate rational functions in kinematic invariants and the space-time dimension d with numerical coefficients in $\mathbb{Q}$.

Rather than over $\mathbb{Q}$, functional interpolations are usually performed over so-called *finite fields*, i.e. fields $\mathbb{Z}_p$ with characteristic p, where p is a prime. Hence, all calculations are carried out with module p avoiding number swell and reducing the memory footprint. The multiplicative inverse in $\mathbb{Z}_p$ is unique and can be determined using the Extended Euclidean Algorithm [230].

Since the performance of these interpolations is crucially dependent on the used algorithms, in this section we present a new algorithm developed within this thesis and partly published in Ref. [203], that is capable of interpolating *sparse*, i.e. functions where the majority of monomial coefficients is zero, and *dense* functions, i.e. functions where the majority of monomial coefficients is non-zero, requiring a minimal number of black-box probes. Our algorithm is based on Ref. [231].

To fix the notation, we start by defining multivariate polynomials as follows. Given a set of n variables $\vec{z} = (z_1, \ldots, z_n)$ and an n-dimensional multi-index $\alpha = (\alpha[1], \ldots, \alpha[n])$ containing integers $\alpha[i] \geq 0$, we define a monomial $\vec{z}^{\,\alpha}$ as

$$\vec{z}^{\,\alpha} \equiv \prod_{i=1}^{n} z_i^{\alpha[i]} \tag{8.37}$$

with a degree d of

$$d = \sum_{i=1}^{n} \alpha[i] \,. \tag{8.38}$$

A polynomial f, which is an element in the polynomial ring $\mathbb{Z}_p[\vec{z}]$ of variables $\vec{z}$, is defined as

$$f(\vec{z}) = \sum_{j=1}^{T} c_{\alpha_j} \vec{z}^{\,\alpha_j} \,, \tag{8.39}$$

where T is the number of non-zero terms. The coefficients c_{α_j} are elements of $\mathbb{Z}_p$ corresponding to different multi-indices α_j.

Rational functions can be constructed by combining two polynomials. Given two polynomials $P, Q \in \mathbb{Z}_p[\vec{z}]$, we define a rational function $f \in \mathbb{Z}_p(\vec{z})$, where $\mathbb{Z}_p(\vec{z})$ is the field of rational functions in the variables $\vec{z}$, as the ratio of P and Q:

$$f(\vec{z}) = \frac{P(\vec{z})}{Q(\vec{z})} = \frac{\sum_{i=1}^{T_\mathrm{n}} n_{\alpha_i} \vec{z}^{\,\alpha_i}}{\sum_{j=1}^{T_\mathrm{d}} d_{\beta_j} \vec{z}^{\,\beta_j}} \,. \tag{8.40}$$

The T_n (T_d) non-zero coefficients n_{α_i} (d_{β_j}) are elements in the field $\mathbb{Z}_p$ corresponding to multi-indices α_i (β_i).

In order to provide a unique normalization of Eq. (8.40), we define the lowest degree coefficient in the denominator to be equal to one. If several monomials contribute to the lowest degree d_min, we choose to define that coefficient of the monomial $\vec{z}^{\,\alpha}$ to be equal to one, whose multi-index α is the smallest in a colexicographical order, e.g.

$$(1,1,0) < (1,0,1) < (0,1,1) \,, \tag{8.41}$$

for $d = 2$.

Our algorithm for multivariate rational-function interpolation is based on Ref. [231], which performs only a univariate interpolation of an auxiliary rational function, whose monomial coefficients are multivariate polynomials and are thus processed by multivariate polynomial interpolation [232–239].[2] Note that there are further algorithms worth mentioning [240–246], but none of them fulfills our performance goal.

In order to build the auxiliary rational function $\tilde{f}$ of a rational function $f(z_1, \ldots, z_n)$, one starts by introducing a homogenization variable t as [247]

$$\tilde{f}(t\vec{z}) = f(tz_1, \ldots, tz_n) \,. \tag{8.42}$$

$\tilde{f}$ can be interpreted as a univariate rational function in t, whose monomial coefficients are multivariate polynomials in $\vec{z}$. In addition, we can set one of the z_i to one and obtain its functional dependence by homogenizing with respect to the corresponding power of t, after the interpolation of the remaining monomials in z_j was successful.

Due to potentially missing constants, which are needed for normalization, and cancellations in t, we cannot ensure that an unambiguous normalization can be found for arbitrary rational functions $\tilde{f}$. Therefore, as proposed in Ref. [231], a variable shift $\vec{s} = (s_1, \ldots, s_n)$ is introduced such that

$$\tilde{f}(t\vec{z}) \to \hat{f}(\vec{z}) \equiv \hat{f}(t\vec{z} + \vec{s}) = f(t + s_1, tz_2 + s_2, \ldots, tz_n + s_n) \,, \tag{8.43}$$

2 For a review of polynomial interpolation techniques, we refer the reader to Ref. [203], for example.

where we have set $z_1 = 1$. Applying $\vec{s}$ as in Eq. (8.43) should lead to a constant term in the numerator or denominator, i.e. the coefficient of $\alpha[i] = 0 \,\forall\, i$ or $\beta[i] = 0 \,\forall\, i$ is non-zero, which can be used as a unique normalization. Ref. [231] proposed to shift all occurring variables by random s_i. However, this prescription will lead to a much denser function $\hat{f}$ that has to be interpolated.

Therefore, in Ref. [203], we made the proposal to first scan different combinations of possible shifts $\vec{s}$ and choose the one, which shifts only a minimal subset of variables, but leads to a constant term in either numerator or denominator. The additional probes needed for this scan are in most cases negligible compared to the full interpolation.

As already outlined above, the general idea is to first interpolate only a rational function univariately in t and then proceed with multivariate polynomial interpolation for each coefficient of monomials in t. This is done as follows. In the first run, we fix a randomized set $\vec{y}^1$ of values, $\vec{y}^1 = \{1, y_{2,1}, y_{3,1}, \ldots, y_{n,1}\}$, that is called *anchor points*[3] to replace the z_i. Then, we use randomized values for t and interpolate the t dependence using Thiele's interpolation formula [249], which expresses $\hat{f}$ as a continued fraction

$$\tau(t) = b_0 + (t - t_1)\left(b_1 + (t - t_2)\left(b_2 + (t - t_3)\left(\cdots + \frac{t - t_N}{b_N}\right)^{-1}\right)^{-1}\right)^{-1}, \tag{8.44}$$

where $t_1, \ldots, t_{N+1}$ are distinct elements in $\mathbb{Z}_p$. The coefficients $b_1, \ldots, b_N$ can be obtained recursively by numerical evaluations of the rational function $\hat{f}$ at $t_1, \ldots, t_{N+1}$ for the chosen values of z_i as

$$b_i \equiv b_{i,i}\,, \tag{8.45}$$

$$b_{i,j} = \frac{t_{i+1} - t_j}{b_{i,j-1} - b_{j-1}}\,, \tag{8.46}$$

$$b_{i,0} = f(t_{i+1})\,. \tag{8.47}$$

The termination criterion is reached if one finds the agreement

$$\tau(t_i) = \hat{f}(t_i + s_1, t_i y_{2,1} + s_2, \ldots, t_i y_{n,1} + s_n)\,. \tag{8.48}$$

$\hat{f}$ is now a function of t with numerical coefficients, which themselves are multivariate polynomials in z_i, evaluated at $\vec{y}^1$ and incorporating effects of the used shift $\vec{s}$. Note that zeros can occur in the denominators of Eq. (8.46) by randomizing the values of t with a probability bounded by the Zippel-Schwartz lemma (cf. Eq. (8.52)) [232, 250]. In addition, Eq. (8.44) is not the only method for rational function interpolation. One can also utilize the Extended Euclidean Algorithm as shown in Refs. [230, 251].

3 Additional probes are evaluated as combinations of powers of these anchor points to utilize the structure of shifted Vandermonde systems (cf. Refs. [203, 233, 235, 248]).

Ref. [231] proposes a sparse approach in which the univariate interpolation of $\hat{f}$ in t is calculated densely and the multivariate polynomial interpolation is only performed for the highest degree of t at first. Note that the latter is unaffected by the shift $\vec{s}$. Afterwards, one proceeds with the next-to-highest degree by using the stored coefficients obtained by Eq. (8.44) and numerically subtracts the effects of $\vec{s}$ originating from the higher degrees in t. If the stored values are not sufficient to complete the polynomial interpolation, new dense interpolations in t are performed. This procedure will be applied until the lowest non-zero degree is reached by decreasing the degree of t and proceeding as described above.

There are two major disadvantages of this algorithm. First, Eq. (8.44) does not scale optimally in the number of black-box probes required to terminate. Secondly, if the rational function is not sparse, a huge number of avoidable black-box probes is requested. These two points could be avoided by:

1. Interpolating all coefficients of degrees of t simultaneously and thus partly densely, i.e. including effects of $\vec{s}$;
2. Removing already interpolated multivariate polynomials from the interpolation in t by subtracting their evaluations from additional black-box probes. This procedure is similar to the *pruning* technique invented in Refs. [237,238] for multivariate polynomial interpolation.

To illustrate the benefits of these modifications, let us first assume a dense case. A multivariate polynomial with n variables of only degree i, i.e. the coefficient of t^i, has T_i non-zero coefficients, where T_i can be calculated by

$$T_i = \binom{n+i}{i} - \binom{n+i-1}{i-1} \quad \text{for} \quad i > 0\,. \tag{8.49}$$

Thus, lower values of i lead to a lower value of T_i and therefore require less black-box probes for the interpolation than higher degrees. Since we are currently assuming a completely dense case, even the effect of $\vec{s}$ does not alter the total number of required probes. Guided by this observation, for each obtained probe, our proposal is now the following:

1. Build a system of equations as

$$\sum_i n_{\mathrm{u},i}(\vec{y})t^i - \hat{f}(\vec{y})\sum_j d_{\mathrm{u},j}(\vec{y})t^j = \hat{f}(\vec{y})\sum_j d_{\mathrm{s},j}(\vec{y})t^j - \sum_i n_{\mathrm{s},i}(\vec{y})t^i, \tag{8.50}$$

   where the subscripts s and u denote the solved and unsolved coefficients, respectively, after one interpolation with Eq. (8.44) is performed. The polynomials $n_{x,i}(\vec{z})$ and $d_{x,i}(\vec{z})$ with $x \in \{\mathrm{s},\mathrm{u}\}$ are built by monomials defined by Eq. (8.40) and fulfill Eq. (8.38) such that their degree is equal to i. Note that at least one usage of Thiele's interpolation formula is required to determine the occurring degrees of numerator and denominator in t. The coefficient of either $d_{s,0}$ or $n_{s,0}$, known after the first interpolation with Eq. (8.44), will serve as normalization and is thus set to one;

2. Solve the system of Eq. (8.50) if possible and interpolate all polynomial coefficients $n_{\mathrm{u},i}(\vec{z})$ and $d_{\mathrm{u},i}(\vec{z})$ including the effects of $\vec{s}$;
3. Whenever one polynomial in either numerator or denominator is interpolated successfully, decrease the size of the system of equations defined in Eq. (8.50) by inserting values $\vec{y}$ for the already interpolated functions $n_{s,i}(\vec{z})$ or $d_{s,i}(\vec{z})$ and setting the corresponding $n_{u,i}$ or $d_{u,i}$ to zero;
4. When all interpolations terminated, remove the effect of the shift $\vec{s}$ from $n_{s,i}(\vec{z})$ and $d_{s,i}(\vec{z})$ degree by degree starting from the highest occurring degree in numerator and denominator, respectively.

Using this prescription, no avoidable probes are requested for dense rational functions and one needs exactly one probe for each monomial. However, for sparse functions this approach generates a huge number of unneeded probes, which is also not optimal. Therefore, we propose a small modification by basically combining the benefits of both dense and sparse prescriptions to a hybrid algorithm that scales at most with the maximum number of possible non-zero terms but, in addition, exploits the sparsity of rational functions.

In practice, the main modifications are with regards to point 2, 3, and 4 of the algorithm mentioned above and are as follows:

2. Solve the system of Eq. (8.50) if possible and interpolate all polynomial coefficients $n_{\mathrm{u},i}(\vec{z})$ and $d_{\mathrm{u},i}(\vec{z})$ including the effects of $\vec{s}$. For illustration, we only focus on the numerator in the following, since the procedure is analogous for the denominator. Let $d_{n,\max}$ be the maximum degree of the numerator. If $n_{\mathrm{u},d_{n,\max}}(\vec{z})$ can be interpolated with less probes than the next lower degree, abort the interpolation of the latter and redo it from scratch by removing the effects of $\vec{s}$ originating from $n_{\mathrm{u},d_{n,\max}}(\vec{z})$ and using stored values. If additional probes are requested, subtract the effect of $\vec{s}$ from the result obtained by solving Eq. (8.50). Proceed in the same manner with all remaining polynomials;
3. Whenever one polynomial in either numerator or denominator is interpolated successfully, decrease the size of the system of equations defined in Eq. (8.50) by inserting values $\vec{y}$ for the already interpolated functions $n_{s,i}(\vec{z})$ or $d_{s,i}(\vec{z})$ and setting the corresponding $n_{u,i}$ or $d_{u,i}$ to zero. If a polynomial is interpolated without the effects of $\vec{s}$, the latter have to be added to Eq. (8.50) to provide consistent results;
4. After all interpolations terminated, remove the effect of the shift $\vec{s}$ from all remaining polynomials that are interpolated including effects of $\vec{s}$.

This algorithm cures the problem of requiring avoidable black-box probes for dense and sparse functions, but comes with additional computational work, that has to be done in exchange, by starting some interpolations from scratch. However, we observe that the computational effort of the interpolation is usually only a fraction of the time spent to

evaluate the required black-box probes. Hence, reducing the required number of the latter seems to be more important for our applications.

We have implemented this hybrid algorithm in the publicly available general purpose multivariate rational-function reconstruction[4] library `FireFly` in combination with a multivariate polynomial-interpolation algorithm, which is based on the sparse/dense racing prescription of Ref. [236]. To our knowledge, `FireFly` is the first open-source implementation of multivariate rational-function interpolation. A different approach, assuming dense functions, is implemented in the code of Ref. [229], however.

As the interpolation is performed over finite fields, there is a non-zero chance that the interpolated function is incorrect. One source of potential errors is the interpolation of multivariate polynomials. Zippel proved that if the anchor points are chosen uniformly randomly from a field $\mathbb{Z}_p$, the probability that the interpolation of a black box f with n variables, degree D, and non-zero terms T fails is less than [233]

$$\frac{nD^2T^2}{p}\,. \tag{8.51}$$

It is based on the Zippel-Schwartz lemma [232, 250]

$$\Pr[f(\vec{y}) = 0] \leq \frac{D}{|S|}\,, \tag{8.52}$$

which provides a bound on the probability (Pr) that a polynomial f of total degree D evaluates to zero when selecting $\vec{y}$ independently and uniformly randomly from a subset S of a field $\mathbb{F}$. The Zippel-Schwartz lemma provides an estimate of the probability of hitting zeroes in Eq. (8.46) in addition.

8.5.4 *Rational reconstruction*

After a successful interpolation over a finite field, we need to promote the monomial coefficients back to the field of rational numbers $\mathbb{Q}$. Generally, there is no inversion of the mapping from rational numbers to elements in a finite field, but one can use a method called *rational reconstruction* (RR). This method is based on the Extended Euclidean Algorithm [230] and the first algorithm to perform this task was described by Wang in 1981 [252].

This RR algorithm leads to a guess for a rational number $a = n/d$ from its image e,

$$e = a \mod m\,, \tag{8.53}$$

where n, d, and $m > e \geq 0$ are integers. The algorithm will succeed if $|n|, |d| \leq \sqrt{m/2}$ and the value of a is then unique [253]. However, the successful application of Wang's algorithm does not guarantee that a is the correct number in $\mathbb{Q}$, because the unique guess can differ

4 See Subsect. 8.5.4 for a definition of the term reconstruction.

for different moduli m. Additionally, the strict bound of $\sqrt{m/2}$ could lead to failures of the RR when one restricts m to be a machine-size integer, i.e. a 64-bit integer on modern CPUs.

Both problems can be solved by the Chinese Remainder Theorem (CRT) [230]. This theorem states that for a set of coprime moduli $m_i > 1$ and images $e_i = a \mod m_i$, there exists one and only one integer $0 \leq x < m_1 \cdot m_2 \cdots m_k$ such that

$$\begin{aligned} x &\equiv e_1 \mod m_1\,, \\ x &\equiv e_2 \mod m_2\,, \\ &\vdots \\ x &\equiv e_k \mod m_k\,, \end{aligned} \tag{8.54}$$

and the remainder of the Euclidean divisor of x by m_i is e_i for every i. In the context of functional interpolations over finite fields this leads to a possible combination of multiple interpolations over fields of coprime characteristic, from which we determine a new x that fulfills the definition from Eq. (8.54) and apply the RR to x with the module $m_1 \cdot m_2 \cdots m_k$. When Wang's algorithm results to the same number a in two consecutive prime fields after applying the CRT, we assume its guess as correct. We proceed for any monomial coefficient with this strategy until we obtain a guess for each of them. Afterwards, the whole function will be evaluated at randomized points and compared to the corresponding black-box probes. When both results coincide, we terminate the interpolation and RR and return the obtained result.

Note that the algorithm by Wang is not optimal for arbitrary n and d, because it will only succeed if both $|n|$ and $|d|$ are smaller than $\sqrt{m/2}$. In Ref. [254] it was observed that the successful guess of the rational number comes together with a huge quotient in the Euclidean Algorithm. Ref. [254] modifies Wang's algorithm to be sensitive to these cases and it is called Maximal Quotient Rational Reconstruction. It comes with the caveat, that it can only be proven to return a unique solution if $|n||d| \leq \sqrt{m}/3$, but performs much better in the average case, because large quotients from random input are rare.

To benefit from the advantages of both algorithms, we proposed in Ref. [203] to race them, i.e. run both algorithms sequentially and consider a guess for a, when either of the two succeeded.

The algorithms presented in this subsection are implemented as part of this thesis in the `FireFly` library [203]. The major part of the development has been done in the course of this thesis, while F. Lange implemented some parts of the interface to `Kira`. In a physical context `FireFly` has been successfully applied to calculate the results presented in Ref. [255], which were not obtainable with conventional methods. Further calculations have been completed using similar interpolation techniques implemented in private codes and should be mentioned here [256–264].

In the next subsection, we discuss how IBP reductions can benefit from the techniques implemented in the `FireFly` library in combination with the reduction program `Kira`. Note that the general prescriptions are in principle independent of the reduction program.

8.5.5 *Integration-by-parts reductions over finite fields*

The usage of finite fields as part of the Laporta algorithm has already been proposed in 2008 by Kauers [265]. Here, one replaces all occurring variables by elements in finite fields and solves the system of equations generated by Eq. (8.36) numerically. In general, this approach is orders of magnitude faster than solving the system algebraically. One of the first applications of this observation was realized in Ref. [266] by first performing the forward elimination over finite fields and removing linearly dependent equations before the actual algebraic reduction. When also performing the back substitution, the master integrals can be identified in addition and one is also able to select only those equations that suffice to reduce a requested subset of integrals. The latter procedure is implemented in `Kira` [221].

In 2014 von Manteuffel and Schabinger proposed in Ref. [226] that one should be able to solve the IBP system several times over finite fields and use the results to interpolate the master integral coefficients in principle. In 2016, they presented the first IBP reduction completed only with finite-field interpolation techniques in Ref. [256]. Recently, three more calculations were concluded [260, 261, 263]. All of them are one-scale problems and, thus, one variable problems. In January 2019 `FIRE6` was published as first public implementation of the Laporta algorithm using interpolation techniques over a finite field [218]. However, it is currently bound to handle at most two scales. The first application to multivariate reductions of, in principle, arbitrarily many variables was presented in Ref. [203] as part of this thesis. A first step towards a full multivariate calculation using interpolation techniques has been performed in Ref. [267]. A combined approach of interpolation and algebraic results within the IBP reduction context has been presented in Ref. [268].

For our work, we combine the interpolation and reconstruction techniques of the `FireFly` library with the IBP reduction code `Kira`. The latter provides us with an already built-in solver `pyRed`, which is used to solve the system of equations over a finite field. This procedure is performed multiple times over different prime fields, where we extract the numerical values provided by `pyRed` and feed them to `FireFly` in order to perform the interpolation and rational reconstruction. Additionally, two integral selections are performed. After the forward elimination not all of the initially required linearly independent equations are needed anymore for the back substitution in general. Therefore, we only select those equations that are required for the reduction of the requested integrals. The same selection is also performed in the algebraic calculation with `Kira`. The second selection only accepts the coefficients of the master integrals for the requested integrals. In a conventional approach, where all computational tasks are performed algebraically, the latter selection does not provide any benefit as the reduction is already completed at this point. However, in our

interpolation approach, this additional selection allows us to omit the interpolation of potentially difficult rational functions that are not required to get the desired result [203].

To illustrate the benefits of the rational-function-interpolation technique for IBP reductions, we consider the topology depicted in Fig. 30, which appears to be the most difficult topology for single top production at the two-loop level. We compare runtime and memory usage

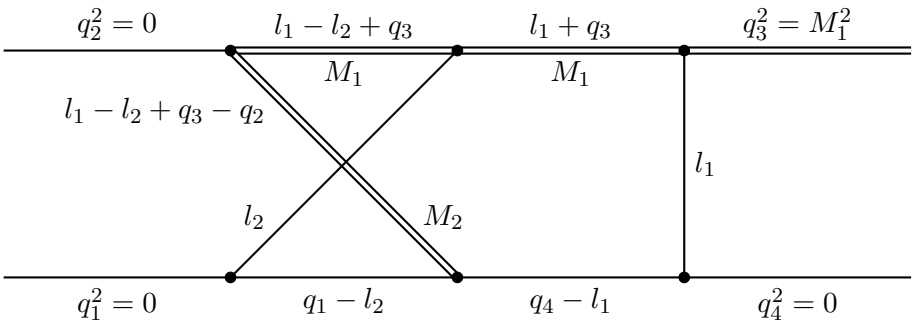

Figure 30: *A non-planar double box which occurs, e.g., in single top production. Double lines indicate massive propagators.*

of both the conventional fully algebraic approach implemented in `Kira 1.2` and `Kira 1.2` in combination with the interpolation techniques of `FireFly 1.3.4` for different values of s. The latter is defined as the absolute value of the sum of all negative powers of a topology:

$$s \equiv \sum_{i=1}^{\#\text{prop.}} \theta\left(\frac{1}{2} - a_i\right) |a_i| \,, \tag{8.55}$$

where $\theta(x)$ is the Heaviside step function. Usually, an integral with higher s is regarded as more difficult than an integral with lower s. The powers a_i are the same as defined in Eq. (8.35). The results are shown in Tab. 3. It is obvious that the interpolation approach is

Table 3: *Runtime and memory usage for `Kira 1.2` and `Kira` with `FireFly` for the reduction of the topology depicted in Fig. 30. M_1 is set to one. The runtime does not include the creation of the system of equations. These tests were run on a computer with two Intel Xeon Gold 6138 and 768 GiB of RAM.*

	`Kira 1.2`		`Kira` with `FireFly`		
s	Runtime	Memory usage	Runtime	CPU time for `pyRed`	Memory usage
1	4 min	7.6 GiB	1 min 21 s	99 %	1.2 GiB
2	1 h 53 min	33 GiB	35 min 8 s	99 %	4.1 GiB
3	18 h 28 min	102 GiB	5 h 39 min	97 %	19 GiB

not only faster by factors up to ~ 3, it also uses only a fraction of the memory required by the conventional approach. In addition, the CPU time is dominated by probing the black box with `pyRed` and not by the interpolation itself. This fact motivates two different types of optimizations:

1. Decrease the number of operations within the system solver, e.g. by reducing the overhead that comes with the solution of a system at a given parameter point. This can be achieved, for example, by solving the system for several points in a vectorized manner on one thread. However, this runtime improvement comes with the cost of a larger memory footprint since more systems of equations have to be kept in memory at the same time. In our studies we observe improvements regarding runtime up to a factor of ≈ 3.
2. In our studies, the forward elimination with `pyRed` takes almost 90% of the total runtime for one probe. Thus, performing the forward elimination algebraically with `Kira`, which is usually significantly faster than the back substitution, and only calculating the back substitution numerically can also help by further reducing the black-box evaluation time [203]. Note, however, that the functions within the system of equations become larger after the forward elimination. Thus, a fast parser, as for example implemented in `FireFly`, that evaluates the occurring functions, is crucial to be competitive. We have studied different IBP reductions up to three scales and could observe runtime improvements of up to an order of magnitude using this hybrid approach that combines algebraic and interpolation techniques. However, if the functions that occur after the forward elimination become too complicated to be parsed reasonably fast, the proposed hybrid approach becomes slower than calculating both forward elimination and back substitution numerically.

In the next section, we apply the interpolation techniques introduced in the previous three subsections to the reduction of the integrals occurring in gluon-induced ZH production at the two-loop level considering QCD corrections.

8.5.6 *Reduction of two-loop integrals for gluon-induced ZH production*

After applying sector relations, the required integral families reduce to the topologies T1, T2b, T2c, T3a, T4a, T4b, T4c, T4d, T7, T8a, T10a, T10c, and T10d as depicted in Fig. 28 for different mass distributions. The number of integrals to be reduced also decreases to roughly 2000, where redundant integrals that can be obtained by the crossing of the incoming gluons have already been dropped.

We only aim to reduce the 2000 integrals occurring in the amplitude instead of performing a full reduction up to given bounds of s, which could be useful for the calculation of the master integrals. However, this would further complicate the reduction significantly. Therefore, for each integral family, we pass the list of integrals to `Kira` and combine it with `FireFly` for the reduction. The coefficients of the master integrals are rational functions of the five scales s, t, h, z, and M_q and the space-time dimension d. By setting one scale to one, whose dependence can be reconstructed by dimensional analysis afterwards, the to be determined coefficients depend on five variables. A first scan of the auxiliary functions $\hat{f}$ for

each integral family revealed maximum degrees around 160, which for five variables would lead to a dense bound of roughly $1.9 \cdot 10^9$ possible monomials following Eq. (8.49). For this number even the interpolation technique could possibly become not feasible anymore and could suffer from probabilistic chances of incorrect interpolations as estimated by Eq. (8.51). Therefore, we fix the mass of the quark q occurring in the loops by a ratio to the Z mass. Within the scope of this thesis, we only focus on the top quark and fix M_t to

$$M_t^2 = \frac{18}{5} z \approx \left(\frac{173}{91}\right)^2 z \,. \tag{8.56}$$

Afterwards, we choose z to be the variable that is set to one. Using this ratio the reduction simplifies significantly by decreasing the possible number of monomials by two orders of magnitude and thus to be bounded by roughly $6 \cdot 10^7$. Note, however, that the substitution imposed by Eq. (8.56) leads to larger rational numbers as coefficients of each monomial, thus requiring more prime fields than without this replacement.

Using `Kira` in combination with `FireFly` and the setup described in the previous paragraphs, we were able to reduce the integral families affiliated with the topologies T1, T2c, T3a, T4a, T4b, T4c, T4d, T7, T8a, T10a, T10c, and T10d. The most complicated ones are those belonging to T2b and T2c, where both reductions are of comparable complexity, but differ in the black-box evaluation time. The most complicated coefficient of the master integrals of T2c has a maximum degree of 166 in the numerator and 163 in the denominator leading to a dense bound of almost $6.5 \cdot 10^7$ possible monomials. Fortunately, only $1.2 \cdot 10^7$ of them are non-zero. In total $1.1 \cdot 10^8$ black-box probes and twelve prime fields were needed to complete the reduction of this integral family using 80 threads on two Intel Xeon Gold 6138. The reduction filled 240 GiB of memory and was completed in one and a half month, where each black-box probe took on average 3.8 s. We applied the non-hybrid approach without any vectorization of black-box probes.

The only missing reduction is currently the one belonging to topology T2b. The maximum degrees of numerator and denominator are comparable to the one of T2c, but the black-box probe takes on average 4.7 s and would therefore run considerably longer than T2c. However, it is conceivable that the reduction of T2b could also be completed, taking additional time.

Since we applied the relation of Eq. (8.56), the full reduction has also to be computed again for the bottom quark with a suitable replacement of M_b or in the limit of $M_b = 0$. Further, the missing one-particle-reducible two-loop diagrams, the contributions of real radiation, and the calculation of all master integrals have to be considered. Therefore, a lot of additional work has to be done in order to receive the result for the cross section of gluon-induced ZH production at NLO QCD incorporating quark-mass effects. However, the technical improvements developed within this thesis strongly support the feasibility of calculations with similar complexity. Additionally, we observed that some kinematical parts and parts related to the space-time dimension d can possibly be factorized, which would

lead to much simpler rational functions to be interpolated. We are currently working on an algorithm for `FireFly` that detects factorizable polynomials automatically for this purpose.

8.6 CONCLUSIONS AND OUTLOOK

In this chapter, we have presented recent progress on the calculation of NLO QCD contributions to gluon-induced ZH production, where we are aiming to incorporate full quark-mass dependence. The computational steps required to obtain the amplitude were summarized and occurring integrals were prepared for further processing. We achieved an almost complete reduction of the involved Feynman integrals to a set of roughly 500 master integrals by imposing a relation between the top-quark mass and the Z-boson mass. The reduction has been computed employing the `Kira` program in combination with the functional-interpolation-library `FireFly` developed within the scope of this thesis. The techniques and algorithms implemented in `FireFly` allow to ease the computational bottleneck of cutting-edge calculations like the one presented in this chapter. Additionally, various other applications like the calculation of projector coefficients can be achieved efficiently using the interpolation approach instead of a fully algebraic computation. As further algorithmic optimizations, e.g. polynomial factorization, promise to make the interpolation technique even more efficient, we are certain that calculations of similar complexity as gluon-initiated ZH production can be completed employing the techniques implemented into the `FireFly` library.

In order to obtain a complete result at NLO QCD, all master integrals have still to be evaluated and the missing integral family has to be reduced. In addition, renormalization has to be performed and the real radiation together with the reducible two-loop subgraphs have to be evaluated. Fortunately, the latter two parts consist only of one-loop diagrams, whose integral structure is well-known.

As the current implementation of `FireFly` into `Kira` is private, it would be a great benefit if their combination becomes publicly available. Therefore, we are currently working together with the `Kira` authors to provide an open-source code. However, this work is beyond the scope of this thesis.

Part III

APPENDICES

A

CONVENTIONS AND FEYNMAN RULES

In this appendix, we summarize notational conventions and introduce all momentum space Feynman rules required in this thesis.

Throughout this work, we use natural units, i.e. $\hbar = c = 1$. Therefore, masses, momenta, and energies are expressed in electronvolts (eV) and distances and time in eV^{-1}.

We define the metric tensor of a four-dimensional Minkowski space-time in the mostly minus convention, i.e.

$$g = \mathrm{diag}(1, -1, -1, -1)\,. \tag{A.1}$$

Hence, scalar products of four-dimensional vectors in Minkowski space are given by

$$a \cdot b \equiv a_\mu b^\mu \equiv a_0 b_0 - \vec{a} \cdot \vec{b}\,. \tag{A.2}$$

The Feynman rules required in this thesis are the ones of QCD in Feynman gauge, the Yukawa coupling of the Higgs boson to a quark, the coupling of the Z boson to a pair of quarks, the coupling of the neutral Goldstone boson to a quark pair, and the coupling of the Z to the Higgs boson. For the propagator of the Z boson, we impose Landau gauge. The mass of the quark is denoted as M_q, its electric charge in units of the elementary electric charge as e_q, and its third component of the isospin as I_q. θ_w is the weak mixing angle, g is the coupling constant of the weak interaction, and g_3 is the coupling constant of the strong interaction. The momenta are assumed to be incoming and labeled as p for the propagators. All used Feynman rules are listed in the following equations:

g: 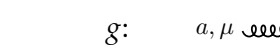 $= -\mathrm{i}\dfrac{g_{\mu\nu}\delta^{ab}}{p^2 + \mathrm{i}0}$ (A.3)

ghost (c): 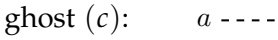 $= \mathrm{i}\dfrac{\delta^{ab}}{p^2 + \mathrm{i}0}$ (A.4)

q: 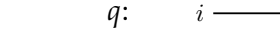 $= \mathrm{i}\dfrac{(\not{p} + M_q)\delta^{ij}}{p^2 - M_q^2 + \mathrm{i}0}$ (A.5)

σ: $= \mathrm{i}\delta^{ab} g_{\alpha\delta} g_{\beta\gamma}$ (A.6)

Z: 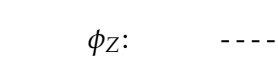 $= -\mathrm{i}\dfrac{g_{\mu\nu} - p_\mu p_\nu / p^2}{p^2 - M_Z^2 + \mathrm{i}0}$ (A.7)

ϕ_Z: $= \dfrac{\mathrm{i}}{p^2 + \mathrm{i}0}$ (A.8)

ggg:

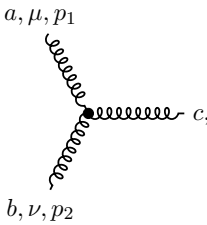

$$= -g_3 f^{abc}\Big[g^{\mu\nu}(p_1-p_2)^{\lambda} + g^{\nu\lambda}(p_2-p_3)^{\mu} + g^{\lambda\mu}(p_3-p_1)^{\nu}\Big] \tag{A.9}$$

$gggg$:

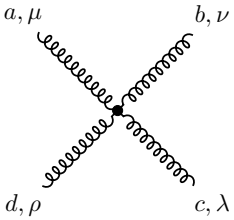

$$= -ig_3^2\Big[f^{abe}f^{cde}\left(g^{\mu\lambda}g^{\nu\rho}-g^{\mu\rho}g^{\nu\lambda}\right) + f^{ace}f^{bde}\left(g^{\mu\nu}g^{\lambda\rho}-g^{\mu\rho}g^{\nu\lambda}\right) + f^{ade}f^{cbe}\left(g^{\mu\lambda}g^{\nu\rho}-g^{\mu\nu}g^{\rho\lambda}\right)\Big] \tag{A.10}$$

$gg\sigma$:

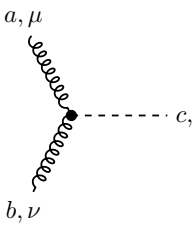

$$= \frac{g_3}{\sqrt{2}} f^{abc}\left(g^{\mu\alpha}g^{\nu\beta}-g^{\mu\beta}g^{\nu\alpha}\right) \tag{A.11}$$

$c\bar{c}g$:

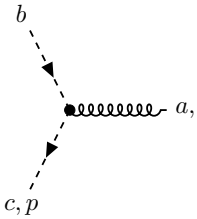

$$= g_3 f^{abc} p^{\mu} \tag{A.12}$$

$q\bar{q}g$:

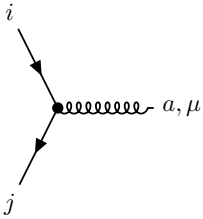

$$= -ig_3\gamma^{\mu}T^a_{ji} \tag{A.13}$$

$q\bar{q}H$:

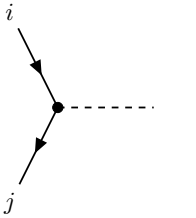

$$= -i\frac{M_q\delta_{ji}}{v} \tag{A.14}$$

$q\bar{q}\phi_Z$:

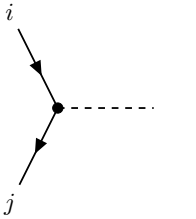

$$= -2\frac{I_q M_q}{v}\gamma_5 \tag{A.15}$$

$q\bar{q}Z$:
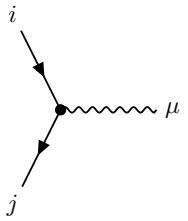

$$= \mathrm{i}\frac{g}{\cos\theta_w}\gamma_\mu\left(\frac{I_q}{2} - e_q \sin^2\theta_w \frac{I_q}{2}\gamma_5\right) \tag{A.16}$$

ZHZ:
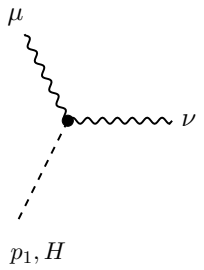

$$= \mathrm{i}\frac{g}{\cos\theta_w} M_Z g_{\mu\nu} \tag{A.17}$$

$H\phi_Z Z$:
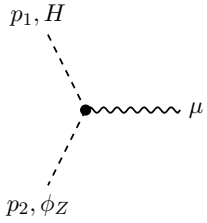

$$= \frac{g}{2\cos\theta_w}\left(p_2 - p_1\right)_\mu \tag{A.18}$$

In this thesis, all Feynman diagrams have been created with TikZ-Feynman [269].

B

EXPLICIT FORMULÆ

In this appendix, we list some formulæ required by some chapters in this work.

B.1 THRESHOLD CORRECTIONS

The following threshold corrections required in Subsect. 3.1.3 are used to relate the SM input parameters of gauge couplings and the top quark pole mass to running $\overline{\text{DR}}'$ parameters. The terms for the gauge couplings read:

$$\begin{aligned}\Delta\alpha_{\text{em}}(M_Z) = \frac{\alpha_{\text{em}}}{2\pi}\Bigg(&\frac{1}{3} - \frac{16}{9}\ln\left(\frac{m_t}{M_Z}\right) - \frac{4}{9}\sum_{i=1}^{6}\ln\left(\frac{m_{\tilde{u}_i}}{M_Z}\right) - \frac{1}{9}\sum_{i=1}^{6}\ln\left(\frac{m_{\tilde{d}_i}}{M_Z}\right)\\ &- \frac{4}{3}\sum_{i=1}^{2}\ln\left(\frac{m_{\tilde{\chi}_i^+}}{M_Z}\right) - \frac{1}{3}\sum_{i=1}^{6}\ln\left(\frac{m_{\tilde{e}_i}}{M_Z}\right) - \frac{1}{3}\ln\left(\frac{m_{H^+}}{M_Z}\right)\Bigg), \qquad \text{(B.1)}\\ \Delta\alpha_s(M_Z) = \frac{\alpha_s}{2\pi}\Bigg[&\frac{1}{2} - 2\ln\left(\frac{m_{\tilde{g}}}{M_Z}\right) - \frac{2}{3}\ln\left(\frac{m_t}{M_Z}\right)\\ &- \frac{1}{6}\sum_{i=1}^{6}\left(\ln\left(\frac{m_{\tilde{u}_i}}{M_Z}\right) + \ln\left(\frac{m_{\tilde{d}_i}}{M_Z}\right)\right)\Bigg]. \qquad \text{(B.2)}\end{aligned}$$

$\tilde{\chi}_i^+$ is the ith positively charged chargino, and $\tilde{u}_i$ ($\tilde{d}_i$) label the up-(down-)type squarks of the ith generation. Consequently, $\tilde{e}_i$ labels the slepton of the ith generation.

The terms required in the extraction of the top quark mass in the $\overline{\text{DR}}'$ scheme read:

$$\begin{aligned}\Delta m_t^{(1),\text{QCD}} = -\frac{\alpha_s}{4\pi}C_F\Bigg[&\left(\frac{m_{\tilde{g}}m_{\tilde{t}_1}^2 s_{2\theta_t}}{m_t(m_{\tilde{t}_1}^2 - m_{\tilde{g}}^2)} - \frac{m_{\tilde{g}}m_{\tilde{t}_2}^2 s_{2\theta_t}}{m_t(m_{\tilde{t}_2}^2 - m_{\tilde{g}}^2)} + \frac{m_{\tilde{t}_1}^4}{2(m_{\tilde{t}_1}^2 - m_{\tilde{g}}^2)^2}\right.\\ &\left. - \frac{m_{\tilde{t}_1}^2}{m_{\tilde{t}_1}^2 - m_{\tilde{g}}^2} + \frac{m_{\tilde{t}_2}^4}{2(m_{\tilde{t}_2}^2 - m_{\tilde{g}}^2)^2} - \frac{m_{\tilde{t}_2}^2}{m_{\tilde{t}_2}^2 - m_{\tilde{g}}^2} + 1\right)\ln\left(\frac{m_{\tilde{g}}^2}{Q^2}\right)\\ &+ \left(-\frac{m_{\tilde{g}}m_{\tilde{t}_1}^2 s_{2\theta_t}}{m_t(m_{\tilde{t}_1}^2 - m_{\tilde{g}}^2)} - \frac{m_{\tilde{t}_1}^4}{2(m_{\tilde{t}_1}^2 - m_{\tilde{g}}^2)^2} + \frac{m_{\tilde{t}_1}^2}{m_{\tilde{t}_1}^2 - m_{\tilde{g}}^2}\right)\ln\left(\frac{m_{\tilde{t}_1}^2}{Q^2}\right)\\ &+ \left(\frac{m_{\tilde{g}}m_{\tilde{t}_2}^2 s_{2\theta_t}}{m_t(m_{\tilde{t}_2}^2 - m_{\tilde{g}}^2)} - \frac{m_{\tilde{t}_2}^4}{2(m_{\tilde{t}_2}^2 - m_{\tilde{g}}^2)^2} + \frac{m_{\tilde{t}_2}^2}{m_{\tilde{t}_2}^2 - m_{\tilde{g}}^2}\right)\ln\left(\frac{m_{\tilde{t}_2}^2}{Q^2}\right)\\ &+ \frac{m_{\tilde{t}_1}^2}{2(m_{\tilde{t}_1}^2 - m_{\tilde{g}}^2)} + \frac{m_{\tilde{t}_2}^2}{2(m_{\tilde{t}_2}^2 - m_{\tilde{g}}^2)} - 3\ln\left(\frac{m_t^2}{Q^2}\right) + \frac{7}{2}\Bigg], \qquad \text{(B.3)}\end{aligned}$$

$$\Delta m_t^{(2),\mathrm{QCD}} = \left(\Delta m_t^{(1),\mathrm{QCD}}\right)^2 - \Delta m_t^{(2),\mathrm{dec}} . \tag{B.4}$$

In Eq. (B.3), it is $C_F = 4/3$ and $s_{2\theta_t}$, where θ_t is the stop mixing angle given by

$$\sin(2\theta_t) = 2\frac{X_t m_t}{m_{\tilde{t}_1}^2 - m_{\tilde{t}_2}^2} . \tag{B.5}$$

The two-loop term $\Delta m_t^{(2),\mathrm{dec}}$ is given in Ref. [93] for general stop, sbottom, and gluino masses.

B.2 PROJECTOR COEFFICIENTS

To obtain the form factors $f_1(t,u),\ldots,f_4(t,u)$[1] as defined by Eq. (8.17), the following set of projector coefficients is used:

$$\begin{aligned}
c_{1,1} &= 4d_1^{-1}D_{2,1}\Delta_{tz}^2 z\big(-4D_{2,2}s^3z^3 + D_{3,1}\Delta_{tz}^3\Delta_{uz}^3 - 4D_{3,2}\Delta_{tz}\Delta_{uz}s^2z^2 \\
&\quad + D_{5,1}\Delta_{tz}^2\Delta_{uz}^2 sz\big) , && \text{(B.6)}\\
c_{1,2} &= -4d_1^{-1}D_{2,1}\Delta_{tz}\Delta_{uz} z\big(D_{3,3}\Delta_{tz}^3\Delta_{uz}^3 - 4D_{3,4}s^3z^3 + 2D_{4,1}\Delta_{tz}\Delta_{uz}s^2z^2 \\
&\quad + D_{5,2}\Delta_{tz}^2\Delta_{uz}^2 sz\big) , && \text{(B.7)}\\
c_{1,3} &= 4d_1^{-1}D_{1,1}^2 D_{2,3}\Delta_{tz}s^2\big(z(\Delta_{uz}+s) - \Delta_{uz}t\big)^3 , && \text{(B.8)}\\
c_{1,4} &= -4d_1^{-1}D_{1,2}^2 D_{1,1}^2\Delta_{tz}^2 s^2 z(-D_{1,2}\Delta_{tz}\Delta_{uz} - 2sz)(D_{2,4}\Delta_{tz}\Delta_{uz} + D_{2,5}sz) , && \text{(B.9)}\\
c_{1,5} &= -4d_1^{-1}D_{2,1}\Delta_{tz}sz\big\{sz\big[2D_{1,1}sz\big(D_{3,5}\Delta_{tz}\Delta_{uz} - 2D_{3,6}sz\big) + D_{6,1}\Delta_{tz}^2\Delta_{uz}^2\big] \\
&\quad - D_{5,3}\Delta_{tz}^3\Delta_{uz}^3\big\} , && \text{(B.10)}\\
c_{1,6} &= 4d_1^{-1}D_{1,2}^2 D_{1,1}s^2 z\big(D_{1,2}\Delta_{tz}\Delta_{uz} + 2sz\big)\big(D_{3,7}\Delta_{tz}^2\Delta_{uz}^2 + D_{4,2}\Delta_{tz}\Delta_{uz}sz \\
&\quad - 2D_{3,8}s^2z^2\big) , && \text{(B.11)}\\
c_{1,7} &= -4d_1^{-1}D_{1,2}^2 D_{1,1}\Delta_{tz}sz\big(-D_{1,2}\Delta_{tz}\Delta_{uz} - 2sz\big)\big(2D_{2,2}\Delta_{tz}^2\Delta_{uz}^2 + 2D_{2,2}s^2z^2 \\
&\quad + D_{3,9}\Delta_{tz}\Delta_{uz}sz\big) , && \text{(B.12)}\\
c_{1,8} &= 4d_1^{-1}D_{1,2}D_{2,1}\Delta_{tz}\Delta_{uz} z\big(4D_{1,1}^2 D_{2,6}s^3z^3 + D_{4,3}\Delta_{tz}^3\Delta_{uz}^3 + 2D_{4,4}\Delta_{tz}^2\Delta_{uz}^2 sz \\
&\quad - 2D_{4,5}\Delta_{tz}\Delta_{uz}s^2z^2\big) , && \text{(B.13)}\\
c_{1,9} &= 4d_1^{-1}D_{1,2}D_{2,1}\Delta_{tz}^2 z\big(4D_{2,7}s^3z^3 + D_{4,6}\Delta_{tz}^3\Delta_{uz}^3 + D_{5,4}\Delta_{tz}^2\Delta_{uz}^2 sz \\
&\quad - 2D_{5,5}\Delta_{tz}\Delta_{uz}s^2z^2\big) , && \text{(B.14)}\\
c_{1,14} &= 2d_1^{-1}D_{1,2}D_{1,1}^2\Delta_{tz}\Delta_{uz}s\big\{sz\big[D_{4,7}\Delta_{tz}^2\Delta_{uz}^2 - 4sz\big(D_{3,6}sz + D_{3,10}\Delta_{tz}\Delta_{uz}\big)\big] \\
&\quad + D_{3,11}\Delta_{tz}^3\Delta_{uz}^3\big\} , && \text{(B.15)}\\
c_{1,15} &= 2d_1^{-1}D_{1,2}D_{1,1}^2\Delta_{tz}^2 s\big\{sz\big[D_{4,8}\Delta_{tz}^2\Delta_{uz}^2 + 2sz(D_{4,9}\Delta_{tz}\Delta_{uz} + 2sz)\big] \\
&\quad + D_{3,11}\Delta_{tz}^3\Delta_{uz}^3\big\} , && \text{(B.16)}\\
c_{1,21} &= 2\frac{c_{1,14}}{\Delta_{uz}} , && \text{(B.17)}
\end{aligned}$$

1 Note that $f_1(u,t),\ldots,f_4(u,t)$ can be obtained by the replacement $t \leftrightarrow u$.

$$c_{1,22} = 2\frac{c_{1,15}}{\Delta_{tz}}\,, \tag{B.18}$$

$$\begin{aligned} c_{2,1} = {} & -4d_2^{-1}D_{2,1}\Delta_{tz}z\big[\Delta_{uz}t - z\big(\Delta_{uz}+s\big)\big]^2 \\ & \times\big\{sz\big[sz\big(4D_{1,1}sz + D_{4,11}\Delta_{tz}\Delta_{uz}\big) + D_{5,6}\Delta_{tz}^2\Delta_{uz}^2\big] - D_{5,7}\Delta_{tz}^3\Delta_{uz}^3\big\} \\ & \times\big\{sz\big[D_{5,8}\Delta_{tz}^2\Delta_{uz}^2 - 4sz\big(D_{3,12}\Delta_{tz}\Delta_{uz} + D_{3,8}sz\big)\big] - D_{4,10}\Delta_{tz}^3\Delta_{uz}^3\big\}\,, \end{aligned} \tag{B.19}$$

$$\begin{aligned} c_{2,2} = {} & -4d_2^{-1}D_{2,1}\Delta_{uz}z\big[\Delta_{uz}t - z\big(\Delta_{uz}+s\big)\big]^2 \\ & \times\big\{sz\big[2D_{1,1}sz\big(D_{3,13}\Delta_{tz}\Delta_{uz} - 2D_{3,6}sz\big) + D_{6,1}\Delta_{tz}^2\Delta_{uz}^2\big] - D_{5,3}\Delta_{tz}^3\Delta_{uz}^3\big\} \\ & \times\big\{sz\big[D_{5,8}\Delta_{tz}^2\Delta_{uz}^2 - 4sz\big(D_{3,12}\Delta_{tz}\Delta_{uz} + D_{3,8}sz\big)\big] - D_{4,10}\Delta_{tz}^3\Delta_{uz}^3\big\}\,, \end{aligned} \tag{B.20}$$

$$\begin{aligned} c_{2,3} = {} & -4d_2^{-1}D_{2,1}sz\big[\Delta_{uz}t - z\big(\Delta_{uz}+s\big)\big]^2 \\ & \times\big(4D_{4,12}\Delta_{tz}\Delta_{uz}s^2z^2 - 4D_{4,13}s^3z^3 - D_{6,2}\Delta_{tz}^3\Delta_{uz}^3 + D_{6,3}\Delta_{tz}^2\Delta_{uz}^2sz\big) \\ & \times\big\{sz\big[D_{5,8}\Delta_{tz}^2\Delta_{uz}^2 - 4sz\big(D_{3,12}\Delta_{tz}\Delta_{uz} + D_{3,8}sz\big)\big] - D_{4,10}\Delta_{tz}^3\Delta_{uz}^3\big\}\,, \end{aligned} \tag{B.21}$$

$$\begin{aligned} c_{2,4} = {} & 4d_2^{-1}D_{1,2}^2D_{1,1}^2\Delta_{tz}s^2z\big[\Delta_{uz}t - z\big(\Delta_{uz}+s\big)\big]^2\big(D_{1,2}\Delta_{tz}\Delta_{uz} + 2sz\big)^2 \\ & \times\big(D_{2,8}sz + D_{3,14}\Delta_{tz}\Delta_{uz}\big)\big[sz\big(2D_{3,8}sz - D_{4,14}\Delta_{tz}\Delta_{uz}\big) + D_{3,11}\Delta_{tz}^2\Delta_{uz}^2\big]\,, \end{aligned} \tag{B.22}$$

$$\begin{aligned} c_{2,5} = {} & 2d_2^{-1}D_{2,1}sz\big(2D_{5,9}\Delta_{tz}^2\Delta_{uz}^2s^2z^2 - 4D_{5,10}\Delta_{tz}\Delta_{uz}s^3z^3 + D_{6,4}\Delta_{tz}^4\Delta_{uz}^4 \\ & + D_{7,1}\Delta_{tz}^3\Delta_{uz}^3sz + 8D_{1,3}D_{1,1}^2s^4z^4\big) \\ & \times\big\{D_{4,10}\Delta_{tz}^4\Delta_{uz}^4 + s^2z^2\big[4sz\big(D_{3,16}\Delta_{tz}\Delta_{uz} - D_{3,8}sz\big) + D_{5,11}\Delta_{tz}^2\Delta_{uz}^2\big] \\ & - D_{5,12}sz\Delta_{tz}^3\Delta_{uz}^3\big\}\,, \end{aligned} \tag{B.23}$$

$$\begin{aligned} c_{2,6} = {} & -2d_2^{-1}D_{1,2}^2D_{1,1}\Delta_{uz}s^2z\big[z\big(\Delta_{uz}+s\big) - \Delta_{uz}t\big]\big(D_{1,2}\Delta_{tz}\Delta_{uz} + 2sz\big)^2 \\ & \times\big(D_{4,15}\Delta_{tz}^2\Delta_{uz}^2 + 2D_{4,16}s^2z^2 - D_{5,13}\Delta_{tz}\Delta_{uz}sz\big) \\ & \times\big[sz\big(2D_{3,8}sz - D_{4,14}\Delta_{tz}\Delta_{uz}\big) + D_{3,11}\Delta_{tz}^2\Delta_{uz}^2\big]\,, \end{aligned} \tag{B.24}$$

$$\begin{aligned} c_{2,7} = {} & -4d_2^{-1}D_{1,2}^2D_{1,1}sz\big[\Delta_{uz}t - z\big(\Delta_{uz}+s\big)\big]^2\big(D_{1,2}\Delta_{tz}\Delta_{uz} + 2sz\big)^2 \\ & \times\big(D_{2,9}\Delta_{tz}\Delta_{uz}sz + D_{3,15}\Delta_{tz}^2\Delta_{uz}^2 - 2D_{1,1}s^2z^2\big) \\ & \times\big[sz\big(D_{4,14}\Delta_{tz}\Delta_{uz} - 2D_{3,8}sz\big) - D_{3,11}\Delta_{tz}^2\Delta_{uz}^2\big]\,, \end{aligned} \tag{B.25}$$

$$\begin{aligned} c_{2,8} = {} & -4d_2^{-1}D_{1,2}D_{2,1}\Delta_{uz}z\big[\Delta_{uz}t - z\big(\Delta_{uz}+s\big)\big]^2 \\ & \times\big(4D_{1,1}^2D_{2,10}s^3z^3 + D_{5,14}\Delta_{tz}^3\Delta_{uz}^3 + D_{5,15}\Delta_{tz}^2\Delta_{uz}^2sz + 2D_{5,16}\Delta_{tz}\Delta_{uz}s^2z^2\big) \\ & \times\big\{sz\big[D_{5,8}\Delta_{tz}^2\Delta_{uz}^2 - 4sz\big(D_{3,12}\Delta_{tz}\Delta_{uz} + D_{3,8}sz\big)\big] - D_{4,10}\Delta_{tz}^3\Delta_{uz}^3\big\}\,, \end{aligned} \tag{B.26}$$

$$\begin{aligned} c_{2,9} = {} & 2d_2^{-1}D_{1,2}D_{2,1}\Delta_{tz}z\big\{D_{4,10}\Delta_{tz}^4\Delta_{uz}^4 \\ & + s^2z^2\big[4sz\big(D_{3,16}\Delta_{tz}\Delta_{uz} - D_{3,8}sz\big) + D_{5,11}\Delta_{tz}^2\Delta_{uz}^2\big] - szD_{5,12}\Delta_{tz}^3\Delta_{uz}^3\big\} \\ & \times\big\{2D_{1,1}s^2z^2\big[2sz\big(2D_{3,14}sz + D_{4,17}\Delta_{tz}\Delta_{uz}\big) + D_{5,17}\Delta_{uz}^2\Delta_{tz}^2\big] \\ & - D_{6,5}sz\Delta_{tz}^3\Delta_{uz}^3 + D_{5,18}\Delta_{tz}^4\Delta_{uz}^4\big\}\,, \end{aligned} \tag{B.27}$$

$$\begin{aligned} c_{2,14} = {} & 2d_2^{-1}D_{1,2}D_{1,1}^2\Delta_{uz}s\big[\Delta_{uz}t - z\big(\Delta_{uz}+s\big)\big]^2 \\ & \times\big\{sz\big[D_{5,19}\Delta_{tz}^2\Delta_{uz}^2 - 2sz\big(2D_{2,11}sz + D_{4,18}\Delta_{tz}\Delta_{uz}\big)\big] + D_{3,11}\Delta_{tz}^3\Delta_{uz}^3\big\} \\ & \times\big\{sz\big[D_{5,8}\Delta_{tz}^2\Delta_{uz}^2 - 4sz\big(D_{3,12}\Delta_{tz}\Delta_{uz} + D_{3,8}sz\big)\big] - D_{4,10}\Delta_{tz}^3\Delta_{uz}^3\big\}\,, \end{aligned} \tag{B.28}$$

$$\begin{aligned} c_{2,15} = {} & -2d_2^{-1}D_{1,2}D_{1,1}^2\Delta_{tz}s\big[\Delta_{uz}t - z\big(\Delta_{uz}+s\big)\big]^2 \\ & \times\big\{sz\big[D_{5,8}\Delta_{tz}^2\Delta_{uz}^2 - 4sz\big(D_{3,12}\Delta_{tz}\Delta_{uz} + D_{3,8}sz\big)\big] - D_{4,10}\Delta_{tz}^3\Delta_{uz}^3\big\} \end{aligned}$$

$$\times \left\{ sz\left[D_{5,20}\Delta_{tz}^2\Delta_{uz}^2 + 2sz\left(D_{4,19}\Delta_{tz}\Delta_{uz} + 2D_{3,17}sz \right) \right] - D_{3,11}\Delta_{tz}^3\Delta_{uz}^3 \right\}, \tag{B.29}$$

$$c_{2,21} = 2\frac{c_{2,14}}{\Delta_{uz}}, \tag{B.30}$$

$$c_{2,22} = 2\frac{c_{2,15}}{\Delta_{tz}}, \tag{B.31}$$

$$c_{3,1} = 4d_3^{-1}D_{1,1}\Delta_{tz}^2\left[z\left(\Delta_{uz} + s \right) - \Delta_{uz}t \right]^3 \left(D_{2,4}\Delta_{tz}\Delta_{uz} + D_{2,5}sz \right), \tag{B.32}$$

$$c_{3,2} = 4d_3^{-1}\left(\Delta_{tz}\Delta_{uz} - sz \right)^3 \left(D_{3,18}\Delta_{tz}^2\Delta_{uz}^2 - D_{4,20}\Delta_{tz}\Delta_{uz}sz + 2D_{3,8}s^2z^2 \right), \tag{B.33}$$

$$c_{3,3} = 4d_3^{-1}D_{1,1}\Delta_{tz}s\left[z\left(\Delta_{uz} + s \right) - \Delta_{uz}t \right]^3 \left(- D_{2,8}sz - D_{3,14}\Delta_{tz}\Delta_{uz} \right), \tag{B.34}$$

$$c_{3,4} = 4d_3^{-1}D_{1,1}^2D_{2,3}\Delta_{tz}^2s^2\left[z\left(\Delta_{uz} + s \right) - \Delta_{uz}t \right]^3, \tag{B.35}$$

$$c_{3,5} = 2d_3^{-1}\Delta_{tz}s\left[\Delta_{uz}t - z\left(\Delta_{uz} + s \right) \right]^2 \left(D_{4,15}\Delta_{tz}^2\Delta_{uz}^2 + 2D_{4,16}s^2z^2 - D_{5,13}\Delta_{tz}\Delta_{uz}sz \right), \tag{B.36}$$

$$c_{3,6} = -2d_3^{-1}s^2\left[\Delta_{uz}t - z\left(\Delta_{uz} + s \right) \right]^2 \left(D_{1,2}^2D_{2,13}\Delta_{tz}^2\Delta_{uz}^2 + 2D_{4,21}s^2z^2 - D_{5,21}\Delta_{tz}\Delta_{uz}sz \right), \tag{B.37}$$

$$c_{3,7} = -4d_3^{-1}D_{1,1}\Delta_{tz}s\left[z\left(\Delta_{uz} + s \right) - \Delta_{uz}t \right]^3 \left(2sz - D_{2,7}\Delta_{tz}\Delta_{uz} \right), \tag{B.38}$$

$$c_{3,8} = -4d_3^{-1}D_{1,1}\left(\Delta_{tz}\Delta_{uz} - sz \right)^3 \left(D_{3,19}\Delta_{tz}^2\Delta_{uz}^2 - 2D_{3,20}\Delta_{tz}\Delta_{uz}sz + 2D_{3,8}s^2z^2 \right), \tag{B.39}$$

$$c_{3,9} = -2d_3^{-1}\Delta_{tz}^2\left(\Delta_{tz}\Delta_{uz} - sz \right)^2 \left(D_{4,22}\Delta_{tz}^2\Delta_{uz}^2 - D_{5,22}\Delta_{tz}\Delta_{uz}sz + 2D_{5,23}s^2z^2 \right), \tag{B.40}$$

$$c_{3,14} = -2d_3^{-1}D_{1,1}^2D_{2,3}\Delta_{tz}\Delta_{uz}s^2\left[z\left(\Delta_{uz} + s \right) - \Delta_{uz}t \right]^3, \tag{B.41}$$

$$c_{3,15} = -c_{3,14}\frac{\Delta_{tz}}{\Delta_{uz}}, \tag{B.42}$$

$$c_{3,21} = 2\frac{c_{3,14}}{\Delta_{uz}}, \tag{B.43}$$

$$c_{3,22} = -2\frac{c_{3,14}}{\Delta_{uz}}, \tag{B.44}$$

$$c_{4,1} = 4d_4^{-1}\Delta_{tz}\left(2D_{2,2}\Delta_{tz}^2\Delta_{uz}^2 + 2D_{2,2}s^2z^2 + D_{3,9}\Delta_{tz}\Delta_{uz}sz \right), \tag{B.45}$$

$$c_{4,2} = -c_{4,1}\frac{\Delta_{uz}}{\Delta_{tz}}, \tag{B.46}$$

$$c_{4,3} = -4d_4^{-1}s\left[sz\left(D_{2,9}\Delta_{tz}\Delta_{uz} - 2D_{1,1}sz \right) + D_{3,21}\Delta_{tz}^2\Delta_{uz}^2 \right], \tag{B.47}$$

$$c_{4,4} = -4d_4^{-1}D_{1,1}\Delta_{tz}s^2\left(2sz - D_{2,7}\Delta_{tz}\Delta_{uz} \right), \tag{B.48}$$

$$c_{4,5} = -c_{4,3}, \tag{B.49}$$

$$c_{4,6} = -c_{4,4}\frac{\Delta_{uz}}{\Delta_{tz}}, \tag{B.50}$$

$$c_{4,7} = d_4^{-1}s\left(- 4D_{2,12}\Delta_{tz}^2\Delta_{uz}^2 - 8D_{2,7}s^2z^2 + 4D_{3,22}\Delta_{tz}\Delta_{uz}sz \right), \tag{B.51}$$

$$c_{4,8} = 4d_4^{-1}\Delta_{uz}\left[D_{3,23}\Delta_{tz}^2\Delta_{uz}^2 + sz\left(D_{3,24}\Delta_{tz}\Delta_{uz} + 2D_{3,25}sz \right) \right], \tag{B.52}$$

$$c_{4,9} = -c_{4,8}\frac{\Delta_{tz}}{\Delta_{uz}}, \tag{B.53}$$

$$c_{4,14} = -2c_{4,4}\frac{\Delta_{uz}}{\Delta_{tz}}, \tag{B.54}$$

$$c_{4,15} = \frac{c_{4,4}}{2}, \tag{B.55}$$

$$c_{4,21} = -\frac{c_{4,4}}{\Delta_{tz}}, \tag{B.56}$$

$$c_{4,22} = \frac{c_{4,4}}{\Delta_{tz}}\,, \tag{B.57}$$

where $c_{i,j}$ is coefficient j corresponding to t_j defined by Eq. (8.22) to obtain the form factor f_i. The denominators $d_1, \ldots, d_4$ are given by

$$\begin{aligned} d_1 = {} & D_{1,2} D_{1,1}^2 D_{2,1} s^3 z \big\{ D_{4,10} \Delta_{tz}^4 \Delta_{uz}^4 \\ & + s^2 z^2 \big[4sz \big(D_{3,16} \Delta_{tz} \Delta_{uz} - D_{3,8} sz \big) + D_{5,11} \Delta_{tz}^2 \Delta_{uz}^2 \big] - D_{5,12} sz \Delta_{tz}^3 \Delta_{uz}^3 \big\}\,, \end{aligned} \tag{B.58}$$

$$\begin{aligned} d_2 = {} & D_{1,2} D_{1,1}^2 D_{2,1} s^2 z \big[\Delta_{uz} t - z \big(\Delta_{uz} + s \big) \big]^2 \\ & \times \big\{ sz \big[D_{5,8} \Delta_{tz}^2 \Delta_{uz}^2 - 4sz \big(D_{3,26} \Delta_{tz} \Delta_{uz} + D_{3,8} sz \big) \big] - D_{4,10} \Delta_{tz}^3 \Delta_{uz}^3 \big\} \\ & \times \big\{ D_{4,10} \Delta_{tz}^4 \Delta_{uz}^4 + s^2 z^2 \big[4sz \big(D_{3,16} \Delta_{tz} \Delta_{uz} - D_{3,8} sz \big) + D_{5,11} \Delta_{tz}^2 \Delta_{uz}^2 \big] \\ & - D_{5,12} sz \Delta_{tz}^3 \Delta_{uz}^3 \big\}\,, \end{aligned} \tag{B.59}$$

$$d_3 = -D_{1,1}^2 s \big(\Delta_{tz} \Delta_{uz} - sz \big)^4 \big[sz \big(2 D_{3,8} sz - D_{4,14} \Delta_{tz} \Delta_{uz} \big) + D_{3,11} \Delta_{tz}^2 \Delta_{uz}^2 \big]\,, \tag{B.60}$$

$$d_4 = D_{1,1}^2 s^2 \big[sz \big(D_{4,23} \Delta_{tz}^2 \Delta_{uz}^2 + D_{4,24} \Delta_{tz} \Delta_{uz} sz - 2 D_{3,8} s^2 z^2 \big) + D_{3,11} \Delta_{tz}^3 \Delta_{uz}^3 \big]\,. \tag{B.61}$$

Additionally, we use the following auxiliary functions

$$D_{1,1} = d - 3\,, \tag{B.62}$$

$$D_{1,2} = d - 4\,, \tag{B.63}$$

$$D_{1,3} = d - 5\,, \tag{B.64}$$

$$D_{2,1} = d^2 - 7d + 12\,, \tag{B.65}$$

$$D_{2,2} = d^2 - 5d + 5\,, \tag{B.66}$$

$$D_{2,3} = d^2 - 6d + 4\,, \tag{B.67}$$

$$D_{2,4} = -2d^2 + 11d - 10\,, \tag{B.68}$$

$$D_{2,5} = d^2 - 6d + 6\,, \tag{B.69}$$

$$D_{2,6} = d^2 - 7d + 8\,, \tag{B.70}$$

$$D_{2,7} = d^2 - 5d + 6\,, \tag{B.71}$$

$$D_{2,8} = d^2 - 8d + 14\,, \tag{B.72}$$

$$D_{2,9} = 2d^2 - 11d + 14\,, \tag{B.73}$$

$$D_{2,10} = d^2 - 7d + 10\,, \tag{B.74}$$

$$D_{2,11} = d^2 - 8d + 15\,, \tag{B.75}$$

$$D_{2,12} = 3d^2 - 15d + 16\,, \tag{B.76}$$

$$D_{2,13} = 2d^2 - 7d + 8\,, \tag{B.77}$$

$$D_{3,1} = -5d^3 + 47d^2 - 132d + 100\,, \tag{B.78}$$

$$D_{3,2} = d^3 - 12d^2 + 40d - 35\,, \tag{B.79}$$

$$D_{3,3} = 3d^3 - 31d^2 + 100d - 100\,, \tag{B.80}$$

$$D_{3,4} = d^3 - 9d^2 + 25d - 21\,, \tag{B.81}$$

$$D_{3,5} = 5d^3 - 50d^2 + 152d - 134\,, \tag{B.82}$$

$$D_{3,6} = d^3 - 10d^2 + 30d - 25\,, \tag{B.83}$$
$$D_{3,7} = -2d^3 + 22d^2 - 73d + 70\,, \tag{B.84}$$
$$D_{3,8} = d^3 - 10d^2 + 30d - 26\,, \tag{B.85}$$
$$D_{3,9} = -d^3 + 4d^2 + d - 8\,, \tag{B.86}$$
$$D_{3,10} = -3d^3 + 30d^2 - 91d + 79\,, \tag{B.87}$$
$$D_{3,11} = 4d^3 - 39d^2 + 116d - 100\,, \tag{B.88}$$
$$D_{3,12} = -3d^3 + 31d^2 - 99d + 96\,, \tag{B.89}$$
$$D_{3,13} = 5d^3 - 50d^2 + 152d - 134\,, \tag{B.90}$$
$$D_{3,14} = d^3 - 10d^2 + 31d - 30\,, \tag{B.91}$$
$$D_{3,15} = d^3 - 9d^2 + 25d - 20\,, \tag{B.92}$$
$$D_{3,16} = 4d^3 - 41d^2 + 129d - 122\,, \tag{B.93}$$
$$D_{3,17} = d^3 - 11d^2 + 38d - 41\,, \tag{B.94}$$
$$D_{3,18} = 2d^3 - 22d^2 + 73d - 70\,, \tag{B.95}$$
$$D_{3,19} = d^3 - 12d^2 + 42d - 40\,, \tag{B.96}$$
$$D_{3,20} = d^3 - 11d^2 + 38d - 40\,, \tag{B.97}$$
$$D_{3,21} = d^3 - 9d^2 + 25d - 20\,, \tag{B.98}$$
$$D_{3,22} = d^3 - 3d^2 - 6d + 16\,, \tag{B.99}$$
$$D_{3,23} = d^3 - 7d^2 + 15d - 10\,, \tag{B.100}$$
$$D_{3,24} = -3d^3 + 24d^2 - 60d + 46\,, \tag{B.101}$$
$$D_{3,25} = d^3 - 9d^2 + 26d - 24\,, \tag{B.102}$$
$$D_{3,26} = -3d^3 + 31d^2 - 99d + 96\,, \tag{B.103}$$
$$D_{4,1} = d^4 - 8d^3 + 12d^2 + 32d - 70\,, \tag{B.104}$$
$$D_{4,2} = d^4 - 9d^3 + 17d^2 + 28d - 70\,, \tag{B.105}$$
$$D_{4,3} = -2d^4 + 27d^3 - 133d^2 + 278d - 200\,, \tag{B.106}$$
$$D_{4,4} = 3d^4 - 39d^3 + 185d^2 - 380d + 282\,, \tag{B.107}$$
$$D_{4,5} = 4d^4 - 52d^3 + 241d^2 - 476d + 338\,, \tag{B.108}$$
$$D_{4,6} = -2d^4 + 28d^3 - 139d^2 + 286d - 200\,, \tag{B.109}$$
$$D_{4,7} = d^4 - 23d^3 + 161d^2 - 424d + 348\,, \tag{B.110}$$
$$D_{4,8} = -3d^4 + 31d^3 - 99d^2 + 88d + 28\,, \tag{B.111}$$
$$D_{4,9} = d^4 - 12d^3 + 48d^2 - 70d + 18\,, \tag{B.112}$$
$$D_{4,10} = 4d^4 - 55d^3 + 272d^2 - 564d + 400\,, \tag{B.113}$$
$$D_{4,11} = 4d^4 - 54d^3 + 264d^2 - 564d + 452\,, \tag{B.114}$$
$$D_{4,12} = 2d^4 - 27d^3 + 132d^2 - 278d + 213\,, \tag{B.115}$$
$$D_{4,13} = d^4 - 14d^3 + 71d^2 - 155d + 123\,, \tag{B.116}$$
$$D_{4,14} = d^4 - 8d^3 + 8d^2 + 52d - 88\,, \tag{B.117}$$

$$D_{4,17} = d^4 - 17d^3 + 99d^2 - 234d + 190\,, \tag{B.118}$$
$$D_{4,18} = -2d^4 + 25d^3 - 112d^2 + 218d - 162\,, \tag{B.119}$$
$$D_{4,19} = d^4 - 19d^3 + 124d^2 - 330d + 302\,, \tag{B.120}$$
$$D_{4,15} = 2d^4 - 21d^3 + 72d^2 - 86d + 20\,, \tag{B.121}$$
$$D_{4,16} = d^4 - 11d^3 + 39d^2 - 48d + 10\,, \tag{B.122}$$
$$D_{4,20} = d^4 - 9d^3 + 17d^2 + 28d - 70\,, \tag{B.123}$$
$$D_{4,21} = d^4 - 12d^3 + 50d^2 - 86d + 52\,, \tag{B.124}$$
$$D_{4,22} = 2d^4 - 25d^3 + 116d^2 - 232d + 160\,, \tag{B.125}$$
$$D_{4,23} = -d^4 + 4d^3 + 31d^2 - 168d + 188\,, \tag{B.126}$$
$$D_{4,24} = d^4 - 6d^3 - 12d^2 + 112d - 140\,, \tag{B.127}$$
$$D_{5,1} = d^5 - 14d^4 + 84d^3 - 281d^2 + 496d - 316\,, \tag{B.128}$$
$$D_{5,2} = d^5 - 16d^4 + 92d^3 - 219d^2 + 160d + 60\,, \tag{B.129}$$
$$D_{5,3} = 2d^5 - 36d^4 + 248d^3 - 811d^2 + 1244d - 700\,, \tag{B.130}$$
$$D_{5,4} = d^5 - 10d^4 + 16d^3 + 116d^2 - 432d + 388\,, \tag{B.131}$$
$$D_{5,5} = d^5 - 14d^4 + 70d^3 - 143d^2 + 86d + 30\,, \tag{B.132}$$
$$D_{5,6} = d^5 - 26d^4 + 228d^3 - 899d^2 + 1644d - 1140\,, \tag{B.133}$$
$$D_{5,7} = 2d^5 - 35d^4 + 236d^3 - 763d^2 + 1180d - 700\,, \tag{B.134}$$
$$D_{5,8} = d^5 - 12d^4 + 32d^3 + 98d^2 - 528d + 552\,, \tag{B.135}$$
$$D_{5,9} = d^5 - 110d^3 + 679d^2 - 1488d + 1080\,, \tag{B.136}$$
$$D_{5,10} = d^5 - 13d^4 + 62d^3 - 138d^2 + 158d - 96\,, \tag{B.137}$$
$$D_{5,11} = d^5 - 12d^4 + 20d^3 + 222d^2 - 924d + 936\,, \tag{B.138}$$
$$D_{5,12} = d^5 - 8d^4 - 23d^3 + 370d^2 - 1092d + 952\,, \tag{B.139}$$
$$D_{5,13} = d^5 - 12d^4 + 52d^3 - 108d^2 + 130d - 88\,, \tag{B.140}$$
$$D_{5,14} = d^5 - 16d^4 + 98d^3 - 285d^2 + 390d - 200\,, \tag{B.141}$$
$$D_{5,16} = 2d^5 - 33d^4 + 210d^3 - 645d^2 + 956d - 546\,, \tag{B.142}$$
$$D_{5,15} = -3d^5 + 46d^4 - 274d^3 + 790d^2 - 1096d + 580\,, \tag{B.143}$$
$$D_{5,17} = d^5 - 16d^4 + 102d^3 - 326d^2 + 516d - 312\,, \tag{B.144}$$
$$D_{5,18} = 2d^5 - 31d^4 + 186d^3 - 538d^2 + 748d - 400\,, \tag{B.145}$$
$$D_{5,19} = d^5 - 19d^4 + 131d^3 - 407d^2 + 568d - 292\,, \tag{B.146}$$
$$D_{5,20} = d^5 - 17d^4 + 123d^3 - 469d^2 + 904d - 668\,, \tag{B.147}$$
$$D_{5,21} = d^5 - 12d^4 + 48d^3 - 62d^2 - 36d + 104\,, \tag{B.148}$$
$$D_{5,22} = d^5 - 10d^4 + 24d^3 + 46d^2 - 244d + 232\,, \tag{B.149}$$
$$D_{5,23} = d^5 - 14d^4 + 72d^3 - 164d^2 + 150d - 28\,, \tag{B.150}$$
$$D_{6,1} = d^6 - 17d^5 + 104d^4 - 250d^3 + 41d^2 + 684d - 692\,, \tag{B.151}$$
$$D_{6,2} = d^6 - 18d^5 + 127d^4 - 441d^3 + 767d^2 - 580d + 100\,, \tag{B.152}$$

$$D_{6,3} = d^6 - 21d^5 + 170d^4 - 674d^3 + 1357d^2 - 1264d + 380\,, \tag{B.153}$$

$$D_{6,4} = -2d^6 + 35d^5 - 238d^4 + 786d^3 - 1278d^2 + 904d - 200\,, \tag{B.154}$$

$$D_{6,5} = d^6 - 14d^5 + 70d^4 - 134d^3 - 14d^2 + 364d - 344\,, \tag{B.155}$$

$$D_{7,1} = d^7 - 20d^6 + 166d^5 - 770d^4 + 2294d^3 - 4608d^2 + 5656d - 3008\,, \tag{B.156}$$

and the short-hand notation $\Delta_{xy} \equiv x - y$. Note that in $D_{i,j}$ the i indicates the maximum degree of the space-time dimension d in the corresponding coefficient.

BIBLIOGRAPHY

[1] M.E. Peskin and D.V. Schroeder, *An Introduction to quantum field theory*, first ed., Addison-Wesley, Reading 1995.

[2] G. Aad *et al.* [ATLAS Collaboration], *Observation of a new particle in the search for the Standard Model Higgs boson with the ATLAS detector at the LHC*, *Phys. Lett.* **B 716** (2012) 1, arXiv:1207.7214 [hep-ex].

[3] S. Chatrchyan *et al.* [CMS Collaboration], *Observation of a New Boson at a Mass of 125 GeV with the CMS Experiment at the LHC*, *Phys. Lett.* **B 716** (2012) 30, arXiv:1207.7235 [hep-ex].

[4] G. Aad *et al.* [ATLAS and CMS Collaborations], *Measurements of the Higgs boson production and decay rates and constraints on its couplings from a combined ATLAS and CMS analysis of the LHC pp collision data at* $\sqrt{s} = 7$ *and 8 TeV*, *JHEP* **1608** (2016) 045, arXiv:1606.02266 [hep-ex].

[5] S.P. Martin, *A Supersymmetry primer*, *Adv. Ser. Direct. High Energy Phys.* **21** (2010) 1, hep-ph/9709356.

[6] S. Dawson, *The MSSM and why it works*, hep-ph/9712464.

[7] A. Djouadi, *The Anatomy of electro-weak symmetry breaking. II. The Higgs bosons in the minimal supersymmetric model*, *Phys. Reports* **459** (2008) 1, hep-ph/0503173.

[8] P. Draper and H. Rzehak, *A Review of Higgs Mass Calculations in Supersymmetric Models*, *Phys. Reports* **619** (2016) 1, arXiv:1601.01890 [hep-ph].

[9] P. Fayet, *Supersymmetry and Weak, Electromagnetic and Strong Interactions*, *Phys. Lett.* **B 64** (1976) 159.

[10] P. Fayet, *Spontaneously Broken Supersymmetric Theories of Weak, Electromagnetic and Strong Interactions*, *Phys. Lett.* **B 69** (1977) 489.

[11] P. Bechtle, K. Desch, M. Uhlenbrock and P. Wienemann, *Constraining SUSY models with Fittino using measurements before, with and beyond the LHC*, *Eur. Phys. J.* **C 66** (2010) 215, arXiv:0907.2589 [hep-ph].

[12] [CMS Collaboration], *Supersymmetry Publications*, http://cms-results.web.cern.ch/cms-results/public-results/publications/SUS/index.html.

[13] G. Hiller and F. Krüger, *More model-independent analysis of* $b \to s$ *processes*, *Phys. Rev.* **D 69** (2004) 074020, hep-ph/0310219.

[14] D.A. Ross and M.J.G. Veltman, *Neutral Currents in Neutrino Experiments*, *Nucl. Phys.* **B 95** (1975) 135.

[15] R.V. Harlander, P. Kant, L. Mihaila and M. Steinhauser, *Higgs boson mass in supersymmetry to three loops*, *Phys. Rev. Lett.* **100** (2008) 191602 [*Phys. Rev. Lett.* **101** (2008) 039901], arXiv:0803.0672 [hep-ph].

[16] P. Kant, R.V. Harlander, L. Mihaila and M. Steinhauser, *Light MSSM Higgs boson mass to three-loop accuracy*, *JHEP* **1008** (2010) 104, arXiv:1005.5709 [hep-ph].

[17] G. Aad *et al.* [ATLAS and CMS Collaborations], *Combined Measurement of the Higgs Boson Mass in pp Collisions at $\sqrt{s} = 7$ and 8 TeV with the ATLAS and CMS Experiments*, *Phys. Rev. Lett.* **114** (2015) 191803, arXiv:1503.07589 [hep-ex].

[18] M. Tanabashi *et al.* [Particle Data Group], *Review of Particle Physics*, *Phys. Rev.* **D 98** (2018) 030001.

[19] R. Hempfling and A.H. Hoang, *Two loop radiative corrections to the upper limit of the lightest Higgs boson mass in the minimal supersymmetric model*, *Phys. Lett.* **B 331** (1994) 99, hep-ph/9401219.

[20] S. Heinemeyer, W. Hollik and G. Weiglein, *Precise prediction for the mass of the lightest Higgs boson in the MSSM*, *Phys. Lett.* **B 440** (1998) 296, hep-ph/9807423.

[21] S. Heinemeyer, W. Hollik and G. Weiglein, *QCD corrections to the masses of the neutral $\mathcal{CP}$-even Higgs bosons in the MSSM*, *Phys. Rev.* **D 68** (1998) 091701, hep-ph/9803277.

[22] S. Heinemeyer, W. Hollik and G. Weiglein, *The Masses of the neutral $\mathcal{CP}$-even Higgs bosons in the MSSM: Accurate analysis at the two loop level*, *Eur. Phys. J.* **C 9** (1999) 343, hep-ph/9812472.

[23] S. Heinemeyer, W. Hollik and G. Weiglein, *The Mass of the lightest MSSM Higgs boson: A Compact analytical expression at the two loop level*, *Phys. Lett.* **B 455** (1999) 179, hep-ph/9903404.

[24] G. Degrassi, P. Slavich and F. Zwirner, *On the neutral Higgs boson masses in the MSSM for arbitrary stop mixing*, *Nucl. Phys.* **B 611** (2001) 403, hep-ph/0105096.

[25] A. Brignole, G. Degrassi, P. Slavich and F. Zwirner, *On the $\mathcal{O}(\alpha_t^2)$ two loop corrections to the neutral Higgs boson masses in the MSSM*, *Nucl. Phys.* **B 631** (2002) 195, hep-ph/0112177.

[26] A. Brignole, G. Degrassi, P. Slavich and F. Zwirner, *On the two loop sbottom corrections to the neutral Higgs boson masses in the MSSM*, *Nucl. Phys.* **B 643** (2002) 79, hep-ph/0206101.

[27] A. Dedes, G. Degrassi and P. Slavich, *On the two loop Yukawa corrections to the MSSM Higgs boson masses at large* $\tan\beta$, *Nucl. Phys.* **B 672** (2003) 144, hep-ph/0305127.

[28] S. Heinemeyer, W. Hollik, H. Rzehak and G. Weiglein, *High-precision predictions for the MSSM Higgs sector at $\mathcal{O}(\alpha_b\alpha_s)$*, *Eur. Phys. J.* **C 39** (2005) 465, hep-ph/0411114.

[29] S. Heinemeyer, W. Hollik, H. Rzehak and G. Weiglein, *The Higgs sector of the complex MSSM at two-loop order: QCD contributions*, *Phys. Lett.* **B 652** (2007) 300, arXiv:0705.0746 [hep-ph].

[30] S. Borowka, T. Hahn, S. Heinemeyer, G. Heinrich and W. Hollik, *Momentum-dependent two-loop QCD corrections to the neutral Higgs-boson masses in the MSSM*, *Eur. Phys. J.* **C 74** (2014) 2994, arXiv:1404.7074 [hep-ph].

[31] W. Hollik and S. Paßehr, *Higgs boson masses and mixings in the complex MSSM with two-loop top-Yukawa-coupling corrections*, *JHEP* **1410** (2014) 171, arXiv:1409.1687 [hep-ph].

[32] S. Borowka, T. Hahn, S. Heinemeyer, G. Heinrich and W. Hollik, *Renormalization scheme dependence of the two-loop QCD corrections to the neutral Higgs-boson masses in the MSSM*, *Eur. Phys. J.* **C 75** (2015) 424, arXiv:1505.03133 [hep-ph].

[33] S. Paßehr and G. Weiglein, *Two-loop top and bottom Yukawa corrections to the Higgs-boson masses in the complex MSSM*, *Eur. Phys. J.* **C 78** (2018) 222, arXiv:1705.07909 [hep-ph].

[34] S. Borowka, S. Paßehr and G. Weiglein, *Complete two-loop QCD contributions to the lightest Higgs-boson mass in the MSSM with complex parameters*, *Eur. Phys. J.* **C 78** (2018) 576, arXiv:1802.09886 [hep-ph].

[35] S.P. Martin, *Two Loop Effective Potential for a General Renormalizable Theory and Softly Broken Supersymmetry*, *Phys. Rev.* **D 65** (2002) 116003, hep-ph/0111209.

[36] S.P. Martin, *Two Loop Effective Potential for the Minimal Supersymmetric Standard Model*, *Phys. Rev.* **D 66** (2002) 096001, hep-ph/0206136.

[37] S.P. Martin, *Complete Two Loop Effective Potential Approximation to the Lightest Higgs Scalar Boson Mass in Supersymmetry*, *Phys. Rev.* **D 67** (2003) 095012, hep-ph/0211366.

[38] A. Dedes and P. Slavich, *Two loop corrections to radiative electroweak symmetry breaking in the MSSM*, *Nucl. Phys.* **B 657** (2003) 333, hep-ph/0212132.

[39] S.P. Martin, *Two loop scalar self energies in a general renormalizable theory at leading order in gauge couplings*, *Phys. Rev.* **D 70** (2004) 016005, hep-ph/0312092.

[40] B.C. Allanach, A. Djouadi, J.L. Kneur, W. Porod and P. Slavich, *Precise determination of the neutral Higgs boson masses in the MSSM*, *JHEP* **0409** (2004) 044, hep-ph/0406166.

[41] S.P. Martin, *Strong and Yukawa two-loop contributions to Higgs scalar boson self-energies and pole masses in supersymmetry*, *Phys. Rev.* **D 71** (2005) 016012, hep-ph/0405022.

[42] S.P. Martin, *Two-loop scalar self-energies and pole masses in a general renormalizable theory with massless gauge bosons*, *Phys. Rev.* **D 71** (2005) 116004, hep-ph/0502168.

[43] S.P. Martin, *Three-loop corrections to the lightest Higgs scalar boson mass in supersymmetry*, *Phys. Rev.* **D 75** (2007) 055005, hep-ph/0701051.

[44] G. Degrassi, S. Di Vita and P. Slavich, *Two-loop QCD corrections to the MSSM Higgs masses beyond the effective-potential approximation*, *Eur. Phys. J.* **C 75** (2015) 61,

arXiv:1410.3432 [hep-ph].

[45] M.D. Goodsell and F. Staub, *The Higgs mass in the CP violating MSSM, NMSSM, and beyond*, *Eur. Phys. J.* **C 77** (2017) 46, arXiv:1604.05335 [hep-ph].

[46] S.P. Martin, *Effective potential at three loops*, *Phys. Rev.* **D 96** (2017) 096005, arXiv:1709.02397 [hep-ph].

[47] R.V. Harlander, J. Klappert and A. Voigt, *Higgs mass prediction in the MSSM at three-loop level in a pure $\overline{DR}$ context*, *Eur. Phys. J.* **C 77** (2017) 814, arXiv:1708.05720 [hep-ph].

[48] A.R. Fazio and E.A. Reyes R., *The Lightest Higgs Boson Mass of the MSSM at Three-Loop Accuracy*, *Nucl. Phys.* **B 942** (2019) 164, arXiv:1901.03651 [hep-ph].

[49] M.D. Goodsell and S. Paßehr, *All two-loop scalar self-energies and tadpoles in general renormalisable field theories*, arXiv:1910.02094 [hep-ph].

[50] S. Heinemeyer, W. Hollik and G. Weiglein, *FeynHiggs: A Program for the calculation of the masses of the neutral CP even Higgs bosons in the MSSM*, *Comp. Phys. Commun.* **124** (2000) 76, hep-ph/9812320.

[51] G. Degrassi, S. Heinemeyer, W. Hollik, P. Slavich and G. Weiglein, *Towards high precision predictions for the MSSM Higgs sector*, *Eur. Phys. J.* **C 28** (2003) 133, hep-ph/0212020.

[52] M. Frank, T. Hahn, S. Heinemeyer, W. Hollik, H. Rzehak and G. Weiglein, *The Higgs Boson Masses and Mixings of the Complex MSSM in the Feynman-Diagrammatic Approach*, *JHEP* **0702** (2007) 047, hep-ph/0611326.

[53] T. Hahn, S. Heinemeyer, W. Hollik, H. Rzehak and G. Weiglein, *High-Precision Predictions for the Light CP -Even Higgs Boson Mass of the Minimal Supersymmetric Standard Model*, *Phys. Rev. Lett.* **112** (2014) 141801, arXiv:1312.4937 [hep-ph].

[54] B.C. Allanach, *SOFTSUSY: a program for calculating supersymmetric spectra*, *Comp. Phys. Commun.* **143** (2002) 305, hep-ph/0104145.

[55] A. Djouadi, J.L. Kneur and G. Moultaka, *SuSpect: A Fortran code for the supersymmetric and Higgs particle spectrum in the MSSM*, *Comp. Phys. Commun.* **176** (2007) 426, hep-ph/0211331.

[56] W. Porod, *SPheno, a program for calculating supersymmetric spectra, SUSY particle decays and SUSY particle production at e^+e^- colliders*, *Comp. Phys. Commun.* **153** (2003) 275, hep-ph/0301101.

[57] W. Porod and F. Staub, *SPheno 3.1: Extensions including flavour, CP-phases and models beyond the MSSM*, *Comp. Phys. Commun.* **183** (2012) 2458, arXiv:1104.1573 [hep-ph].

[58] P. Athron, J.h. Park, D. Stöckinger and A. Voigt, *FlexibleSUSY—A spectrum generator generator for supersymmetric models*, *Comp. Phys. Commun.* **190** (2015) 139, arXiv:1406.2319 [hep-ph].

[59] P. Athron, M. Bach, D. Harries, T. Kwasnitza, J.-h. Park, D. Stöckinger, A. Voigt, J. Ziebell, *FlexibleSUSY 2.0: Extensions to investigate the phenomenology of SUSY and non-SUSY models*, *Comp. Phys. Commun.* **230** (2018) 145, arXiv:1710.03760 [hep-ph].

[60] J. Pardo Vega and G. Villadoro, *SusyHD: Higgs mass Determination in Supersymmetry*, *JHEP* **1507** (2015) 159, arXiv:1504.05200 [hep-ph].

[61] G. Lee and C.E.M. Wagner, *Higgs bosons in heavy supersymmetry with an intermediate m_A*, *Phys. Rev.* **D 92** (2015) 075032, arXiv:1508.00576 [hep-ph].

[62] R.V. Harlander, J. Klappert, A.D. Ochoa Franco and A. Voigt, *The light CP-even MSSM Higgs mass resummed to fourth logarithmic order*, *Eur. Phys. J.* **C 78** (2018) 874, arXiv:1807.03509 [hep-ph].

[63] P. Draper, G. Lee and C.E.M. Wagner, *Precise estimates of the Higgs mass in heavy supersymmetry*, *Phys. Rev.* **D 89** (2014) 055023, arXiv:1312.5743 [hep-ph].

[64] E. Bagnaschi, G.F. Giudice, P. Slavich and A. Strumia, *Higgs Mass and Unnatural Supersymmetry*, *JHEP* **1409** (2014) 092, arXiv:1407.4081 [hep-ph].

[65] E. Bagnaschi, J. Pardo Vega and P. Slavich, *Improved determination of the Higgs mass in the MSSM with heavy superpartners*, *Eur. Phys. J.* **C 77** (2017) 334, arXiv:1703.08166 [hep-ph].

[66] E. Bagnaschi, G. Degrassi, S. Paßehr and P. Slavich, *Full two-loop QCD corrections to the Higgs mass in the MSSM with heavy superpartners*, *Eur. Phys. J.* **C 79** (2019) 910, arXiv:1908.01670 [hep-ph].

[67] N. Murphy and H. Rzehak, *Higgs-Boson Masses and Mixings in the MSSM with CP Violation and Heavy SUSY Particles*, arXiv:1909.00726 [hep-ph].

[68] H. Bahl and W. Hollik, *Precise prediction for the light MSSM Higgs boson mass combining effective field theory and fixed-order calculations*, *Eur. Phys. J.* **C 76** (2016) 499, arXiv:1608.01880 [hep-ph].

[69] H. Bahl, S. Heinemeyer, W. Hollik and G. Weiglein, *Reconciling EFT and hybrid calculations of the light MSSM Higgs-boson mass*, *Eur. Phys. J.* **C 78** (2018) 57, arXiv:1706.00346 [hep-ph].

[70] B.C. Allanach and A. Voigt, *Uncertainties in the Lightest CP Even Higgs Boson Mass Prediction in the Minimal Supersymmetric Standard Model: Fixed Order Versus Effective Field Theory Prediction*, *Eur. Phys. J.* **C 78** (2018) 573, arXiv:1804.09410 [hep-ph].

[71] P. Athron, J.h. Park, T. Steudtner, D. Stöckinger and A. Voigt, *Precise Higgs mass calculations in (non-)minimal supersymmetry at both high and low scales*, *JHEP* **1701** (2017) 079, arXiv:1609.00371 [hep-ph].

[72] F. Staub and W. Porod, *Improved predictions for intermediate and heavy Supersymmetry in the MSSM and beyond*, *Eur. Phys. J.* **C 77** (2017) 338, arXiv:1703.03267 [hep-ph].

[73] H. Bahl and W. Hollik, *Precise prediction of the MSSM Higgs boson masses for low M_A*, *JHEP* **1807** (2018) 182, arXiv:1805.00867 [hep-ph].

[74] R.V. Harlander, J. Klappert and A. Voigt, *The light CP-even MSSM Higgs mass including N^3LO+N^3LL QCD corrections*, arXiv:1910.03595 [hep-ph].

[75] E.A. Reyes R. and A.R. Fazio, *Comparison of the EFT Hybrid and Three-Loop Fixed-Order Calculations of the Lightest MSSM Higgs Boson Mass*, *Phys. Rev.* **D 100** (2019) 115017, arXiv:1908.00693 [hep-ph].

[76] H.P. Nilles, *Supersymmetry, Supergravity and Particle Physics*, *Phys. Reports* **110** (1984) 1.

[77] G.F. Giudice and R. Rattazzi, *Theories with gauge mediated supersymmetry breaking*, *Phys. Reports* **322** (1999) 419, hep-ph/9801271.

[78] P.Z. Skands *et al.*, *SUSY Les Houches accord: Interfacing SUSY spectrum calculators, decay packages, and event generators*, *JHEP* **0407** (2004) 036, hep-ph/0311123.

[79] D.M. Pierce, J.A. Bagger, K.T. Matchev and R.-J. Zhang, *Precision corrections in the minimal supersymmetric standard model*, *Nucl. Phys.* **B 491** (1997) 3, hep-ph/9606211.

[80] B.C. Allanach *et al.*, *The Snowmass Points and Slopes: Benchmarks for SUSY Searches*, *Eur. Phys. J.* **C 25** (2002) 113, hep-ph/0202233.

[81] J.A. Aguilar-Saavedra *et al.*, *Supersymmetry parameter analysis: SPA convention and project*, *Eur. Phys. J.* **C 46** (2006) 43, hep-ph/0511344.

[82] H. Bahl, T. Hahn, S. Heinemeyer, W. Hollik, S. Paßehr, H. Rzehak and G. Weiglein, *Precision calculations in the MSSM Higgs-boson sector with FeynHiggs 2.14*, arXiv:1811.09073 [hep-ph].

[83] A. Pak, M. Steinhauser and N. Zerf, *Supersymmetric next-to-next-to-leading order corrections to Higgs boson production in gluon fusion*, *JHEP* **1209** (2012) 118, arXiv:1208.1588 [hep-ph].

[84] W. Siegel, *Supersymmetric Dimensional Regularization via Dimensional Reduction*, *Phys. Lett.* **B 84** (1979) 193.

[85] D. Stöckinger, *Regularization by dimensional reduction: consistency, quantum action principle, and supersymmetry*, *JHEP* **0503** (2005) 076, hep-ph/0503129.

[86] W.A. Bardeen, A.J. Buras, D.W. Duke and T. Muta, *Deep Inelastic Scattering Beyond the Leading Order in Asymptotically Free Gauge Theories*, *Phys. Rev.* **D 18** (1978) 3998.

[87] S.P. Martin and M.T. Vaughn, *Two loop renormalization group equations for soft supersymmetry breaking couplings*, *Phys. Rev.* **D 50** (1994) 2282 [Erratum: *Phys. Rev.* **D 78** (2008) 039903], hep-ph/9311340.

[88] I. Jack and D.RT. Jones, *Soft supersymmetry breaking and finiteness*, *Phys. Lett.* **B 333** (1994) 372, hep-ph/9405233.

[89] Y. Yamada, *Two loop renormalization group equations for soft SUSY breaking scalar interactions: Supergraph method*, *Phys. Rev.* **D 50** (1994) 3537, hep-ph/9401241.

[90] I. Jack, D.R.T. Jones, S.P. Martin, M.T. Vaughn and Y. Yamada, *Decoupling of the ϵ-scalar mass in softly broken supersymmetry*, *Phys. Rev.* **D 50** (1994) R5481, hep-ph/9407291.

[91] D. Stöckinger and J. Unger, *Three-loop MSSM Higgs-boson mass predictions and regularization by dimensional reduction*, *Nucl. Phys.* **B 935** (2018) 1, arXiv:1804.05619 [hep-ph].

[92] T. Hermann, L. Mihaila and M. Steinhauser, *Three-loop anomalous dimensions for squarks in supersymmetric QCD*, *Phys. Lett.* **B 703** (2011) 51, arXiv:1106.1060 [hep-ph].

[93] A. Bednyakov, A. Onishchenko, V. Velizhanin and O. Veretin, *Two loop $\mathcal{O}(\alpha_s^2)$ MSSM corrections to the pole masses of heavy quarks*, *Eur. Phys. J.* **C 29** (2003) 87, hep-ph/0210258.

[94] A. Bednyakov, D.I. Kazakov and A. Sheplyakov, *On the two-loop $\mathcal{O}(\alpha_s^2)$ corrections to the pole mass of the t-quark in the MSSM*, *Phys. Atom. Nucl.* **71** (2008) 343, hep-ph/0507139.

[95] A.V. Bednyakov, *Running mass of the b-quark in QCD and SUSY QCD*, *Int. J. Mod. Phys.* **A 22** (2007) 5245, arXiv:0707.0650 [hep-ph].

[96] A. Bauer, L. Mihaila and J. Salomon, *Matching coefficients for α_s and m_b to $\mathcal{O}(\alpha_s^2)$ in the MSSM*, *JHEP* **0902** (2009) 037, arXiv:0810.5101 [hep-ph].

[97] I. Jack, D.R.T. Jones and A.F. Kord, *Three loop soft running, benchmark points and semiperturbative unification*, *Phys. Lett.* **B 579** (2004) 180, hep-ph/0308231.

[98] I. Jack, D.R.T. Jones and A.F. Kord, *Snowmass benchmark points and three-loop running*, *Ann. Phys.* **316** (2005) 213, hep-ph/0408128.

[99] L.N. Mihaila, J. Salomon and M. Steinhauser, *Gauge Coupling Beta Functions in the Standard Model to Three Loops*, *Phys. Rev. Lett.* **108** (2012) 151602, arXiv:1201.5868 [hep-ph].

[100] A.V. Bednyakov, A.F. Pikelner and V.N. Velizhanin, *Anomalous dimensions of gauge fields and gauge coupling beta-functions in the Standard Model at three loops*, *JHEP* **1301** (2013) 017, arXiv:1210.6873 [hep-ph].

[101] A.V. Bednyakov, A.F. Pikelner and V.N. Velizhanin, *Yukawa coupling beta-functions in the Standard Model at three loops*, *Phys. Lett.* **B 722** (2013) 336, arXiv:1212.6829 [hep-ph].

[102] K.G. Chetyrkin and M.F. Zoller, *Three-loop β-functions for top-Yukawa and the Higgs self-interaction in the Standard Model*, *JHEP* **1206** (2012) 033, arXiv:1205.2892 [hep-ph].

[103] A.V. Bednyakov, A.F. Pikelner and V.N. Velizhanin, *Higgs self-coupling beta-function in the Standard Model at three loops*, *Nucl. Phys.* **B 875** (2013) 552, arXiv:arXiv:1303.4364 [hep-ph].

[104] M. Sperling, D. Stöckinger and A. Voigt, *Renormalization of vacuum expectation values in spontaneously broken gauge theories*, *JHEP* **1307** (2013) 132, arXiv:1305.1548 [hep-ph].

[105] M. Sperling, D. Stöckinger and A. Voigt, *Renormalization of vacuum expectation values in spontaneously broken gauge theories: Two-loop results*, *JHEP* **1401** (2014) 068,

arXiv:1310.7629 [hep-ph].

[106] B.C. Allanach, A. Bednyakov and R. Ruiz de Austri, *Higher order corrections and unification in the minimal supersymmetric standard model: SOFTSUSY3.5*, *Comp. Phys. Commun.* **189** (2015) 192, arXiv:1407.6130 [hep-ph].

[107] D. Kunz, L. Mihaila and N. Zerf, $\mathcal{O}(\alpha_S^2)$ *corrections to the running top-Yukawa coupling and the mass of the lightest Higgs boson in the MSSM*, *JHEP* **1412** (2014) 136, arXiv:1409.2297 [hep-ph].

[108] P. Kant et al., *H3m*, https://www.ttp.kit.edu/Progdata/ttp10/ttp10-23/H3m-v1.3/.

[109] J.L. Feng, P. Kant, S. Profumo and D. Sanford, *Three-Loop Corrections to the Higgs Boson Mass and Implications for Supersymmetry at the LHC*, *Phys. Rev. Lett.* **111** (2013) 131802, arXiv:1306.2318 [hep-ph].

[110] The ATLAS, CDF, CMS, and D0 Collaborations, *First combination of Tevatron and LHC measurements of the top-quark mass*, arXiv:1403.4427 [hep-ex].

[111] S. Bethke, *The 2009 World Average of* α_s, *Eur. Phys. J.* **C 64** (2009) 689, arXiv:0908.1135 [hep-ph].

[112] S.P. Martin and D.G. Robertson, *Higgs boson mass in the Standard Model at two-loop order and beyond*, *Phys. Rev.* **D 90** (2014) 073010, arXiv:1407.4336 [hep-ph].

[113] S.P. Martin, *Four-Loop Standard Model Effective Potential at Leading Order in QCD*, *Phys. Rev.* **D 92** (2015) 054029, arXiv:1508.00912 [hep-ph].

[114] L.N. Mihaila, J. Salomon and M. Steinhauser, *Renormalization constants and beta functions for the gauge couplings of the Standard Model to three-loop order*, *Phys. Rev.* **D 86** (2012) 096008, arXiv:1208.3357 [hep-ph].

[115] D. Buttazzo, G. Degrassi, P.P. Giardino, G.F. Giudice, F. Sala, A. Salvio and A. Strumia, *Investigating the near-criticality of the Higgs boson*, *JHEP* **1312** (2013) 089, arXiv:1307.3536 [hep-ph].

[116] A.V. Bednyakov and A.F. Pikelner, *Four-loop strong coupling beta-function in the Standard Model*, *Phys. Lett.* **B 762** (2016) 151, arXiv:1508.02680 [hep-ph].

[117] K.G. Chetyrkin and M.F. Zoller, *Leading QCD-induced four-loop contributions to the* β*-function of the Higgs self-coupling in the SM and vacuum stability*, *JHEP* **1606** (2016) 175, arXiv:1604.00853 [hep-ph].

[118] S. Fanchiotti, B.A. Kniehl and A. Sirlin, *Incorporation of QCD effects in basic corrections of the electroweak theory*, *Phys. Rev.* **D 48** (1993) 307, hep-ph/9212285.

[119] K.G. Chetyrkin and M. Steinhauser, *The Relation between the* $\overline{MS}$ *and the on-shell quark mass at order* α_s^3, *Nucl. Phys.* **B 573** (2000) 617, hep-ph/9911434.

[120] K. Melnikov, T. van Ritbergen, *The three-loop relation between the* $\overline{MS}$ *and the pole quark masses*, *Phys. Lett.* **B 482** (2000) 99, hep-ph/9912391.

[121] K.G. Chetyrkin, J.H. Kühn and M. Steinhauser, *RunDec: A Mathematica package for running and decoupling of the strong coupling and quark masses*, *Comp. Phys. Commun.* **133** (2000) 43, hep-ph/0004189.

[122] G. Degrassi, S. Di Vita, J. Elias-Miro, J.R. Espinosa, G.F. Giudice, G. Isidori and A. Strumia, *Higgs mass and vacuum stability in the Standard Model at NNLO*, *JHEP* **1208** (2012) 098, arXiv:1205.6497 [hep-ph].

[123] R. Harlander, L. Mihaila and M. Steinhauser, *Two-loop matching coefficients for the strong coupling in the MSSM*, *Phys. Rev.* **D 72** (2005) 095009, hep-ph/0509048.

[124] A.V. Bednyakov, *Some two-loop threshold corrections and three-loop renormalization group analysis of the MSSM*, arXiv:1009.5455 [hep-ph].

[125] S.P. Martin, *Top-quark pole mass in the tadpole-free $\overline{MS}$ scheme*, *Phys. Rev.* **D 93** (2016) 094017, arXiv:1604.01134 [hep-ph].

[126] H. Bahl, S. Heinemeyer, W. Hollik and G. Weiglein, *Theoretical uncertainties in the MSSM Higgs boson mass calculation*, arXiv:1912.04199 [hep-ph].

[127] S.L. Glashow, D.V. Nanopoulos and A. Yildiz, *Associated Production of Higgs Bosons and Z Particles*, *Phys. Rev.* **D 18** (1978) 1724.

[128] S. Dawson, *Radiative corrections to Higgs boson production*, *Nucl. Phys.* **B 359** (1991) 283.

[129] M. Aaboud *et al.* [ATLAS Collaboration], *Observation of $H \to b\bar{b}$ decays and VH production with the ATLAS detector*, *Phys. Lett.* **B 786** (2018) 59, arXiv:1808.08238 [hep-ex].

[130] A.M. Sirunyan *et al.* [CMS Collaboration], *Observation of Higgs boson decay to bottom quarks*, *Phys. Rev. Lett.* **121** (2018) 121801, arXiv:1808.08242 [hep-ex].

[131] D. de Florian *et al.* [LHC Higgs Cross Section Working Group], *Handbook of LHC Higgs Cross Sections: 4. Deciphering the Nature of the Higgs Sector*, arXiv:1610.07922 [hep-ph].

[132] T. Aaltonen *et al.* [CDF and D0 Collaborations], *Evidence for a particle produced in association with weak bosons and decaying to a bottom-antibottom quark pair in Higgs boson searches at the Tevatron*, *Phys. Rev. Lett.* **109** (2012) 071804, arXiv:1207.6436 [hep-ex].

[133] M. Aaboud *et al.* [ATLAS Collaboration], *Evidence for the $H \to b\bar{b}$ decay with the ATLAS detector*, *JHEP* **1712** (2017) 024, arXiv:1708.03299 [hep-ex].

[134] A.M. Sirunyan *et al.* [CMS Collaboration], *Evidence for the Higgs boson decay to a bottom quark–antiquark pair*, *Phys. Lett.* **B 780** (2018) 501, arXiv:1709.07497 [hep-ex].

[135] O. Brein, A. Djouadi and R. Harlander, *NNLO QCD corrections to the Higgs-strahlung processes at hadron colliders*, *Phys. Lett.* **B 579** (2004) 149, hep-ph/0307206.

[136] R. Hamberg, W.L. van Neerven and T. Matsuura, *A complete calculation of the order α_s^2 correction to the Drell-Yan K factor*, *Nucl. Phys.* **B 359** (1991) 343 [Erratum: *Nucl. Phys.* **B 644** (202) 403].

[137] R.V. Harlander and W.B. Kilgore, *Next-to-next-to-leading order Higgs production at hadron colliders*, *Phys. Rev. Lett.* **88** (2002) 201801, hep-ph/0201206.

[138] G. Ferrera, M. Grazzini and F. Tramontano, *Associated WH production at hadron colliders: a fully exclusive QCD calculation at NNLO*, *Phys. Rev. Lett.* **107** (2011) 152003, arXiv:1107.1164 [hep-ph].

[139] G. Ferrera, M. Grazzini and F. Tramontano, *Associated ZH production at hadron colliders: the fully differential NNLO QCD calculation*, *Phys. Lett.* **B 740** (2015) 51, arXiv:1407.4747 [hep-ph].

[140] J.M. Campbell, R.K. Ellis and C. Williams, *Associated production of a Higgs boson at NNLO*, *JHEP* **1606** (2016) 179, arXiv:1601.00658 [hep-ph].

[141] Y. Li, A. von Manteuffel, R.M. Schabinger and H.X. Zhu, *N^3LO Higgs boson and Drell-Yan production at threshold: The one-loop two-emission contribution*, *Phys. Rev.* **D 90** (2014) 053006, arXiv:1404.5839 [hep-ph].

[142] M.C. Kumar, M.K. Mandal and V. Ravindran, *Associated production of Higgs boson with vector boson at threshold N^3LO in QCD*, *JHEP* **1503** (2015) 037, arXiv:1412.3357 [hep-ph].

[143] B.A. Kniehl, *Associated Production of Higgs and Z Bosons From Gluon Fusion in Hadron Collisions*, *Phys. Rev.* **D 42** (1990) 2253.

[144] D.A. Dicus and C. Kao, *Higgs Boson - Z^0 Production From Gluon Fusion*, *Phys. Rev.* **D 38** (1988) 1008 [Erratum: *Phys. Rev.* **D 42** (1990) 2412].

[145] L. Altenkamp, S. Dittmaier, R.V. Harlander, H. Rzehak and T.J.E. Zirke, *Gluon-induced Higgs-strahlung at next-to-leading order QCD*, *JHEP* **1302** (2013) 078, arXiv:1211.5015 [hep-ph].

[146] R.V. Harlander, A. Kulesza, V. Theeuwes and T. Zirke, *Soft gluon resummation for gluon-induced Higgs Strahlung*, *JHEP* **1411** (2014) 082, arXiv:1410.0217 [hep-ph].

[147] A. Hasselhuhn, T. Luthe and M. Steinhauser, *On top quark mass effects to $gg \to ZH$ at NLO*, *JHEP* **1701** (2017) 073, arXiv:1611.05881 [hep-ph].

[148] B. Hespel, F. Maltoni and E. Vryonidou, *Higgs and Z boson associated production via gluon fusion in the SM and the 2HDM*, *JHEP* **1506** (2015) 065, arXiv:1503.01656 [hep-ph].

[149] D. Goncalves, F. Krauss, S. Kuttimalai and P. Maierhöfer, *Higgs-Strahlung: Merging the NLO Drell-Yan and loop-induced $0+1$ jet multiplicities*, *Phys. Rev.* **D 92** (2015) 073006, arXiv:1509.01597 [hep-ph].

[150] O. Brein, R. Harlander, M. Wiesemann and T. Zirke, *Top-Quark Mediated Effects in Hadronic Higgs-Strahlung*, *Eur. Phys. J.* **C 72** (2012) 1868, arXiv:1111.0761 [hep-ph].

[151] T. Ahmed, A.H. Ajjath, L. Chen, P.K. Dhani, P. Mukherjee and V. Ravindran, *Polarised Amplitudes and Soft-Virtual Cross Sections for $b\bar{b} \to ZH$ at NNLO in QCD*,

arXiv:1910.06347 [hep-ph].

[152] M.L. Ciccolini, S. Dittmaier and M. Krämer, *Electroweak radiative corrections to associated WH and ZH production at hadron colliders*, *Phys. Rev.* **D 68** (2003) 073003, hep-ph/0306234.

[153] A. Denner, S. Dittmaier, S. Kallweit and A. Mück, *Electroweak corrections to Higgs-strahlung off W/Z bosons at the Tevatron and the LHC with HAWK*, *JHEP* **1203** (2012) 075, arXiv:1112.5142 [hep-ph].

[154] F. Granata, J.M. Lindert, C. Oleari and S. Pozzorini, *NLO QCD+EW predictions for HV and HV+jet production including parton-shower effects*, *JHEP* **1709** (2017) 012, arXiv:1706.03522 [hep-ph].

[155] J. Butterworth *et al.*, *PDF4LHC recommendations for LHC Run II*, *J. Phys. G* **43** (2016) 023001, arXiv:1510.03865 [hep-ph].

[156] W. Astill, W. Bizoń, E. Re and G. Zanderighi, *NNLOPS accurate associated HW production*, *JHEP* **1606** (2016) 154, arXiv:1603.01620 [hep-ph].

[157] W. Astill, W. Bizoń, E. Re and G. Zanderighi, *NNLOPS accurate associated HZ production with $H \to b\bar{b}$ decay at NLO*, *JHEP* **1811** (2018) 157, arXiv:1804.08141 [hep-ph].

[158] J.M. Campbell, R.K. Ellis and C. Williams, *Vector boson pair production at the LHC*, *JHEP* **1107** (2011) 018, arXiv:1105.0020 [hep-ph].

[159] J.M. Campbell, R.K. Ellis and W.T. Giele, *A Multi-Threaded Version of MCFM*, *Eur. Phys. J.* **C 75** (2015) 246, arXiv:1503.06182 [physics.comp-ph].

[160] O. Brein, R.V. Harlander and T.J.E. Zirke, *vh@nnlo - Higgs Strahlung at hadron colliders*, *Comp. Phys. Commun.* **184** (2013) 998, arXiv:1210.5347 [hep-ph].

[161] R.V. Harlander, J. Klappert, S. Liebler and L. Simon, *vh@nnlo-v2: New physics in Higgs Strahlung*, *JHEP* **1805** (2018) 089, arXiv:1802.04817 [hep-ph].

[162] W.T. Giele and S. Keller, *Determination of W boson properties at hadron colliders*, *Phys. Rev.* **D 57** (1998) 4433, hep-ph/9704419.

[163] R.V. Harlander, J. Klappert, C. Pandini and A. Papaefstathiou, *Exploiting the WH/ZH symmetry in the search for New Physics*, *Eur. Phys. J.* **C 78** (2018) 760, arXiv:1804.02299 [hep-ph].

[164] C. Englert, M. McCullough and M. Spannowsky, *Gluon-initiated associated production boosts Higgs physics*, *Phys. Rev.* **D 89** (2014) 013013, arXiv:1310.4828 [hep-ph].

[165] R.V. Harlander, S. Liebler and T. Zirke, *Higgs Strahlung at the Large Hadron Collider in the 2-Higgs-Doublet Model*, *JHEP* **1402** (2014) 023, arXiv:1307.8122 [hep-ph].

[166] S. Dittmaier *et al.* [LHC Higgs Cross Section Working Group], *Handbook of LHC Higgs Cross Sections: 1. Inclusive Observables*, arXiv:1101.0593 [hep-ph].

[167] S. Dittmaier *et al.* [LHC Higgs Cross Section Working Group], *Handbook of LHC Higgs Cross Sections: 2. Differential Distributions*, arXiv:1201.3084 [hep-ph].

[168] S. Heinemeyer *et al.* [LHC Higgs Cross Section Working Group], *Handbook of LHC Higgs Cross Sections: 3. Higgs Properties*, arXiv:1307.1347 [hep-ph].

[169] M. Cacciari, G.P. Salam and G. Soyez, *The anti-k_t jet clustering algorithm*, *JHEP* **0804** (2008) 063, arXiv:0802.1189 [hep-ph].

[170] A. Denner, S. Dittmaier, S. Kallweit and A. Mück, *HAWK 2.0: A Monte Carlo program for Higgs production in vector-boson fusion and Higgs strahlung at hadron colliders*, *Comp. Phys. Commun.* **195** (2015) 161, arXiv:1412.5390 [hep-ph].

[171] A. Denner, S. Dittmaier and J.N. Lang, *Renormalization of mixing angles*, *JHEP* **1811** (2018) 104, arXiv:1808.03466 [hep-ph].

[172] R.D. Ball *et al.* [NNPDF Collaboration], *Parton distributions for the LHC Run II*, *JHEP* **1504** (2015) 040, arXiv:1410.8849 [hep-ph].

[173] A.V. Manohar, P. Nason, G.P. Salam and G. Zanderighi, *The Photon Content of the Proton*, *JHEP* **1712** (2017) 046, arXiv:1708.01256 [hep-ph].

[174] V. Bertone *et al.* [NNPDF Collaboration], *Illuminating the photon content of the proton within a global PDF analysis*, *SciPost Phys.* **5** (2018) 008, arXiv:1712.07053 [hep-ph].

[175] J. Alwall, M. Herquet, F. Maltoni, O. Mattelaer and T. Stelzer, *MadGraph 5 : Going Beyond*, *JHEP* **1106** (2011) 128, arXiv:1106.0522 [hep-ph].

[176] J. Alwall *et al.*, *The automated computation of tree-level and next-to-leading order differential cross sections, and their matching to parton shower simulations*, *JHEP* **1407** (2014) 079, arXiv:1405.0301 [hep-ph].

[177] J. Bellm *et al.*, *Herwig 7.0/Herwig++ 3.0 release note*, *Eur. Phys. J.* **C 76** (2016) 196, arXiv:1512.01178 [hep-ph].

[178] J. Bellm *et al.*, *Herwig 7.1 Release Note*, arXiv:1705.06919 [hep-ph].

[179] M. Czakon, P. Fiedler and A. Mitov, *Total Top-Quark Pair-Production Cross Section at Hadron Colliders Through $\mathcal{O}(\alpha_s^4)$*, *Phys. Rev. Lett.* **110** (2013) 252004, arXiv:1303.6254 [hep-ph].

[180] M. Cacciari and G.P. Salam, *Dispelling the N^3 myth for the k_t jet-finder*, *Phys. Lett.* **B 641** (2006) 57, hep-ph/0512210.

[181] M. Cacciari, G.P. Salam and G. Soyez, *FastJet User Manual*, *Eur. Phys. J.* **C 72** (2012) 1896, arXiv:arXiv:1111.6097 [hep-ph].

[182] J.R. Andersen *et al.*, *Les Houches 2017: Physics at TeV Colliders Standard Model Working Group Report*, , arXiv:1803.07977 [hep-ph].

[183] W.H. Furry, *A Symmetry Theorem in the Positron Theory*, *Phys. Rev.* **51** (1937) 125.

[184] L.D. Landau, *On the angular momentum of a system of two photons*, *Dokl. Akad. Nauk SSSR* **60** (1948) 207.

[185] C.N. Yang, *Selection Rules for the Dematerialization of a Particle Into Two Photons*, *Phys. Rev.* **77** (1950) 242.

[186] P. Nogueira, *Automatic Feynman graph generation*, *J. Comp. Phys.* **105** (1993) 279.

[187] R. Harlander, T. Seidensticker and M. Steinhauser, *Corrections of $\mathcal{O}(\alpha\alpha_s)$ to the decay of the Z boson into bottom quarks*, *Phys. Lett.* **B 426** (1998) 125, hep-ph/9712228.

[188] T. Seidensticker, *Automatic application of successive asymptotic expansions of Feynman diagrams*, hep-ph/9905298.

[189] J.A.M. Vermaseren, *New features of FORM*, math-ph/0010025.

[190] T. van Ritbergen, A.N. Schellekens and J.A.M. Vermaseren, *Group theory factors for Feynman diagrams*, *Int. J. Mod. Phys.* **A 14** (1999) 41, hep-ph/9802376.

[191] L. Chen, *A prescription for projectors to compute helicity amplitudes in D dimensions*, arXiv:1904.00705 [hep-ph].

[192] C.G. Bollini and J.J. Giambiagi, *Dimensional Renormalization: The Number of Dimensions as a Regularizing Parameter*, *Nuovo Cim.* **12B** (1972) 20.

[193] G. 't Hooft and M.J.G. Veltman, *Regularization and Renormalization of Gauge Fields*, *Nucl. Phys.* **B 44** (1972) 189.

[194] S. Moch, J.A.M. Vermaseren and A. Vogt, *On γ_5 in higher-order QCD calculations and the NNLO evolution of the polarized valence distribution*, *Phys. Lett.* **B 748** (2015) 432, arXiv:1506.04517 [hep-ph].

[195] D.A. Akyeampong and R. Delbourgo, *Dimensional regularization, abnormal amplitudes and anomalies*, *Nuovo Cim.* **17A** (1973) 578.

[196] S.A. Larin and J.A.M. Vermaseren, *The α_s^3 corrections to the Bjorken sum rule for polarized electroproduction and to the Gross-Llewellyn Smith sum rule*, *Phys. Lett.* **B 259** (1991) 345.

[197] S.A. Larin, *The Renormalization of the axial anomaly in dimensional regularization*, *Phys. Lett.* **B 303** (1993) 113, hep-ph/9302240.

[198] E.B. Zijlstra and W.L. van Neerven, *Order α_s^2 correction to the structure function $F_3(x, Q^2)$ in deep inelastic neutrino - hadron scattering*, *Phys. Lett.* **B 297** (1992) 377.

[199] C. Anastasiou and K. Melnikov, *Pseudoscalar Higgs boson production at hadron colliders in NNLO QCD*, *Phys. Rev.* **D 67** (2003) 037501, hep-ph/0208115.

[200] S.A. Larin, F.V. Tkachov, J.A.M. Vermaseren, *The FORM version of MINCER*, 1991.

[201] M. Steinhauser, *MATAD: a program package for the computation of massive tadpoles*, *Comp. Phys. Commun.* **134** (2001) 335, hep-ph/0009029.

[202] M. Prausa, *Towards Light Quark Mass Effects in Higgs Production and Decay at Next-to-Next-to-Leading Order*, https://dx.doi.org/doi:10.18154/RWTH-2018-224331.

[203] J. Klappert and F. Lange, *Reconstructing Rational Functions with* `FireFly`, *Comp. Phys. Commun.* **247** (2020) 106951, arXiv:1904.00009 [cs.SC].

[204] F.V. Tkachov, *A theorem on analytical calculability of 4-loop renormalization group functions*, *Phys. Lett.* **B 100** (1981) 65.

[205] K.G. Chetyrkin, F.V. Tkachov, *Integration By Parts: The algorithm to calculate beta functions in four loops*, *Nucl. Phys.* **B 192** (1981) 159.

[206] A.V. Smirnov and A.V. Petukhov, *The Number of Master Integrals is Finite*, *Lett. Math. Phys.* **97** (2011) 37, arXiv:1004.4199 [hep-th].

[207] S.G. Gorishny, S.A. Larin, L.R. Surguladze, F.V. Tkachov, *Mincer: Program for multiloop calculations in quantum field theory for the Schoonschip system*, *Comp. Phys. Commun.* **55** (1989) 381.

[208] D.J. Broadhurst, *Three loop on-shell charge renormalization without integration: $\Lambda^{\overline{MS}}_{QED}$ to four loops*, *Z. Phys.* **C 54** (1992) 599.

[209] K. Melnikov, T. van Ritbergen, *Three-Loop Slope of the Dirac Form Factor and the 1S Lamb Shift in Hydrogen*, *Phys. Rev. Lett.* **84** (2000) 1673, hep-ph/9911277.

[210] K. Melnikov, T. van Ritbergen, *The three-loop on-shell renormalization of QCD and QED*, *Nucl. Phys.* **B 591** (2000) 515, hep-ph/0005131.

[211] R.N. Lee, *Presenting* `LiteRed`*: a tool for the Loop InTEgrals REDuction*, arXiv:1212.2685 [hep-ph].

[212] R.N. Lee, `LiteRed` *1.4: a powerful tool for reduction of multiloop integrals*, *J. Phys. Conf. Ser.* **523** (2014) 012059, arXiv:1310.1145 [hep-ph].

[213] S. Laporta, *High-precision calculation of multi-loop Feynman integrals by difference equations*, *Int. J. Mod. Phys.* **A 15** (2000) 5087, hep-ph/0102033.

[214] C. Anastasiou, A. Lazopoulos, *Automatic Integral Reduction for Higher Order Perturbative Calculations*, *JHEP* **0407** (2004) 046, hep-ph/0404258.

[215] A.V. Smirnov, *Algorithm FIRE – Feynman Integral REduction*, *JHEP* **0810** (2008) 107, arXiv:0807.3243 [hep-ph].

[216] A.V. Smirnov, V.A. Smirnov, *FIRE4, LiteRed and accompanying tools to solve integration by parts relations*, *Comp. Phys. Commun.* **184** (2013) 2820, arXiv:1302.5885 [hep-ph].

[217] A.V. Smirnov, *FIRE5: a C++ implementation of Feynman Integral REduction*, *Comp. Phys. Commun.* **189** (2015) 182, arXiv:1408.2372 [hep-ph].

[218] A.V. Smirnov, F.S. Chukharev, *FIRE6: Feynman Integral REduction with Modular Arithmetic*, *Comp. Phys. Commun.* **247** (2020) 106877, arXiv:1901.07808 [hep-ph].

[219] C. Studerus, *Reduze - Feynman Integral Reduction in C++*, *Comp. Phys. Commun.* **181** (2010) 1293, arXiv:0912.2546 [physics.comp-ph].

[220] A. von Manteuffel, C. Studerus, *Reduze 2 - Distributed Feynman Integral Reduction*, arXiv:1201.4330 [hep-ph].

[221] P. Maierhöfer, J. Usovitsch, P. Uwer, *Kira - A Feynman Integral Reduction Program*, *Comp. Phys. Commun.* **230** (2018) 99, arXiv:1705.05610 [hep-ph].

[222] P. Maierhöfer, J. Usovitsch, *Kira 1.2 Release Notes*, arXiv:1812.01491 [hep-ph].

[223] A.G. Grozin, *Integration by parts: An introduction*, *Int. J. Mod. Phys.* **A 26** (2011) 2807, arXiv:1104.3993 [hep-ph].

[224] A.V. Kotikov, S. Teber, *Multi-Loop Techniques for Massless Feynman Diagram Calculations*, *Phys. Part. Nuclei* **50** (2019) 1, arXiv:1805.05109 [hep-th].

[225] R.H. Lewis, *Fermat: A Computer Algebra System for Polynomial and Matrix Computation*, http://home.bway.net/lewis/.

[226] A. von Manteuffel, R.M. Schabinger, *A novel approach to integration by parts reduction*, *Phys. Lett.* **B 744** (2015) 101, arXiv:1406.4513 [hep-ph].

[227] T. Peraro, *Scattering amplitudes over finite fields and multivariate functional reconstruction*, *JHEP* **1612** (2016) 030, arXiv:1608.01902 [hep-ph].

[228] G. Laurentis and D. Maître, *Extracting analytical one-loop amplitudes from numerical evaluations*, *JHEP* **1907** (2019) 123, arXiv:1904.04067 [hep-ph].

[229] T. Peraro, *FiniteFlow: multivariate functional reconstruction using finite fields and dataflow graphs*, *JHEP* **1907** (2019) 031, arXiv:1905.08019 [hep-ph].

[230] J. von zur Gathen, J. Gerhard, *Modern Computer Algebra*, third ed., Cambridge University Press, 2013.

[231] A. Cuyt, W.-s. Lee, *Sparse interpolation of multivariate rational functions*, *Theor. Comp. Sci.* **412** (2011) 1445.

[232] R. Zippel, *Probabilistic algorithms for sparse polynomials*, *Symbolic Algebraic Comp. EUROSAM* **1979** (1979) 216.

[233] R. Zippel, *Interpolating Polynomials from their Values*, *J. Symb. Comp.* **9** (1990) 375.

[234] M. Ben-Or, P. Tiwari, *A Deterministic Algorithm for Sparse Multivariate Polynomial Interpolation*, *Proc. ACM Symp. Theory Comp.* **20** (1988) 301.

[235] E. Kaltofen, Lakshman Y., *Improved Sparse Multivariate Polynomial Interpolation Algorithms*, *Symbolic Algebraic Comp. ISSAC* **1988** (1989) 467.

[236] E. Kaltofen, Lakshman Y.N., J.-M. Wiley, *Modular Rational Sparse Multivariate Polynomial Interpolation*, *Proc. Int. Symp. Symbolic Algebraic Comp.* **1990** (1990) 135.

[237] E. Kaltofen, W.-s. Lee, A.A. Lobo, *Early Termination in Ben-Or/Tiwari Sparse Interpolation and a Hybrid of Zippel's Algorithm*, *Proc. Int. Symp. Symbolic Algebraic Comp.* **2000** (2000) 192.

[238] E. Kaltofen, W.-s. Lee, *Early termination in sparse interpolation algorithms*, *J. Symb. Comp.* **36** (2003) 365.

[239] S.M.M. Javadi, M. Monagan, *Parallel Sparse Polynomial Interpolation over Finite Fields*, *Proc. Int. Workshop Parallel Symbolic Comp.* **4** (2010) 160.

[240] E. Kaltofen, B.M. Trager, *Computing with Polynomials Given by Black Boxes for Their Evaluations: Greatest Common Divisors, Factorization, Separation of Numerators and Denominators*, *J. Symb. Comp.* **9** (1990) 301.

[241] E. Kaltofen, Z. Yang, *On Exact and Approximate Interpolation of Sparse Rational Functions*, *Proc. Int. Symp. Symbolic Algebraic Comp.* **2007** (2007) 203.

[242] D.Y. Grigoriev, M. Karpinski, M.F. Singer, *Interpolation of Sparse Rational Functions Without Knowing Bounds on Exponents*, *Proc. Symp. Foundations Comp. Sci.* **31** (1990) 840.

[243] D.Y. Grigoriev, M. Karpinski, *Algorithms for Sparse Rational Interpolation*, *Proc. Int. Symp. Symbolic Algebraic Comp.* **1991** (1991) 7.

[244] D. Grigoriev, M. Karpinski, M.F. Singer, *Computational Complexity of Sparse Rational Interpolation*, *SIAM J. Comp.* **23** (1994) 1.

[245] J. de Kleine, M. Monagan, A. Wittkopf, *Algorithms for the Non-monic Case of the Sparse Modular GCD Algorithm*, *Proc. Int. Symp. Symbolic Algebraic Comp.* **2005** (2005) 124.

[246] Q.-L. Huang, X.-S. Gao, *Sparse Rational Function Interpolation with Finitely Many Values for the Coefficients*, *Math. Aspects Comp. Information Sci.* **2017** (2017) 227, `arXiv:1706.00914[cs.SC]`.

[247] A. Díaz, E. Kaltofen, FoxBox*: A System for Manipulating Symbolic Objects in Black Box Representation*, *Proc. Int. Symp. Symbolic Algebraic Comp.* **1998** (1998) 30.

[248] J. Hu, M. Monagan, *A Fast Parallel Sparse Polynomial GCD Algorithm*, *Proc. Int. Symp. Symbolic Algebraic Comp.* **2016** (2016) 271.

[249] M. Abramowitz, I.A. Stegun (Eds.), *Handbook of Mathematical Functions With Formulas, Graphs, and Mathematical Tables*, first ed., Dover Publications, 1964.

[250] J.T. Schwartz, *Fast Probabilistic Algorithms for Verification of Polynomial Identities*, *J. ACM* **27** (1980) 701.

[251] S. Khodadad, M. Monagan, *Fast Rational Function Reconstruction*, *Proc. Int. Symp. Symbolic Algebraic Comp.* **2006** (2006) 184.

[252] P.S. Wang, *A p-adic Algorithm for Univariate Partial Fractions*, *Proc. ACM Symp. Symbolic Algebraic Comp.* **1981** (1981) 212.

[253] P.S. Wang, M.J.T. Guy, J.H. Davenport, *P-adic Reconstruction of Rational Numbers*, *ACM SIGSAM Bulletin* **16, 2** (1982) 2.

[254] M. Monagan, *Maximal Quotient Rational Reconstruction: An Almost Optimal Algorithm for Rational Reconstruction*, *Proc. Int. Symp. Symbolic Algebraic Comp.* **2004** (2004) 243.

[255] J. Artz, R.V. Harlander, F. Lange, T. Neumann and M. Prausa, *Results and techniques for higher order calculations within the gradient-flow formalism*, *JHEP* **1906** (2019) 121 [Erratum: *JHEP* **1910** (2019) 032], arXiv:1905.00882 [hep-lat].

[256] A. von Manteuffel, R.M. Schabinger, *Quark and gluon form factors to four-loop order in QCD: the N_f^3 contributions*, *Phys. Rev.* **D 95** (2017) 034030, arXiv:1611.00795 [hep-ph].

[257] S. Badger, C. Brønnum-Hansen, H.B. Hartanto, T. Peraro, *Analytic helicity amplitudes for two-loop five-gluon scattering: the single-minus case*, *JHEP* **1901** (2019) 186, arXiv:1811.11699 [hep-ph].

[258] S. Abreu, J. Dormans, F. Febres Cordero, H. Ita, B. Page, *Analytic Form of Planar Two-Loop Five-Gluon Scattering Amplitudes in QCD*, *Phys. Rev. Lett.* **122** (2019) 082002, arXiv:1812.04586 [hep-ph].

[259] R.N. Lee, A.V. Smirnov, V.A. Smirnov and M. Steinhauser, *Four-loop quark form factor with quartic fundamental colour factor*, *JHEP* **1902** (2019) 172, arXiv:1901.02898 [hep-ph].

[260] J.M. Henn, T. Peraro, M. Stahlhofen and P. Wasser, *Matter dependence of the four-loop cusp anomalous dimension*, *Phys. Rev. Lett.* **122** (2019) 201602, arXiv:1901.03693 [hep-ph].

[261] A. von Manteuffel, R.M. Schabinger, *Quark and gluon form factors in four loop QCD: the N_f^2 and $N_{q\gamma}N_f$ contributions*, *Phys. Rev.* **D 99** (2019) 094014, arXiv:1902.08208 [hep-ph].

[262] S. Abreu, J. Dormans, F. Febres Cordero, H. Ita, B. Page and V. Sotnikov, *Analytic Form of the Planar Two-Loop Five-Parton Scattering Amplitudes in QCD*, *JHEP* **1905** (2019) 084, arXiv:1904.00945 [hep-ph].

[263] A. von Manteuffel, R.M. Schabinger, *Planar master integrals for four-loop form factors*, *JHEP* **1905** (2019) 073, arXiv:1903.06171 [hep-ph].

[264] S. Badger *et al.*, *Analytic form of the full two-loop five-gluon all-plus helicity amplitude*, *Phys. Rev. Lett.* **123** (2019) 071601, arXiv:1905.03733 [hep-ph].

[265] M. Kauers, *Fast solvers for dense linear systems*, *Nucl. Phys. Proc. Suppl.* **183** (2008) 245.

[266] P. Kant, *Finding Linear Dependencies in Integration-By-Parts Equations: A Monte Carlo Approach*, *Comp. Phys. Commun.* **185** (2014) 1473, arXiv:1309.7287 [hep-ph].

[267] H.B. Hartanto, S. Badger, C. Brønnum-Hansen and T. Peraro, *A numerical evaluation of planar two-loop helicity amplitudes for a W-boson plus four partons*, *JHEP* **1909** (2019) 119, arXiv:1906.11862 [hep-ph].

[268] D. Bendle, J. Boehm, W. Decker, A. Georgoudis, F.J. Pfreundt, M. Rahn, P. Wasser and Y. Zhang, *Integration-by-parts reductions of Feynman integrals using Singular and GPI-Space*, arXiv:1908.04301 [hep-th].

[269] J. Ellis, *TikZ-Feynman: Feynman diagrams with TikZ*, *Comp. Phys. Commun.* **210** (2017) 103, arXiv:1601.05437 [hep-ph].

DANKSAGUNG

Zuallererst gilt mein Dank Prof. Robert Harlander, der mir die Promotion in seiner Arbeitsgruppe ermöglicht hat. Die wissenschaftliche Zusammenarbeit, die hervorrangende Betreuung und die Möglichkeit, auch eigenen Projekten nachzugehen, haben mich sehr bereichert.

Bei Prof. Michael Krämer bedanke ich mich für die Übernahme des Zweitgutachtens.

Für das Führen von hilfreichen Diskussionen, die angenehme Arbeitsatmosphäre und das Korrekturlesen meiner Arbeit bedanke ich mich herzlich bei Benjamin Summ und Fabian Lange. In diesem Zuge bin ich auch Dr. Alexander Voigt für die Zusammenarbeit und Unterstützung sehr dankbar. Außerdem danke ich Dr. Mario Prausa für die nützlichen Diskussionen gerade zu Beginn dieser Arbeit.

Dr. Andreas Papaefstathiou danke ich für das Bereitstellen der Monte-Carlo-Daten, die in dieser Arbeit verwendet wurden.

Großer Dank gilt allen Personen, die mich während dieser Arbeit abseits der Physik begleitet und unterstützt haben. Besonders für den Rückhalt durch meine Mutter Michaela, meinen Großvater Ewald und meiner Partnerin Katrin bin ich sehr dankbar. Ich danke zudem all meinen Freunden, die mich auf diesem Weg begleitet und unterstützt haben. Insbesondere gilt dies für Benjamin, der mich in die Kunst des schwedischen Basketballs eingeführt hat, und Nina, die mich speziell in der Anfangsphase dieser Arbeit bestärkt hat.

In liebevoller Erinnerung an Klaus, Sabine und Kläre.

EIDESSTATTLICHE ERKLÄRUNG

Ich, Jonas Klappert, erkläre hiermit, dass diese Dissertation und die darin dargelegten Inhalte die eigenen sind und selbstständig, als Ergebnis der eigenen originären Forschung, generiert wurden.

Hiermit erkläre ich an Eides statt

1. Diese Arbeit wurde vollständig oder größtenteils in der Phase als Doktorand dieser Fakultät und Universität angefertigt;
2. Sofern irgendein Bestandteil dieser Dissertation zuvor für einen akademischen Abschluss oder eine andere Qualifikation an dieser oder einer anderen Institution verwendet wurde, wurde diesklar angezeigt;
3. Wenn immer andere eigene- oder Veröffentlichungen Dritter herangezogen wurden, wurden diese klar benannt;
4. Wenn aus anderen eigenen- oder Veröffentlichungen Dritter zitiert wurde, wurde stets die Quelle hierfür angegeben. Diese Dissertation ist vollständig meine eigene Arbeit, mit der Ausnahme solcher Zitate;
5. Alle wesentlichen Quellen von Unterstützung wurden benannt;
6. Wenn immer ein Teil dieser Dissertation auf der Zusammenarbeit mit anderen basiert, wurde von mir klar gekennzeichnet, was von anderen und was von mir selbst erarbeitet wurde;
7. Ein Teil oder Teile dieser Arbeit wurden zuvor veröffentlicht und zwar in:

[JK1] R.V. Harlander, J. Klappert and A. Voigt, *Higgs mass prediction in the MSSM at three-loop level in a pure $\overline{DR}$ context*, *Eur. Phys. J.* **C 77** (2017) 814, arXiv:1708.05720 [hep-ph].

[JK3] R.V. Harlander, J. Klappert, C. Pandini and A. Papaefstathiou, *Exploiting the WH/ZH symmetry in the search for New Physics*, *Eur. Phys. J.* **C 78** (2018) 760, arXiv:1804.02299 [hep-ph].

[JK4] R.V. Harlander, J. Klappert, A. D. Ochoa Franco and A. Voigt, *The light CP-even MSSM Higgs mass resummed to fourth logarithmic order*, *Eur. Phys. J.* **C 78** (2018) 874, arXiv:1807.03509 [hep-ph].

[JK5] J. Klappert and F. Lange, *Reconstructing Rational Functions with* `FireFly`, *Comp. Phys. Commun.* **247** (2020) 106951, arXiv:1904.00009 [cs.SC].

[JK6] R.V. Harlander, J. Klappert and A. Voigt, *The light CP-even MSSM Higgs mass including N^3LO+N^3LL QCD corrections*, arXiv:1910.03595 [hep-ph].